



## **Design of Implantable Antennas for Biomedical Applications**

**Dr Nabeel Ahmed Malik**

This is a digitised version of a dissertation submitted to the University of Bedfordshire.

It is available to view only.

This item is subject to copyright.



# Design of Implantable Antennas for Biomedical Applications

by

Nabeel Ahmed Malik

Department of Computer Science and Technology

Institute for Research and Applied Computing

Centre for Wireless Research

A thesis submitted to the University of Bedfordshire, in fulfilment of the requirements for the  
degree of Doctor of Philosophy

January 2022

## **Declaration**

I, Nabeel Ahmed Malik declare that this thesis and the work presented in it are my own and has been generated by me as the result of my own original research.

I confirm that:

- This work was done wholly or mainly while in candidature for a research degree at this University.
- Where any part of this thesis has previously been submitted for a degree or any other qualification at this University or any other institution, this has been clearly stated.
- Where I have drawn on or cited the published work of others, this is always clearly attributed.
- Where I have quoted from the work of others, the source is always given. With the exception of such quotations, this thesis is entirely my own work.
- I have acknowledged all main sources of help.
- Where the thesis or any part of it is based on work done by myself jointly with others, I have made clear exactly what was done by others and what I have contributed myself.
- Parts of this work have been published as indicated on “List of Publications”.

## **Abstract**

Biomedical telemetry has gained a lot of attention with recent developments in the healthcare industry. This technology has made it feasible to monitor the physiological signs of a patient remotely without traditional hospital appointments and follow up check-ups. Implantable Medical Devices (IMDs) play an important role in monitoring patients through wireless telemetry. IMDs have a wide range of applications which includes wireless endoscopy, blood pressure monitoring, wireless drug delivery, cardiac defibrillation, pacemakers and blood sugar level monitoring etc. IMDs consist of nodes and sensors in which the antenna is a major component. The selection of the antenna is a challenging task in IMD design as it dictates performance of the whole implant. Various factors need to be considered for implantable antennas such as miniaturization, patient safety, biocompatibility, low power consumption and providing robust and continuous operation within a harsh environment. The human body is a very lossy medium and affects the working of the antenna significantly. Therefore, designing an antenna to operate from inside the body is a very challenging task.

Three novel implantable antennas are designed using a simple methodology. Computer Simulation Technology (CST) Microwave Studio software is used to design and simulate the antennas. The antennas are compact in size, light weight and show good performance in implantable conditions. A circular patch antenna is designed for operating in Industrial, Scientific and Medical (ISM) band at 915 MHz using coaxial probe feed. The overall volume of the antenna is  $(\pi \times 4^2 \times 0.38) \text{ mm}^3$ . At 915 MHz the antenna has a peak gain of -28.8 dBi and has a bandwidth of 90 MHz when simulated in simplified skin layer phantom of the human body. The radiation efficiency of the antenna is -31.6 dB at resonant frequency. The 1-gram(g) and 10-gram(g) average(avg) SAR values for this antenna are 1218 and 125.2 W/Kg when the input power of the antenna was 0.5W. The antenna satisfies the requirements for implantable applications. A microstrip rectangular patch antenna is designed operating in Medical Implantable Communication Service (MICS) band (402-405) MHz and ISM bands of (902-928) MHz and (2.4-2.45) GHz. The antenna resonates at 402 MHz, 915 MHz and 2.4 GHz when simulated in simplified fat layer phantom of the human. The size of the antenna is  $(6 \times 5 \times 0.5) \text{ mm}^3$ . At resonant

frequencies the peak gain of the antenna is (-47.7, -37.2, -25.5) dBi. This antenna offers a bandwidth of (108, 170, 250) MHz with a radiation efficiency of (-52, -42, -32) dB at operating frequencies. The 1g avg. SAR values of rectangular patch antenna at operating frequencies are (122, 184, 863) W/Kg and 10g avg. SAR values of rectangular patch antenna at operating frequencies are (12.25, 18.42, 86.42) W/Kg when the antenna was excited with an input power of 0.5W. Finally, design of a compact size antenna operating at 915 MHz is presented. The antenna has a size of ( $4 \times 4 \times 0.26$ ) mm<sup>3</sup>. When simulated in simplified skin layer phantom the antenna offers a bandwidth of 170 MHz with a peak gain of -34.7 dBi at resonant frequency. The radiation efficiency of the antenna is -36.5 dB. SAR values of this antenna are 1069 W/Kg for 1g avg. and 108 W/Kg for 10g avg. with 0.5W input power.

All of the designed antennas are simulated in simplified human body phantom model and multilayer tissues. After that the antennas are subjected to different implant depths to investigate their performance with varying implant depths. Different thicknesses of insulation layer are used to analyse the effects on antenna resonance. To check the antenna integration with sensors, dummy electronic components are used, and antennas are simulated which shows the diversity of designed antennas. The designed antennas are simulated in anatomical body model and the results showed a good match between anatomical body model and phantom body model. A size reduction of 15%, 29% and 47% and overall performance improvement of 9%, 15% and 12% is achieved for the designed circular patch antenna, rectangular patch antenna and compact size antenna which proves that the designed antennas are best match for the implantable applications.

## **Dedication**

*This thesis is dedicated to my parents with love & respect.*

## **Acknowledgment**

First and foremost, I am thankful to Almighty Allah for having given me the strength to do this research work and complete my thesis.

I would like to express my sincere gratitude to my Director of Studies, Dr. Paul Sant for his continuous guidance, valuable suggestions and huge support throughout my PhD studies. I would also like to thank my second supervisor, Dr. Tahmina Ajmal for her help and guidance throughout my academic journey. I would also like to thank Dr. Masood Ur Rehman for his valuable support and guidance to complete this research work. They are all highly committed persons and have motivated me always. I greatly respect them for their patience, vast knowledge and their helping nature. The achievements we accomplished together during my PhD studies are highly commendable. The successful completion of my thesis would have not been possible without their help.

I would like to immensely thank my parents for making me a capable and a better person. This research work would have been just a dream without my father help and guidance. His love and undying support have been a strong factor for the completion of my research work. I would like to express my appreciation to my technical manager, Robert Keane and other team members for their support. Last but not the least, I thank my friends and colleagues in the IRAC department for being with me at times of need. I wish them all success in their endeavours.

## **Publications**

1. N. A. Malik, P. Sant, T. Ajmal and M. Ur-Rehman, "A Tri-band Implantable Antenna for Biotelemetry Applications," *2020 International Conference on UK-China Emerging Technologies (UCET)*, Glasgow, UK, 2020, pp. 1-4.
2. N. A. Malik, P. Sant, T. Ajmal and M. Ur-Rehman, "A Compact Size Implantable Antenna for Bio-medical Applications," *2020 International Conference on UK-China Emerging Technologies (UCET)*, Glasgow, UK, 2020, pp. 1-4.
3. N. A. Malik, P. Sant, T. Ajmal and M. Ur-Rehman, "Implantable Antennas for Bio-Medical Applications," *IEEE Journal of Electromagnetics, RF and Microwaves in Medicine and Biology*", vol. 5, no. 1, pp. 84-96, March 2021.

## **List of Abbreviations**

AT	Ambient Temperature
AUT	Antenna Under Test
AVG	Average
BER	Bitt Error Rate
BSN	Body Sensor Network
CSRR	Complementary Split Ring Resonator
CST	Computer Simulation Technology
EIRP	Effective Isotropic Radiated Power
SAR	Specific Absorption Rate
MICS	Medical Implantable Communication Service
MedRadio	Medical Device Radio Communication Service
ISM	Industrial, Scientific and Medical
IMDs	Implantable Medical Devices
LOS	Line of Sight
PIFA	Planar Inverted F Antenna
TX	Transmitter
RX	Receiver
WBAN	Wireless Body Area Networks
PVC	Polyvinyl Chloride
EBG	Electromagnetic Band Gap

MIMO	Multiple Input Multiple Output
RFID	Radio Frequency Identification
FCC	Federal Communication Commission
ICNIRP	International Commission on Non-Ionizing Radiation Protection
PDMS	Poly Dimethyl Siloxane
CPW	Coplanar Waveguide
FDTD	Finite Difference Time Domain
FIT	Finite Integral Technique
IE3D	Integral Equation Three Dimensional
FEKO	Feldberechnung für Körper mit beliebiger Oberfläche
MATLAB	Matrix Laboratory
ADE	Antenna Design Explorer
HFSS	High Frequency Structure Simulator
MoM	Method of Moments
FEM	Finite Element Method
PBA	Perfect Boundary Approximation
TST	Thin Sheet Technique
TLM	Transmission Line Matrix
CMA	Characteristics Mode Analysis
RAM	Random-Access Memory
EM	Electromagnetic

EMI	Electromagnetic Interference
EMC	Electromagnetic Compatibility
CST MPS	CST Mphysics Studio
CST CS	CST Cable Studio
CST DS	CST Design Studio
CST PS	CST Particle Studio
PCB	Printed Circuit Board
CST PCBS	CST PCB Studio
CST EMS	CST EM Studio
CST MWS	CST Microwave Studio

## List of Tables

Table 2.1: Comparative analysis of different miniaturization techniques for implantable antennas ....	16
Table 2.2: Comparative analysis of implantable antennas .....	29
Table 2.3: Human body tissues conductivity and permittivity .....	34
Table 4.1- Circular patch antenna dimensions .....	59
Table 4.2- Circular patch antenna comparison with previous work.....	66
Table 4.3- Rectangular patch antenna detailed dimensions .....	70
Table 4.4- Rectangular patch antenna comparison with previous work.....	76
Table 4.5- Compact size antenna dimensions .....	79
Table 4.6- Compact size antenna optimized dimensions .....	81
Table 4.7- Compact size antenna comparison with previous work.....	86
Table 4.8- Comparison of the designed antennas with each other .....	87
Table 5.1- Electrical properties of human body tissues at different frequencies.....	91
Table 5.2- Simulation time and memory used by designed antennas in anatomical body model .....	107

## List of Figures

Figure 1.1: Block diagram of implantable device [5].....	2
Figure 2.1: Schematic of antenna design process [20] .....	9
Figure 2.2: (a) Geometry of probe fed wideband antenna (b) Radiation pattern of the antenna [61] ..	17
Figure 2.3: (a) Structure of implantable meander line antenna (b) Surface current density of the antenna at 402.5 MHz [63] .....	18
Figure 2.4: (a) Geometry of implantable fractal patch antenna (b) Radiation pattern of antenna at 2.45 GHz [9].....	18
Figure 2.5: (a) Structure of helical antenna for ingestible capsule (b) Reflection coefficient of the antenna [64].....	19
Figure 2.6: Structure of implantable helical antenna using two magnetic sheets [65] .....	19
Figure 2.7: Scattering parameters of the helical antenna [65].....	20
Figure 2.8: (a) Conical spiral implantable antenna geometry (b) Reflection coefficient of the antenna [66] .....	20
Figure 2.9: (a) Geometry of implantable CP conformal antenna (b) Reflection coefficient of the antenna [67] .....	21
Figure 2.10: (a) Geometry of implantable conformal patch antenna (b) S11 curve of the antenna [68] .....	22
Figure 2.11: (a) Reflection coefficient of differentially fed implantable antenna in flat and conformal form (b) Radiation patterns of the antenna at 915 MHz [69] .....	22
Figure 2.12: (a) Structure of implantable bow-tie antenna (b) S11 curve of the antenna [70].....	23
Figure 2.13: (a) Top and side view of implantable CP ring antenna (b) Radiation pattern of the antenna at 2.45 GHz [71].....	24
Figure 2.14: (a) Structure of spiral shape implantable antenna (b) Reflection coefficient of the antenna with different ground planes [72] .....	25
Figure 2.15: (a) Geometry of implantable dual band CP antenna (b) Radiation pattern of the antenna [73] .....	25

Figure 2.16: (a) Structure of loop antenna (b) Reflection coefficient [8].....	26
Figure 2.17: (a) Geometry of implantable triangular slot antenna (b) Reflection coefficient [11] .....	27
Figure 2.18: (a) Geometry of implantable flexible metamaterial antenna (b) Reflection coefficient of the antenna [74].....	27
Figure 2.19: (a) Geometry of implantable broadband PIFA antenna (b) Radiation pattern of the antenna at 402 MHz [76] .....	28
Figure 2.20: (a) Structure of implantable PIFA with slotted ground plane (b) Radiation pattern at 2.45 GHz [77].....	29
Figure 2.21: (a) Radiation efficiency of the antenna (b) Radiation efficiency of antenna after modification with a 4% improvement [97] .....	39
Figure 2.22: Bandwidth enhancement of dipole antenna [99].....	39
Figure 3.1- Design Methodology .....	44
Figure 4.1- Slot creation in the patch of circular patch antenna (a)- case 0 (b)- case 1 (c)-case 2 (d)- case 3.....	54
Figure 4.2- (a) Slotted patch of the circular patch antenna (b) Slotted patch of the circular patch antenna with labelled parameters.....	54
Figure 4.3- Simulated return loss plot of the circular patch antenna in free space in different stages of slots creation in the patch with solid ground plane .....	55
Figure 4.4- Slots creation in the ground plane of the circular patch antenna (a)- case 0 (b)- case 1 (c)-case 2 (d)- case 3 .....	56
Figure 4.5- (a) Slotted ground plane of the circular patch antenna (b) Slotted ground plane of the circular patch antenna with labelled parameters.....	57
Figure 4.6- Circular patch antenna side view .....	57
Figure 4.7- Simulated return loss plot of the circular patch antenna in free space in different stages of slot creation in the ground plane with slotted patch .....	58
Figure 4.8- Block representation of circular patch antenna in simplified skin layer phantom.....	60
Figure 4.9- Return loss of the circular patch antenna in free space and in skin layer phantom .....	60

Figure 4.10- Return loss of the circular patch antenna in skin layer phantom after design optimization .....	61
Figure 4.11- 3D radiation pattern of the circular patch antenna in skin layer phantom at 915 MHz ....	62
Figure 4.12- Polar plot of radiation pattern of the circular patch antenna in skin layer phantom at 915 MHz (a) E-Plane (b) H-Plane .....	63
Figure 4.13- Circular patch antenna SAR in skin layer phantom at 915 MHz (a) 1g avg. (b) 10g avg.	63
Figure 4.14-Return loss of the circular patch antenna in skin layer phantom with changing parameters .....	65
Figure 4.15- (a) Rectangular patch antenna patch view (b) Rectangular patch antenna ground plane view .....	68
Figure 4.16- (a) Rectangular patch antenna patch with labelled parameters (b) Rectangular patch antenna ground plane with labelled parameters.....	69
Figure 4.17- Rectangular patch antenna perspective view .....	69
Figure 4.18- Block representation of rectangular patch antenna inside fat layer phantom .....	69
Figure 4.19- Return loss of the rectangular patch antenna in fat layer phantom.....	71
Figure 4.20- 3D radiation pattern of the rectangular patch antenna (a) 402 MHz (b) 915 MHz (c) 2.4 GHz .....	72
Figure 4.21- (a) E-plane radiation pattern of the rectangular patch antenna (b) H-plane radiation pattern of the rectangular patch antenna.....	73
Figure 4.22- 1g avg. SAR of the rectangular patch antenna (a) 402 MHz (b) 915 MHz (c) 2.4 GHz ..	73
Figure 4.23- 10g avg. SAR of the rectangular patch antenna (a) 402 MHz (b) 915 MHz (c) 2.4 GHz	74
Figure 4.24- Return loss of the rectangular patch antenna with changing parameters .....	75
Figure 4.25- (a) Compact size antenna patch (b) Compact size antenna labelled patch .....	77
Figure 4.26- (a) Compact size antenna ground plane (b) Compact size antenna labelled ground plane .....	77
Figure 4.27- Compact size antenna side view .....	78
Figure 4.28- Block representation of compact size antenna inside skin layer phantom.....	78
Figure 4.29- Return loss of the compact size antenna in free space and skin layer phantom .....	79

Figure 4.30- Compact size antenna optimized design (a) Patch view (b) Labelled patch view .....	80
Figure 4.31- Compact size antenna optimized design (a) ground plane view (b) Labelled ground plane view .....	81
Figure 4.32- Return loss of the compact size optimized antenna.....	82
Figure 4.33- 3D radiation pattern of the compact size antenna at 915 MHz.....	83
Figure 4.34- Polar plot of radiation pattern of the compact size antenna at 915 MHz (a) E-plane (b) H-plane .....	83
Figure 4.35- Compact size antenna SAR at 915 MHz (a) 1g avg. (b) 10g avg.....	84
Figure 4.36- Return loss of compact size antenna with changing parameters.....	85
Figure 5.1- Block representation of simplified multilayer tissue phantom .....	91
Figure 5.2- Circular patch antenna return loss in multilayer tissues (skin, fat and muscle).....	92
Figure 5.3- Polar plot of radiation pattern of the circular patch antenna in multilayer tissues (skin, fat and muscle) at 915 MHz (a) E-plane (b) H-plane .....	93
Figure 5.4- Return loss of the rectangular patch antenna in multilayer tissues (skin, fat and muscle) .	94
Figure 5.5- Polar plot of radiation pattern of the rectangular patch antenna in multilayer tissues (skin, fat and muscle) at 2.4 GHz (a) E-plane (b) H-plane.....	95
Figure 5.6- Return loss of compact size antenna at 915 MHz in multilayer tissues (skin, fat and muscle) .....	96
Figure 5.7- Polar plot of radiation pattern of compact size antenna in multilayer tissues (skin, fat and muscle) at 915 MHz (a) E-plane (b) H-plane.....	96
Figure 5.8- Return loss of compact size antenna in skin layer phantom with different implant depths	98
Figure 5.9- Polar plot of the radiation pattern of the compact size antenna with different implant depths in skin layer phantom at 915 MHz (a) E-plane (b) H-plane.....	99
Figure 5.10- Return loss of circular patch antenna with different implant depths in skin layer.....	99
Figure 5.11- Polar plot of radiation pattern of the circular patch antenna with different implant depths in skin layer at 915 MHz (a) E-plane (b) H-plane.....	100
Figure 5.12- Return loss of the rectangular patch antenna with different implant depths in fat layer	101

Figure 5.13- Radiation pattern of rectangular patch antenna at 2.4 GHz with varied implant depths (a)-E plane (b)- H plane .....	102
Figure 5.14- Antenna placement in circular and rectangular phantoms.....	102
Figure 5.15- Gain of compact size antenna at 915 MHz in rectangular and circular shape phantoms	103
Figure 5.16- Return loss of rectangular patch antenna with insulation layer .....	104
Figure 5.17- Block representation of antenna and circuit components .....	105
Figure 5.18- Return loss of rectangular patch antenna when simulated without and with circuit components.....	105
Figure 5.19- Return loss of the circular patch antenna without and with circuit components .....	106
Figure 5.20- Return loss of the compact size antenna when simulated without and with circuit components.....	106
Figure 5.21- Block diagram of antenna inside anatomical body model .....	107
Figure 5.22- Return loss of compact size antenna in anatomical body model and simplified skin layer phantom.....	108
Figure 5.23- 3D Radiation pattern of the compact size antenna at 915 MHz (a) anatomical body model (b) simplified skin layer phantom .....	109
Figure 5.24- Polar plot of radiation pattern of the compact size antenna in anatomical body model and simplified skin layer phantom at 915 MHz (a) E-plane (b) H-plane.....	109
Figure 5.25- Compact size antenna 1g avg. SAR (a) anatomical body model (b) simplified skin layer phantom.....	110
Figure 5.26- Compact size antenna 10g avg. SAR (a) anatomical body model (b) simplified skin layer phantom.....	110
Figure 5.27- Return loss of the rectangular patch antenna in anatomical body model and simplified fat layer phantom .....	111
Figure 5.28- 3D radiation pattern of the rectangular patch antenna in anatomical body model (a) 402 MHz (b) 915 MHz (c) 2.4 GHz.....	112
Figure 5.29- 3D radiation pattern of the rectangular patch antenna in simplified fat layer phantom (a) 402 MHz (b) 915 MHz (c) 2.4 GHz .....	112

Figure 5.30- Polar plot of radiation pattern of rectangular patch antenna in anatomical body model (a) E-plane (b) H-plane .....	113
Figure 5.31- Polar plot of radiation pattern of rectangular patch antenna in simplified fat layer phantom (a) E-plane (b) H-plane.....	113
Figure 5.32 - 1g avg. SAR of the rectangular patch antenna in anatomical body model (a) 402 MHz (b) 915 MHz (c) 2.4 GHz.....	114
Figure 5.33- 1g avg. SAR of the rectangular patch antenna in simplified fat layer phantom (a) 402 MHz (b) 915 MHz (c) 2.4 GHz .....	114
Figure 5.34- 10g avg. SAR of the rectangular patch antenna in anatomical body model (a) 402 MHz (b) 915 MHz (c) 2.4 GHz.....	114
Figure 5.35- 10g avg. SAR of the rectangular patch antenna in simplified fat layer phantom (a) 402 MHz (b) 915 MHz (c) 2.4 GHz.....	114
Figure 5.36- Return loss plot of the circular patch antenna in anatomical body model and simplified skin layer phantom .....	115
Figure 5.37- Circular patch antenna 3D radiation pattern (a) anatomical body model (b) simplified skin layer phantom .....	116
Figure 5.38- Polar plot of the radiation pattern of the circular patch antenna in anatomical body model and simplified skin layer phantom (a) E-plane (b) H-plane .....	116
Figure 5.39- Circular patch antenna 1g avg. SAR (a) anatomical body model (b) simplified skin layer phantom.....	117
Figure 5.40- Circular patch antenna 10g avg. SAR (a) anatomical body model (b) simplified skin layer phantom.....	117
Figure 5.41- SAR of the compact size antenna in anatomical body model at 915 MHz when excited with maximum allowed input power (a) 1g (b) 10g.....	118
Figure 5.42- 1g avg. SAR of the rectangular patch antenna in anatomical body model when excited with maximum allowed input power (a) 402 MHz (b) 915 MHz (c) 2.4 GHz.....	119
Figure 5.43- 10g avg. SAR of the rectangular patch antenna in anatomical body model when excited with maximum allowed input power (a) 402 MHz (b) 915 MHz (c) 2.4 GHz.....	119

Figure 5.44- SAR of the circular patch antenna at 915 MHz in anatomical body model when excited with maximum allowed input power (a) 1g (b) 10 g.....120

## Contents

Abstract .....	i
Dedication .....	iii
Acknowledgment .....	iv
Publications .....	v
List of Abbreviations.....	vi
List of Tables.....	ix
List of Figures .....	x
Contents.....	xvii
1. Introduction .....	1
1.1 Research Background.....	1
1.2 Problem Statement .....	2
1.3 Motivation and objectives .....	3
1.4 Thesis Contribution .....	5
1.5 Thesis Organization.....	6
2. Implantable Antennas.....	8
2.1 Introduction .....	8
2.2 Implantable Sensors and Antennas.....	9
2.3 Implantable Antenna Design: Requirements and Challenges .....	10
2.3.1 Miniaturization .....	10
2.3.2 Patient Safety.....	12
2.3.3 Biocompatibility .....	13

2.3.4	Implantable Antenna Fabrication Methods and Materials .....	14
2.4	Types of Implantable Antennas.....	16
2.4.1	Planar Antennas.....	16
2.4.2	Wire Antennas.....	18
2.4.3	Conformal Antennas.....	21
2.4.4	Spiral Antennas .....	23
2.4.5	Slot Antennas .....	26
2.4.6	Planar Inverted F antennas (PIFA).....	28
2.5	Human Body Effect on Antenna Performance .....	33
2.5.1	Human Body Effects on Antenna Radiation Efficiency and Antenna Radiated Power	37
2.5.2	Human Body Effect on Antenna Bandwidth.....	38
2.5.3	Human Body Effect on Antenna Radiation Pattern.....	38
2.5.4	Methods to improve Implantable Antennas Radiation Efficiency .....	38
2.5.5	Implantable Antenna Bandwidth and Gain Improvement .....	39
2.6	Channel Modelling for Implantable Antennas .....	40
2.7	Chapter Summary.....	42
3.	Methodology .....	43
3.1	Introduction .....	43
3.2	Methodology of the Designed Antennas .....	43
3.2.1	Methodology Parameters.....	44
3.3	Project Milestones .....	45
3.3.1	Literature Review on Implantable Antennas.....	45
3.3.2	Design of Implantable Antenna.....	45

3.3.3	Human Body Effect Analysis.....	46
3.4	Numerical Modelling Techniques .....	46
3.4.1	Finite Difference Time Domain (FDTD) .....	47
3.4.2	Finite Integral Technique (FIT).....	48
3.5	Antenna Design Software.....	48
3.6	CST Microwave Studio® .....	49
3.7	Chapter Summary.....	51
4.	Design of Implantable Antennas .....	52
4.1	Introduction .....	52
4.2	Circular Patch Antenna .....	53
4.2.1	Circular Patch Antenna Optimization .....	61
4.2.2	Parametric Study of Circular Patch Antenna.....	64
4.3	Rectangular Patch Antenna .....	66
4.3.1	Rectangular patch antenna parametric study.....	74
4.4	Compact Size Antenna .....	76
4.4.1	Compact size antenna optimization.....	80
4.4.2	Parametric study of compact size antenna.....	84
4.5	Chapter summary .....	87
5.	Performance Evaluation of Designed Antennas in Simplified Body Model and Anatomical Body Model .....	90
5.1	Introduction .....	90
5.2	Designed Antennas Performance in Multilayer Tissues.....	91
5.2.1	Performance analysis of circular patch antenna in multilayer tissues .....	91

5.2.2	Performance analysis of rectangular patch antenna in multilayer tissues .....	93
5.2.3	Performance analysis of compact size antenna in multilayer tissues .....	95
5.3	Performance Evaluation of Designed Antennas with Different Implant depths .....	97
5.3.1	Performance evaluation of compact size antenna with different implant depths in skin layer phantom.....	97
5.3.2	Performance evaluation of circular patch antenna with different implant depths in skin layer phantom.....	99
5.3.3	Performance evaluation of rectangular patch antenna in fat layer phantom with different implant depths .....	100
5.4	Performance Evaluation of Compact Size Antenna in Different Size Phantoms .....	102
5.5	Effect of Insulation Layer on Rectangular Patch Antenna performance.....	103
5.6	Analysis of Circuit Components Effect on Designed Antennas Performance .....	104
5.7	Designed Antennas Performance Evaluation in Anatomical Body Model .....	107
5.7.1	Performance evaluation of compact size antenna in anatomical body model .....	108
5.7.2	Performance evaluation of rectangular patch antenna in anatomical body model .....	111
5.7.3	Performance evaluation of circular patch antenna in anatomical body model .....	115
5.8	Designed Antennas SAR Calculation in Anatomical Body Model with Maximum Allowed Input Power .....	118
5.9	Chapter Summary .....	120
6.	Conclusion and Future Work .....	122
6.1	Conclusion.....	122
6.2	Future Work .....	124
6.2.1	Antenna Fabrication .....	124
6.2.2	Wireless power transfer.....	124

6.2.3	Antenna design .....	124
6.2.4	Realization of the implantable device .....	125
References .....		126
Appendix A .....		136
Appendix B .....		140

# **Chapter 1**

## **1. Introduction**

### **1.1 Research Background**

Wireless communication technologies have received significant attention from the research community in recent years. The growth in portable and wearable wireless devices has made body-centric applications an integral part of our daily life resulting in the fast-growing field of Body-Centric Wireless Networks (BCWNs). For BCWNs antennas and propagation play an important role because the antenna effects both transmission and reception. So, if the performance of the antenna is poor it will affect the performance of the whole system.

In biomedical telemetry, implantable medical devices (IMDs) are capable of monitoring a patient's physiological data wirelessly in real time [1], [2]. In biomedical telemetry, the implantable devices are of greater significance and have many applications such as hyperthermia for cancer treatment, remote drug delivery and vital signs monitoring [3], [4]. The implantable devices are placed inside the body where they monitor data (such as blood pressure and temperature) and send the information to an external device. The external device can be used to process the information, transmit signals to an implantable device such as wakeup signals and wireless power transfer for RF energy harvesting.

Implantable devices are made up of many components including an antenna, battery, and sensors. A block diagram of an implantable device is shown in Figure 1.1 [5].

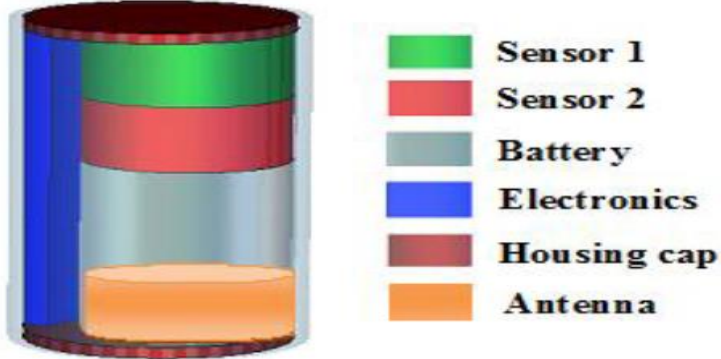


Figure 1.1: Block diagram of implantable device [5]

Reliability and robustness of the communication link between the internal and external device depends largely on the implantable antenna. Moreover, it also affects the overall size and weight of the implantable device. Furthermore, the environment within the body electromagnetically is very harsh and lossy and therefore adds to the design complexity. Additionally, it is general requirement that IMDs exhibit long battery life to extend the operation and avoid their frequent replacements through surgical procedures. Hence, miniaturization, patient safety, biocompatibility, operational frequency band, strong wireless link and wireless energy charging can be summarised as key requirements for IMDs.

## 1.2 Problem Statement

Though medical implantable devices have improved human life due to their wide-ranging applications, the design of these devices particularly the antenna is a complex and multi-faceted task. The implantable antenna could be subjected to bending conditions, so the flexibility of the antenna needs to be considered. As the radio frequency (RF) exposure could damage human body tissues, the SAR and EIRP values for the implantable antenna should be within safe levels [6], [7].

The size of the implantable device is dependent on the implantable antenna, so the size of the antenna should be small while maintaining the correct resonance, impedance matching, radiation level and communication link. An implantable antenna also needs to use bio-compatible materials to ensure safety of the human organs. As the human body is a lossy medium, when the antenna is implanted inside the body the performance of the antenna will diminish. This would result as a difference between simulated results and actual results. The optimization of the design to get the desired results is a challenging task.

The propagation losses are greater at higher frequencies, so the antenna needs to be designed at a lower frequency while keeping the size of the antenna as small as possible. The issue with a lower frequency of operation is that if the antenna size is reduced the frequency will shift to a higher value. So, an adequate approach is needed to minimize this trade-off. Several researchers have considered these issues, however there is still gap. This research aims to address this gap.

### **1.3 Motivation and objectives**

With the rapid growth in the world's population, demand for biomedical telemetry has significantly increased in order to improve people's health and lifestyle. A lot of research has been done in this field.

A number of implantable antenna designs are proposed in open literature. However, most of these antenna designs do not fulfil the stringent requirements of miniaturization, patient safety, biocompatibility, high radiation efficiency, good bandwidth, high gain, low power consumption and reliable communication.

A miniaturized circularly polarized loop antenna for biomedical applications was proposed in [8]. The size of the antenna is  $13 \times 13 \times 1.27$  mm<sup>3</sup>. The antenna offers a bandwidth of 245 MHz at a resonant frequency of 915 MHz. Radiation efficiency of this antenna is not reported. The gain of the antenna is -32 dBi and 1g avg. SAR value of this antenna is 599 W/Kg. The antenna gain is low despite having large volume. The implantable antenna proposed in [9] operates at 2.45 GHz with dimensions of  $11.44 \times 11.44 \times 0.275$  mm<sup>3</sup>. A bandwidth of 100 MHz is reported while other parameters are not mentioned to quantify antenna performance. The antenna resonates at higher frequency of ISM band at 2.4 GHz incurring more losses. Though the gain of the antenna increases with increasing operating frequency, but it does not compensate for the losses because in the human body the conductivity of the body tissues increases with an increase in frequency. The size of the antenna decreases with increasing frequency. A flexible implantable antenna with dimensions of  $11 \times 11 \times 2$  mm<sup>3</sup> was presented in [10]. At 2.4 GHz the antenna has a bandwidth of 500 MHz with a gain of -20.8 dBi. The antenna 1g. avg. SAR is 356 W/Kg. Shunt capacitances are used in the design which makes it a complex design. A coplanar waveguide fed implantable antenna was proposed in [11]. The antenna size is  $10 \times 12 \times 0.65$  mm<sup>3</sup> with a resonant frequency of 2.4 GHz. The gain and bandwidth of this antenna are -7.9 dBi and 180 MHz with

a radiation efficiency of -23 dB at 2.45 GHz. SAR value of this antenna is 136 W/Kg for 1g avg. The gain of this antenna is good but it operates at a higher frequency. In [12] an ultrawideband conformal capsule antenna operating at 2.4 GHz with dimensions of  $14 \times 30 \times 10$  mm $^3$  is proposed. The antenna has a very wide bandwidth of 4500 MHz with a gain of -25 dBi. The radiation efficiency of this antenna is -32.2 dB and it has 1g avg. SAR value of 295 W/Kg. This antenna size is quite large. The implantable antenna presented in [13] resonates at 402 MHz. The dimensions of the antenna are  $17.5 \times 69 \times 2.25$  mm $^3$ . The antenna offers a bandwidth of 17 MHz and its gain is -25.3 dBi. SAR value of this antenna is 186 W/Kg for 1g avg. with a radiation efficiency of -28.7 dB. The antenna size is very large and the efficiency of the antenna is low as compared to its large size. The antenna also has a narrow bandwidth.

An ultrawideband liver implanted antenna was presented in [14]. The dimensions of the antenna are  $16.2 \times 7.9 \times 1.25$  mm $^3$  with a resonant frequency of 6 GHz. Bandwidth of this antenna is 6200 MHz. Though the antenna yields a wider bandwidth but it resonates at high frequency and all of the antenna performance parameters are not listed. In [15] the design of a dual band implantable antenna operating at 403 MHz and 2.45 GHz is proposed. The size of the antenna is  $26 \times 8 \times 1.25$  mm $^3$ . At resonant frequencies the bandwidth of this antenna is 450 MHz and 500 MHz with a radiation efficiency of -5.82 dB and -3.95 dB. The efficiency of the antenna is good but channel propagation losses are not considered. The antenna presented in [16] has dimensions of  $1.4 \times 9.05 \times 9.45$  mm $^3$  and it resonates at 406 MHz and 2.38 GHz. The bandwidth of this antenna is 83 MHz and 900 MHz with a 1g avg. SAR value of 490 W/Kg. The gain and efficiency of this antenna are not reported. An implantable antenna operating at 434 MHz for capsule applications was presented in [17]. The gain and bandwidth of this antenna is -22.4 dBi and 17 MHz. Radiation efficiency of this antenna is -24 dB. The proposed antenna is designed using bio-compatible material but the bandwidth of the antenna is quite narrow.

Absence of an adept solution capable of dealing with the two major issues of efficient antenna design and channel characterisation is the motivating force behind this research. Systematic research will be conducted in order to devise an efficient implantable solution achieving the following objectives:

- To understand adequate approaches and methods required to design implantable antennas.

- To design implantable antennas by employing suitable techniques to ensure the design requirements are met.
- To study the human body effects on antenna performance for different implant depths and mounting scenarios.
- To optimize the antenna design for mitigation of human body effects on antenna performance.

#### **1.4 Thesis Contribution**

The main contributions in this thesis are following.

Three Implantable antennas were designed for biomedical applications. Design of a circular patch antenna was presented first. The antenna was simulated in multi-layer tissues and different implant depths. The antenna maintains its performance in implantable conditions. The antenna has a small volume of  $\pi \times 4^2 \times 0.38 \text{ mm}^3$ . Gain of the antenna is -28.8 dBi when simulated in simplified body model. The proposed antenna has a bandwidth of 90 MHz which covers the 915 MHz frequency band. The 1g avg. SAR of the designed antenna is 1218 W/Kg and 10g avg. SAR is 125.2 W/Kg. It can be seen in the comparison Table 4.2 that in this design, a size reduction of around 15% is achieved with an overall performance improvement of 9%.

A rectangular patch antenna was designed for biomedical applications. The antenna has multiband operation. These frequency bands can be used for data transmission, wakeup signal and wireless power transfer applications. The antenna yields a wider bandwidth in implantable conditions. Both free space and implantable simulation results were analysed and showed a good match. The antenna performed well in multilayer tissues and at different implant depths. The antenna has compact size of  $6 \times 5 \times 0.5 \text{ mm}^3$ . The antenna operates at 402 MHz, 915 MHz and 2.4 GHz. Gain and bandwidth of the antenna at resonant frequency are (-47.7, -37.2, -25.5) dBi and (108, 170, 250) MHz. The 1g avg. SAR of the antenna is (122, 184, 863) W/Kg and 10g avg. SAR is (12.25, 18.42, 86.42) W/Kg. The gain of our antenna seems lower but the design objectives have been met as the designed antenna has a smaller size, tri-band frequency operation and wider bandwidth. The comparison Table 4.4 shows that a size reduction of 29% is achieved with performance improvement of around 15%. The work on this antenna is published in [18].

A Compact size antenna was designed which is light weight and has very small overall volume. The antenna operates at the same frequency in multilayer tissues (skin, fat and muscle) which is the novelty of this antenna as it maintains its operating frequency despite the different conducting properties of the body tissues and the fact that its size is very small. A small size antenna often gives narrow bandwidth and higher frequency of operation but this antenna has wider bandwidth of 170 MHz and lower ISM resonant frequency of 915 MHz. This antenna has an overall volume of  $4 \times 4 \times 0.26$  mm<sup>3</sup>. This antenna has a peak gain of -34.7 dBi despite its small size. The designed antenna has SAR values of 1069 W/Kg and 108 W/Kg for 1g and 10g avg. The compact size antenna has a size reduction of around 47% with an overall performance improvement of 12% as compared to the similar antennas in Table 4.7. The work on this antenna is published in [19].

## 1.5 Thesis Organization

This thesis is organised into six chapters. Chapter 1 gives the background theory of implantable medical devices and importance of antennas in these devices. Problem statement is given to elaborate the needs to conduct this research. All the motivational aspects are presented and based on motivations the objectives of this research work are identified. Chapter 2 details the implantable antenna basics and literature review on implantable antennas. The dependency of implantable sensors on antennas is briefly discussed. All the design approaches and techniques required to design implantable antennas are critically analysed and comments are made based on discussion. The advantages and disadvantages of each technique are formulated. Various implantable antenna types are analysed and comparisons made. Human body effects on antenna performance are discussed and different approaches are presented to enhance antenna performance based on the literature review. The patch loss estimation for different communication scenarios is also discussed. In chapter 3 the methodology used to accomplish this research work is presented. Numerical modelling techniques are discussed. An insight was given to the available commercial software programs used for antenna design. An introduction to CST Microwave Studio software is presented as we have used this software to design the antennas. Chapter 4 gives the detailed explanation of the designed antennas. The simulations are carried out in free space and in simplified body model to dictate the antenna performance in implantable scenarios. There are three

antennas designed and simulations are carried out in different tissues of the human body phantom. The human body effects on designed antenna performance were detailed in chapter 5. The designed antenna performance was compared in different human body phantom tissues of the simplified body model. The antennas were subjected to different mounting conditions and implantable depths and results are examined and compared to see how the antennas are performing in simplified human body phantom model and anatomical body model. As the software simulations are subjected to the limited environment, so there is a difference between the simulation results of simplified human body phantom model of different shapes for same human body tissue. So, the designed antennas are simulated in different shape body phantoms. Conclusions are made in chapter 6 based on the research work and possible improvements and future work is suggested.

# Chapter 2

## 2. Implantable Antennas

### 2.1 Introduction

Biomedical telemetry has gained a lot of attention with the development in the healthcare industry. This technology has made it feasible to monitor the physiological signs of patients remotely without traditional hospital appointments and routine check-ups. Implantable Medical Devices (IMDs) play an important role in monitoring patients through wireless telemetry. IMDs consist of sensor nodes in which the antenna is a major component. Various factors need to be considered for designing implantable antennas such as miniaturization, patient safety, biocompatibility, efficiency, lower frequency band of operation and dual-band operation to have a robust and continuous operation. The selection of the antenna is a challenging task in implantable sensor design as it dictates performance of the whole implant. In this chapter a critical review on implantable antennas for biomedical applications is presented. This chapter summarizes the design requirements, techniques and challenges given in the open literature and comments are made on advantages and disadvantages of various techniques. Different examples of implantable antennas are given and comparisons made. A detailed review on antenna performance in the human body and the effects of the lossy nature of human body is presented. Methods are explored to improve antenna performance parameters. Finally, the different communication scenarios for path loss estimation are given. A schematic of implantable antenna design procedure, requirements, challenges, implantable antenna types and human body effects is shown in Figure 2.1 [20].

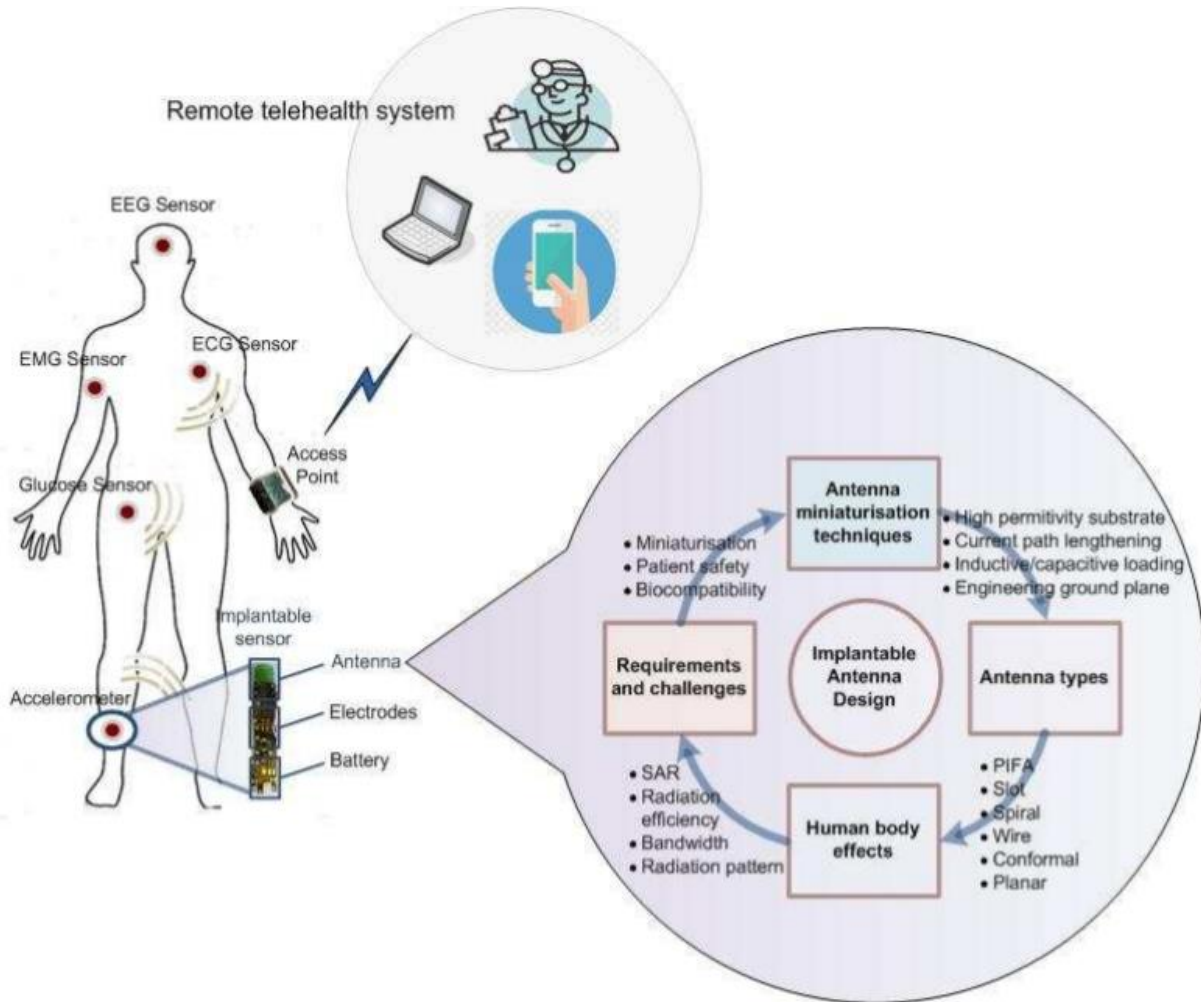


Figure 2.1: Schematic of antenna design process [20]

## 2.2 Implantable Sensors and Antennas

Various implantable sensors are presented in the literature. A wireless implantable sensor based on magnetoelectric (ME) antennas named as NanoNeuro Radio Frequency Identification (RFID) is proposed in [21] for neural recording. An array of ME antennas is used in this sensor because of their smaller size enabling miniaturization of the sensor. The ME antennas can also harvest energy which increases the sensor lifetime.

A dual band antenna is designed based on impulse radio technology for wireless capsule endoscopic image transmission system in [22]. The antenna is fed by a battery powered radio transceiver. The antenna received power is used to estimate the image transmission requirement of the system. In [23], a miniaturized four element Multiple Input Multiple Output (MIMO) antenna with Electromagnetic

Band Gap (EBG) structure for implantable medical devices is proposed. The antenna is tested in pork slab and operates in the ISM band with dimensions of  $18.5 \times 18.5 \times 1.27$  mm<sup>3</sup> and a peak gain of -15 dBi. Utilization of implantable antenna for oral cancer detection is presented in [24] employing a Planar Inverted F Antenna (PIFA). The CST voxel model Katja is used to design the human mouth. Resonant frequency showed a considerable shift when a malignant tissue is detected.

An implantable RFID sensor tag for continuous glucose monitoring is discussed in [25]. This sensor system is powered by an inductive link and consists of multiple units including RFID tag, ferrite antenna, glucose sensor, potentiostat, Analog-to-Digital converter (ADC), temperature sensor and a digital baseband for signal processing. The glucose sensor has a range of 0-30 mm. It is evident that implantable antennas play a pivotal role in these applications as implantable sensors have a large dependency on the antennas.

### **2.3 Implantable Antenna Design: Requirements and Challenges**

The operation of implantable antennas within the human body is completely different from those of conventional antennas operating in free space because of lossy nature of human body tissues. Though, sometimes their design requirements are application dependent, some key design provisions are common and are discussed here in this section.

#### *2.3.1 Miniaturization*

The implantable antenna is a major component of an implantable device so the miniaturization of the implantable antenna is a very crucial factor. The implantable antennas operate in Medical Implantable Communication Service (MICS) band (402 – 405 MHz), Medical Device Radio Communication Service (MedRadio) band (401 MHz – 406 MHz) and Industrial, Scientific and Medical (ISM) band (902 – 928 MHz) and (2.4– 2.45 GHz)[26]-[28]. There are different miniaturization techniques being employed to reduce the antenna size. Some popular methods are as follows:

### *2.3.1.1 Use of High Permittivity Dielectric Substrate*

The size of the implantable antenna can be reduced by using high permittivity dielectric substrate or high permittivity dielectric superstrate. The high permittivity substrate would result in shorter wavelength which would cause the resonant frequency to be lowered [29]. In [30], Rogers 6002 substrate with relative permittivity of  $\epsilon_r=10.2$  is used to reduce the size of the antenna.

A very high permittivity substrate,  $MgTa_{1.5}Nb_{0.5}O_6$  with relative permittivity of  $\epsilon_r=28$  is used for size reduction in [31]. The antenna was placed inside of a tissue fluid for testing by taking into account the electrical properties of the tissue fluid ( $\epsilon_r= 45.2$  and  $\sigma = 0.61 \text{ S/m}$  at 402 MHz). In first case, 14% size reduction is achieved while in later case, the size is reduced by 29%. Use of very high permittivity substrate or superstrate can cause the input power of the antenna to be converted into surface waves that affects the radiation efficiency of the antenna. The dielectric constant of human body tissues also needs to be considered because each layer of the human body tissue has different dielectric constant. The resonant frequency of the implantable antenna will shift to a higher or lower value depending on the type of the tissue layer in which antenna is implanted.

### *2.3.1.2 Planar Inverted F Antennas (PIFAs)*

Planar Inverted F Antenna (PIFA) structures are one of the techniques used to get miniaturization for the implantable antennas. Microstrip patch antennas are also used for this purpose. The resonant length of a patch antenna is half of its wavelength while the resonant length of PIFA is quarter of its wavelength [32]. So, the PIFAs are preferred over the microstrip patch antennas where the size reduction is needed.

### *2.3.1.3 Radiator Current Path Lengthening*

Lengthening the current path of the radiator is another way of getting size reduction in implantable antennas. An increased current path brings the resonant frequency of the implantable antenna to a lower band [29]. Radiator stacking is an effective technique to lengthen the current path of the radiator in which two radiators are stacked one above the other, either vertically or horizontally [33]. A size reduction of 33% can be achieved through this technique.

#### *2.3.1.4 Inductive/Capacitive Loading*

Loading techniques can be used to get the impedance matching at the desired frequency of operation. The loading could be inductive or capacitive which would minimize the imaginary part of the impedance helping in the size reduction. Inductive loading technique has been used in [34]. In [35], the capacitive loading technique is used to achieve the size reduction. Using inductive/capacitive loading can result in 72% reduction in the antenna size.

#### *2.3.1.5 Use of Higher Operating Frequency*

The easiest way to reduce the size of the antenna is to use a higher operating frequency [36]. If the size of the antenna is reduced, the resonant frequency of the antenna will shift to a higher value and vice versa. The problem with the higher frequency operation is that the losses are more which affect the overall performance of the system. Since the implantable antennas operate in three frequency bands which are MICS band, MedRadio band and ISM band [37], [38]. The MICS band is more commonly used to avoid the increased level of losses.

#### *2.3.1.6 Engineering Ground Plane*

Impedance matching plays an important role in the efficient working of the antenna. If the ground plane structure is changed, the impedance matching and hence the size of the antenna changes [39]. One way to achieve that is making slots in the ground plane to alter the path of return current. This slows the current as the displacement of the current from one edge of the slot to the other causes a phase shift resulting in a smaller antenna size [38].

### *2.3.2 Patient Safety*

Implantable medical devices are positioned inside the human body. Careful considerations are therefore, needed to rule out damage to the human body tissues due to electromagnetic exposure. Different precautions are taken to ensure the patient safety as discussed below.

#### *2.3.2.1 Specific Absorption Rate (SAR)*

Specific Absorption Rate (SAR) is the amount of RF energy absorbed by the human body tissues. It is used as a metric to ensure the safety of biological tissues in the event of electromagnetic exposure. There

are two standards for SAR which are internationally adopted. According to IEEE C95.1-1999 standard, the SAR should be less than 1.6 W/kg averaged over 1 g cubic volume of the tissue [6]. The IEEE C95.1-2005 standard specifies that the SAR should be less than 2 W/kg averaged over 10 g cubic volume of the tissue [40].

The Federal Communications Commission (FCC) uses 1 g averaging while the International Commission on Non-Ionizing Radiation Protection (ICNIRP) recommends 10 g averaging [41], [42]. 2W/kg over 10 g cubic tissue would be equal to 4-6 W/kg averaged over 1 g cubic tissue. To maintain standard SAR levels, the implantable devices are required to use low output power. Usually the Specific Absorption (SA) per pulse is determined by [43]:

$$SA = SAR \times T_p \quad (2.1)$$

Where  $T_p$  denotes the pulse duration. The electromagnetic power absorbed by the body tissue can raise temperature of the tissue. The temperature of the human body tissue near the implanted device should not increase more than 1-2  $^{\circ}\text{C}$  [43].

### 2.3.2.2 *Effective Isotropic Radiated Power (EIRP)*

A high level of EIRP of the implantable antenna can be harmful to the human body and will interfere with nearby radio devices. The standardized limit of EIRP for an implantable antenna operating in MedRadio band is -16 dBm and -20 dBm for ISM band [44]. If the implantable antenna is used for data telemetry, the input power should be limited to avoid damage to the tissues. If the implantable antenna acts as a receiver, the external source power should adhere to these standards.

### 2.3.3 *Biocompatibility*

Biocompatibility is also an important factor for implantable antennas to ensure the safety of the human subject. Direct contact between the antenna and human body tissues would cause a short circuit because the body tissues are electrically conductive. Two approaches are commonly used to ensure biocompatibility. One, is to use a biocompatible material for antenna fabrication and the other, is to encapsulate the antenna with a biocompatible superstrate [45].

Some of the biocompatible materials used for the implantable antenna design are Ceramic Alumina ( $\epsilon_r = 9.4$ ;  $\tan\delta = 0.006$ ), Teflon ( $\epsilon_r = 2.1$ ;  $\tan\delta = 0.001$ ) and MACOR ( $\epsilon_r = 6.1$ ;  $\tan\delta = 0.005$ ). However, it is difficult to drill and make round cuts in ceramic substrates [46], [47]. The materials used for biocompatible encapsulation are Zirconia ( $\epsilon_r = 29$ ;  $\tan\delta \approx 0$ ), Silastic MDX-4210 Biomedical-Grade Base Elastomer ( $\epsilon_r = 3.3$ ;  $\tan\delta \approx 0$ ) and PEEK ( $\epsilon_r = 3.2$ ;  $\tan\delta = 0.01$ ) [48], [49]. Zirconia is a better candidate for bio-encapsulation due to its electromagnetic properties. Its loss tangent is very low and permittivity value is very high which helps to reduce power loss by concentrating the near field of antenna inside the encapsulation. The advantage of PEEK and Silastic MDX-4210 is that they have simple fabrication and are easy to handle.

#### 2.3.4 *Implantable Antenna Fabrication Methods and Materials*

The fabrication of implantable antennas needs the utmost level of care due to their intended usage. There are a number of different fabrication methods being proposed in literature including antennas embroidered on fabric, polymer composites encapsulation, microfluidic antennas, photolithography and 3D printed antennas [50]-[52]. In [53], conductive fabric was embedded with Poly Dimethyl Siloxane (PDMS). Fabricating the antenna using the conductive fabric along with PDMS (acting as the substrate and a protective encapsulation simultaneously) allows for an easier realization and more robust flexible antenna structure than the conventional fabrication methods.

An ultra-wideband antenna is fabricated using the same technique to achieve the flexibility and robustness in [54]. Implantable antennas are also designed using metamaterials where normal materials cannot give the desired performance. The use of these materials for implantable antenna design is based on the application for which the antenna is to be used. Their applications include wireless charging to pacemakers, microwave hyperthermia and medical imaging [55], [56].

A metamaterial inspired implantable wideband antenna is proposed in [57]. The antenna is operating at 2.3 GHz with overall dimensions of  $0.42\lambda \times 0.42\lambda \times 0.0072\lambda$  where  $\lambda$  is the guided wavelength and its value is 38.1 mm. The antenna approximate physical dimensions are  $16 \times 16 \times 0.275$  mm<sup>3</sup>. Characteristics modal analysis is performed to estimate the maximum miniaturization and the bandwidth enhancement.

The antenna uses complimentary split ring resonators to achieve the desired miniaturization. The biocompatibility of the antenna is maintained by using silicon and gold as substrate layer and the radiating element. The antenna has a fractional bandwidth of 93.5%. Simplified body model is used to validate the antenna performance. A metamaterial loaded dual band circularly polarized implantable antenna was proposed in [58]. The antenna dimensions are  $7 \times 6 \times 0.254$  mm<sup>3</sup> with operating frequencies of 915 MHz and 2.4 GHz. Gain of the antenna is recorded as -17.1 dBi and -9.81 dBi at 915 MHz and 2.4 GHz while offering an impedance bandwidth of 35.8% and 17.8% at relevant frequencies. Wider bandwidth and circular polarization of this implantable antenna are achieved by introducing a metamaterial structure with very large value of epsilon on the top of superstrate layer. The proposed antenna was integrated with dummy electronic components to evaluate the antenna performance in minced pork.

Khan *et al.* [59] proposed a triband compact metamaterial embedded implantable antenna for biotelemetry applications. The antenna operates in Medical Implant Communications Services band of 402-405 MHz and Industrial Scientific and Medical bands of 902-928 MHz and 2.4-2.45 GHz. The volume of the antenna is  $15.8 \times 13.2 \times 2$  mm<sup>3</sup>. The split ring resonator (SRR) metamaterial radiator is integrated in open ended stubs in the top layer whereas the slots are also etched in the bottom layer to adjust the lower frequency of operation. The antenna was designed and optimized using CST Microwave Studio software.

A dual band implantable antenna with short circuited SRR was proposed in [60]. The antenna operates in MICS band of 402-405 MHz and in ISM band of 2.4-2.45 GHz. The ground plane and radiating element of the antenna are short circuited to achieve miniaturization. The radiating element is a split ring resonator connected with a spiral. Antenna dimensions are 14mm×14mm. CST Microwave Studio was used to design the antenna. Performance of the antenna was analysed using anatomical human body model. Despite some good features of the proposed antenna, it offers only a narrow bandwidth. A comparative analysis of different miniaturization techniques is given in Table 2.1.

Table 2.1: Comparative analysis of different miniaturization techniques for implantable antennas

Technique	Pros.	Cons.
1) <i>PIFA Structures</i>	Compact size implantable antenna can be designed using this structure at lower frequencies. PIFA has low backward radiation.	Results in low gain as currents at adjacent arms cancels each other far field radiation [32].
2) <i>High Frequency Use</i>	The easiest technique to reduce the size of the antenna.	The antenna would incur more losses due to power absorption at higher frequencies [36].
3) <i>Inductive Loading / Capacitive Loading</i>	Helps in impedance mismatch, minimize frequency shift while keeping size small.	This technique may lead to low antenna gain [35].
4) <i>Current Path Lengthening</i>	Slows the current flow which makes the physically small antenna, an electrically large antenna.	The current on the edges may cancel each other effect due to phase shift which effects the antenna performance [33].
5) <i>Engineering Ground Plane</i>	Helps in size reduction by creating slots in ground plane.	Radiated signal from the edges of ground slot may lead to electromagnetic compatibility problem if not controlled [39].
6) <i>High Permittivity Dielectric Substrate</i>	Helps to minimize dielectric losses.	Can cause the input power of the antenna to be converted into surface waves resulting in lower efficiency [29].

## 2.4 Types of Implantable Antennas

There are different types of implantable antennas depending on the application. Key types are discussed in this section.

### 2.4.1 Planar Antennas

A probe-fed wideband implantable antenna with dimensions of  $12 \times 7.5 \times 0.25$  mm<sup>3</sup> using Rogers 6010 LM (with  $\epsilon_r=10.2$ ) substrate is proposed in [61]. The antenna operates in five frequency bands of 403-405 MHz, 433.1-434.8 MHz, 868-868.6 MHz, 902.8-928.0 MHz and 2.4-2.48 GHz as shown in Figure 2.2 [61]. It exhibits a radiation efficiency of 80% with a bandwidth of 168.85% whereas the gain and SAR of the antenna are not reported. A flexible antenna using Poly-dimethyl Siloxane (PMDS) with  $\epsilon_r$

$\epsilon_r = 2.8$  as base material is proposed by Fu et al. [10]. The overall dimensions of the antenna are  $11 \times 11 \times 2$  mm<sup>3</sup>. The antenna centre frequency is 2.42 GHz with realized gain of -20.8 dBi. It has a bandwidth of 10.4% while the efficiency is not reported. The antenna measurements were taken using single layer tissue model having dimensions of  $150 \times 150 \times 90$  mm<sup>3</sup> with  $\epsilon_r = 37.88$  and  $\sigma = 1.44$  S/m at 2.42 GHz. SAR value of this antenna is 156 W/Kg for 1g avg. The proposed antenna has a good gain but the use of shunt capacitances to minimize impedance mismatch makes it a complex antenna design.

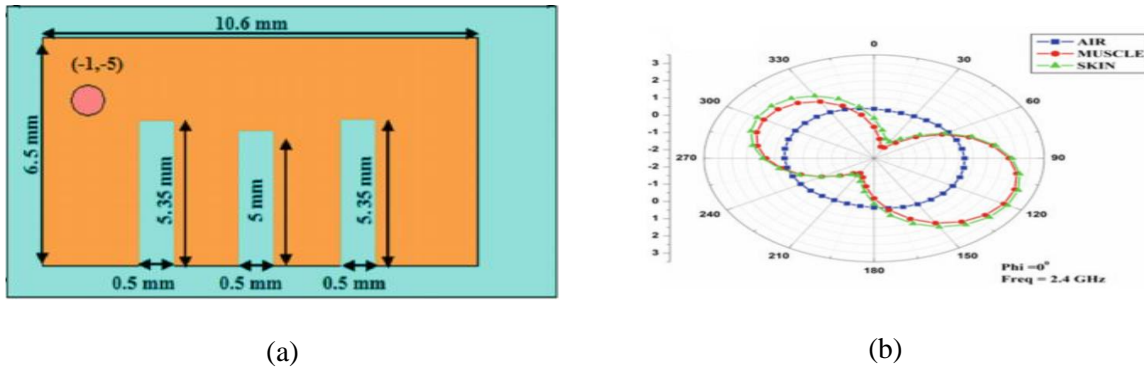


Figure 2.2: (a) Geometry of probe fed wideband antenna (b) Radiation pattern of the antenna [61]

Shah *et al.* have proposed a meandered line implantable antenna for intracranial pressure monitoring at 915 MHz and 2.45 GHz [62]. The antenna has a volume of  $8 \times 6 \times 0.5$  mm<sup>3</sup> and uses Rogers 6010 as the substrate. For biocompatibility, it is encapsulated in ceramic alumina. Human skin tissue model with dimensions of  $200 \times 200 \times 200$  mm<sup>3</sup> is used to test the performance. The antenna has a gain and bandwidth of -28.5 dBi and 9.84% at 915MHz and -22.8 dBi and 8.57% at 2.45 GHz while efficiency is not reported. The 1g avg. SAR values of this antenna at resonant frequencies are 971.56 W/Kg and 807.34 W/Kg whereas the 10g avg. SAR values at resonant frequencies are 118.26 W/Kg and 102.04 W/Kg. SAR of this antenna needs to be lowered to be used for actual implants. A meander line antenna for pacemaker application operating at 402.5 MHz with a bandwidth of 33.5% is proposed by Samsuri *et al.* in [63]. The antenna is designed on FR-4 substrate with  $\epsilon_r = 4.7$  and  $\tan \delta = 0.025$  having a size of  $30.5 \times 21.02 \times 6.4$  mm<sup>3</sup>. The antenna structure and surface current density is shown in Figure 2.3 [63]. The gain, efficiency and SAR of this antenna are not given. Moreover, the volume of the antenna is quite large. Maity *et al.* have proposed a microstrip patch antenna with fractal geometry in [9]. The antenna has a volume of  $11.44 \times 11.44 \times 0.275$  mm<sup>3</sup> and Silicon with  $\epsilon_r = 11.7$  is used as the substrate.

Gain and efficiency of the antenna are not reported while the bandwidth is 1.5%. Despite the considerable size, the antenna offers a narrow bandwidth. The geometry and radiation pattern of the antenna are shown in Figure 2.4 [9].

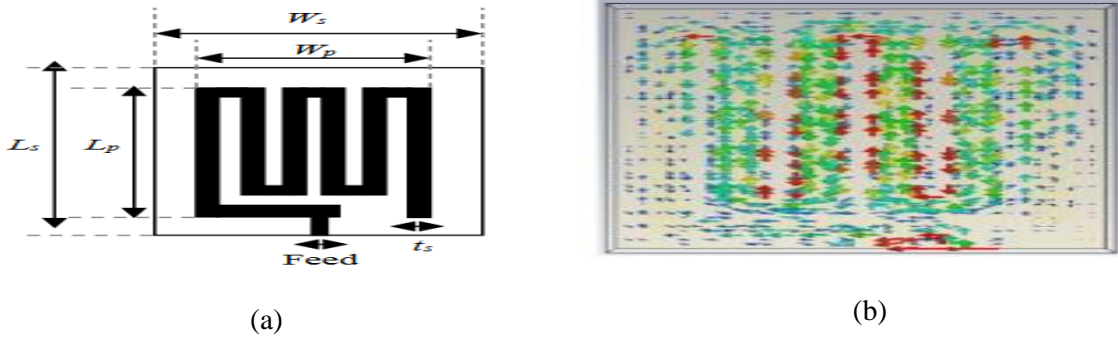


Figure 2.3: (a) Structure of implantable meander line antenna (b) Surface current density of the antenna at 402.5 MHz [63]

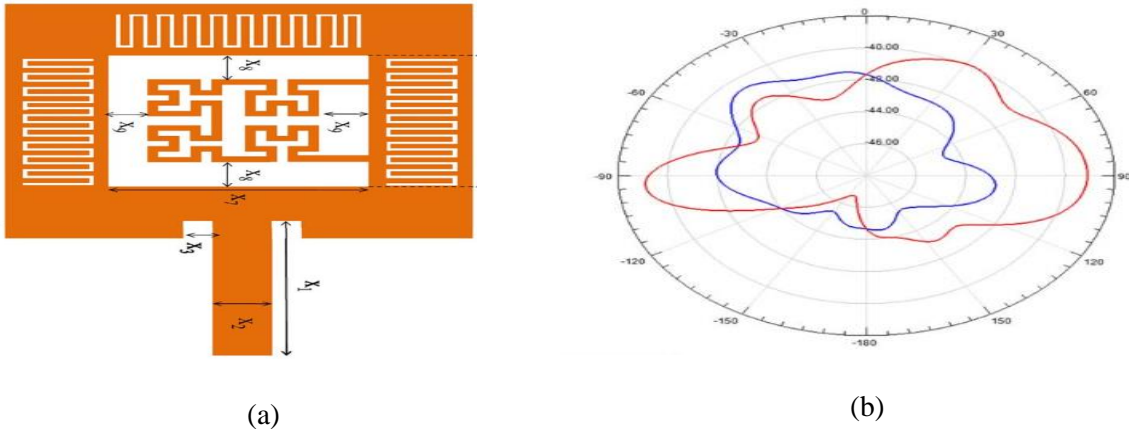


Figure 2.4: (a) Geometry of implantable fractal patch antenna (b) Radiation pattern of antenna at 2.45 GHz [9]

#### 2.4.2 Wire Antennas

A circularly polarized (CP) helical implantable antenna for ingestible capsule application is proposed in [64]. The antenna operates at 2.4 GHz with a gain of -19.83 dBi and bandwidth of 290 MHz. The 3D capsule model and reflection coefficient of the antenna are given in Figure 2.5 [64]. The radiation efficiency of the antenna is -24.8 dB. SAR of this antenna is not given which shows that the patient safety considerations are not taken into account.

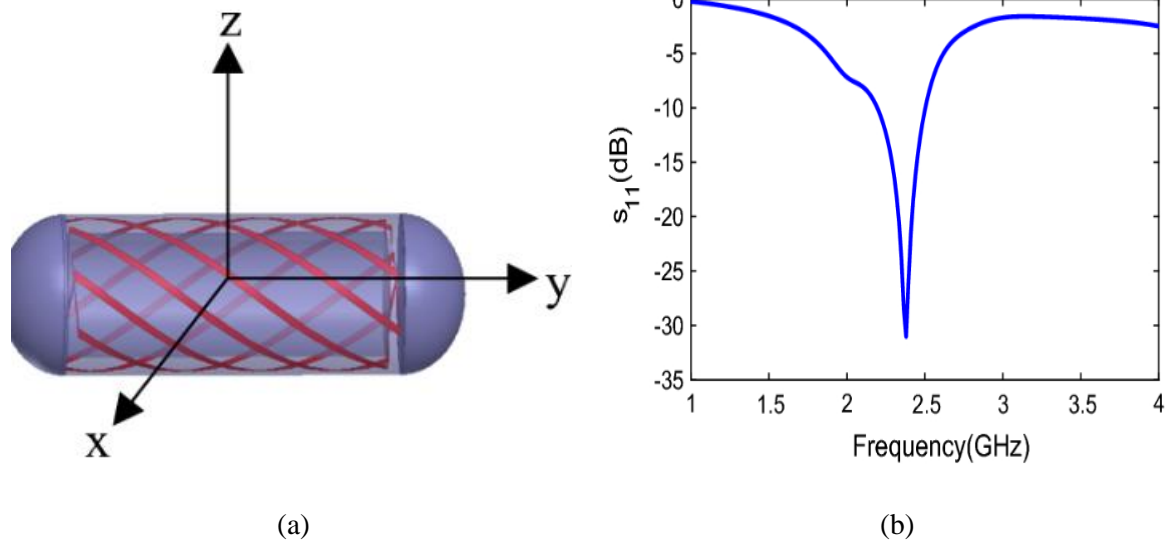


Figure 2.5: (a) Structure of helical antenna for ingestible capsule (b) Reflection coefficient of the antenna [64]

Xin *et al.* have designed a 30 mm long helical antenna in [65]. To achieve the dual resonance, two non-equally spaced helical copper foil layers are used. The antenna is tested in a  $280 \times 160 \times 280$  mm<sup>3</sup> phantom model with  $\epsilon_r=56.05$  and  $\sigma=0.52$  S/m at 30 MHz. The gain of the antenna is -67 dBi while the impedance bandwidth is 15.66 MHz (48.21%). The SAR and efficiency of the antenna are not reported. The gain of the antenna is very low. Geometry and scattering parameters of the antenna are shown in Figure 2.6 and Figure 2.7 [65].

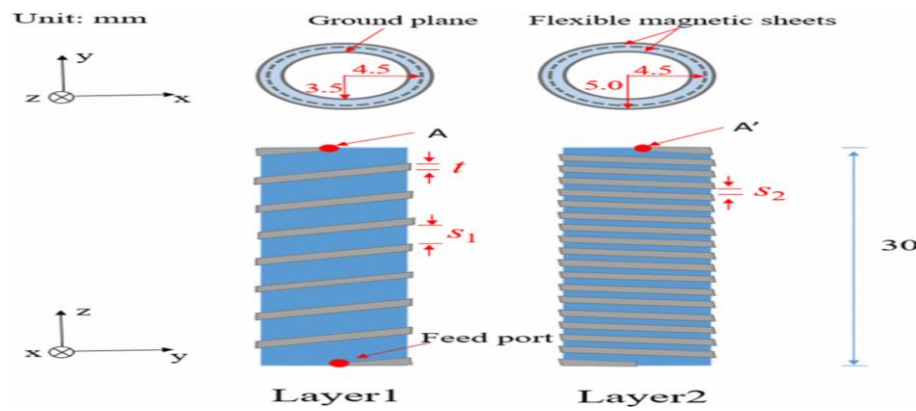


Figure 2.6: Structure of implantable helical antenna using two magnetic sheets [65]

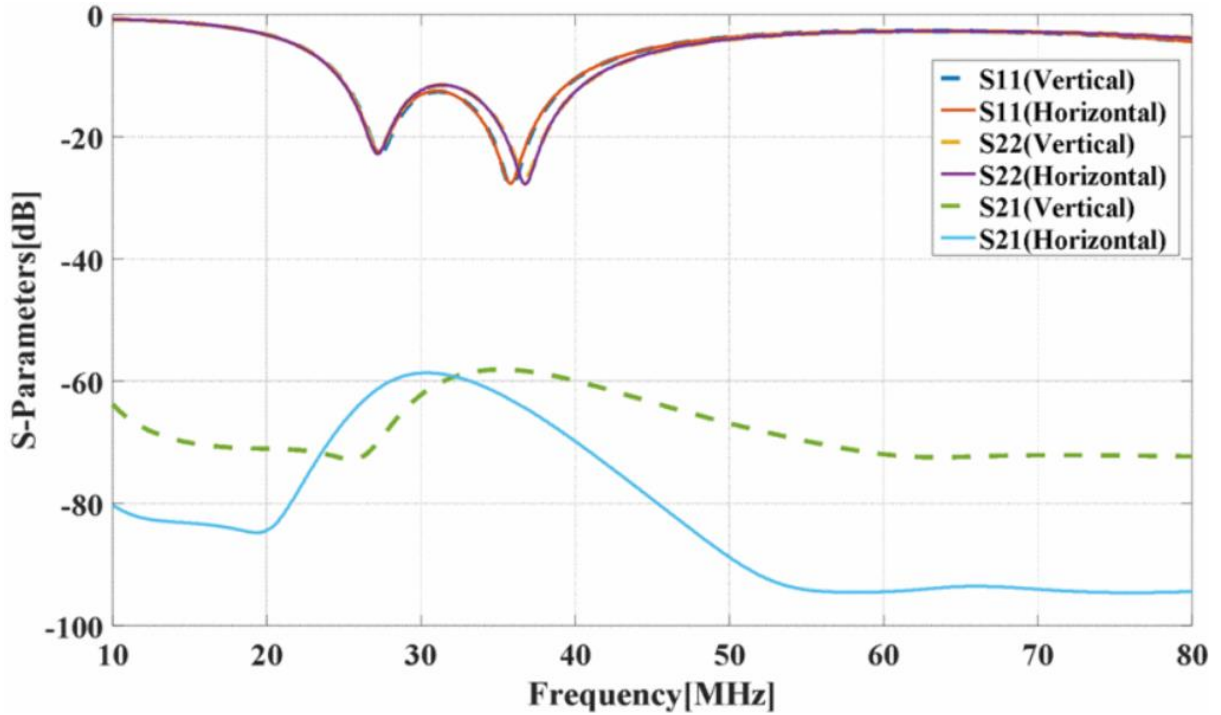


Figure 2.7: Scattering parameters of the helical antenna [65]

A  $50 \Omega$  coaxial probe fed conical spiral antenna operating at 450 MHz with a bandwidth of 101 MHz is presented in [66]. A liquid phantom with  $\epsilon_r=56$  and  $\sigma=0.83 \text{ S/m}$  is used for the measurements. The antenna design and reflection coefficient are shown in Figure 2.8 [66]. The gain, efficiency and SAR of the antenna are not listed. So, the performance of this antenna cannot be quantified.

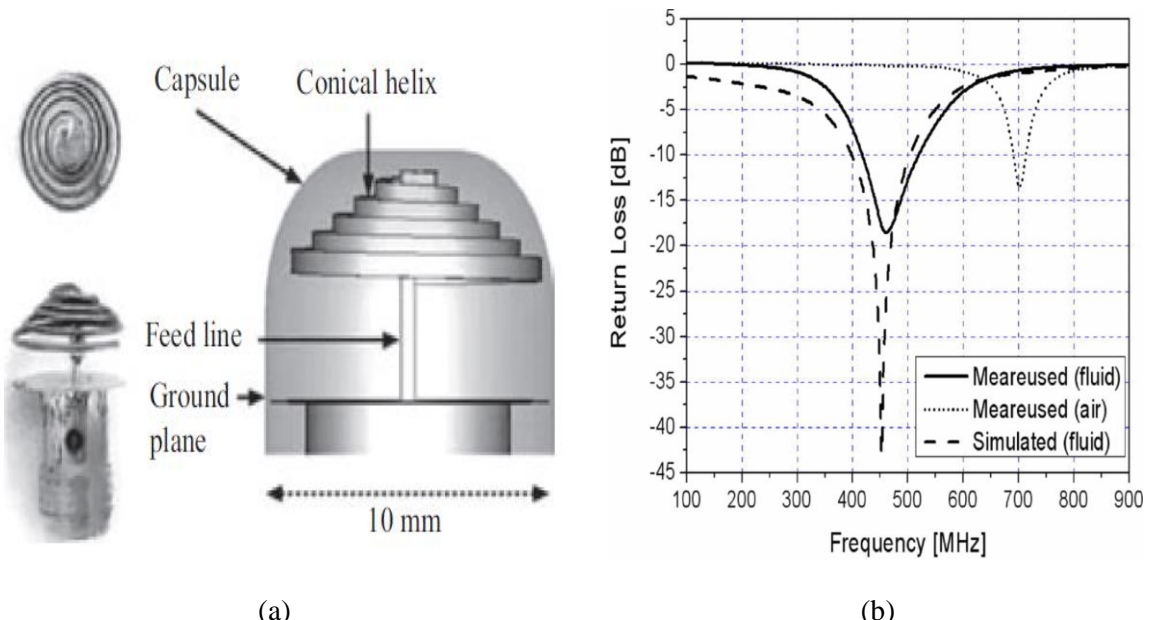


Figure 2.8: (a) Conical spiral implantable antenna geometry (b) Reflection coefficient of the antenna [66]

### 2.4.3 Conformal Antennas

A conformal CP implantable antenna operating at 2.45 GHz and using Rogers RO6010 as substrate with  $\epsilon_r=10.2$  and  $\tan \delta=0.0023$  is discussed in [67]. The size of the antenna is  $14.2\times16.64\times0.254$  mm<sup>3</sup>. The antenna offers a gain and bandwidth of -29.1 dBi and 31%. The efficiency of antenna is not reported. The antenna is tested using muscle phantom having dimensions of  $100\times100\times100$  mm<sup>3</sup> with  $\epsilon_r=52.74$  and  $\sigma=1.74$  S/m. The 1g avg. SAR of this antenna is 368.7 W/Kg. As this antenna has a large size, the gain of the antenna could have been improved. The geometry and reflection coefficient of the antenna are illustrated in Figure 2.9 [67].

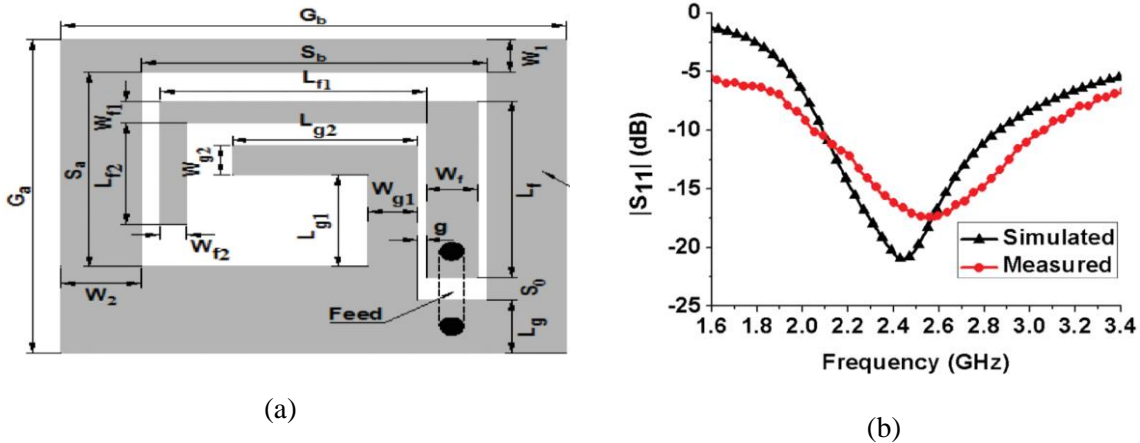


Figure 2.9: (a) Geometry of implantable CP conformal antenna (b) Reflection coefficient of the antenna [67]

In [68], a conformal patch antenna operating at 2.48 GHz is presented by Ketavath *et al.* The high permittivity substrate employed has  $\epsilon_r=10.2$  with  $\tan\delta=0.008$  making the overall dimensions of the antenna as  $24\times22\times0.07$  mm<sup>3</sup>. The antenna gain and bandwidth are -19.7 dBi and 24%. Gain of the antenna is good but the size of the antenna is large. The geometry and S11 of the proposed antenna are illustrated in Figure 2.10 [68].

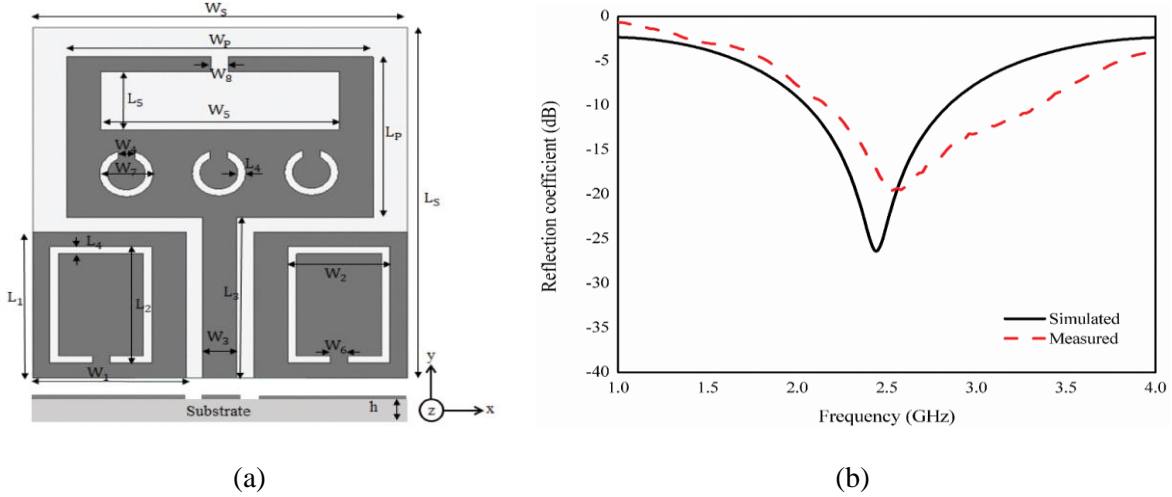


Figure 2.10: (a) Geometry of implantable conformal patch antenna (b) S11 curve of the antenna [68]  
 Zhang *et al.* have proposed a differentially fed antenna for ingestible capsule system in [69]. Polyimide with  $\epsilon_r=3.5$  and  $\tan \delta=0.008$  is used as substrate with thickness of 0.15 mm. The overall volume of the antenna is  $30 \text{ mm}^3$ . The antenna operates at 915 MHz with a gain of -21 dBi and bandwidth of 8.9%. Efficiency of the antenna is not reported. SAR of this antenna is 150 W/Kg for 1g avg. and 27.5 W/Kg for 10g avg. The antenna has a good gain but the size of the antenna is large. The reflection coefficient and radiation pattern of the antenna are depicted in Figure 2.11 [69].

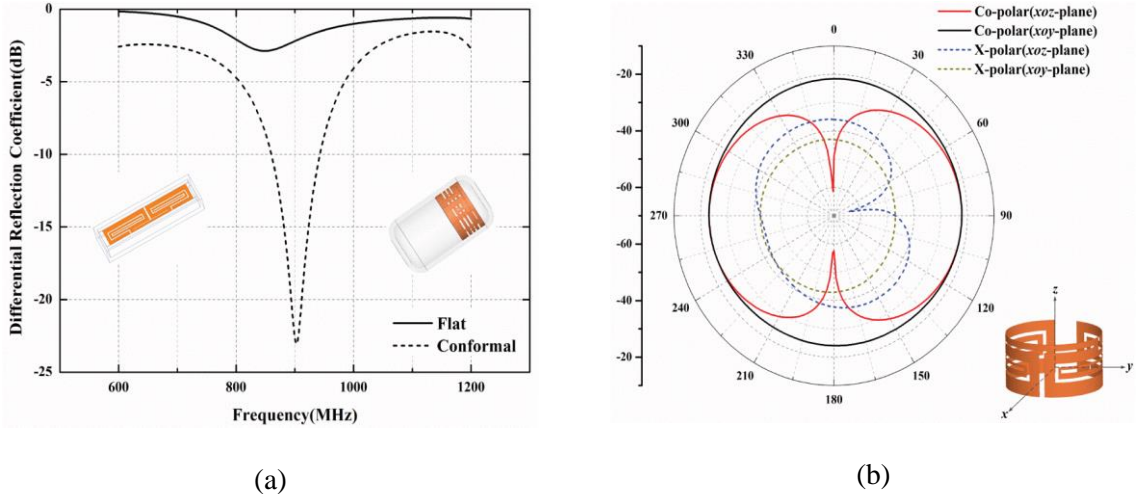


Figure 2.11: (a) Reflection coefficient of differentially fed implantable antenna in flat and conformal form (b) Radiation patterns of the antenna at 915 MHz [69]

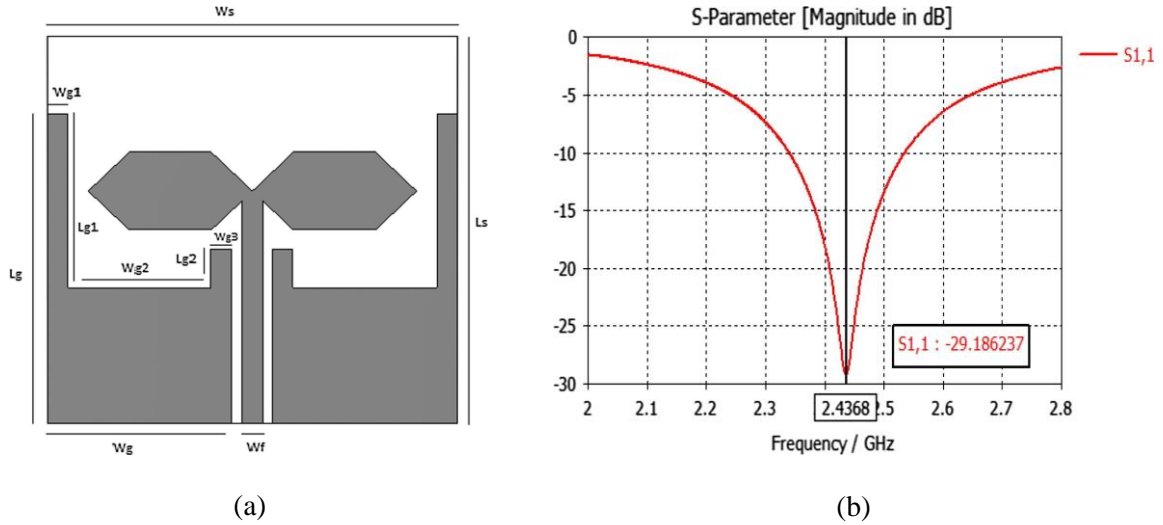


Figure 2.12: (a) Structure of implantable bow-tie antenna (b) S11 curve of the antenna [70]

A hexagon bow-tie patch antenna using  $\text{Al}_2\text{O}_3$  with  $\epsilon_r=9.8$  as substrate operating at 2.45 GHz is proposed by Mahalakshmi *et al.* in [70] as shown in Figure 2.12. The antenna has dimensions of  $10\times10\times1 \text{ mm}^3$  and offers a gain of -14.5 dBi. The antenna bandwidth, radiation efficiency and SAR values are not mentioned.

#### 2.4.4 Spiral Antennas

A CP ring antenna is proposed by Xu *et al.* [71]. The antenna operates at 2.45 GHz with a size of  $\pi\times5^2\times1.27 \text{ mm}^3$ . It uses Rogers 3010 with  $\epsilon_r=10.23$ ,  $\tan \delta = 0.0035$  having thickness of 0.635 mm as substrate and is shown in Figure 2.13. The antenna is tested using muscle tissues with  $\epsilon_r=52.7$  and  $\sigma=1.74 \text{ S/m}$ . It offers a gain of -22.7 dBi and bandwidth of 12.4%. The 1g avg. SAR value of the antenna is 508 W/Kg at 2.45 GHz. The efficiency of the antenna is not reported. The gain should be higher than -22.7 dBi with that size of the antenna.

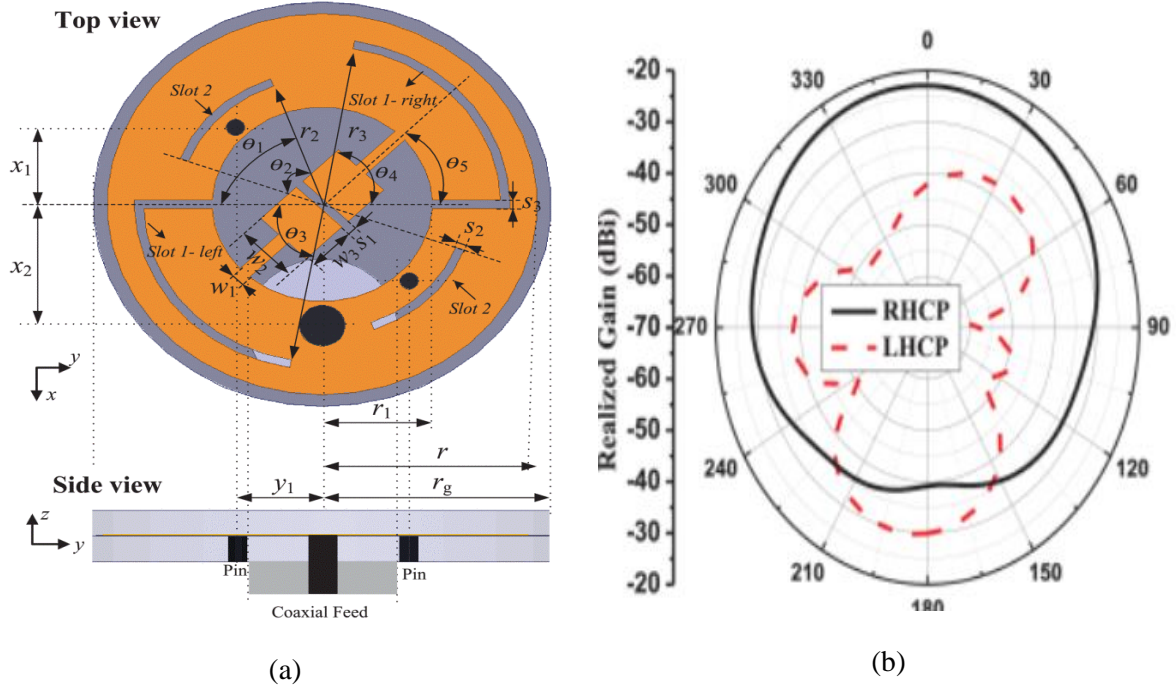
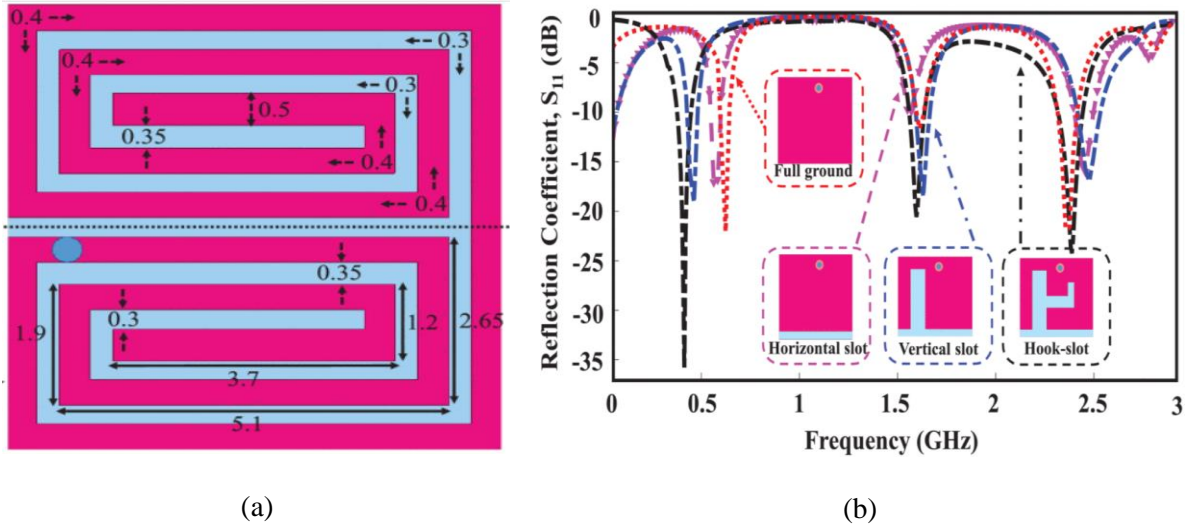


Figure 2.13: (a) Top and side view of implantable CP ring antenna (b) Radiation pattern of the antenna at 2.45 GHz [71]

A tri-band spiral shaped implantable antenna with slotted ground operating at 402 MHz, 1.6 GHz and 2.45 GHz is discussed by Shah *et al.* [72] as shown in Figure 2.14. The size of the antenna is  $7 \times 6.5 \times 0.377$  mm $^3$  while Rogers RT/Duroid 6010 with  $\epsilon_r=10.2$  and  $\tan \delta=0.0035$  is used as superstrate and substrate. The gain of the antenna at the three frequencies is noted to be -30.5 dBi, -22.6 dBi, -18.2 dBi, respectively while it has a bandwidth of 36.8%, 10.8% and 3.4% respectively. At resonant frequencies the 1g avg. SAR values are 588 W/Kg, 441 W/Kg and 305 W/Kg while the 10g avg. SAR values of this antenna are 92.7 W/Kg, 85.3 W/Kg and 81.7 W/Kg. Efficiency of the antenna is not reported. The proposed antenna has a compact size but it has higher SAR values.



(a)

(b)

Figure 2.14: (a) Structure of spiral shape implantable antenna (b) Reflection coefficient of the antenna with different ground planes [72]

Smanta *et al.* have proposed a dual band CP antenna having a size of  $10 \times 10 \times 0.6$  mm<sup>3</sup> in [73]. The antenna is operating at 902 MHz and 2.45 GHz and makes use of Rogers 3010 as reactive impedance substrate with  $\epsilon_r=10.2$  and  $\tan \delta=0.0035$ . The antenna gain, bandwidth and efficiency at 920 MHz are -29.33 dBi, 12.2% and 2.6% while these parameters at 2.45 GHz are -21.0 dBi, 123% and 3.8%. The geometry and radiation pattern of the antenna are given in Figure 2.15. Skin mimicking gel is used to test the antenna. The 1g avg. SAR values at resonant frequencies are 812 W/Kg and 680 W/Kg. This antenna offers a good efficiency but it has a large size.

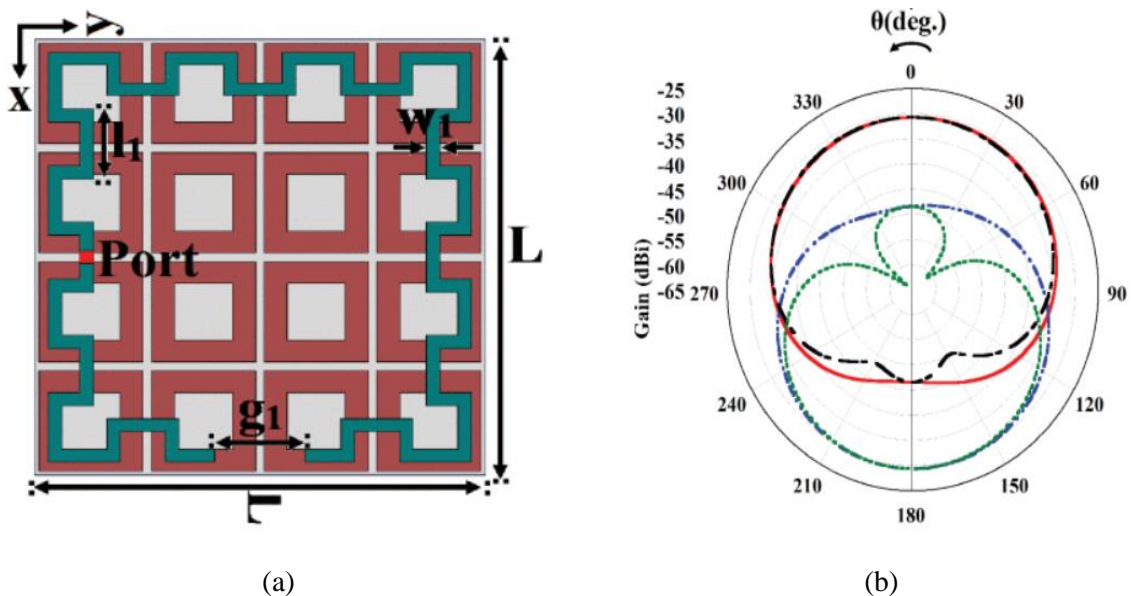


Figure 2.15: (a) Geometry of implantable dual band CP antenna (b) Radiation pattern of the antenna [73]

A CP loop antenna is proposed by Xu et al. in [8]. The substrate and superstrate material for this antenna is 0.635 mm Roger 3010 with  $\epsilon_r=10.2$  and  $\tan \delta =0.0035$ . The size of the antenna is  $13\times13\times1.27$  mm<sup>3</sup> with centre frequency of 915 MHz. The antenna has a gain of -32 dBi and bandwidth of 18.2%. It is tested in skin tissue model, minced pork and skin mimicking gel. The 1g avg. SAR of the antenna at 915 MHz is 599W/Kg. Despite the large size, the antenna has a low gain. The structure and reflection coefficient of loop antenna are shown in Figure 2.16 [8].

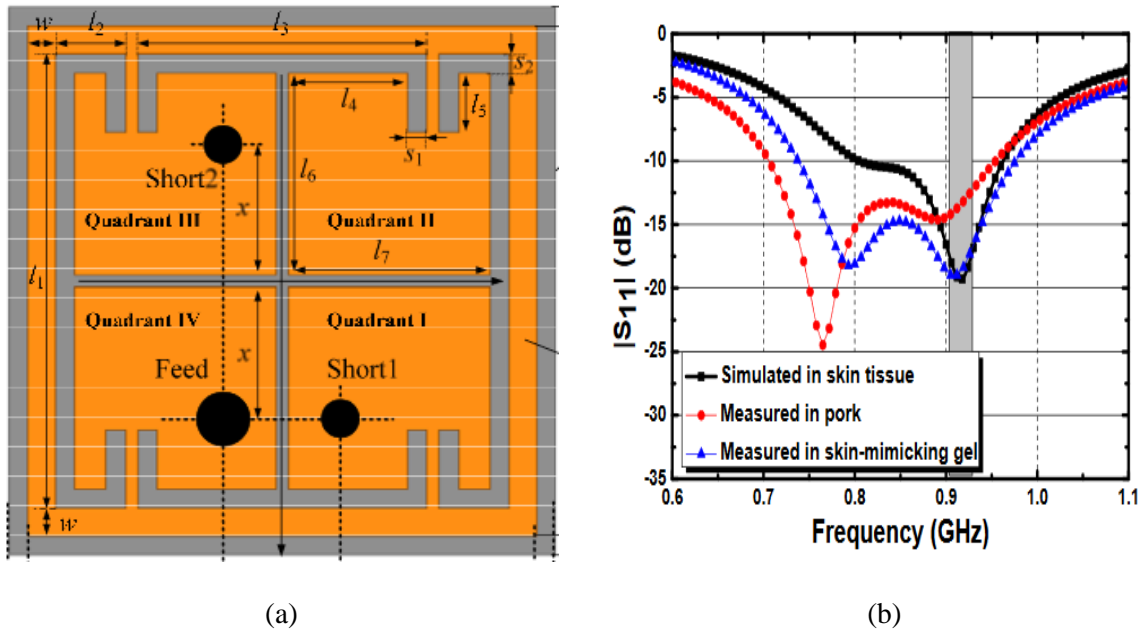


Figure 2.16: (a) Structure of loop antenna (b) Reflection coefficient [8]

#### 2.4.5 Slot Antennas

A coplanar waveguide fed triangular slot antenna is proposed in [11]. The antenna has a size of  $10\times10\times0.65$  mm<sup>3</sup> with a resonant frequency of 2.45 GHz as shown in Figure 2.17. Al<sub>2</sub>O<sub>3</sub> is used as substrate and the antenna is tested in liquid phantom showing a peak gain of -7.9 dBi and a bandwidth of 8.2%. The radiation efficiency of antenna is 0.5%. The 1g avg. SAR of this antenna is 136 W/Kg. The proposed antenna has a very good gain but the size of the antenna is large.

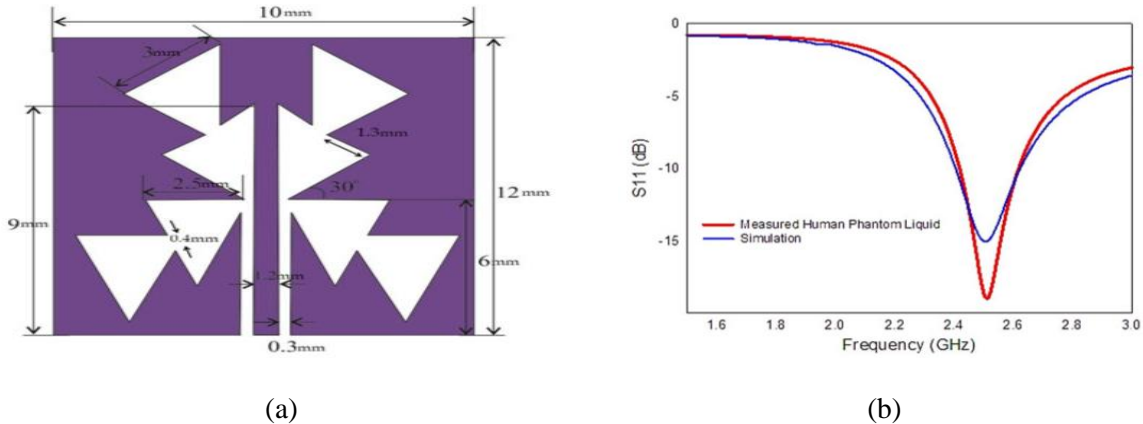


Figure 2.17: (a) Geometry of implantable triangular slot antenna (b) Reflection coefficient [11]

A wideband flexible antenna is presented in [74] by Das *et al.* The antenna is designed on Kapton polyimide substrate having  $\epsilon_r=2.91$  and  $\tan \delta=0.005$ . Rogers 6010 with  $\epsilon_r=10.2$  and  $\tan \delta=0.0023$  is used as superstrate. A metamaterial array is used at the top of the superstrate to enhance the gain. The antenna has dimensions of  $10\times10\times0.4$  mm<sup>3</sup> operating at 2.45 GHz as illustrated in Figure 2.18. It offers a bandwidth of 57%, a gain of -9 dBi and efficiency of 2.3%. The 1g avg. SAR of this antenna is 131 W/Kg at 2.45 GHz. The antenna offers a wider bandwidth but it operates at higher frequency despite its large size. A CP implantable slot antenna operating at 915 MHz is discussed in[75]. The antenna size is  $15\times15\times1.27$  mm<sup>3</sup> and it uses Rogers 3010 ( $\epsilon_r=10.2$  and  $\tan \delta=0.0035$ ) as substrate. Gain of the antenna is -27 dBi and it exhibits a bandwidth of 5.7%. The antenna is tested using skin phantom ( $\epsilon_r =41.35$  and  $\sigma=0.87$  S/m). The 1g avg. SAR value of this antenna is 517 W/Kg. The size of the antenna is quite large.

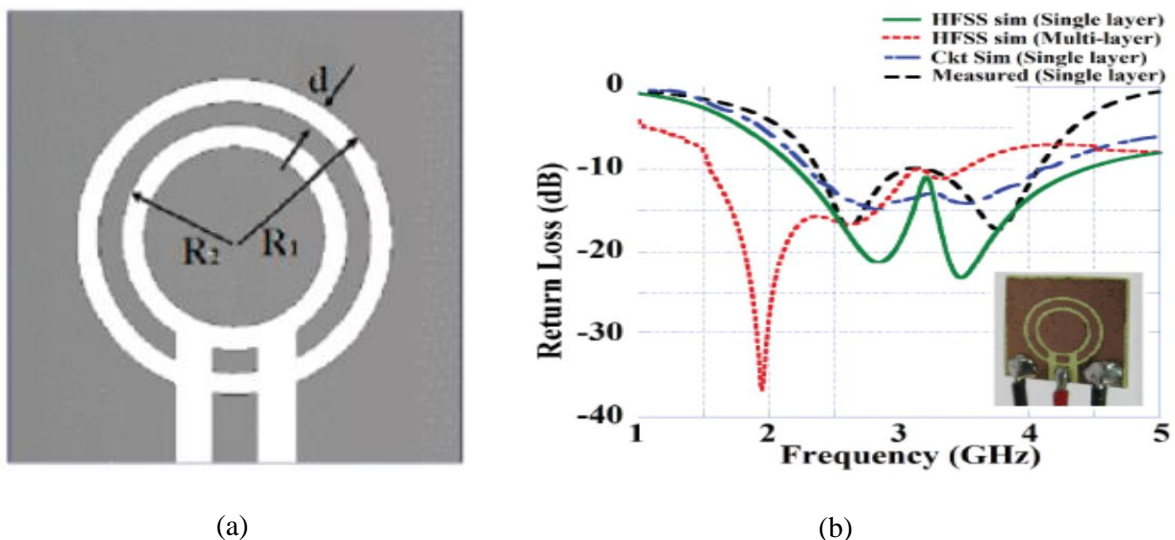


Figure 2.18: (a) Geometry of implantable flexible metamaterial antenna (b) Reflection coefficient of the antenna [74]

#### 2.4.6 Planar Inverted F antennas (PIFA)

A compact broadband implantable PIFA having a size of  $23 \times 16.4 \times 1.27$  mm<sup>3</sup> and operating at 402 MHz is proposed in [76]. The substrate has  $\epsilon_r=10.2$  and  $\tan\delta=0.0023$ . A gain of -34.9 dBi and bandwidth of 52 MHz (13%) is being achieved by the antenna shown in Figure 2.19. The 1g avg. SAR of this antenna is 284.5 W/Kg at resonant frequency. The gain of the antenna is low as compared to its large size.

Luo *et al.* have designed a PIFA with slotted ground plane in [77]. The antenna makes use of 0.635 mm thick layer of Rogers 3010 ( $\epsilon_r=10.2$  and  $\tan\delta=0.005$ ) as substrate and superstrate with an overall size of  $\pi \times 5.35^2 \times 1.34$  mm<sup>3</sup>. The antenna resonates at 402 MHz and 2.45 GHz. The antenna structure and radiation pattern are shown in Figure 2.20 [77]. The gain and bandwidth of the antenna at 402 MHz are -41 dBi and 41% while these parameters are -21.3 dBi and 27.8% at 2.45 GHz. Minced pork is used for the measurements. The 1g avg. SAR of the antenna is 666 W/Kg and 676 W/Kg at operating frequencies. The efficiency of the antenna is not reported.

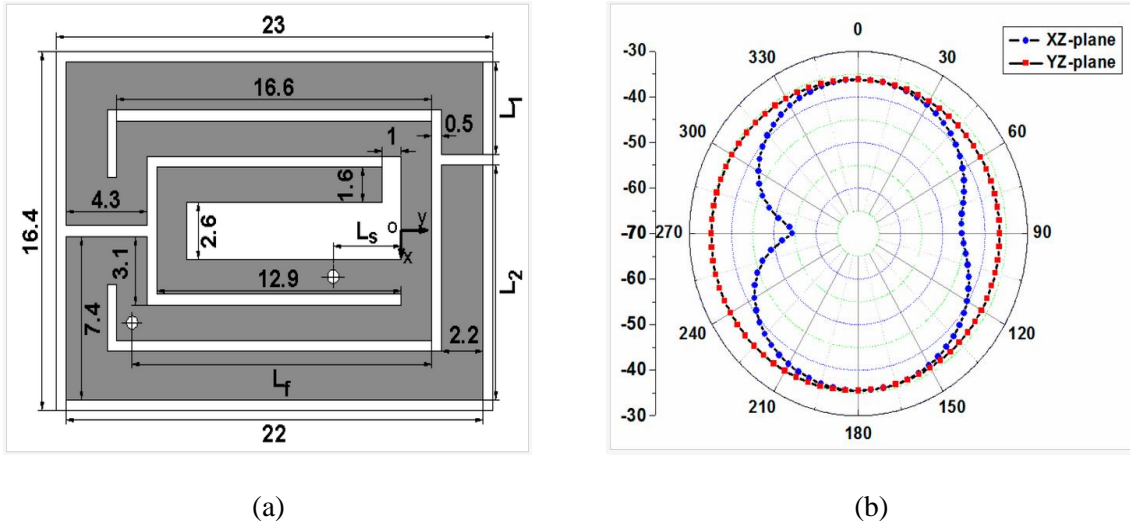
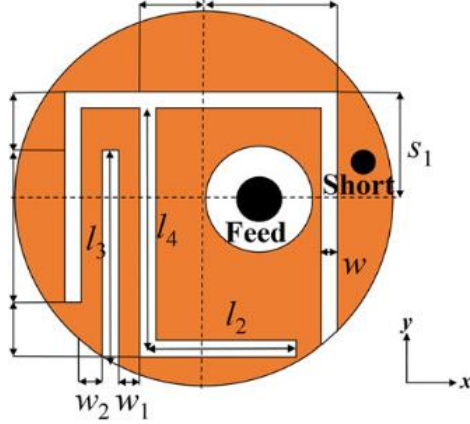
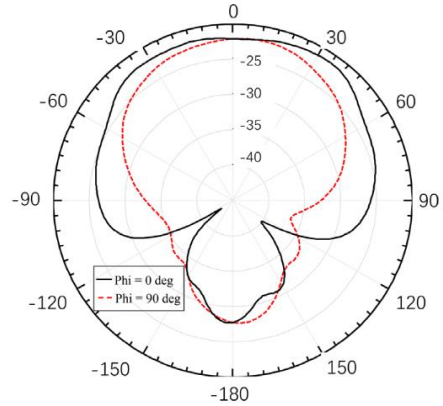


Figure 2.19: (a) Geometry of implantable broadband PIFA antenna (b) Radiation pattern of the antenna at 402 MHz [76]



(a)



(b)

Figure 2.20: (a) Structure of implantable PIFA with slotted ground plane (b) Radiation pattern at 2.45 GHz [77]

Table 2.2: Comparative analysis of implantable antennas

Reference	Antenna type	Volume (mm <sup>3</sup> )	$f_o$ (GHz)	Gain (dBi)	Bandwidth (%)	$\eta$ (%)	Substrate
[8]	Loop antenna	13×13×1.27	0.915	-32	18.2	-	sub: $\epsilon_r=10.2$ ; tan $\delta=0.0035$
[9]	Microstrip patch antenna	11.44×11.44×0.275	2.45	-	1.5	-	Sub; Silicon $\epsilon_r=11.7$
[10]	Flexible antenna	11×11×2	2.42	-20.8	10.4	-	Sub: PMDS $\epsilon_r=2.8$
[11]	Triangular slot antenna	10×10×0.65	2.45	-7.9	8.2	0.5	Sub; Al <sub>2</sub> O <sub>3</sub>

<b>Reference</b>	<b>Antenna type</b>	<b>Volume (mm<sup>3</sup>)</b>	<b><math>f_o</math> (GHz)</b>	<b>Gain (dBi)</b>	<b>Bandwidth (%)</b>	<b><math>\eta</math> (%)</b>	<b>Substrate</b>
[61]	Patch antenna	12×7.5×0.25	0.403- 0.405 0.4331- 0.4348 0.868- 0.8686 0.9028- 0.9280 2.4-2.48	-	168.85	80	Sub: $\epsilon_r=10.2$
[62]	Patch antenna	8×6×0.5	0.915; 2.45	-28.5; -22.8	9.84; 8.57	-	sub: $\epsilon_r=10.2$ ; tan $\delta =0.0023$
[63]	Meander line antenna	30.5×21.02×6.4	0.4025	-	33.5	-	Sub; FR-4 $\epsilon_r=4.7$ ; tan $\delta=0.025$
[67]	Conformal CP antenna	14.2×16.64×0.254	2.45	-29.1	31	-	sub: $\epsilon_r=10.2$ ; tan $\delta =0.0022$
[68]	Patch antenna	24×22×0.07	2.48	-19.7	24	-	Sub: $\epsilon_r=3.5$ tan $\delta=0.008$
[69]	Conformal antenna	34.5×5.8×0.15	0.915	-21	8.9	-	Sub; $\epsilon_r=3.5$ ; tan $\delta=0.008$
[70]	Bow-tie antenna	10×10×1	2.43	-14.5	-	-	Sub; Al <sub>2</sub> O <sub>3</sub> $\epsilon_r=9.8$

<b>Reference</b>	<b>Antenna type</b>	<b>Volume (mm<sup>3</sup>)</b>	<b><math>f_o</math> (GHz)</b>	<b>Gain (dBi)</b>	<b>Bandwidth (%)</b>	<b><math>\eta</math> (%)</b>	<b>Substrate</b>
[71]	Ring antenna	$\pi \times 5^2 \times 1.27$	2.45	-22.7	12.4	-	sub: $\epsilon_r=10.2$ ; tan $\delta = 0.0035$
[72]	Spiral shape	$7 \times 6.5 \times 0.377$	0.402; 1.6; 2.45	-30.5; -22.6; -18.2	36.8; 10.8; 3.4	-	sub: $\epsilon_r=10.2$ ; tan $\delta = 0.0035$
[73]	Loop antenna	$10 \times 10 \times 0.6$	0.92;2.4 5	-29.33; -21.0	12.2; 123	2.6; 3.8	Sub: $\epsilon_r=10.2$ tan $\delta=0.0035$
[74]	Slot antenna	$10 \times 10 \times 0.4$	2.45	-9	57	2.3	sub: $\epsilon_r=2.91$ ; tan $\delta = 0.005$
[75]	CP antenna	$15 \times 15 \times 1.27$	0.915	-27	5.7	-	Sub; $\epsilon_r=10.2$ ; tan $\delta=0.0022$
[76]	PIFA	$23 \times 16.4 \times 1.27$	0.402	-34.9	13	-	sub: $\epsilon_r=10.2$ ; tan $\delta = 0.0023$
[77]	PIFA	$\pi \times 5.35^2 \times 1.34$	0.402;2. 45	-41; -21.3	41; 27.8	-	Sub: $\epsilon_r=10.2$ tan $\delta=0.005$
[78]	CP antenna	$11 \times 11 \times 1.27$	0.915	-29	1.2	23	sub: $\epsilon_r=10.2$ ; tan $\delta = 0.0023$

<b>Reference</b>	<b>Antenna type</b>	<b>Volume (mm<sup>3</sup>)</b>	<b><math>f_o</math> (GHz)</b>	<b>Gain (dBi)</b>	<b>Bandwidth (%)</b>	<b><math>\eta</math> (%)</b>	<b>Substrate</b>
[79]	Circular antenna	$\pi \times 7.5^2 \times 1.92$	0.4035; 0.4339; 2.45	-	28; 10	-	Sub; $\epsilon_r=10.2$ ; tan $\delta=0.0022$
[80]	Flower shape antenna	$7 \times 7.2 \times 0.2$	0.928; 2.45	-28.44; -25.65	19.8; 8.9	-	Sub; $\epsilon_r=2.9$ ; tan $\delta=0.0025$
[81]	SRR Antenna	$10 \times 12 \times 1.27$	0.420; 2.45	-	34.5; 58.5	-	sub: $\epsilon_r=10.2$ ; tan $\delta=0.0023$
[82]	Clover slot antenna	$14 \times 12 \times 0.8$	2.45	-6	7.3	-	Sub; $\text{Al}_2\text{O}_3$ $\epsilon_r=9.8$ ; tan $\delta$ $=0.001$
[83]	Ferrite antenna	$10 \times 10 \times 1.28$	2.45	-17	-	-	sub: $\epsilon_r=10.2$ ; tan $\delta=0.0022$
[84]	CP antenna	$10 \times 10 \times 1.27$	2.45	-22.33	14.03	-	sub: $\epsilon_r=10.2$ ; tan $\delta =0.003$
[85]	U Slot monopole antenna	$29 \times 29 \times 0.5$	2.45	-	8.5	-	sub: $\epsilon_r=10.2$
[86]	Bow tie antenna	$26 \times 22 \times 0.65$	2.45	-6	7.7	0.2	-
[87]	Monopole antenna	$18 \times 24 \times 1$	2.4	-	2.5	-	Sub; $\epsilon_r=28$
[88]	Meander slot antenna	$12.5 \times 14.7 \times 1.27$	2.45	5.7	16.9	98	sub: $\epsilon_r=10.2$ ; tan $\delta =0.0023$

Comparison of various implantable antennas is presented in Table 2.2. It can be seen that each implantable antenna has different performance characteristics. Different miniaturization techniques are employed to design these antennas. In [9] the antenna miniaturization is achieved by using high permittivity dielectric substrate while capacitive loading technique is used in [10] for this purpose. The radiator current path lengthening technique is used for miniaturization in [72] while a PIFA structure is used for miniaturization in [76]. The slotted ground plane technique is employed in [77] to get a miniaturized antenna whereas a higher frequency of operation is selected in [82] for antenna miniaturization. The implantable antenna in [72] has a compact size but the efficiency of the antenna is not reported. In [76] the antenna has a low frequency of operation but the antenna has low gain and narrow bandwidth despite its large volume. The bandwidth of antenna in [61] is wider as compared to the other antennas reviewed in literature but it has a large volume. The gain and efficiency of the antenna proposed in [88] are the highest of all the antennas listed in comparison Table 2.2 but the size of the antenna is large. The gain of the antennas given in comparison Table 2.2 varies from -41 dBi to -6 dBi. However, some of the antennas reported in literature has a lower gain than -41 dBi. The gain of the antenna in [65] is -67 dBi. The gain of our designed antennas is within the range of -47.7 dBi to -25.5 dBi. There are number of factors which cause the gain variation in implantable antennas. The antenna size has an effect on antenna gain. Normally the bigger size antennas have higher gain. The miniaturization techniques employed in antenna design could also impact the gain of the antenna. In some cases, the slotted antennas have lower gain than the antennas with solid ground plane and patch. The implantation depth and the type of tissue layer of the human body in which the antenna is implanted also contribute to the gain variation as each layer of the human body tissues has different permittivity and conductivity at different frequencies.

## 2.5 Human Body Effect on Antenna Performance

The environment of human body forms an integral part of the implantable medical devices. It is very lossy medium where electric properties of the tissues change with the change in operating frequency as shown in Table 2.3 [89].

Table 2.3: Human body tissues conductivity and permittivity

Tissue	Conductivity( $\sigma$ =S/m) at 403 MHz	Conductivity( $\sigma$ =S/m) at 2.45 GHz	Relative Permittivity( $\epsilon_r$ ) at 403 MHz	Relative Permittivity( $\epsilon_r$ ) at 2.45 GHz
Small intestine	1.9	3.17	66	54.4
Stomach	1	2.2	67.5	62.1
Colon	0.86	2	62.5	53.8
Skin	0.69	1.46	47	38
Muscle	0.79	1.74	57.1	52.7

The high conductivity and permittivity of the human body tissues causes attenuation losses inside the body which is given by the following equation [90]:

$$L_\alpha = 20 \log_{10}(e^{-\alpha l}) \quad (2.2)$$

Where  $\alpha$ (N<sub>p</sub>/m) is the attenuation constant and  $l$  (m) is the distance travelled by the signal in the human body tissue. The attenuation constant can be calculated by the following equation [90]:

$$\alpha = \omega \sqrt{\frac{\mu\epsilon}{2} \left( 1 + \left( \frac{\sigma}{\omega\epsilon} \right)^2 - 1 \right)} \quad (2.3)$$

$$\omega = 2\pi f \quad (2.4)$$

Where  $\omega$ (rad/m) and  $\mu$ (H/m) are angular frequency and permeability of human body tissue whereas the  $\epsilon$  and  $\sigma$  are the permittivity and conductivity, respectively. The permeability and permittivity in the above equations are complex quantities. As the body tissues are non-magnetic in nature, the imaginary

part of permeability is zero. Apart from the attenuation losses, the losses due to the reflections at the boundary between the tissues is calculated as [90]:

$$\eta = \sqrt{\frac{j\omega\mu}{\sigma+j\omega\varepsilon}} \quad (2.5)$$

$$\Gamma = \frac{\eta^2 - \eta_1}{\eta^2 + \eta_1} \quad (2.6)$$

$$L_r = 20\log_{10}(\Gamma) \quad (2.7)$$

Where  $\Gamma$  is the reflection coefficient at the tissues boundary and  $\eta$  is the intrinsic impedance. The losses are more at higher frequencies. So, the MICS band and MedRadio band are preferred for data transmission by implantable devices. Lower frequencies of ISM band can also be used. The reflection of the transmitted signal also occurs at the boundary between free space and the outer layer of the skin as both mediums have different impedances and electromagnetic properties. The signal power received by the external receiver is calculated by the following equation [29], [91]:

$$P_{RX} = P_{TX} + G_{TX} + G_{RX} - L_P - e_P - ML_{TX} - ML_{RX} \quad (2.8)$$

Where  $P$ (dBm) is the power,  $G$ (dB) is the gain and  $ML$  (dB) is impedance mismatch loss. The subscript  $TX$  and  $RX$  represents transmitter and receiver.  $L_P$ (dB) is the path loss and  $e_P$  (dB) is the polarization mismatch factor. The gain of the implantable antennas is usually negative because of the lossy nature of the human body tissues. The path loss  $L_P$  can be calculated as follows [92]:

$$L_P = 10n\log\left(\frac{d}{d_0}\right) + 10\log\left(\frac{4\pi d_0}{\lambda_0}\right)^2 + S \quad (2.9)$$

Where  $n$  is a component of path loss and it depends on the environment. For non-line of sight propagation, the value of  $n = 3$  and for the line of sight LOS propagation the value of  $n = 1.5$ . The free space propagation value of  $n$  is 2.  $d_0$  is the reference distance whereas  $\lambda$ (m) is the wavelength.  $S$  is the random scatter around the mean. If we assume the value of  $d_0$  as 1m then free space path loss  $L_f$  is calculated by the following equation [92]:

$$L_f = 20\log_{10}\left(\frac{20\pi d}{\lambda_0}\right) \quad (2.10)$$

The free space gain  $G$  is defined as the ratio of radiation intensity in a given direction to the total input power. Mathematically it is given by following formula [93]:

$$G = \frac{4\pi U}{P_{in}} \quad (2.11)$$

Where  $U$  is the radiation intensity in watt per unit solid angle.  $P_{in}$  is the total input power in watts. The relationship between radiation intensity and average radiated power  $S_{avg}$  is as follows [93]:

$$U = r^2 S_{avg} \quad (2.12)$$

$S_{avg}$  is in watt per meter square. The gain of a conductive medium ( $G_{con}$ ) is given by [94]:

$$G_{con} = \frac{4\pi R g^2}{R_r} \quad (2.13)$$

Where  $R$  is intrinsic resistance and  $R_r$  is the radiation resistance. The intrinsic resistance can be calculated by the following equation [94]:

$$R_{intrinsic} = \sqrt{\frac{\omega\mu}{2\sigma}} \quad (2.14)$$

$g$  represents a function which involves the parameters of medium and its value is given by [94]:

$$g = \frac{|H|de^{\frac{d}{\delta}}}{I_i} \quad (2.15)$$

$|H|$ (A/m) is the magnetic field.  $d$  is the distance in meters.  $I_i$  is the input current in amperes. Whereas  $\delta$  represents the skin depth. The radiation resistance is given by [95]:

$$R_{rad} = \frac{P_{rad}}{I_i^2} \quad (2.16)$$

$P_{rad}$  is the radiated power. From equations (2.13) and (2.15) it can be seen that if the magnetic field inside the human body increases the value of  $g$  will increase. The higher value of  $g$  will increase the gain of the implantable antenna [94].

### 2.5.1 Human Body Effects on Antenna Radiation Efficiency and Antenna Radiated Power

Antenna radiation efficiency and antenna radiated power are affected by the loss in the human body tissues. The radiation efficiency of implantable antennas is given by the following equation [44]:

$$\eta = \frac{P_{rad}}{P_{in}} \quad (2.17)$$

$P_{in}$  is the input power. In case of implantable antennas, the input power consists of three power components which are reflected, absorbed and radiated powers ( $P_{ref} + P_{abs} + P_{rad}$ ). Due to the near field coupling in the implantable antennas, the absorbed power is larger than the reflected power which would result in low radiation efficiency and radiated power. The absorbed power is given by the following equation [96]:

$$P_{abs} = \frac{\omega}{2} \int_v \epsilon_0 \epsilon_r |E|^2 dv \quad (2.18)$$

An increase in the absorbed power also increases the specific absorption rate which affects the antenna radiation efficiency. The SAR is given by [93]:

$$SAR = \frac{P_L}{\rho} = \frac{\sigma |E|^2}{2\rho} \quad (2.19)$$

Where  $\rho$ (kg/m<sup>3</sup>) is the mass density and E(V/m) is electric field. Radiation resistance and loss resistance can be used to represent the radiation efficiency [91]:

$$\eta = \frac{R_{rad}}{R_{rad} + R_L} \quad (2.20)$$

Where  $R_{rad}$  and  $R_L$  are radiation and loss resistances in ohms. So, the gain of the antenna would be:

$$G = \eta D \quad (2.21)$$

Where D is the directivity of the radiated power. Directivity is a ratio of radiation intensity in a specific direction to the average radiation intensity. The average directivity is given by:

$$D = \frac{U(\theta, \phi)}{U(\theta, \phi)_{avg}} = \frac{4\pi U(\theta, \phi)}{P_t} \quad (2.22)$$

Where  $P_t$  is the total radiated power. If the antenna radiation resistance increases, the antenna radiation efficiency also increases. The radiation resistance of the antenna depends largely on the antenna radiated power. Hence, the radiation efficiency of the antenna decreases inside human body tissues because of the coupling between the antenna radiating element and the body tissues. The insulation of the antenna would be beneficial by taking biocompatibility issue into consideration.

### *2.5.2 Human Body Effect on Antenna Bandwidth*

The implantable antennas are of compact sizes, so they are expected to have narrow bandwidth. However, bandwidth increases due to losses and detuning inside the body. All the radiated power does not reach the receiver because of absorption and reflection by the body tissues. The absorbed power is much more than the reflected power for implantable antennas which causes the bandwidth to be wider at the cost of lower radiation efficiency [44]. These losses can be avoided using different techniques like bio-encapsulation and impedance matching. By using these techniques, the losses might become lower resulting in a narrow bandwidth. But the implantable antennas with narrow bandwidth always suffer frequency detuning inside the human body. A careful consideration is therefore, needed to be taken to tackle this issue.

### *2.5.3 Human Body Effect on Antenna Radiation Pattern*

The radiation pattern of an antenna is the plot of the radiated field of the antenna as a function of angle at a fixed distance [93]. The radiation pattern of an implantable antenna is completely different from that of conventional antenna in free space. The lossy medium of human body might broaden the radiation pattern. The antenna position is also associated with the radiation pattern. The radiation pattern of an implantable antenna would also be different in same medium if mounting scenarios and positions differ.

### *2.5.4 Methods to improve Implantable Antennas Radiation Efficiency*

Antenna radiation efficiency can be improved in number of ways. One technique is to suppress the surface waves of the antenna. This technique is applied in [97] as shown in Figure 2.21. A coplanar

waveguide (CPW) fed ring antenna gives an efficiency improvement. This is done by removing little portion of the substrate in the patch vicinity. In this way the surface waves would be eliminated causing the radiation efficiency to be stable. Another method to improve implantable antenna radiation efficiency is to apply high permittivity biocompatible superstrate. This would lower the antenna coupling and power absorption inside the human body by increasing the radiation efficiency. This technique is applied in [98].

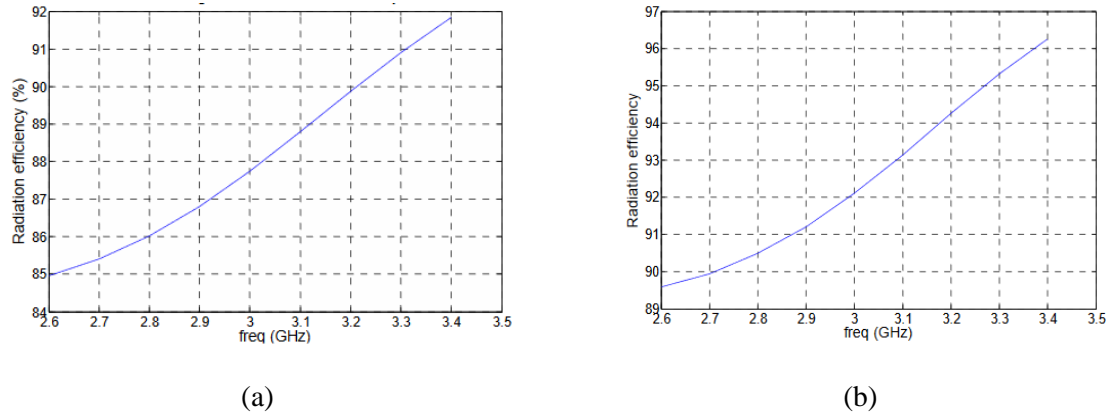


Figure 2.21: (a) Radiation efficiency of the antenna (b) Radiation efficiency of antenna after modification with a 4% improvement [97]

### 2.5.5 *Implantable Antenna Bandwidth and Gain Improvement*

The bandwidth of the antenna can be increased by using a thicker substrate. There are different methods to increase the bandwidth of an implantable antenna. In [99] the bandwidth of a dipole antenna is increased by connecting a small strip line with dipole. The result is shown in Figure 2.22.

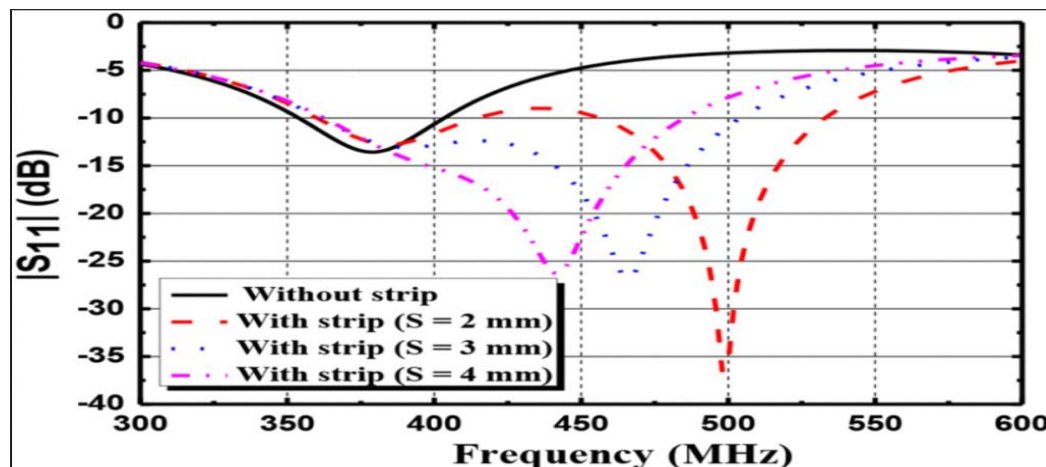


Figure 2.22: Bandwidth enhancement of dipole antenna [99]

Another technique is given in [100] for PIFA. The ground plane of the antenna is partially connected to RFID circuit to increase the bandwidth of the antenna. The gain of the implantable antenna can be improved by applying different techniques. In [101] the gain of compact broadband monopole antenna is improved by inserting a U-shaped extension to the ground plane. This will improve the gain of the antenna by improving the capacitive coupling and directivity.

## 2.6 Channel Modelling for Implantable Antennas

There are different communication channels for implantable devices. Some of the communication scenarios for implantable antennas are discussed in this section. The communication between an implantable antenna and an external device is referred as in/off-body communication. The external device is normally a control device to send and receive data which is observed by a physician or another person depending on the received signal. A 3-D compact broadband implantable antenna was proposed in [102]. Link margin was calculated by inserting antenna into simplified body model. MedRadio band (401-406) MHz was used for communication and ISM band (2.4-2.48) GHz was used for wakeup signal. Gain of the antenna is -28.95 dBi and 25.5 dBi. The communication link calculation showed that the communication distance for communication is 18.95m which means the antenna can transmit the information up to the specified distance but for the wakeup communication the distance was measured as 1.8m. For mm-size neural implants the wireless channel was characterized in [103]. Signal propagation model for different biological materials was built by employing full wave electromagnetic model. The simulated results were validated over a frequency range of 100 MHz to 6 GHz by performing tests on animals. The effects of dielectric properties of human body tissues in anatomical body model were also discussed.

All these channels characterizations described earlier are for near field propagation. Wireless power transfer techniques have gained a lot attention from researchers in field of medical implants which is an example of in/off-body communication [104]. A distance of 50 cm is considered more preferable for wireless power transfer so far which makes use of lower frequency of operation around 433 MHz. A system for wireless power transfer in implantable devices is proposed in [105]. Parasitic patches are used for wireless power transfer. The system has good gain and size of the antennas is compact but in

this system the propagation losses and patient safety considerations are not considered. In [106] a triple band antenna for data telemetry, wireless power transfer and power conservation is studied. The antenna operates in MICS and ISM bands. The sleep mode is introduced to conserve the energy. The implantable antennas also communicate with a node or sensor on the body forming an in/on-body communication channel. Various examples of in/on-body communication channels are proposed in literature. Alomainy *et al.* [107] proposed modelling and characterization of biotelemetric radio channel from ingested implants considering organ contents. In this study the channel modelling was carried out on the frequencies which are very common for bio-medical applications. These frequencies include 402 MHz, 868 MHz and 2.4 GHz. Numerical model was developed for in/on-body communication channel to which the electromagnetic analysis was applied. For the digestive track system, the calculated parameters have shown that the accuracy of digital phantom is also important factor for wave propagation with organ content. A nearfield scanner was used to measure the path gain variations over radio channel. Simulated results were validated with actual measurement.

A wireless capsule endoscopy system was proposed in [108]. Path loss variations are calculated on different sliced body tissues but not on the whole body. 300 MHz to 2450 MHz frequency range was used to calculate the path loss. It was found that the losses were much less on the frequencies lower than 900 MHz as compared to higher frequencies. For wireless capsule endoscopy an implantable loop antenna with a buffer layer is proposed in [109]. This loop antenna communicate with an external loop antenna and the buffer layer helps to reduce the reflection on the human body tissue boundaries. The application of directive antennas for medical implants was investigated in [110]. It was found in this study that the use of directive antennas can reduce interference with nearby bands and radiation exposure to body tissues which in turn reduce power loss. In case of multi-medical implants the implantable antennas and devices communicate with each other forming an in/in-body communication channel. In-body channel characterization in 400 MHz MICS band was proposed in [111]. At very short distances multipath effects and human body movements were analysed and statistical data was used to calculate the path loss.

## **2.7 Chapter Summary**

In this chapter a comprehensive review on implantable antennas used for biomedical applications is presented. Since, the antenna is a key component of a biosensor operating in a harsh in-body environment, its design becomes a very challenging task. Several factors need to be considered while designing such an antenna including size, gain, efficiency, radiation pattern and patient safety. A detailed critical review is conducted into different implantable antenna designs available in open literature including planar, wire, conformal, spiral, slotted and PIFA structures. Though, the selection of antenna type is generally application specific, patch structures have exhibited greater potential of meeting most of the requirements efficiently.

Key requirements and challenges in implantable antenna design are summarized in terms of miniaturization, patient safety and biocompatibility as well as different techniques employed to meet these requirements. Widely used miniaturization methods include using high permittivity substrates, PIFAs, larger current path on the radiator, inductive or capacitive loading, higher operating frequencies and altered ground plane. Each method has been evaluated for its merits and demerits. The design of implantable antennas is application dependent, so the selection of miniaturization technique also depends on the type of antenna needs to be designed. A detailed comparative study has shown that despite having greater potential of miniaturization, use of higher frequencies suffer from higher losses. However, further investigations are required in this direction as exposure studies at these frequencies are not yet fully established. Patient safety is paramount in implantable devices and it is strictly governed through SAR and EIRP limits. Implantable antennas are bound to meet these regulations and further ensures the safety through use of biocompatible materials. Human body effects on these antennas make it pertinent to consider the human body as part of the antenna design. Channel modelling for implantable antennas has also been investigated.

# Chapter 3

## 3. Methodology

### 3.1 Introduction

The goal is to design compact implantable antennas for bio-medical applications. The study followed the general procedures of systems engineering including gathering the user requirements, translating them into system requirements, development of a system architecture based on the functional analysis. The antennas are designed using numerical methods and validated through a series of simulations.

CST Microwave Studio<sup>®</sup>, a specialised electromagnetic solver tool, is used to design the antenna numerically. Detailed performance evaluations were carried out to analyse antenna performance in free space using the simulated results of reflection coefficient response, impedance matching, gain, radiation efficiency and radiation pattern. Since the antenna has to be used by implanting it into a series of human body scenarios, a detailed investigation was carried out to study the in-vitro antenna performance using a numerical phantom of the human body in CST Microwave Studio. The effects of varying in-body antenna position are analysed. A comparison between the simulation results of free space and implantable scenario is used to validate and benchmark the antenna performance in required working conditions for telemetry.

### 3.2 Methodology of the Designed Antennas

The implantable antennas are application dependent so their design methodology could be different for each design. There are many requirements for a compact size efficient implantable antenna e.g. lighter weight, high gain, larger radiation efficiency, low SAR and good radiation pattern. Methodology used to design the implantable antennas involve various steps. First of all, a thorough review on implantable antennas was carried out. The tools and techniques used for implantable antennas were critically analysed. After considering the advantages and disadvantages of different design strategies and the types of implantable antennas, the methodology parameters were set. The designed antenna performance was

analysed in simplified human body phantom layers and then in anatomical body model to satisfy the requirements for implantable applications. Optimizations were carried out where necessary.

The following flow chart elaborates the design methodology.

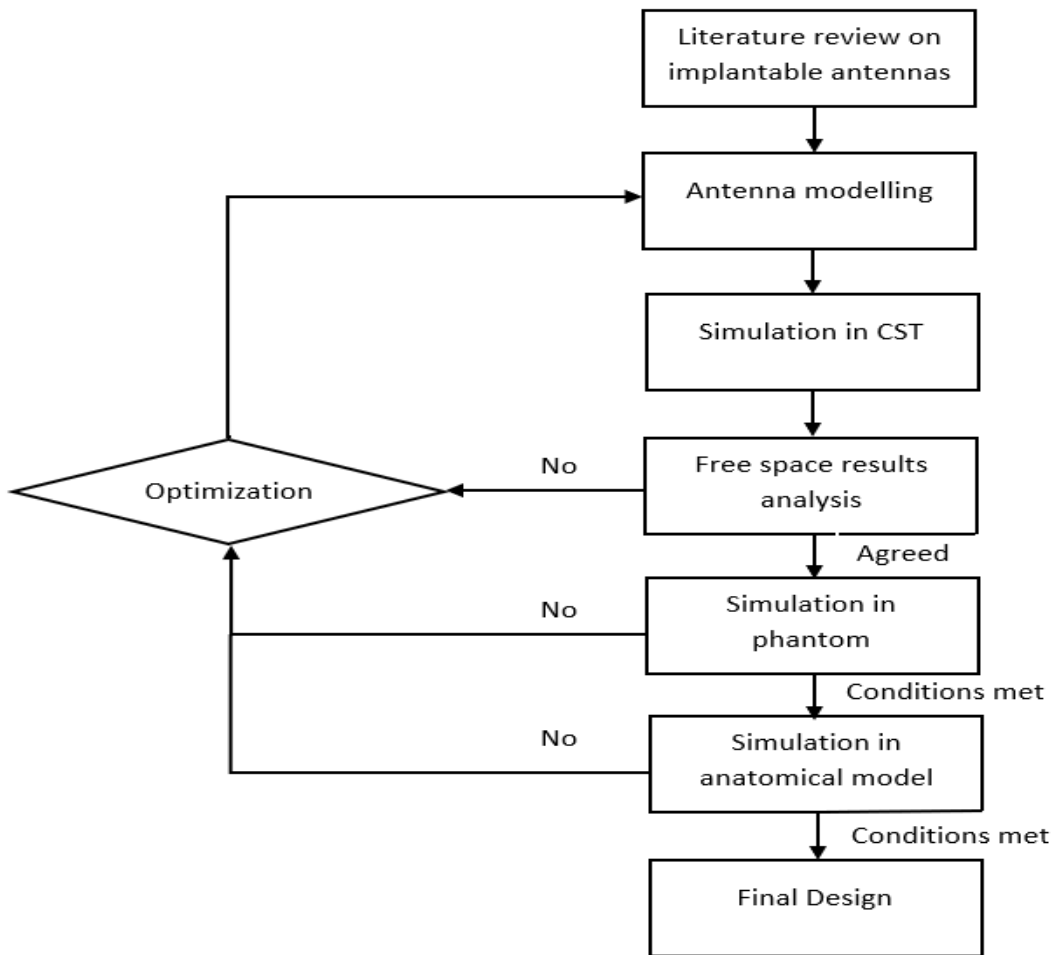


Figure 3.1- Design Methodology

### 3.2.1 Methodology Parameters

The parameters which were defined for the implantable antennas based on the requirements for implantable applications are as follows.

- The return loss of the antenna should be measured around  $S11 \leq -10$  dB. The implantable antennas often show an increase in return loss when implanted inside the body. If the initial

return loss was measured around -6dB the return loss will increase inside the body and antenna will not resonate on that frequency.

- The -10 dB bandwidth of the antenna should be wide enough to cover the desired frequency bands, either MICS band or ISM band.
- Achieve the maximum gain and radiation efficiency while keeping the antenna size as small as possible.
- Evaluate the antenna performance in different tissue layer and anatomical body model to validate the robustness of the antenna.
- To make sure that the SAR values for the designed antennas are within allowed limits.

When all these conditions are met the implantable antenna design is finalized. The next step is to fabricate the simulated antennas to validate the results. In this thesis only simulated antenna designs are presented.

### **3.3 Project Milestones**

The main goal of the research is to design compact size implantable antennas for biomedical applications. The research is completed in different stages which are as follows.

#### *3.3.1 Literature Review on Implantable Antennas*

An extensive literature survey has been carried out to study implantable antennas. The existing techniques used for implantable antenna design are reviewed. The implantable antennas studied and analysed in the literature review have been used to identify the problem with existing solutions.

#### *3.3.2 Design of Implantable Antenna*

The antennas were designed using CST Microwave Studio Suit. The antennas are simulated in free space and results are analysed. As the antennas have to operate in implantable conditions, the antennas are simulated in simplified human body phantom layers. The simplified human body phantom layers were designed using CST Microwave Studio.

### 3.3.3 Human Body Effect Analysis

The designed antennas were subjected to different implant depth and positions in simplified human body phantom. The antennas were also simulated in anatomical body model. The effects of the lossy tissues of human body were analysed. The results of the different simulations were compared to satisfy the designed antennas performance.

## 3.4 Numerical Modelling Techniques

The analysis and solution of electromagnetic problems has been made easy by the use of computer modelling techniques. Generally, there are three categories of computer modelling techniques to solve the electromagnetic problems which are analytical, numerical and expert systems techniques. The analytical modelling technique solves the problem by applying a closed form solution based on simplified assumptions. The field equations are solved directly to solve a problem in numerical modelling technique by taking into account the boundary conditions of the problem geometry. The expert systems technique is different from the analytical and numerical modelling techniques. A rules database which is set into the system is used to estimate the values of the desired parameters. The values of these parameters are applied to solve an electromagnetic problem [112].

Modelling techniques are used to solve the electromagnetic problems by solving Maxwell equations. In 1873, James Clark Maxwell represented the relationship between electric and magnetic fields and fluxes and charges in the form of equations which are known as Ampere, Faraday, Guass and magnetic field law. The modern electromagnetic theory is based on these laws [113]. There are different ways to represent Maxwell's equations. Maxwell's equations in differential form are given below [113]:

$$\text{Ampere's law} \quad \nabla \times H = J + \frac{\partial D}{\partial t} \quad (3.1)$$

$$\text{Faraday's law} \quad \nabla \times E = - \frac{\partial D}{\partial t} \quad (3.2)$$

$$\text{Guass's law} \quad \nabla \cdot D = \rho \quad (3.3)$$

$$\text{Guass's law for magnetism} \quad \nabla \times B = 0 \quad (3.4)$$

$E$  represents the electric field intensity (V/m) whereas  $H$  is magnetic field intensity (A/m).  $D$  is electric flux density and  $B$  is magnetic flux density. Maxwell's equations in integral form are represented as [113]:

$$\text{Ampere's law} \quad \oint_C H \cdot dl = \int_S J \cdot dA + \frac{d}{dt} \int_S D \cdot dA \quad (3.5)$$

$$\text{Faraday's law} \quad \oint_C E \cdot dl = -\frac{d}{dt} \int_S B \cdot dA \quad (3.6)$$

$$\text{Guass's law} \quad \oint_S D \cdot dA = \int_V \rho dV \quad (3.7)$$

$$\text{Guass's law for magnetism} \quad \oint_S B \cdot dA = 0 \quad (3.8)$$

In electromagnetic problems the relationship between the properties of the medium and the field is described by using following equations [113]:

$$D = \epsilon E \quad (3.9)$$

$$B = \mu H \quad (3.10)$$

$$J_e = \sigma E \quad (3.11)$$

$$J_m = \sigma_m H \quad (3.12)$$

Where  $\epsilon$  is electric permittivity and  $\mu$  is magnetic permeability.  $J_e$  is electric current density ( $A/m^2$ ) and  $\sigma$  is electric conductivity ( $S/m$ ).  $J_m$  is equivalent magnetic conduction current density ( $V/m^2$ ) and  $\sigma_m$  is the equivalent magnetic resistivity ( $\Omega/m$ ). As the use of a numerical technique for solving an electromagnetic problem depends on the type of problem, so there are number of frequency domain and time domain numerical algorithms are in use. Time domain numerical techniques are chosen in this study because they show their strength and stability for modelling the complex inhomogeneous dispersive media as compared to other techniques [114].

### 3.4.1 Finite Difference Time Domain (FDTD)

Finite Difference Time Domain technique (FDTD) was introduced by K.S. Yee in 1966 to solve the Maxwell's equations in discrete form [115]. In software this technique is implemented to provide the

solution of Maxwell's equations. In FDTD Maxwell's equations are converted to central difference equations and then discretized. The solution to these equations is provided by solving at a given instant in time, the electric field and at the next instant in time, the magnetic field. The process repeats itself over and over again in a leapfrog manner [112].

### 3.4.2 *Finite Integral Technique (FIT)*

A time domain numerical technique which solves the integral forms of Maxwell's equations known as Finite Integral Technique (FIT) was introduced by Weiland in 1977 [116]. A manner similar to FDTD is used by this technique for solving electromagnetic problems. For energy and charge conservation with respect to Maxwell's equations, the FIT gets matrix equations for integral quantities which has the inherent properties of Maxwell's equations. In this way the stability in numerical implementation is achieved.

## 3.5 Antenna Design Software

The antenna design software programs which are used by the antenna designers are given as follows:

1. Integral Equation Three Dimensional (IE3D)
2. Feldberechnung für Körper mit beliebiger Oberfläche (FEKO)
3. Matrix Laboratory (MATLAB)
4. Antenna Design Explorer (ADE)
5. High-frequency structure simulator (HFSS)
6. Computer Simulation Technology (CST)

IE3D is provided by Zeland Inc. IE3D uses Method of Moments (MoM) technique to solve electromagnetic problems while FEKO uses MoM and asymptotic high frequency techniques. MATLAB has antenna toolbox for antenna design analysis and visualization and it is based on MoM technique. ADE is a graphical user interface-based tool and it works in MATLAB environment. HFSS uses Finite Element Method (FEM) for solving electromagnetic problems. CST Microwave Studio has different solvers [117], [118]. The MATLAB antenna toolbox and ADE are comparatively new as compared to other antenna design software programs. IE3D is good for simple structures but it is not

suitable for complex structures. FEKO is suitable for large structures, but it requires very large Random-Access Memory (RAM) [117]. HFSS and CST are the two main competitors for antenna design. The CST time domain solver is more accurate than HFSS time domain solver. The accuracy of CST Microwave Studio is also greater than HFSS for wide range of frequency spectrum [119]-[124]. The CST has different studios for multiple applications. The design and analysis of static and low frequency applications is achieved by using CST EM (Electromagnetic) Studio. Its applications include motors, sensors, shielding enclosures, actuators and transformers. CST employs CST Mphysics Studio (CST MPS) for the analysis of mechanical and thermal stress. Free moving charged particles simulation is done with the help of CST Particle Studio (CST PS). CST Cable Studio (CST CS) is used for Electromagnetic Compatibility (EMC) and Electromagnetic Interference (EMI) analysis of a cable and its signal integrity simulation. The EMC and EMI analysis and signal integrity simulation for Printed Circuit Boards (PCB) is done by using CST PCB Studio (CST PCBS). Moreover, the CST Design Studio (CST DS) allows the user to combine it with other studios for simulation of integrated electronics and Multiphysics [125], [126]. We have used CST Microwave studio for our antennas design because of its advantages as compared to other software programs.

### **3.6 CST Microwave Studio®**

For accurate measurement of high frequency problems and 3-D electromagnetic simulation CST Microwave Studio is the perfect tool. It uses Finite Integration Technique (FIT). It works in window-based environment on computer for calculation of antenna parameters. CST Microwave Studio® provides an excellent interface for modelling which simplifies the inputting process of the structure. The device definition is more simplified by strong graphic. After component modelling the meshing procedure is applied before the start of simulation engine. CST Microwave studio gives you the facility to improve and analyse your design in an efficient way with its post processing feature and advanced visualisation engine [122]. The complete technology approach in this software enables the user to choose the most appropriate mesh type or solver for a particular problem. As different methods are needed for different applications, this software has different solvers which are integral equation solver, multilayer solver, asymptotic solver, time domain solver, eigenmode solver and frequency domain

solver. Mesh type of each technique depends on the type of simulation. Perfect Boundary Approximation (PBA) feature comes in combination with hexahedral meshes. Hexahedral meshes also has a combination with Thin Sheet Technique (TST) extension for some solvers. CST Microwave Studio also features the combination of octree based meshing algorithm and hexahedral meshes. These techniques of combining hexahedral meshes with other features reduces overall cell count and it also improves the simulation accuracy as compared to conventional hexahedral meshes. Time domain solvers support hexahedral mesh. Tetrahedral and hexahedral meshes both are supported by eigenmode and frequency domain solver. Multilayer solver and integral equation solver support linear, curved surface and multilayer meshes. The time domain solver is so flexible that it can obtain the whole broadband frequency behaviour of a device in one calculation run. The time domain solver is the best tool for high frequency applications such as transmission lines, antennas, connectors and waveguide components [122].

In CST Microwave Studio there are two-time domain solvers and they both use hexahedral mesh. One is based on Transmission Line Matrix (TLM) method and the other one is based on FIT method. Frequency domain solvers are used for the structures which are very small electrically than their shortest wavelength because for such kind of structures the efficiency of the time domain solvers gets reduced. A very fine mesh is needed for electrically large structures. For that purpose, the CST Microwave studio has integral equation-based solver. Quadrilateral and curved triangular surface mesh are used by integral equation-based solver for electrically large structure. Characteristics Mode Analysis (CMA) tool facilitates the design of antennas of different shapes. This tool is built into multilayer solver and integral equation solver. Asymptotic solver is used for electrically extremely large structures. The ray tracing technique is employed in asymptotic solver. Multilayer solver is mainly used for planar structures and it employs the MoM technique for problem solving. In applications such as filter design the calculation of operating modes is required. The CST Microwave Studio has eigenmode solver for such applications. In a closed electromagnetic device, the eigenmode solver can efficiently calculate a finite number of modes. There are number of options to visualize the simulation results of each solver. CST Microwave Studio also has other features which include structure modeler full parameterization, parameter sweep

tool and built-in optimizer. Based on the applications of CST Microwave Studio, it is the best software for design and analysis of electromagnetic devices [122].

### **3.7 Chapter Summary**

In this chapter the design methodology for implantable antennas is discussed. The schematic of design procedure is given to explain the process. Tools and techniques employed to design the antenna are discussed. A flow chart is also added to elucidate the antenna design procedure. Theoretical model of antenna was developed based on the literature review. Simulations were carried out in CST Microwave Studio. To analyse the antenna performance in implantable scenario the human phantom was used. Project milestones are explained to divide the whole project into different stages. Numerical modelling techniques are discussed and the software programs available for antenna design are listed. Detailed introduction of CST Microwave Studio<sup>®</sup> software is given.

# Chapter 4

## 4. Design of Implantable Antennas

### 4.1 Introduction

Implantable devices are mainly dependent on implantable antennas for communication. Overall size of an implantable device can be reduced and its weight can be lowered by using compact size antennas. The small size of the antenna gives more room for the batteries and other circuitry components. The antenna with larger size may yield to wider bandwidth and high gain values but they make the implantable device bigger in size and weight. Patch antennas are the best option for such applications. Their easy design and ease of integration with sensors makes them the best candidate for the purpose [127]. The low profile and low cost are also the characteristics of the patch antennas. Various patch antennas for implantable applications were presented in the open literature which are discussed in chapter 2 and are critically analysed.

The design of compact size antennas which meet the requirements for the implantable application are the main focus of this thesis. These requirements include high gain, wider bandwidth, small size, low cost, light weight, larger radiation efficiency, good radiation pattern, low SAR, smallest frequency detuning and ease of integration with implantable sensors. It is quite difficult to avoid frequency detuning inside the human body tissues especially in case of patch antennas as they have narrow bandwidth. The frequency detuning can be minimized by antenna design optimization. Various factors need to be considered for antenna design optimization such as resonant frequency, substrate dielectric constant, type of the tissue layer of human body phantom, thickness of tissue layer, implant position and implant depth etc. In this chapter the design of implantable antennas is presented first. Each design process is elaborated thoroughly. The parameters are studied and the optimization process for the antennas is explained. The antennas are simulated in simplified body model and results are explained with any amendments in design to meet the requirements for the implantable applications. Simplified

body model refers to low resolution model based on high level discretization using basic geometrical shapes (such as rectangular or circular bricks) as compared to high resolution inhomogeneous whole body human model. Single tissue layers of simplified human body phantom are used to evaluate the designed antenna performance in implantable conditions. The designed antennas performance in multilayer tissues is evaluated in chapter 5. Antenna designs are compared with the antennas presented in the literature.

## 4.2 Circular Patch Antenna

As explained earlier patch antennas has many advantages over other antennas for implantable applications. We have designed a circular patch antenna for such an application operating at 915 MHz in ISM band. While designing this antenna we have assumed the lossy surrounding media as human body tissues are lossy in nature. As electrical properties of the human body tissues are different at different frequencies, so the human body tissues are taken as part of design process. Careful considerations are taken to choose the substrate material for antenna design for body tissue safety. The conductivity of the body tissues also contributes to impedance mismatch which is reduced by applying appropriate design techniques. Following equations are used as a reference to start the circular patch antenna design [113], [128]. However, the final antenna design dimensions are obtained through optimizations in CST Microwave Studio software.

$$a_{eff} = \frac{x'_{11}c}{2\pi f_r \sqrt{\epsilon_r}} \quad (4.1)$$

$$a = \sqrt{\frac{a_{eff}}{\left\{1 + \frac{2h}{\pi\epsilon_r a_{eff}} \left[ \ln\left(\frac{\pi a_{eff}}{2h}\right) \right]\right\}}} \quad (4.2)$$

Where  $a_{eff}$  is effective radius of the patch. The effective radius of patch is calculated for taking into account the fringing effect.  $x'_{11}$  represents the first order derivative of the Bessel function and its value is 1.8412. The value of  $c$  is  $3 \times 10^8$  m/sec and it denotes the speed of light.  $f_r$  is the resonant frequency of 915 MHz and  $\epsilon_r$  is the dielectric constant of the substrate with a value of 10.2.  $a$  is the actual radius of the patch whereas  $h$  denotes the height of substrate which is 0.13 mm. By solving the equations (4.1)

and (4.2), the radius of patch comes out as 30 mm which is very large. If the size of the antenna is reduced the resonant frequency will shift to a higher value. The miniaturization is one of the basic requirements for an antenna to be used with implantable sensors. So, different miniaturization techniques have been used to reduce the size of circular patch antenna which include the use of high permittivity dielectric superstrate, slotted patch and ground plane and the use of shorting pin loading.

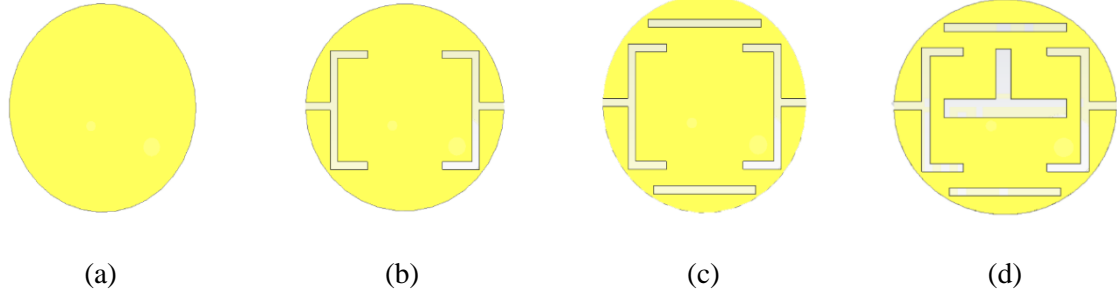


Figure 4.1- Slot creation in the patch of circular patch antenna (a)- case 0 (b)- case 1 (c)-case 2 (d)- case 3

The patch of the antenna is sandwiched between a substrate layer and superstrate layer. The superstrate layer prevents the direct contact between the radiating patch and human body tissues. It also helps to lower antenna operating frequency while keeping the size of the antenna small. The ground plane and patch material are copper annealed with a thickness of 0.035 mm. The substrate material is Rogers RO3010 with a dielectric constant ( $\epsilon_r = 10.2$ ) and loss tangent ( $\tan \delta = 0.0023$ ). The superstrate material is same as substrate with a thickness of 0.25 mm. A shorting pin between patch and ground plane is used in the design with a radius of 0.2 mm and a position of  $P = (X = -0.5; Y = -0.7)$  and its material is PEC. The antenna is excited by a  $50-\Omega$  coaxial probe feed which is located at  $P = (X = 2.1; Y = -1.5)$ .

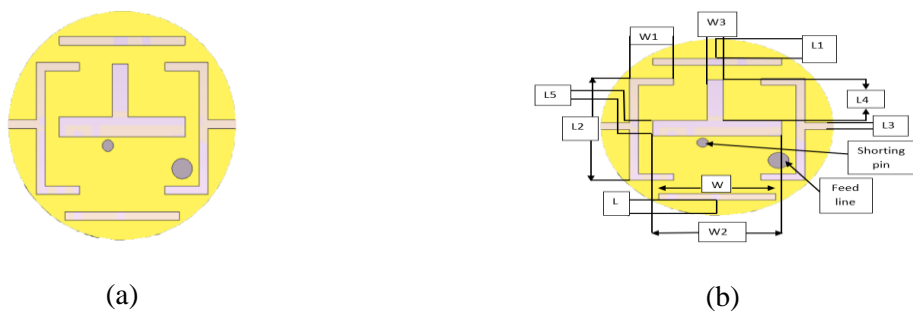


Figure 4.2- (a) Slotted patch of the circular patch antenna (b) Slotted patch of the circular patch antenna with labelled parameters

Slots are etched in the patch and ground plane at positions where current is maximum. Figure 4.1 demonstrates how the slots are created in the patch of the circular patch antenna in different stages from case 0 to case 3. The purpose of the slots is to elongate the current path which makes a physically small antenna an electrically large antenna. Slots also help in miniaturization by shifting the resonant frequency of the antenna to a higher or lower value depending on the size and position of the slots. In antennas some of the power is converted into surface waves which lowers the antenna radiation efficiency. The insertion of slots provide discontinuity in the path of these waves causing them to be radiated instead of staying in the structure. Labelled diagram of the patch of the circular patch antenna is shown in Figure 4.2.

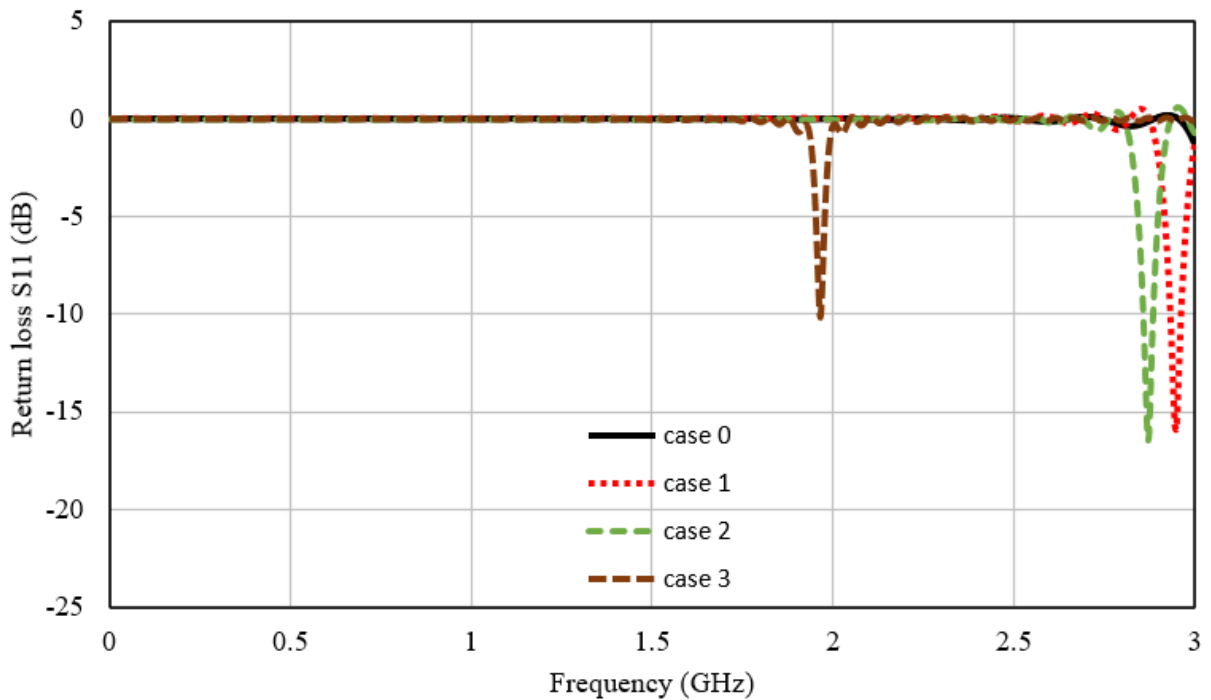


Figure 4.3- Simulated return loss plot of the circular patch antenna in free space in different stages of slots creation in the patch with solid ground plane

For an antenna to resonate the standard is that the antenna return loss (S11) should be less than or equal to -10 dB ( $S11 \leq -10$ ). The lower value of S11 would indicate that the maximum power is transmitted to the medium and reflected back power is small and vice versa. The return loss of the circular patch antenna in different stages of slots creation when simulated in free space with solid ground plane is shown in Figure 4.3. Case 0 represents the solid patch and solid ground plane. It is evident from case 0 curve in Figure 4.3 that there is not any resonance for frequency range from 0 to 3 GHz. The insertion

of slots on left and right side of the circular patch antenna as shown in Figure 4.1(b), creates a resonance around 2.9 GHz which is given as case 1 plot curve in Figure 4.3. The resonant frequency of the circular patch antenna is further shifted to a lower value of around 2.8 GHz by inserting two horizontal slots on upper top and lower bottom side of the patch as depicted in Figure 4.1(c). The return loss plot curve labelled as case 2 in Figure 4.3 represents this frequency shift. A horizontal slot is etched in centre of the patch and a vertical slot is created in the middle of upper half of the patch which is connected with the central horizontal slot. These slots are shown in Figure 4.1(d) and the return loss of the circular patch antenna after creating these slots is given in Figure 4.3 which is labelled as case 3. It can be seen that the frequency has shifted from around 2.8 GHz to 1.9 GHz but the value of the S11 was changed from -16 dB to -10 dB. The detailed dimensions of the patch slots of the circular patch antenna are given in Table 4.1.

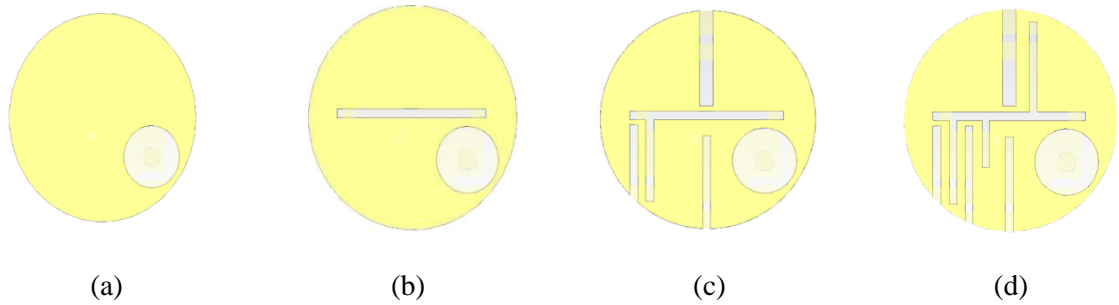


Figure 4.4- Slots creation in the ground plane of the circular patch antenna (a)- case 0 (b)- case 1 (c)- case 2 (d)- case 3

After etching the slots in the patch, the circular patch antenna was resonating at 1.9 GHz but our aim is to design the antenna to resonate at 915 MHz. For that purpose, we engineered the ground plane of the circular patch antenna. The creation of the slots in the ground plane of the circular patch antenna in different stages of the design process is depicted in Figure 4.4 (a), (b), (c) and (d). The slotted ground plane of the circular patch antenna with labelled parameters is shown in Figure 4.5. Figure 4.6 shows the side view of the circular patch antenna.

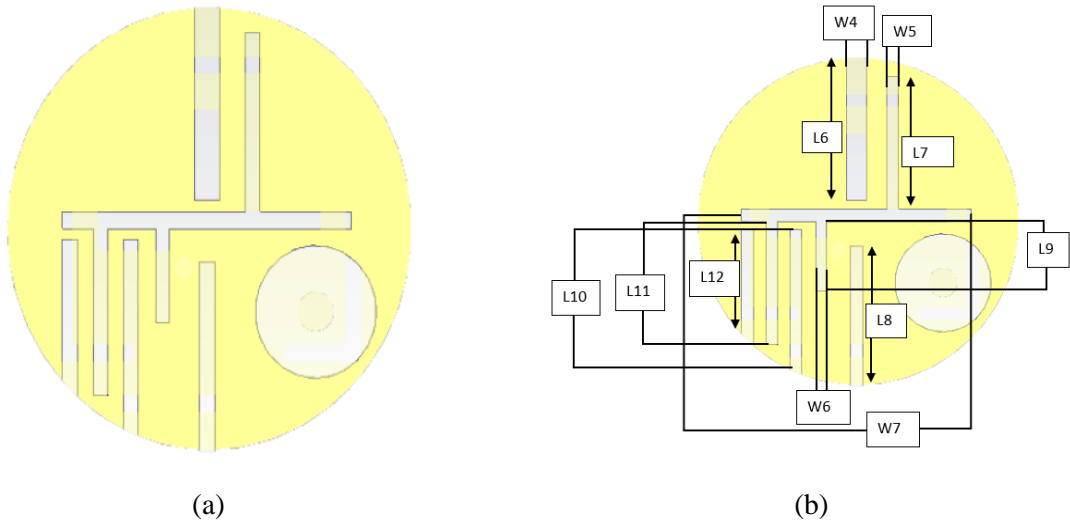


Figure 4.5- (a) Slotted ground plane of the circular patch antenna (b) Slotted ground plane of the circular patch antenna with labelled parameters

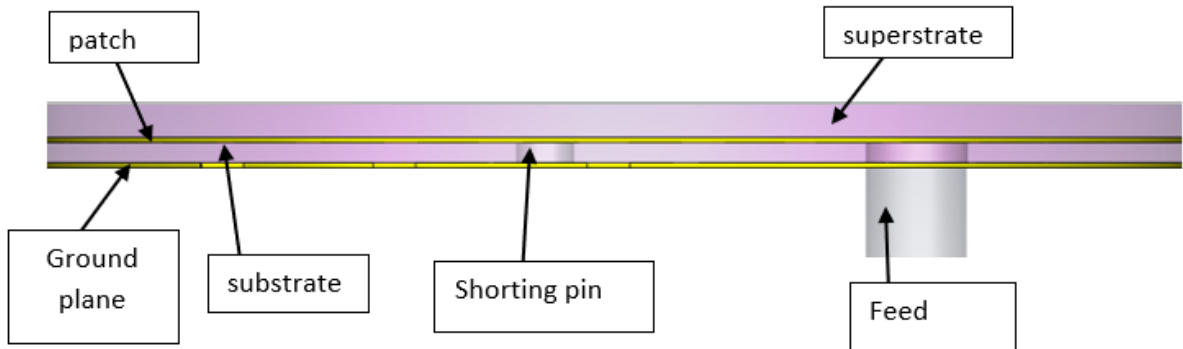


Figure 4.6- Circular patch antenna side view

The simulated return loss of the circular patch antenna in free space in different stages of slot creation in ground plane is shown in Figure 4.7. Case 0 plot curve represents the return loss of the circular patch antenna with solid ground plane and slotted patch. When a horizontal slot is etched in the centre of the ground plane as shown in Figure 4.4(b), the resonant frequency of the antenna is shifted from 1.9 GHz to 1.5 GHz. This frequency shift is labelled as case 1 plot curve in Figure 4.7. Case 2 plot curve in Figure 4.7 is the return loss plot of the circular patch antenna when vertical slots are added in the middle of upper and lower half of the ground plane and in the lower left side of the ground plane. These slots are shown in Figure 4.4(c). The introduction of these slots in the ground plane has changed the resonant

curve but the value of the S11 is not less than -10 dB which is a standard condition for an antenna to resonate. The 915 MHz resonance is achieved by inserting two more vertical slots in lower left of the ground plane and one more vertical slot in upper right side of the ground plane as shown in Figure 4.4(d). Case 3 plot curve in Figure 4.7 shows the simulated return loss after the addition of these slots. It can be seen that the antenna is resonating at 915 MHz and 2.6 GHz but our frequency of interest is 915 MHz. After applying the miniaturization techniques and through extensive optimizations in CST Microwave studio, we have a miniature antenna with overall volume of  $\pi \times 4^2 \times 0.38$  mm<sup>3</sup>. The final design dimensions of the circular patch antenna obtained from CST Microwave Studio software are given in Table 4.1.

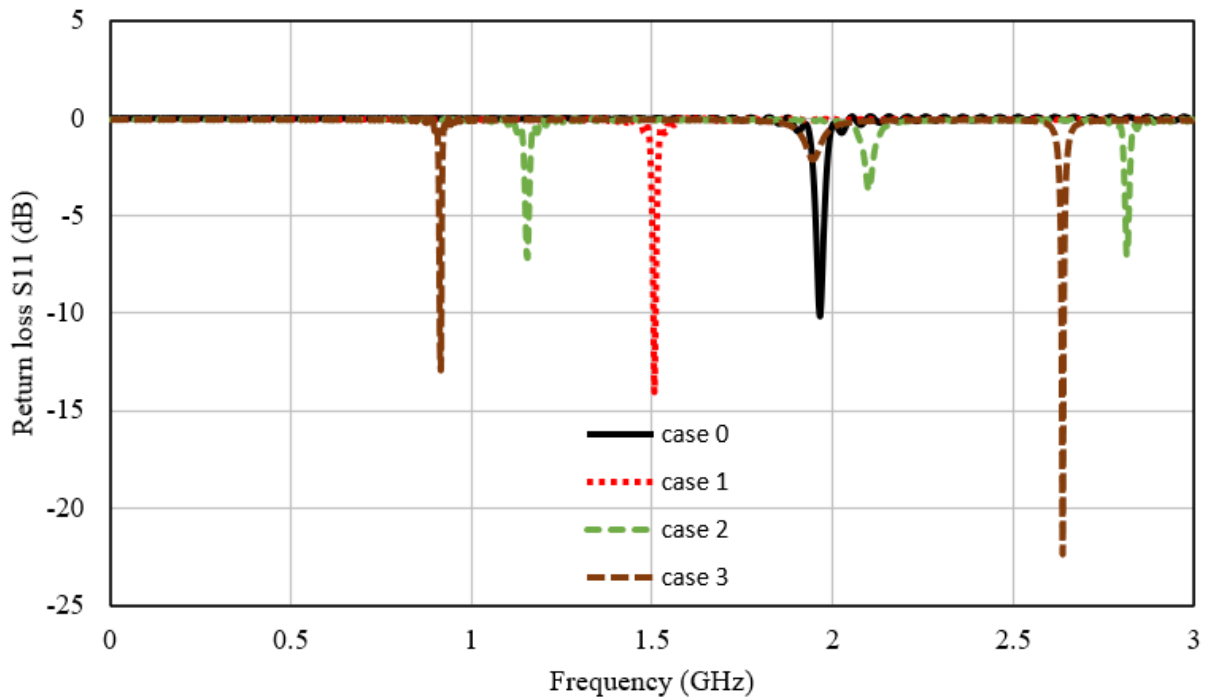


Figure 4.7- Simulated return loss plot of the circular patch antenna in free space in different stages of slot creation in the ground plane with slotted patch

The dimensions of the antenna impact the antenna resonant frequency and its performance. If the dimensions of the parameters in Table 4.1 are changed the circular patch antenna resonant frequency would shift to a higher or lower frequency band. If we increase the value of L, W, W1 and W4-W5 the resonant frequency will shift to higher frequency bands. Decreasing the values of these parameters will have the opposite effect. The resonant frequency of the antenna will shift to lower frequency band with an increase in values of the parameters W2-W3, L1 and L4-L12. The bandwidth of the circular patch

antenna becomes wider with a decrease in W6 and L2-L3 values. The bandwidth is not effected by the change in values of W2-W3. If we increase the values of L2-L3 and W6, the bandwidth of the antenna would become narrow.

Table 4.1- Circular patch antenna dimensions

Parameter	Dimensions (mm)	Parameter	Dimensions (mm)	Parameter	Dimensions (mm)
L	0.7	L7	3.23	W1	1.5
L1	0.9	L8	3.4	W2	4.4
L2	4.6	L9	1.7	W3	0.55
L3	0.3	L10	3.55	W4	0.5
L4	1.85	L11	3	W5	0.3
L5	0.7	L12	2.85	W6	0.25
L6	3.5	W	4	W7	5.7

We aim to design this antenna to resonate at 915 MHz to be used for the implants inside the skin layer. We have implanted the circular patch antenna inside the simplified skin layer phantom to test its performance in implantable conditions as shown in Figure 4.8. The dimensions of the simplified skin layer phantom of the human body are  $(\pi \times 35^2 \times 30)$  mm. The electrical properties of human skin tissue layer at 915 MHz are  $\epsilon_r = 41.6$  and  $\sigma = 0.87$  S/m [129]. The 30mm height of the phantom seems unrealistic but literature has been followed for the design process. In [15] a 30 mm height of the human body phantom is used for antenna simulation. The implantable antennas presented in [71],[79] and [129] are designed using the phantom height of 60 mm, 20 mm and 45 mm. So, we have used a 30 mm height of the skin layer phantom in our antenna design.

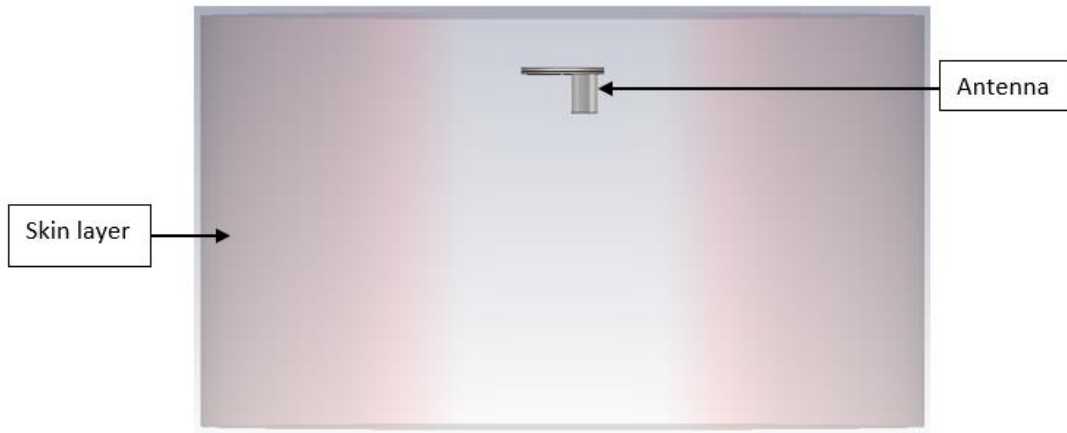


Figure 4.8- Block representation of circular patch antenna in simplified skin layer phantom

The simulated return loss plot of the circular patch antenna in free space and in skin layer phantom is shown in Figure 4.9. It is evident from Figure 4.9 that the return loss at 915 MHz is -13 dB in free space which shows that the antenna is operating at this frequency whereas the antenna is not working in skin layer. The bandwidth of the antenna in free space is 5 MHz at an operating frequency of 915 MHz. As explained in chapter 2, different human body tissues have different conductivity and permittivity at different frequencies. Moreover, the implantable antennas are application dependent whether the application is for skin, fat, muscle, brain, stomach, bone or any other type. The circular patch antenna design was optimized to operate in skin layer of the human body.

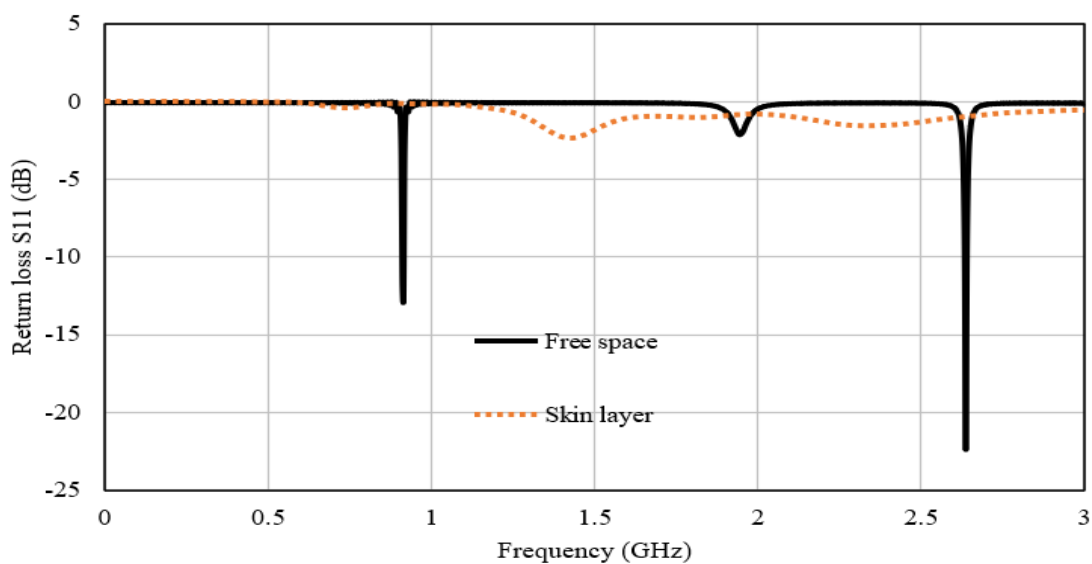


Figure 4.9- Return loss of the circular patch antenna in free space and in skin layer phantom

#### 4.2.1 Circular Patch Antenna Optimization

The circular patch antenna was optimized to operate in skin layer at 915 MHz. Following changes are made in the above design for optimization.

- The position of shorting pin was changed from  $P = (X = -0.5; Y = -0.7)$  to  $P = (X = -1; Y = 1)$ .
- The width of the slot W4 was changed from 0.5mm to 0.3mm.
- Slots with length L7, L9 and L10 were removed.
- The length of slot L11 was reduced from 3mm to 2.4mm.
- Slot L12 length was changed from 2.85mm to 2.4mm.

The simulated return loss of the circular patch antenna in simplified skin layer phantom after design optimization is shown in Figure 4.10. It can be seen in Figure 4.10 that the antenna resonates at 915 MHz with a -10 dB bandwidth of around 90 MHz. The bandwidth of the implantable antennas keeps changing if human body phantoms of different dimensions are used. The radiation efficiency of the antenna is -31.6 dB when simulated in skin layer phantom at 915 MHz.

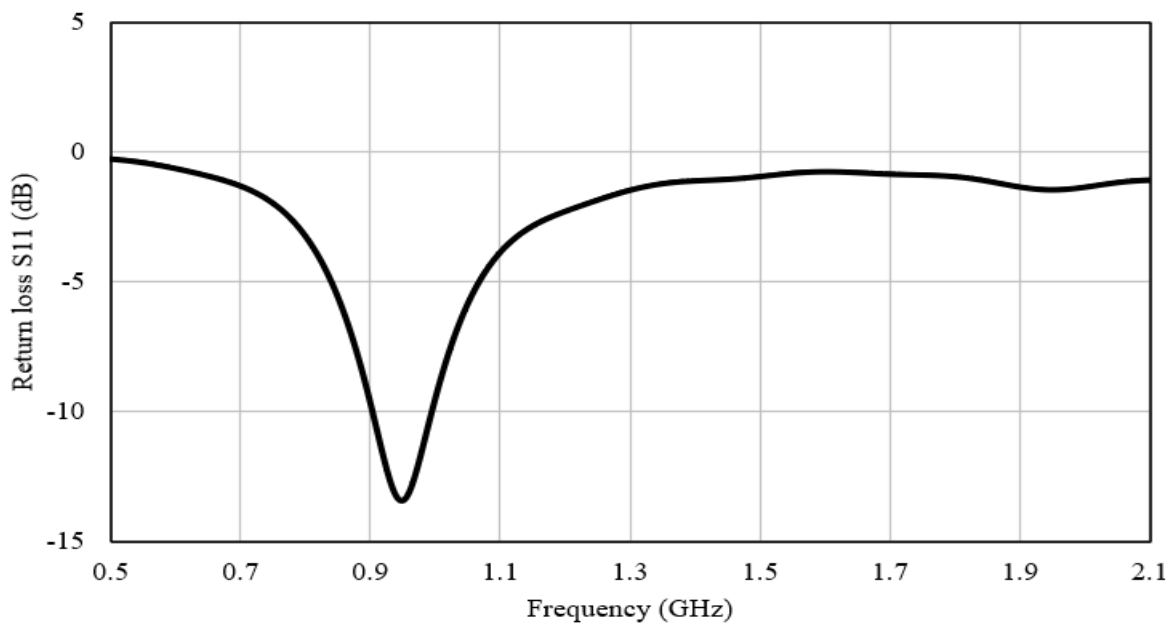


Figure 4.10- Return loss of the circular patch antenna in skin layer phantom after design optimization  
The 3D radiation pattern of the antenna is given in Figure 4.11. The radiation pattern and skin layer phantom are set to be transparent in Figure 4.11 to show the antenna inside radiation pattern diagram.

The radiation pattern of the antenna gets changed when implanted inside the phantom due to power absorption, reflection or diffraction from the tissue boundaries. The dimensions of phantom and antenna orientation has also effect on antenna performance. This antenna has a directivity of 3.2 dBi with a peak realized gain of -28.8 dBi.

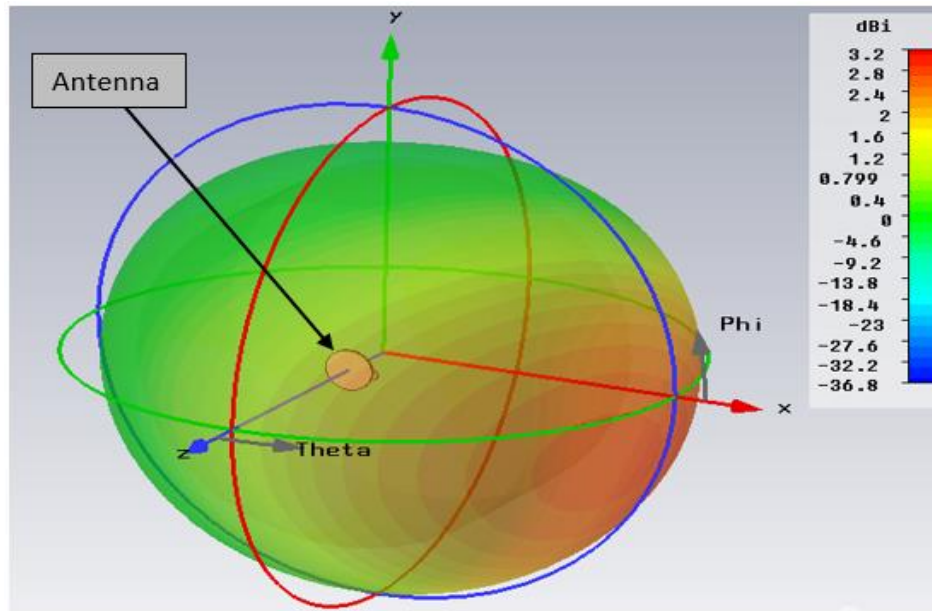


Figure 4.11- 3D radiation pattern of the circular patch antenna in skin layer phantom at 915 MHz

The E-plane (electric field plane) of an antenna is defined as the plane which contains the electric field vector and direction of maximum radiation whereas the H-plane (magnetic field plane) is defined as the plane which contains the magnetic field vector and direction of maximum radiation. The H-plane lies at 90 degrees to the E-plane [113]. Figure 4.12(a) shows the E-plane radiation pattern of the circular patch antenna at 915 MHz. The magnitude of main lobe of radiation is 3.12 dBi. Main lobe direction is 69 degrees with 3 dB angular width of 194.4 degrees. The H-plane radiation pattern of the circular patch antenna is shown in Figure 4.12(b). It is evident from the graph that the magnitude of main lobe of radiation is 1.5 dBi with an angle of 3 degrees. The 3 dB angular width of main lobe of radiation is 174.8 degrees.

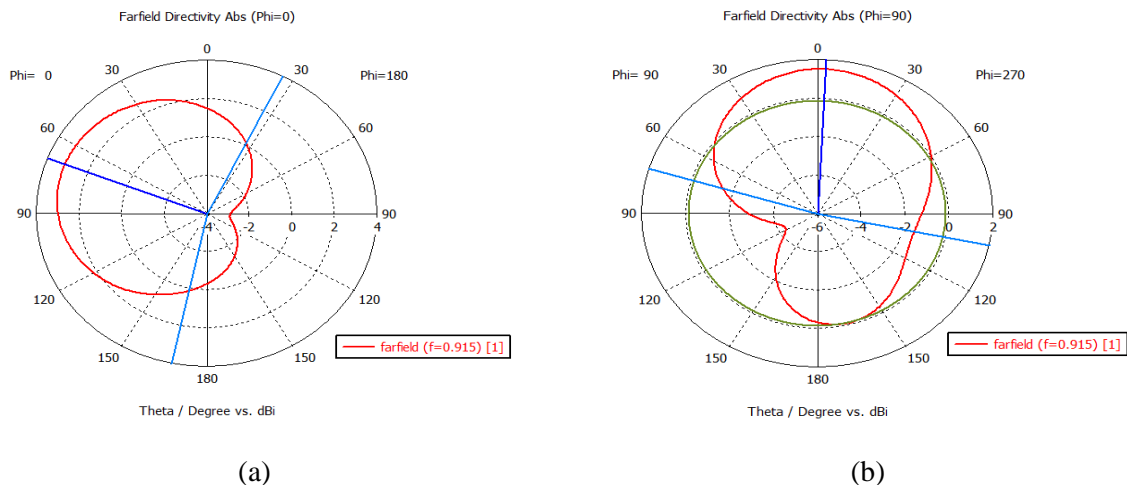


Figure 4.12- Polar plot of radiation pattern of the circular patch antenna in skin layer phantom at 915 MHz (a) E-Plane (b) H-Plane

When an antenna is implanted inside the human body, the antenna power is absorbed by the body tissues because of their lossy nature. The power absorption in tissues is different at different frequencies. A large amount of absorbed power by the body tissues will damage them. There are two standards for SAR to protect the human body tissues from harmful electromagnetic radiations. SAR should be less than 1.6 w/kg averaged over 1g cubic volume of tissue according to IEEE C95.1-1999 standard and 2 w/kg averaged over 10g cubic volume of the tissue according to IEEE C95.1-2005 standard [6]. The 1g and 10g SAR graph of the circular patch antenna is given in Figure 4.13.

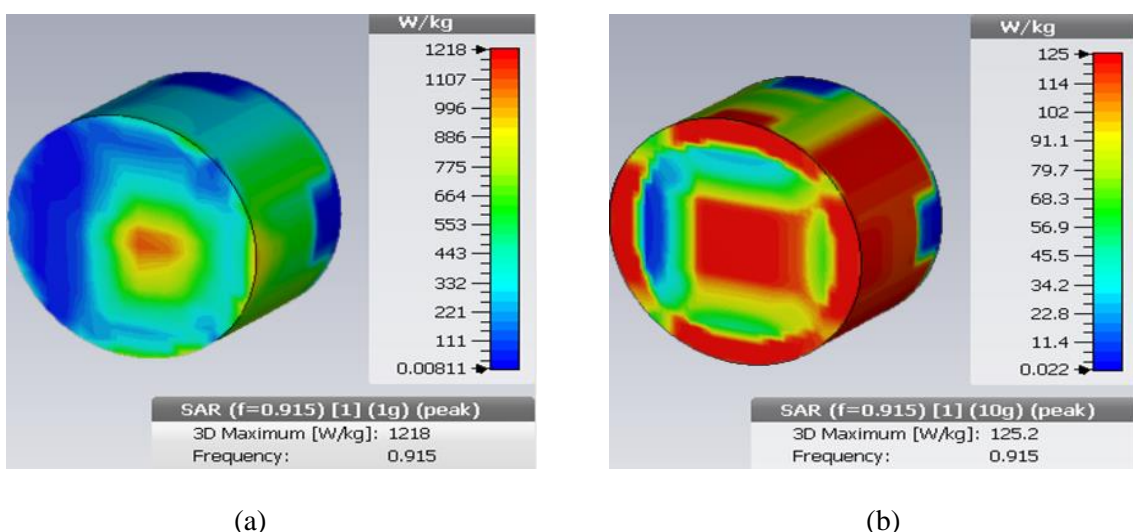


Figure 4.13- Circular patch antenna SAR in skin layer phantom at 915 MHz (a) 1g avg. (b) 10g avg.

It can be seen in above Figure 4.13 that the 1g avg. SAR is 1218 W/Kg and 10g avg. SAR is 125.2 W/Kg at 915 MHz when the input power of the antenna was 0.5W. These SAR values seems higher than the standards specified. To meet the SAR requirements for 1g avg. the maximum allowed input power of the antenna should be limited to 1.3 mW and for 10g avg. the maximum allowed input power should be limited to 16 mW [130]. Hence the SAR values for this antenna are within allowable limits.

#### 4.2.2 *Parametric Study of Circular Patch Antenna*

The antenna parameters are of great importance when analysing its performance. In the proposed antenna design we have used a superstrate layer on the top of patch as well which is not very common in conventional antenna design that are to be used either on-body or for outer body applications. The purpose of using superstrate layer is to prevent the direct contact between the human body tissues and the radiating element which is patch in this design. The superstrate layer minimizes the harmful effect of electromagnetic radiations. To make the implantable antennas resonate on a lower frequency by keeping their size compact is very difficult because the resonant frequency and the size of antenna are inversely proportional to each other. The larger the size of the antenna the lower the resonant frequency will be and vice versa.

A high value of the dielectric constant of substrate material also helps to shift the frequency to a lower value. When we use the superstrate layer the dielectric constant of substrate and superstrate layer adds up and makes the antenna to resonate on a lower frequency. Another reason for using the high permittivity dielectric substrate and superstrate is to make the antenna biocompatible. The human body tissues have high permittivity values, so if the antenna substrate and superstrate have high value of permittivity then the antenna will be more biocompatible. Slots are etched in the patch in this design. The purpose of slots is to make a physically small antenna an electrically large antenna as the slots elongate the current path. Slots also help to adjust the resonant frequency. The electric and magnetic field path is disturbed by the slots and the point at which their magnitude become maximum they leave the patch generating a frequency of resonance. The slots in the ground plane helps to lower the resonant frequency and to improve the antenna bandwidth. The thickness of substrate and superstrate also effect the antenna performance. A higher value of thickness of substrate or superstrate layer would yield into

a higher frequency, but a lower value of thickness would have an opposite effect on resonance. The purpose of shorting pin is to minimize the resistance of the patch which was increased because of slots. The shorting pin also helps to lower the resonant frequency.

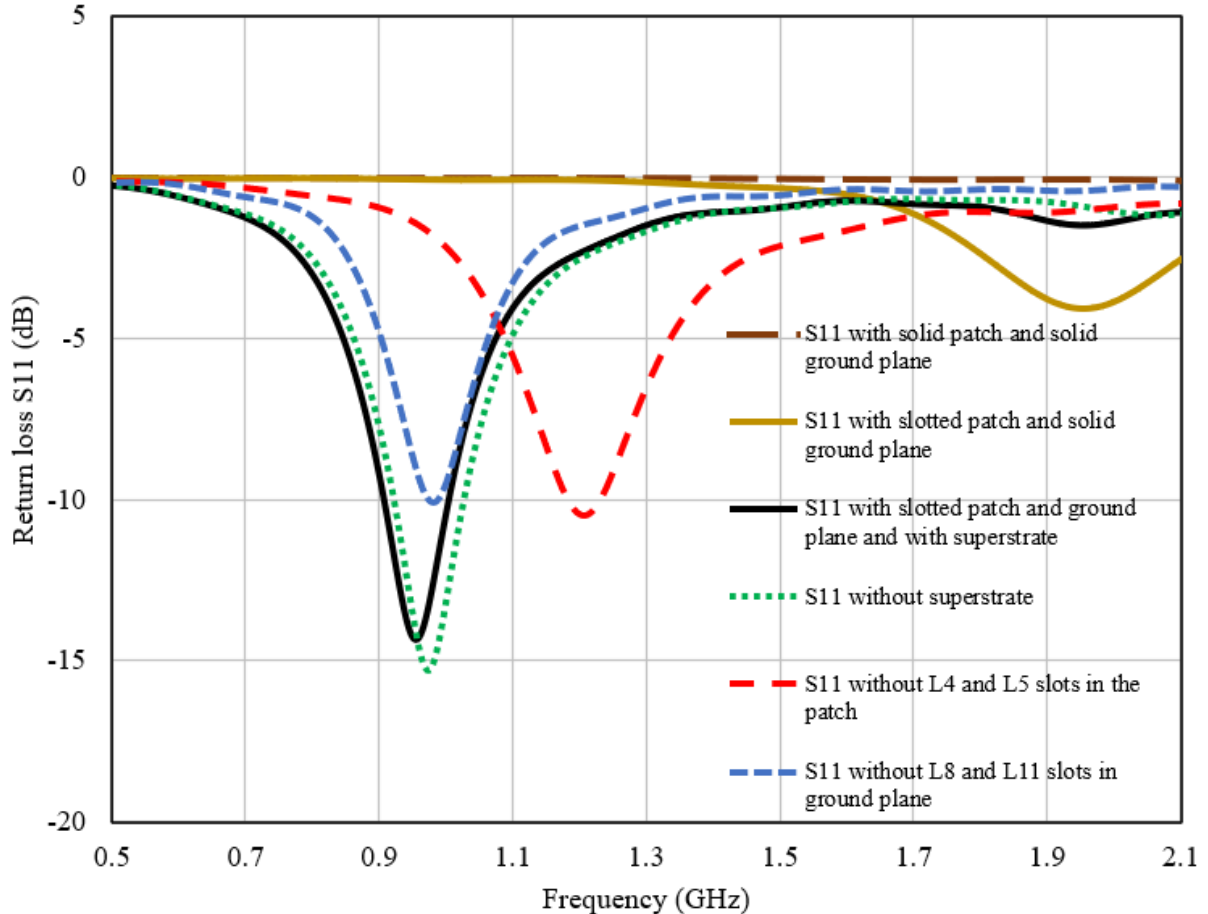


Figure 4.14-Return loss of the circular patch antenna in skin layer phantom with changing parameters  
The return loss plot of the antenna with different changing parameters is given in Figure 4.14. It can be seen in Figure 4.14 that the antenna is not resonating on any frequency with solid patch and ground plane. The antenna resonates at 915 MHz when slots are inserted in patch and ground plane. The resonant frequency of the circular patch antenna is shifted to a higher value and the value of S11 was increased from -14 dB to -10.5 dB when the slots L4 and L5 were removed from patch. The removal of slots L8 and L11 causes a minor shift in the frequency but the value of S11 has increased from -14 dB to -10 dB. The absence of superstrate layer also shows a shift in frequency.

The comparison of the circular patch antenna with similar designs presented in literature is given in Table 4.2. The size of the designed circular patch antenna is smallest than all of the antennas presented

in Table 4.2. The gain of the proposed circular patch antenna is higher than the gain of the antenna in [129] at 915 MHz. The gain of some of the antennas is higher than our designed antenna but they operate at higher frequency and they have large size. As the small size antennas have narrow bandwidth, so our designed antenna has a narrow bandwidth. But in comparison with the other antennas, their bandwidth is not wider as it should be because of their large dimensions. The SAR values of our designed circular patch antenna seems higher but they were calculated when the input power of the antenna was 0.5 W. Because of the small size of the antenna, the maximum allowed power of the antenna should be limited. In comparison with similar antennas in Table 4.2, the circular patch antenna has a size reduction of around 15% with an overall performance improvement of 9%.

Table 4.2- Circular patch antenna comparison with previous work

Reference	Antenna volume( $\text{mm}^3$ )	Frequency (GHz)	Gain (dBi)	Bandwidth (MHz)	SAR(W/Kg)	
					1g	10g
[71]	$\pi \times 5^2 \times 1.27$	2.45	-22.7	303.8	508	-
[77]	$\pi \times 5.35^2 \times 1.34$	0.402; 2.45	-41; -21.3	165; 681	666,676	-
[79]	$\pi \times 7.5^2 \times 1.92$	0.4035; 0.4339; 2.45	-	114; 260	239.5; 159.4	38.21; 34.75
[129]	$\pi \times 4.7^2 \times 1.27$	0.915	-32.8	112	778	-
This work	$\pi \times 4^2 \times 0.38$	0.915	-28.8	90	1218	125.2

### 4.3 Rectangular Patch Antenna

The designed circular patch antenna is a miniaturized antenna with improved performance. However, the circular patch antenna cannot be further miniaturized. The size reduction in circular patch antenna would cause a frequency shift to a higher value and to adjust the resonant frequency, more slots need to be added in the patch and ground plane. The circular patch antenna has already slots in the patch and ground plane. The addition of more slots will decrease the antenna efficiency. A shorting pin has already

been inserted between patch and ground plane of the circular patch antenna to lower the antenna operating frequency. So, more shorting pins cannot be used in the design. Because of these challenges, a rectangular patch was selected to design a smaller size antenna with improved performance. The rectangular patch gives more ease to apply miniaturization techniques because of its geometry. The rectangular patch antenna is designed to be used for the implants in fat layer. To start the rectangular patch antenna design following equations are used as a reference [113],[131]. However, the final antenna dimensions are obtained through optimizations in CST Microwave Studio Software.

$$W = \frac{C}{2f_r \sqrt{\frac{\epsilon_r+1}{2}}} \quad (4.3)$$

Where  $W$  is the width of patch in mm.  $C$  is the speed of light and its value is  $300 \times 10^9$  mm/s.  $f_r$  is the resonant frequency of 2.4 GHz and  $\epsilon_r$  is the dielectric constant of the substrate with a value of 10.2. The effective dielectric constant ( $\epsilon_{eff}$ ) and effective length ( $L_{eff}$ ) of the patch are calculated to take into account the fringing effect in the patch antenna.  $L_{eff}$  consists of actual physical length ( $L$ ) and the incremental length ( $\Delta L$ ) of the patch which is introduced by fringing effect. The value of  $\epsilon_{eff}$ ,  $L_{eff}$ ,  $\Delta L$  and  $L$  is given by following equations [113],[131].

$$\epsilon_{eff} = \frac{\epsilon_r+1}{2} + \frac{\epsilon_r-1}{2} \left\{ \frac{1}{\sqrt{1+\frac{2h}{W}}} \right\} \quad (4.4)$$

$h$  is the height of the substrate which is 0.25 mm.

$$L_{eff} = \frac{C}{2f_r \sqrt{\epsilon_{eff}}} \quad (4.5)$$

$$\Delta L = h \times 0.412 \left\{ \frac{(\epsilon_{eff}+0.3)(\frac{W}{h}+0.264)}{(\epsilon_{eff}-0.258)(\frac{W}{h}+0.8)} \right\} \quad (4.6)$$

$$L = L_{eff} - 2\Delta L \quad (4.7)$$

By solving the equations (4.3)-(4.7), we get the length and width of the patch of patch as 19.5 mm and 26 mm. These dimensions are very large for an antenna to be used with implantable sensors. Extensive optimizations have been carried out by applying different miniaturization techniques to reduce the size

of the rectangular patch antenna. The miniaturization techniques used are the slotted patch and ground plane, use of high permittivity dielectric substrate and the shorting pin loading. The antenna is designed by using Rogers RT6010 ( $\epsilon_r = 10.2$ ;  $\tan\delta = 0.0023$ ) substrate. The superstrate layer is also used for human body tissue safety and to lower the operating frequency. The superstrate layer material and thickness are same as substrate. Copper cladding is used for antenna ground plane and patch material. The antenna is excited by a 50-ohm microstrip line. Slots are etched in the patch to elongate the current path which makes physically small antenna an electrically large antenna. Multiband operation of the antenna is also achieved with the help of slots in the patch. The insertion of slots in the patch introduces more electrical resistance which is reduced by a shorting pin P ( $X = -1.05$ ;  $Y = 1.45$ ). The shorting pin also helps to lower the operating frequency. Slots are also introduced in the ground plane to adjust the resonant frequency and to achieve the wider bandwidth. The overall size of the antenna is  $(6 \times 5 \times 0.5)$  mm<sup>3</sup>.

The slotted patch and ground plane of the rectangular patch antenna are shown in Figure 4.15(a) and (b). Figure 4.16(a) and (b) shows the rectangular patch antenna patch and ground plane with labelled parameters whereas Figure 4.17 shows the rectangular patch antenna perspective view. The simulated antenna design is placed inside a  $(180 \times 180 \times 50)$  mm<sup>3</sup> fat layer box as represented in Figure 4.18 to analyse the antenna performance. The rectangular patch antenna detail dimensions obtained from CST Microwave Studio software are presented in Table 4.3.

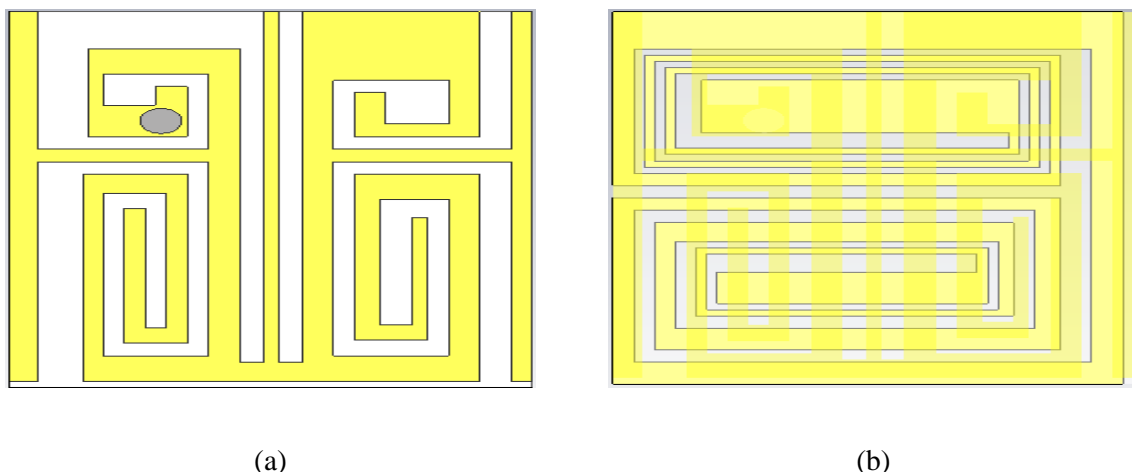


Figure 4.15- (a) Rectangular patch antenna patch view (b) Rectangular patch antenna ground plane view

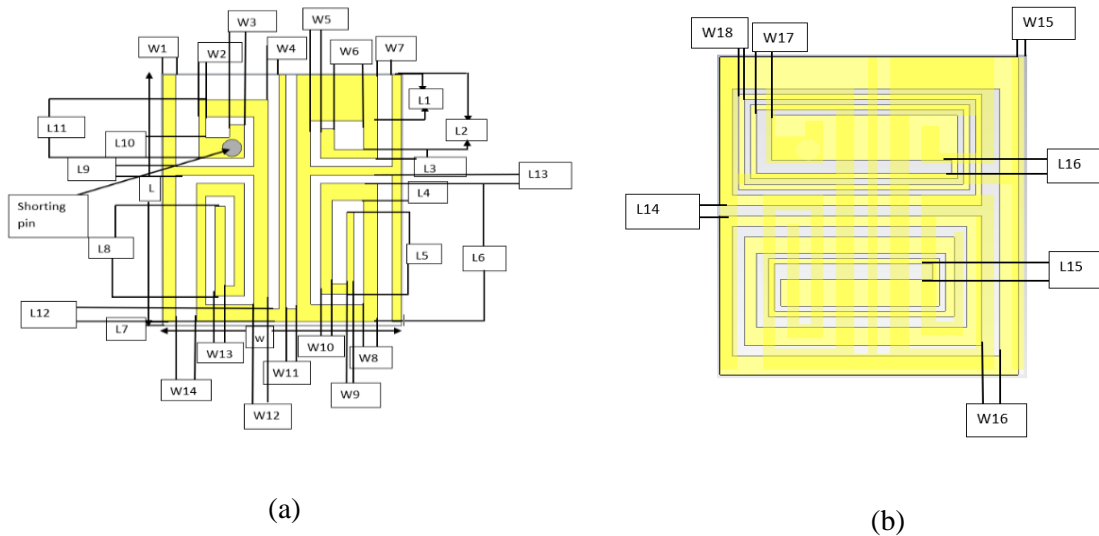


Figure 4.16- (a) Rectangular patch antenna patch with labelled parameters (b) Rectangular patch antenna ground plane with labelled parameters

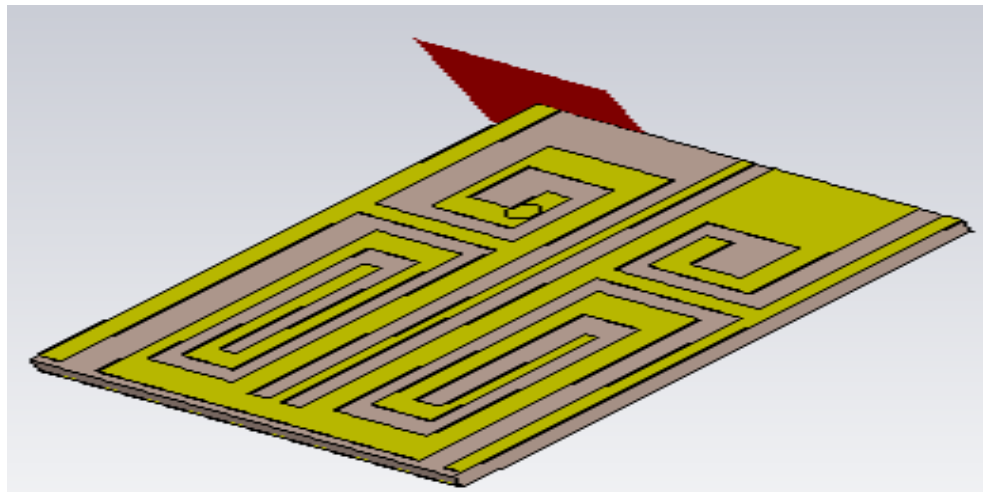


Figure 4.17- Rectangular patch antenna perspective view

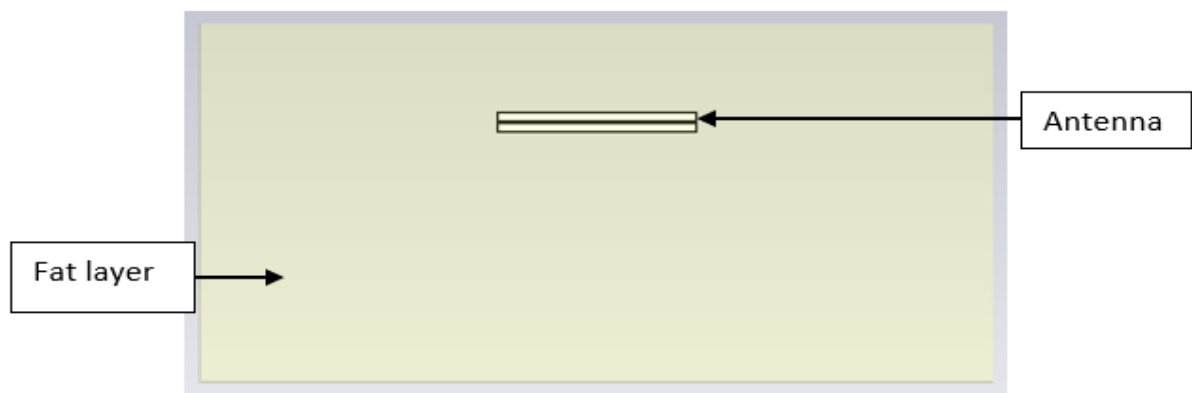


Figure 4.18- Block representation of rectangular patch antenna inside fat layer phantom

Table 4.3- Rectangular patch antenna detailed dimensions

Parameter	Dimensions(mm)	Parameter	Dimensions(mm)	Parameter	Dimensions(mm)
L	6	L12	0.3	W7	0.3
L1	1.1	L13	0.2	W8	0.3
L2	2	L14	0.2	W9	0.15
L3	0.2	L15	0.3	W10	0.25
L4	0.4	L16	0.25	W11	0.2265
L5	1.7	W	5	W12	0.3
L6	2.9	W1	0.275	W13	0.2
L7	0.1	W2	0.15	W14	0.425
L8	2.15	W3	0.3	W15	0.1
L9	0.2	W4	0.226	W16	0.3
L10	0.5	W5	0.2	W17	0.25
L11	1.4	W6	0.6	W18	0.1

The antenna dimensions impact the antenna resonant frequency and its performance. The change in parameters dimensions in Table 4.3 will have the effect on the resonant frequencies of the rectangular patch antenna. The rectangular patch antenna is designed to operate at three frequencies of 402 MHz, 915 MHz and 2.4 GHz. If we increase the values of W4-W5, L7 and L9 the resonant frequency of 402 MHz will shift to higher frequency band. The resonant frequency of 402 MHz will shift to lower frequency band with an increase in values of W2, L5-L6 and L16. The -10 dB bandwidth of rectangular patch antenna at 402 MHz will increase with an increase in values of W3, W7, W11 and L2 while an increase in values of W15, L11 and L15 will increase the bandwidth at 915 MHz. The bandwidth at 2.4 GHz will increase with increase in values of L12 and W17. The decrease in values of these parameters would have the opposite effect. If the value of W9, W13, W18 and L14 is increased, it will shift the 915 MHz resonant frequency to higher frequency band. The 915 MHz frequency will be shifted to a lower frequency band with an increase in values of L3, W8 and W12. Similarly, increasing the values of W10,

W16, L1 and L10 will shift the 2.4 GHz frequency to higher frequency band while this frequency will shift to a lower frequency band with an increase in values of W6, W14, L4 and L8.

The return loss of the antenna in fat layer phantom is shown in Figure 4.19. It can be seen in the graph that the antenna is resonating at 402 MHz, 2.1 GHz and 2.43 GHz and the antenna has narrow bandwidth around these frequencies in free space. When the antenna was implanted inside the fat layer the return loss plot changed because of the lossy nature of the medium. In fat layer the resonance curve shows that at 402 MHz the frequency has a downward shift but it still covers the desired frequency band from (328-436) MHz. The frequency has shifted to a lower value in the lower ISM band generating 915 MHz band (0.91-1.08) GHz. In higher ISM band the antenna resonates at 2.4 GHz (2.32-2.57) GHz. The bandwidth of the antenna depends on many factors such as size of the phantom, depth of the implant and orientation of the antenna etc. The -10 dB bandwidth of rectangular patch antenna at 402 MHz is 108 MHz, at 915 MHz is 170 MHz and at 2.4 GHz is 250 MHz.

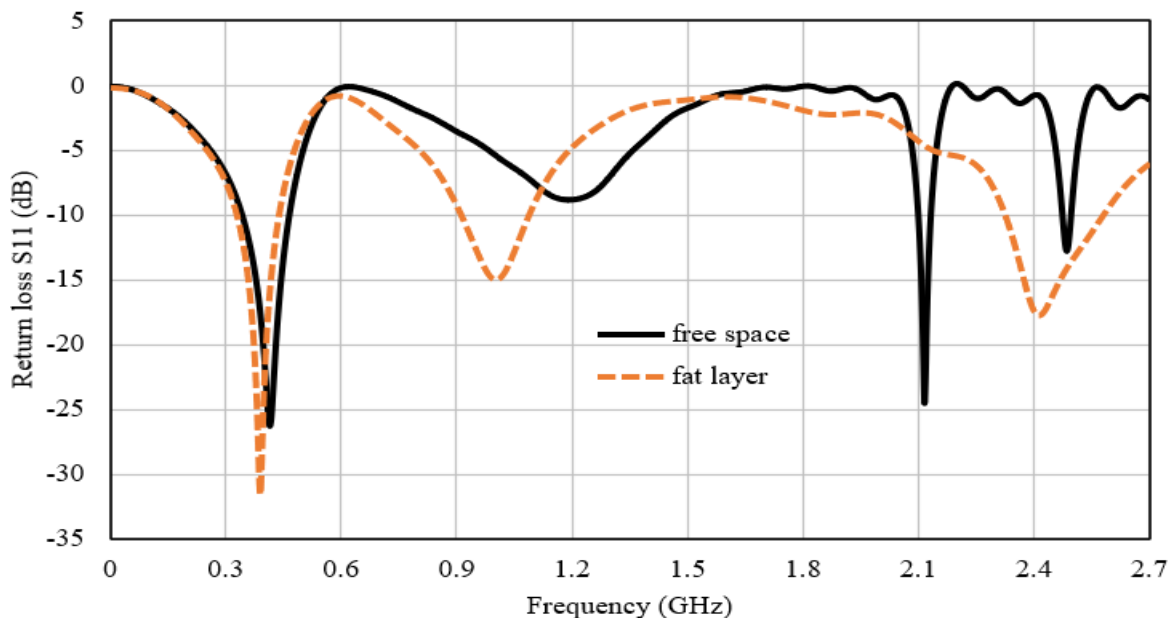


Figure 4.19- Return loss of the rectangular patch antenna in fat layer phantom

Figure 4.20 shows the 3D radiation pattern of the rectangular patch antenna when implanted inside simplified fat layer phantom. The directivity of the antenna at resonant frequencies is 1.94 dBi, 5.34 dBi and 6.41 dBi. As we approach the higher frequencies the value of directivity is increasing. The gain of the rectangular patch antenna at resonant frequencies is -47.7 dBi, -37.2 dBi and -25.5 dBi. The radiation

efficiency of the antenna at relevant frequencies is -50 dB, -42 dB and -32 dB. The directivity and gain of the antenna increase with the increasing frequency because the electrical length of the antenna increases at higher frequencies. The lower frequency of operation in implantable antennas is preferred because the conductivity of body tissues increases with frequency. It is evident from Figure 4.22 and Figure 4.23 that the specific absorption rate has increased at higher frequencies. The higher frequencies of ISM band are used by other applications as well but MICS band is dedicated to implantable applications only. So, at higher frequencies the signals could be lost during data transmission and reception because of signal interference.

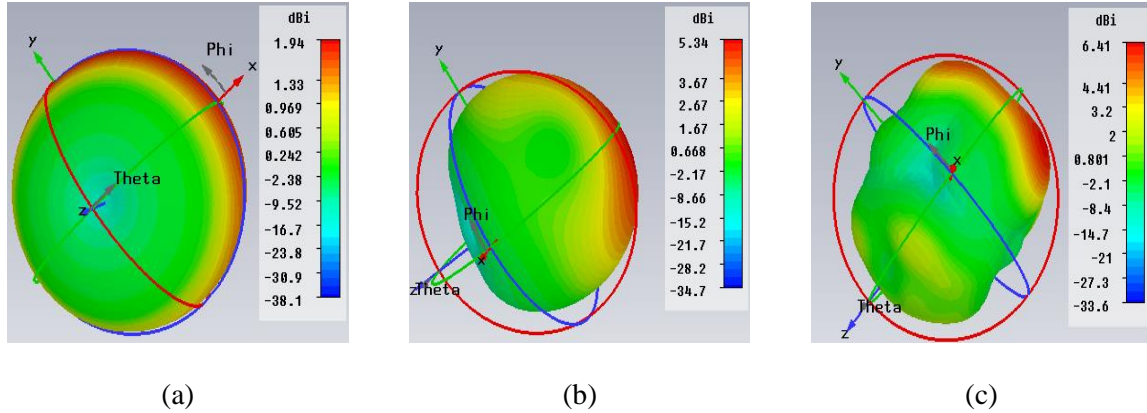


Figure 4.20- 3D radiation pattern of the rectangular patch antenna (a) 402 MHz (b) 915 MHz (c) 2.4 GHz

The E-plane and H-plane radiation pattern of rectangular patch antenna at resonant frequencies is given in Figure 4.21. The antenna has quite omnidirectional radiation pattern at resonant frequencies. The directivity of the antenna is different at different frequencies. Because of the antenna geometry the current distribution is similar across E and H-plane. This results in identical E and H-plane at single frequency in Figure 4.21 [132], [133].

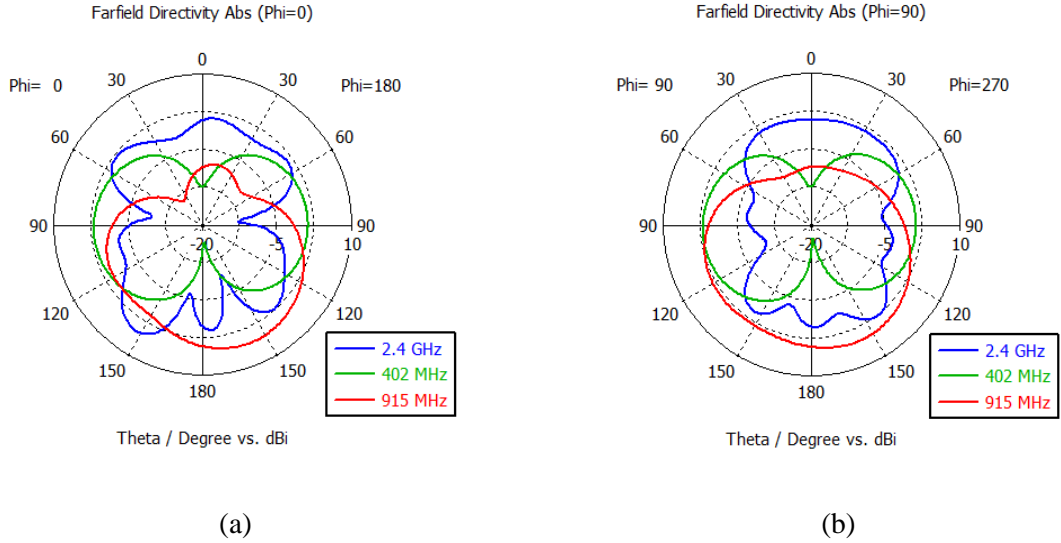


Figure 4.21- (a) E-plane radiation pattern of the rectangular patch antenna (b) H-plane radiation pattern of the rectangular patch antenna

The specific absorption rate (SAR) 1g avg. of the rectangular patch antenna at resonant frequencies is shown in Figure 4.22. At 402 MHz the 1g avg. SAR is 122.1 W/Kg, 183.7 W/Kg at 915 MHz and 862.6 at 2.4 GHz. These values were calculated with an input power of 0.5W. These values are higher than the standard 1.6 W/Kg [6]. To keep the SAR within allowed limits the input power of the antenna should be reduced. The maximum allowed input power of the antenna at 402 MHz should be 13 mW, 8.7 mW at 915 MHz and 1.85 mW.

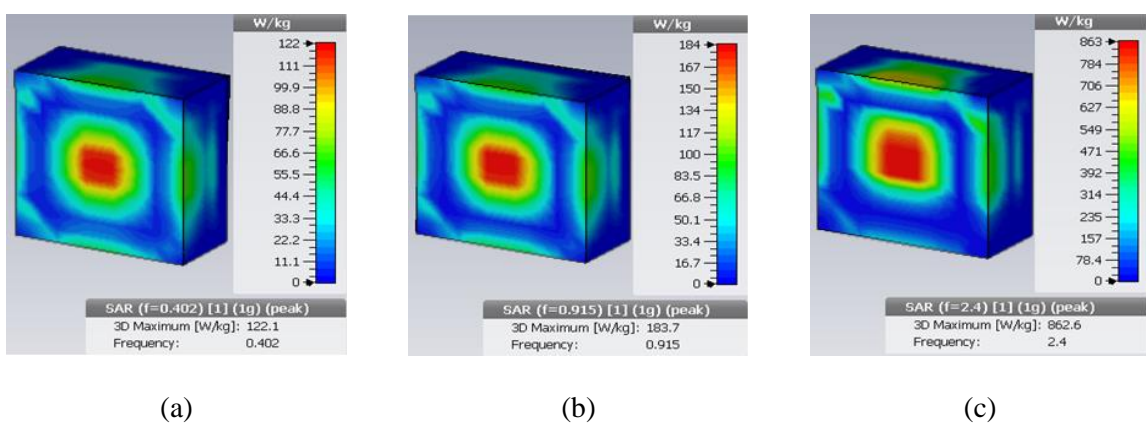


Figure 4.22- 1g avg. SAR of the rectangular patch antenna (a) 402 MHz (b) 915 MHz (c) 2.4 GHz

Figure 4.23 describes the 10g avg. SAR of the rectangular patch antenna at resonant frequencies. The 10g avg. SAR at 402 MHz is 12.25 W/Kg, 18.42 W/Kg and 86.42 W/Kg at 2.4 GHz provided that the input power of the antenna was 0.5W. The calculated SAR values are higher than the 10g avg. standard which is 2 W/Kg. To meet the SAR requirement the maximum allowed input power of the antenna

should be limited to 163 mW at 402 MHz, 108.6 mW at 915 MHz and 23 mW at 2.4 GHz. The SAR is more at higher frequencies because of the losses.

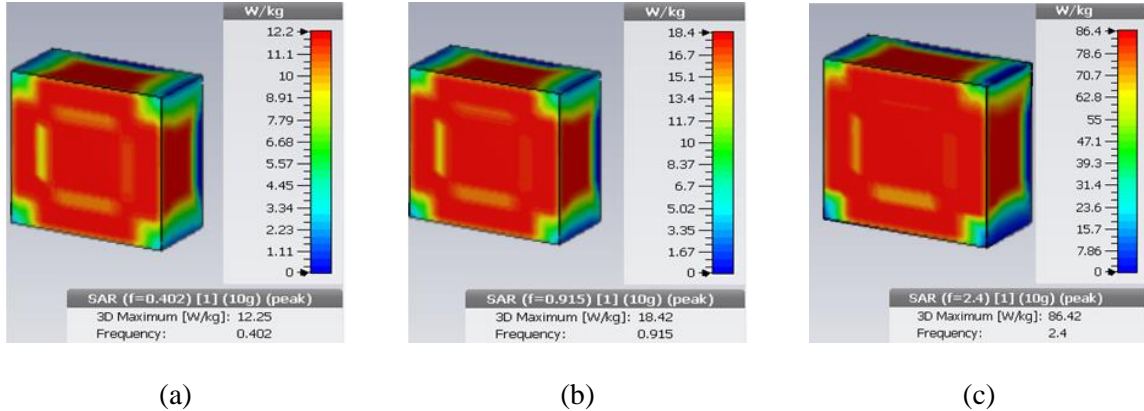


Figure 4.23- 10g avg. SAR of the rectangular patch antenna (a) 402 MHz (b) 915 MHz (c) 2.4 GHz

#### 4.3.1 Rectangular patch antenna parametric study

The antenna parameters effect its resonating frequency and performance. The above designed antenna is a microstrip patch antenna. The width of microstrip line has a huge impact on impedance matching. If the width of line is too large it will bring the line impedance to a lower value and vice versa. So, the feed line should be designed carefully to match the impedance to the standard characteristics impedance of  $50\text{-}\Omega$ . A poorly matched antenna does not perform well in free space and when it is implanted inside the body tissues its performance will be more degraded. The thickness of the superstrate and substrate play an important role for frequency adjustment and gain improvement.

A thick substrate layer will shift the resonant frequency to a higher value but it improves the gain. A thin cladding of substrate will have the opposite effect. The superstrate layer has not much effect on gain of the antenna. However, a high value of dielectric constant of superstrate material will shift the resonant frequency to a lower value. The position of shorting should be at optimum position to ensure the right resonance. The slots in the ground plane helps to improve bandwidth and to adjust resonant frequency. The slots in the patch help to generate more frequency bands. Figure 4.24 shows the effect of changing parameters on the return loss of the antenna.

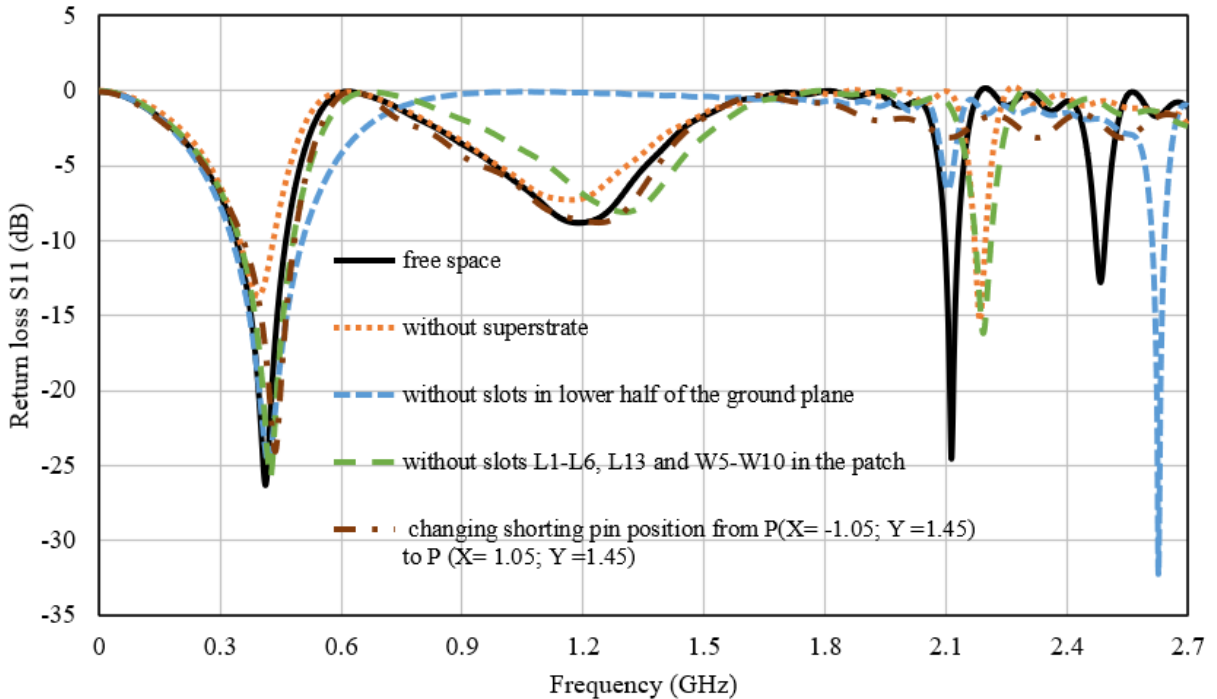


Figure 4.24- Return loss of the rectangular patch antenna with changing parameters

When the antenna was simulated without superstrate layer the resonance curve shows that the value of S11 has changed from lower to a higher value with a slight shift in frequency around MICS band. Without superstrate layer the antenna operates at two frequencies but with superstrate layer the antenna operates at three frequencies. When the slots are removed on the lower half of the ground plane the 402 MHz frequency is same but the higher ISM band frequency is shifted to a higher value. The effect of slots (L1-L6, L13, W5-W10) removal on the right half of the patch is also plotted in Figure 4.24. This effect is much similar to the results when antenna was simulated without superstrate layer but the value of S11 has changed from higher to a lower value around 402 MHz. When the shorting pin position was changed to the right side of the patch the antenna is resonating at only one frequency band.

The rectangular patch antenna comparative analysis with previous work is given in the Table 4.4. It can be seen that the designed rectangular patch antenna has smallest size than all of the antennas presented in Table 4.4. Our designed antenna operates in three frequency bands whereas the other antennas either operate at single band or dual band frequency. The gain of the antenna in [67] is lower than the gain of our designed antenna at 2.4 GHz. The gain of the other antennas is higher than the proposed rectangular patch antenna but they have larger dimensions. The bandwidth of our designed antenna is wider than

the antennas bandwidth in [11], [62] and [76]. At 402 MHz the antenna presented in [76] have higher 1g SAR value than our designed rectangular patch antenna. The 1g and 10g avg. SAR values of our designed antenna at 915 MHz are lower than the SAR values of the antenna presented in [62]. Although some of the antennas presented in Table 4.4 has one or two better performance parameters than our designed antenna but an overall size reduction of 29% is achieved in our antenna design with an overall performance improvement of 15%.

Table 4.4- Rectangular patch antenna comparison with previous work

Reference	Size(mm <sup>3</sup> )	$f_0$ (GHz)	Gain (dBi)	Bandwidth (MHz)	Shorting pin used	SAR (W/Kg)	
						1g	10g
[10]	11×11×2	2.4	-20.8	500	NO	356.4	-
[11]	10×10×0.65	2.45	-7.9	180	NO	136	-
[62]	8×6×0.5	0.915; 2.45	-28.5; -22.8	90; 210	NO	971.56; 807.34	118.26; 102.04
[67]	14.2×16.64×0.254	2.45	-29.1	780	NO	368.7	-
[76]	23×16.4×1.27	0.402	-34.9	52	YES	284.5	-
Proposed work	6×5×0.5	0.402; 0.915; 2.4	-47.7; -37.2; -25.5	108;170;250	YES	122; 184; 863	12.25; 18.42; 86.42

#### 4.4 Compact Size Antenna

We have designed the compact size patch antenna to be used for the implants in skin layer of the human body. To start the compact size antenna design we have used equations (4.3-4.7) as a reference. The length and width of the patch for a frequency of 915 MHz comes out as 51mm and 69mm by solving the equations (4.3-4.7). These dimensions are very large and need to be reduced to fulfil the requirement of a miniature antenna for implantable applications. We have used the shorting pin loading technique, slotted patch and ground plane and high permittivity dielectric superstrate to reduce the size of the

antenna. The final dimensions of the compact size antenna are obtained through optimizations in CST Microwave Studio software. The compact size antenna patch view is shown in Figure 4.25 and ground plane is shown in Figure 4.26. This antenna design includes 0.25 mm substrate layer of Rogers RT3010 ( $\epsilon_r = 10.2$ ;  $\tan\delta = 0.0023$ ).

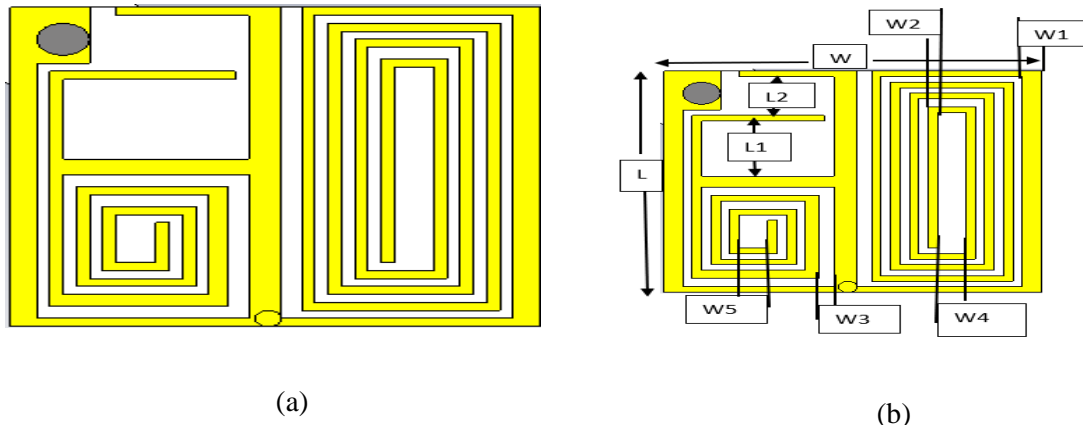


Figure 4.25- (a) Compact size antenna patch (b) Compact size antenna labelled patch

The superstrate layer is useful to protect the human body tissues from harmful radiation and to lower the operating frequency. The superstrate layer has a thickness of 0.05mm and its material is polyimide ( $\epsilon_r = 4.3$ ;  $\tan\delta = 0.004$ ). A 50-ohm coaxial probe is used to excite the antenna. The position of feed is p ( $x = -1.6$ ;  $y = 1.6$ ). Shorting pin is also used to further lower the frequency of the antenna p ( $x = -0.05$ ;  $y = -1.9$ ). The shorting pin also decreases the patch resistance. The copper cladding is used for patch and ground plane.

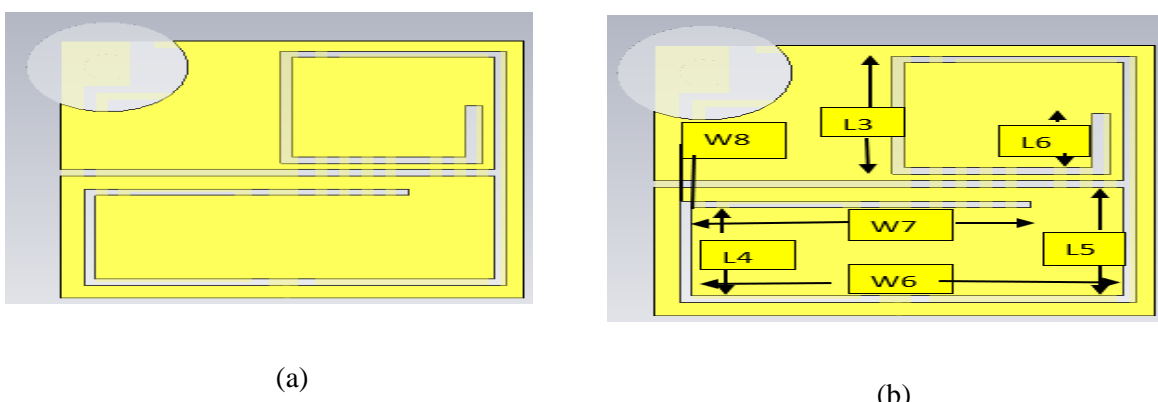


Figure 4.26- (a) Compact size antenna ground plane (b) Compact size antenna labelled ground plane

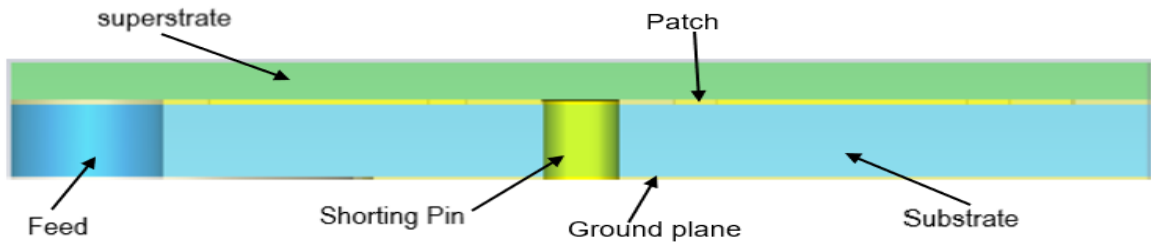


Figure 4.27- Compact size antenna side view

The size of the antenna is  $(4 \times 4 \times 0.3) \text{ } 4.8 \text{ mm}^3$ . The CST Microwave Studio software is used to design the antenna. The side view of the compact size antenna is shown in Figure 4.27. The antenna was simulated in skin box with dimensions of  $(110 \times 110 \times 28) \text{ mm}^3$  as shown in Figure 4.28. The rectangular patch antenna was simulated inside the fat layer phantom because it was designed for the implantable devices to be used inside the fat tissue layer of the human body. However, the compact size antenna is simulated inside the skin layer phantom because it is designed for the implantable devices to be used inside the skin tissue layer of the human body. The dimensions of antenna are given in Table 4.5.

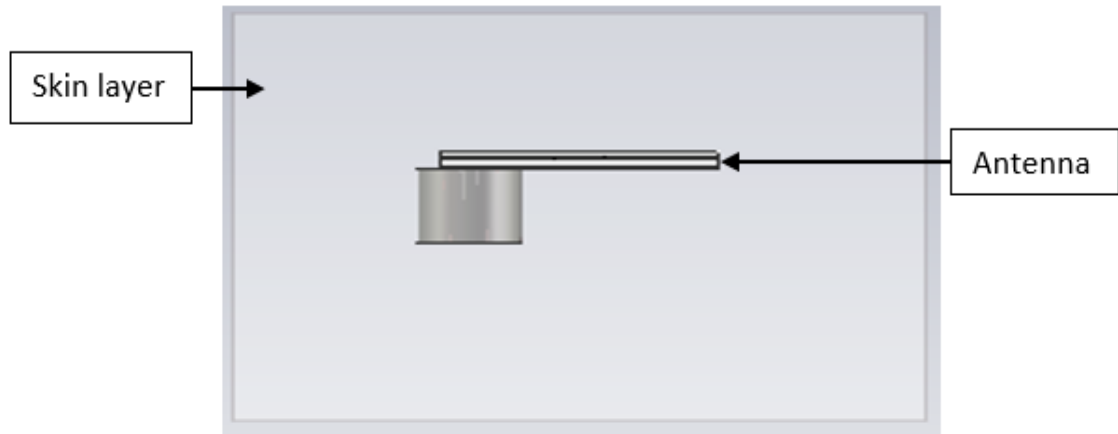


Figure 4.28- Block representation of compact size antenna inside skin layer phantom

Table 4.5- Compact size antenna dimensions

Parameters	Dimensions (mm)	Parameters	Dimensions (mm)	Parameters	Dimensions (mm)
L	4	L6	0.8	W5	0.4
L1	1	W	4	W6	3.45
L2	0.7	W1	0.2	W7	2.7
L3	1.5	W2	0.1	W8	0.1
L4	1.5	W3	0.15		
L5	1.6	W4	0.45		

Figure 4.29 shows the return loss of the compact size antenna in free space and in simplified skin layer phantom. It can be seen in the Figure 4.29 that the antenna is resonating at 915 MHz and 2.2 GHz in free space. However, our frequency of interest is 915 MHz. The resonant frequency of the compact size antenna has shifted downwards from 915 MHz to 800 MHz in skin layer phantom but it still covers the 915 MHz band. The radiation efficiency of this antenna in skin layer is -39 dB. To minimize the frequency shift the compact size antenna was optimized for better performance.

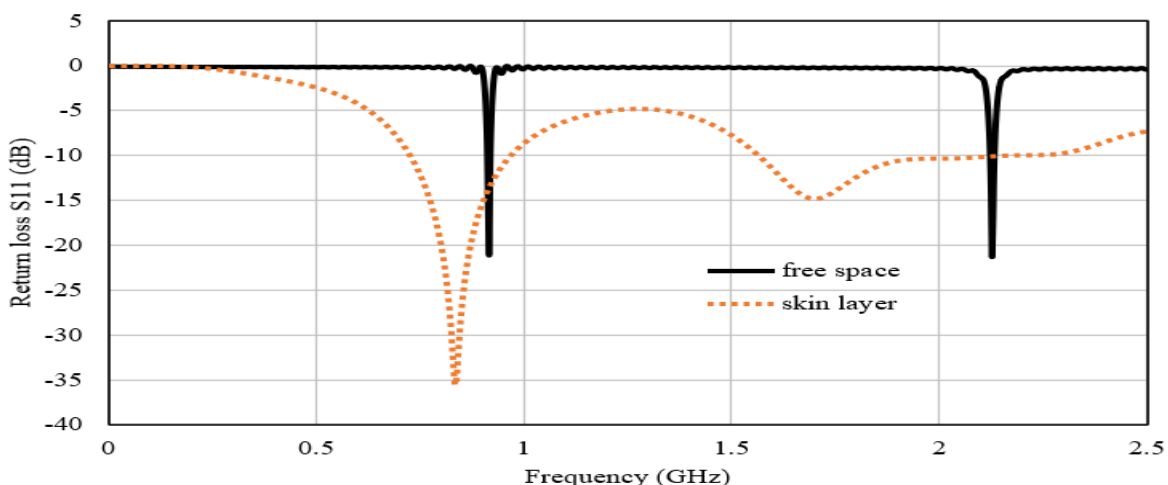


Figure 4.29- Return loss of the compact size antenna in free space and skin layer phantom

#### 4.4.1 Compact size antenna optimization

The compact size antenna design was optimized for the better performance and to adjust the operating frequency in implantable conditions. Optimized antenna patch and ground plane are shown in Figure 4.30 and Figure 4.31. The detailed dimensions of the optimized antenna design are given in Table 4.6.

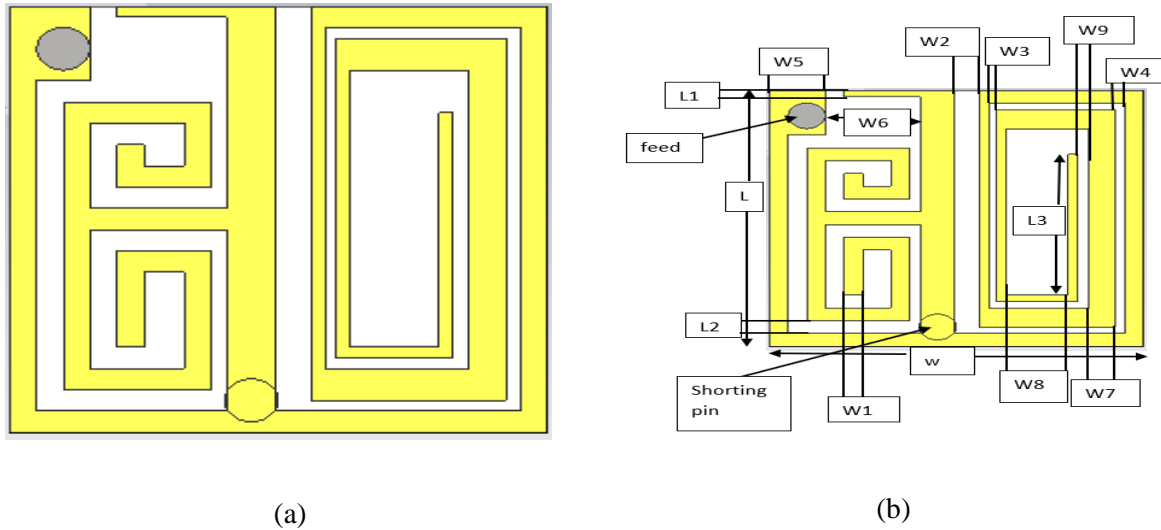
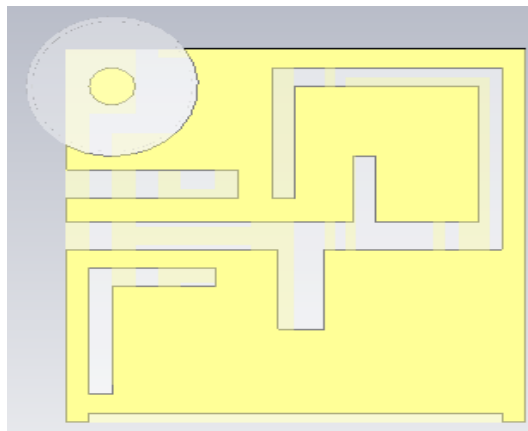


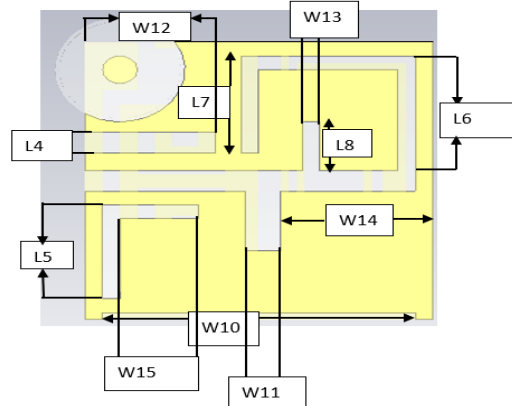
Figure 4.30- Compact size antenna optimized design (a) Patch view (b) Labelled patch view

Following changes were made in the above design.

- Thickness of substrate was changed from 0.25 mm to 0.13 mm.
- The superstrate material was changed from polyimide to Rogers RO3010 and its thickness was changed from 0.05 mm to 0.13 mm.
- Slots position and size was changed in the patch.
- Slots size and position was also changed in the ground plane.
- The position of shorting pin was changed from P ( $X= -0.05$ ;  $Y= -1.9$ ) to P ( $X= -0.2$ ;  $Y= -1.7$ ).
- The size of the antenna is  $4 \times 4 \times 0.26$  mm<sup>3</sup>.



(a)



(b)

Figure 4.31- Compact size antenna optimized design (a) ground plane view (b) Labelled ground plane view

Table 4.6- Compact size antenna optimized dimensions

Parameters	Dimensions (mm)	Parameters	Dimensions (mm)	Parameters	Dimensions (mm)
L	4	W	4	W9	0.12
L1	0.1	W1	0.2	W10	3.8
L2	0.2	W2	0.27	W11	0.4
L3	2.2	W3	0.08	W12	1.5
L4	0.3	W4	0.1	W13	0.2
L5	1.35	W5	0.6	W14	1.75
L6	1.65	W6	1.014	W15	1.55
L7	1.4	W7	0.28		
L8	0.7	W8	0.67		

The return loss of the optimized compact size antenna when simulated in simplified skin layer phantom is given in Figure 4.32. The antenna is resonating at 915 MHz and 1.6 GHz. The -10 dB bandwidth of the antenna around 915 MHz is 170 MHz. The radiation efficiency of the antenna at 915 MHz is -36.5 dB.

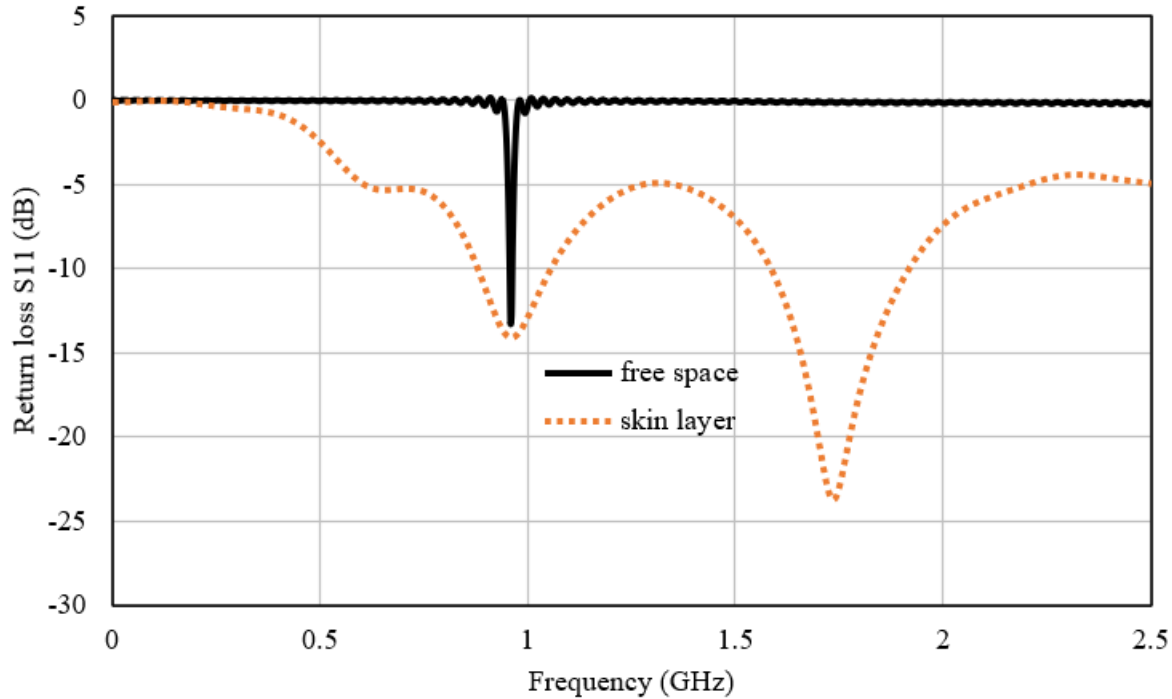


Figure 4.32- Return loss of the compact size optimized antenna

The 3D radiation pattern of the antenna is shown in Figure 4.33. The radiation pattern of the antenna gets changed when implanted inside the body tissues. Antenna has a directivity of 2 dBi. The IEEE gain of the antenna is defined as the ratio of radiation intensity of the antenna in a given direction to the radiation intensity that would be obtained if the power accepted by the antenna were radiated isotropically. The IEEE gain does not include any losses. On contrary, the realized gain is lower than the IEEE gain as it includes antenna impedance mismatch losses as well [134]. The realized gain of the antenna at 915 MHz is -34.7 dBi. The gain of the compact size antenna does not seem very high, however the design objectives have been met as the antenna has very small size with a wider bandwidth of 170 MHz.

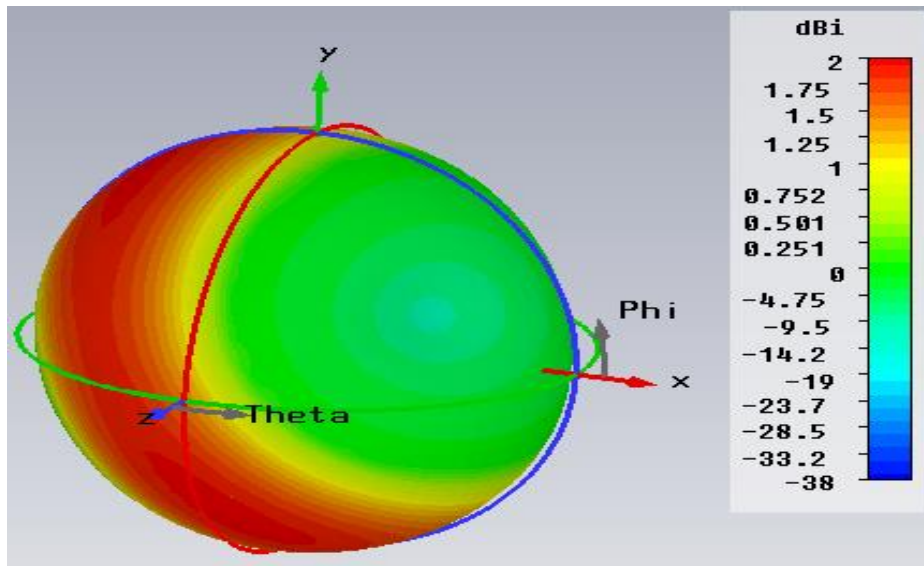


Figure 4.33- 3D radiation pattern of the compact size antenna at 915 MHz

E-plane and H-plane radiation pattern of the antenna at 915 MHz is given in Figure 4.34. The main lobe of radiation in E-plane has a magnitude of 1.89 dBi with a direction of 17 degrees. The 3dB angular width of main lobe of radiation is 97.6 degrees. The side lobe level is -1.2 dB. The H-plane radiation pattern at 915 MHz has main lobe direction around 30 degrees. The magnitude of main lobe of radiation is 1.99 dBi at 915 MHz in H-plane.

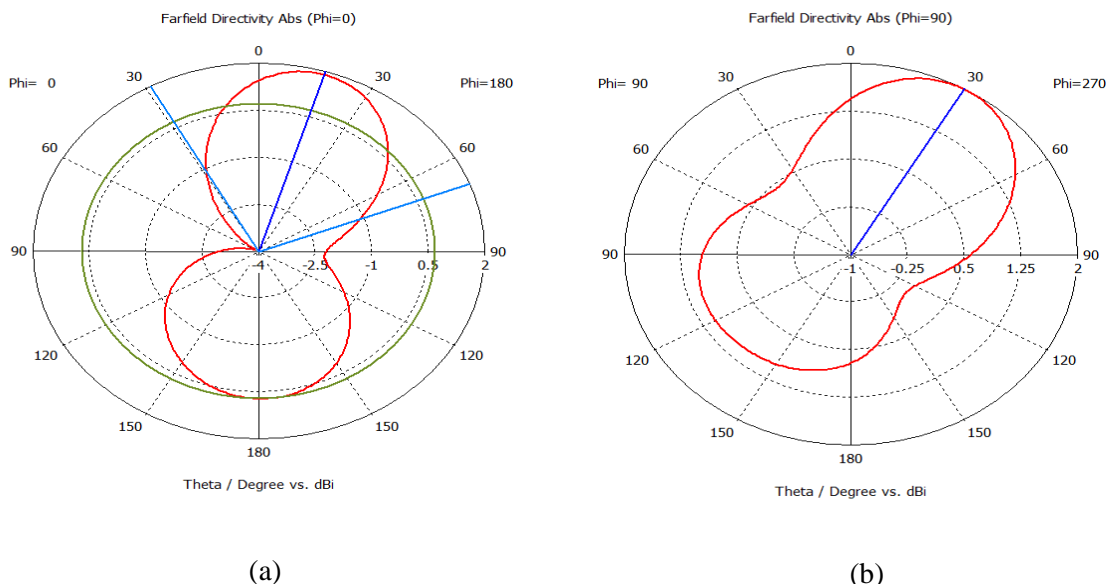


Figure 4.34- Polar plot of radiation pattern of the compact size antenna at 915 MHz (a) E-plane (b) H-plane

Figure 4.35 gives the 1g and 10g avg. SAR at 915 MHz for the compact size antenna in simplified skin layer phantom with an antenna input power of 0.5W. The 1g avg. SAR is 1069 W/Kg and 10g avg. SAR is 108 W/Kg which is higher than 1.6 W/Kg for 1g and 2W/Kg for 10g [6]. To meet the SAR requirements the maximum allowed input power of the antenna should be reduced. The maximum allowed input power at 915 MHz for this antenna should be limited to 1.4 mW to satisfy 1g avg. SAR standard and 18.5 mW for 10g avg. SAR standard.

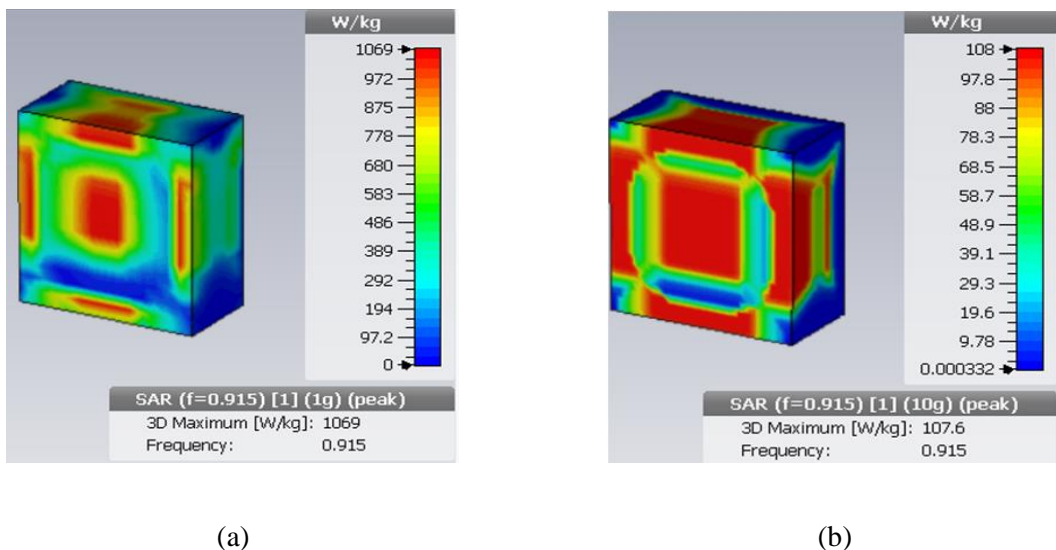


Figure 4.35- Compact size antenna SAR at 915 MHz (a) 1g avg. (b) 10g avg.

#### 4.4.2 Parametric study of compact size antenna

The antenna performance is dependent on its parameters. Figure 4.36 gives the compact size antenna return loss when it was simulated with changing parameters. When the thickness of the superstrate layer was increased from 0.13 mm to 0.25 mm the value of S11 was changed from -14 dB to -11 dB at 915 MHz and the higher band frequency was shifted from 1.6 GHz to 2 GHz. Because of the increase in superstrate layer thickness, the realized gain of the compact size antenna was decreased from -34.7 dBi to -45 dBi and the radiation efficiency of the antenna was decreased from -36.5 dB to -47 dB. If the thickness is decreased the frequency will shift to a lower value.

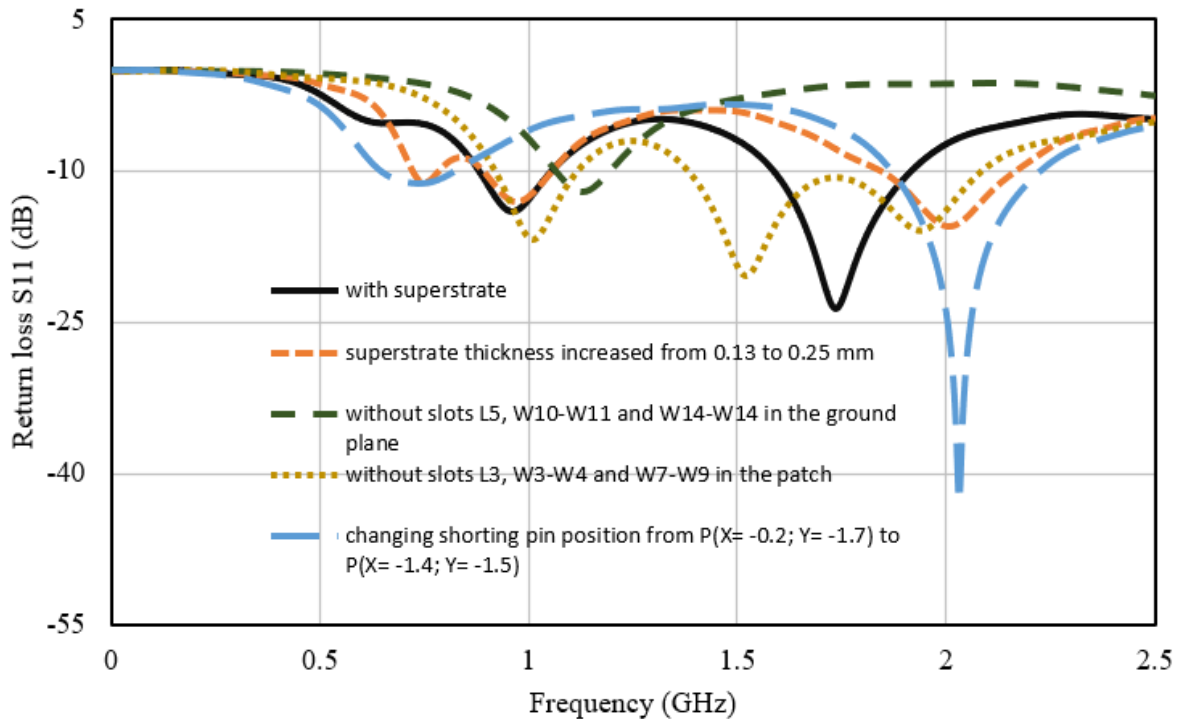


Figure 4.36- Return loss of compact size antenna with changing parameters

The removal of slots (L5, W10-W11, W14-W15) from the bottom half of the ground plane make the antenna to resonate on a higher frequency in lower ISM band with increased return loss. The slots in the ground plane have major impact on resonance and bandwidth. It can be seen in the Figure 4.36 that when the slots (L3, W3-W4, W7-W9) from the right half of the patch were removed the resonance curve has changed. With this effect the antenna is resonating around 1 GHz and -10 dB bandwidth of antenna in the upper band has increased (1.4-2.1 GHz). The shorting pin effect the resonant frequency as well. When the position of shorting pin was changed from  $P(X = -0.2; Y = -1.7)$  to  $P(X = -1.4; Y = -1.5)$  the return loss plot shows that the antenna is now resonating at 700 MHz with a return loss of -11 dB while the higher resonating frequency of 2.05 GHz has lower return loss of around -42 dB. The antenna comparison with previous work is given in Table 4.7.

Table 4.7- Compact size antenna comparison with previous work

Reference	Size(mm <sup>3</sup> )	$f_0$ (GHz)	Gain(dBi)	Bandwidth (MHz)	Shorting pin used	SAR (W/Kg)	
						1g	10g
[8]	13×13×1.27	0.915	-32	245	YES	599	-
[62]	8×6×0.5	0.915; 2.45	-28.5; -22.8	90; 210	NO	971.56; 807.34	118.26; 102.04
[69]	34.5×5.8×0.15	0.915	-21	81	NO	150	27.5
[75]	15×15×1.27	0.915	-27	97	NO	517	-
[78]	11×11×1.27	0.915	-29	35	NO	-	-
This work	4×4×0.26	0.915	-34.7	170	YES	1069	108

Table 4.7 gives the comparison of the compact size antenna with other antennas operating at 915 MHz. Our designed antenna has smallest size than all of the antennas in Table 4.7. The gain of the antenna is lower than other antennas but they have larger dimensions. The bandwidth of our designed antenna is wider than all antennas in Table 4.7 except the antenna in [8]. At 915 MHz the 10g SAR value of our designed antenna is lower than the 10g SAR value of the antenna in [62]. Some of the performance parameters of the antennas presented in Table 4.7 are better than our designed compact size antenna. However, the compact size antenna offers a size reduction of 47% with an overall performance improvement of 12%.

The comparison of the designed antennas with each other is given in Table 4.8. The compact size antenna has the smallest overall volume of 4.16 mm<sup>3</sup>. The overall volume of circular patch antenna is 19.1 mm<sup>3</sup> whereas the overall volume of rectangular patch antenna is 15 mm<sup>3</sup>. The circular patch antenna and compact size antenna operate at single frequency while the rectangular patch antenna operates at three frequencies. The gain of the circular patch antenna is higher than the rectangular patch antenna and compact size antenna at 915 MHz but the compact size antenna gain at 915 MHz is higher than the gain of rectangular patch antenna at this frequency. The -10 dB bandwidth of circular patch

antenna is lowest among all of the designed antennas but the SAR values are the highest than the other two designed antennas.

Table 4.8- Comparison of the designed antennas with each other

Antenna Type	Size( $\text{mm}^3$ )	$f_0$ (GHz)	Gain(dBi)	Bandwidth (MHz)	Shorting pin used	SAR (W/Kg)	
						1g	10g
Circular patch antenna	$\pi \times 4^2 \times 0.38$	0.915	-28.8	90	YES	1218	125.2
Rectangular patch antenna	$6 \times 5 \times 0.5$	0.402;0.915; 2.4	-47.7; -37.2; -25.5	108;170;250	YES	122;184; 863	12.25; 18.42; 86.42
Compact size antenna	$4 \times 4 \times 0.26$	0.915	-34.7	170	YES	1069	108

#### 4.5 Chapter summary

A brief introduction about patch antenna and their advantages is given. Short discussion is made on overall chapter content. A circular patch antenna was designed. The antenna was simulated in free space and then implanted inside simplified skin layer phantom. The free space and implanted simulation results were compared. The antenna was not working in the skin layer. Optimization was carried out and steps were explained. Return loss plot of the optimized circular patch antenna when simulated inside simplified skin layer phantom dictates that this antenna performs well in implantable conditions at 915 MHz. Radiation pattern of the antenna is quite omnidirectional. The E-plane and H-plane radiation pattern of the antenna was discussed. The simulated results of the circular patch antenna were compared with the published work. The circular patch antenna has a size reduction of around 15% with an overall performance improvement of 9% as compared to the other antennas presented in Table 4.2 which makes it suitable for implantable sensors.

A rectangular microstrip patch antenna operating in MICS band at 402 MHz and ISM band at 915 MHz and 2.4 GHz was designed on a Rogers RO3010 substrate. Single layer of the simplified body phantom was used to evaluate the antenna performance in implantable conditions. The antenna was operating at two frequencies but when it was implanted inside the simplified fat layer phantom the resonance curve shows another operating frequency at 915 MHz. As the antenna results in the fat layer were better than those in free space the optimization was not needed in the free space design. The antenna bandwidth was measured at three frequencies and gain was calculated. The upper frequencies showed higher values of gain and bandwidth because of more losses at higher frequencies. SAR was also calculated at individual frequencies. The E-plane and H-plane radiation pattern of the antenna was critically analysed. The antenna comparison with other antenna shows that this antenna is the best choice where three frequency band operation is needed for data transmission, wakeup signal and wireless power transfer applications.

Design of a compact size antenna excited by  $50\text{-}\Omega$  coaxial probe feed was presented. The performance of the implantable antennas inside the human body tissues is unpredictable because of the lossy nature of the human body tissues. So, when the compact size antenna was placed inside the simplified skin layer phantom the antenna resonant frequency showed a downward shift. Optimization on the compact size antenna design was carried out. The substrate thickness was decreased and superstrate thickness was increased with material changed as well. The position and size of the slots was changed in the patch and ground plane. The electrical properties of the skin layer of the human body at 915 MHz are taken into account in the design process to minimize the frequency shift. Overall size of the antenna is  $4\times 4\times 0.26 \text{ mm}^3$ . The dimensions of the optimized antenna were presented separate from the original design. Simulation results in simplified skin layer phantom shows a good agreement between free space and implanted results as shown in Figure 4.32. The antenna operates in ISM band at 915 MHz and bandwidth, gain and SAR values are recorded at this frequency. E-plane and H-plane radiation pattern of the antenna shows that this antenna has quite omnidirectional radiation when simulated in simplified skin layer phantom. The antenna comparison with similar work was presented. The compact size antenna has a size reduction of around 47% with an overall performance improvement of 12% than the

other antennas given in Table 4.7 which justify the novelty of this work. All the simulations were carried out in a single layer tissue of simplified body phantom. Square shape phantoms were used for rectangular patch antenna and compact size antenna while the circular shape phantom was used for circular patch antenna. Implantable antennas are designed for the specific tissue layer of the human body because each tissue layer has different electrical properties. Circular patch antenna and compact size patch antenna were designed for the implants inside skin layer of the human body. So, their simulations were done in simplified skin layer phantom while the rectangular patch antenna was designed for the implants inside the fat layer of the human body and it was simulated inside the simplified fat layer phantom. The antenna performance can change if phantoms of different sizes are used and implantation depth is changed depending on the robustness of the antenna. If the antenna operating frequency is changed, the electrical properties of the human body tissues would also get changed. Because of this, the impact of phantom size and implant depth on antenna performance would vary with varying frequency. Detailed antenna performance evaluation in multilayer tissues, different implant depths, phantoms of different shapes and sizes and antenna robustness check is carried out in next chapter. All the simulation work is done using CST Microwave Studio software.

# Chapter 5

## 5. Performance Evaluation of Designed Antennas in Simplified Body Model and Anatomical Body Model

### 5.1 Introduction

Implantable antennas are application dependent and they are designed to operate in a specific tissue layer of the human body. Their performance will be different in the various human body tissues even in the same tissue layer at a different frequency. The simplified body phantom and full body phantom has also variations in the results obtained but they do not have very large differences. The size of the phantoms and their resolution also effect the antenna performance. The depth of the implant also plays an important role in antenna overall performance. The antenna integration with sensors circuit components can alter the resonance if not integrated properly. The insulation layer around antennas for biocompatibility is a major constraint for antenna operating frequency adjustment. Therefore, it is necessary to evaluate the antenna performance in multilayer tissues and different size phantoms by employing different implant depths and position of the antennas. The antenna should be checked with circuit equivalent components for integration check. Different thickness of insulation layer should be introduced to analyse its effect on antenna performance. This chapter is organized as follows.

Firstly, all of the designed antennas performance was analysed in multilayer tissues (skin, fat and muscle). The return loss and radiation pattern results are presented to compare the performance. After that the antennas simulation results are presented for different depths of implant in single tissue layer of the simplified body phantom. Different size phantoms are also used to evaluate antenna performance. The antenna integration with circuit equivalent components is explained and the effects of insulation layer on antenna performance are analysed. Finally, the antennas are simulated in anatomical body model to evaluate their performance.

## 5.2 Designed Antennas Performance in Multilayer Tissues

The block representation of simplified multilayer tissue phantom which is used for designed antennas performance evaluation is given in Figure 5.1. The electrical properties of different tissues of the human body at 402 MHz, 915 MHz and 2.4 GHz are given in Table 5.1 [89]. It can be seen in Table 5.1 that the electrical properties of body tissues are different at each frequency.

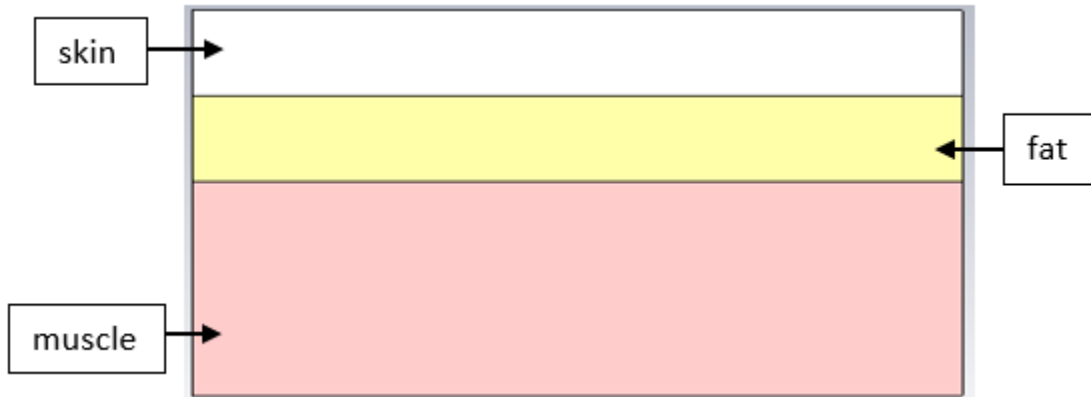


Figure 5.1- Block representation of simplified multilayer tissue phantom

Table 5.1- Electrical properties of human body tissues at different frequencies

Tissue layer	Conductivity( $\sigma=S/m$ )			Relative Permittivity( $\epsilon_r$ )		
	at 402 MHz	at 915 MHz	at 2.4 GHz	at 402 MHz	at 915 MHz	at 2.4 GHz
Skin	0.688	0.872	1.464	46.74	41.33	38.00
Fat	0.041	0.051	0.104	5.57	5.46	5.28
Muscle	0.796	0.948	1.739	57.11	54.99	52.73

### 5.2.1 Performance analysis of circular patch antenna in multilayer tissues

The circular patch antenna was simulated in simplified multilayer tissue (skin, fat and muscle) phantom. The return loss of the antenna in three layers of the human body phantom is shown in Figure 5.2. The resonance curve for the skin layer in Figure 5.2 is identical to the return loss of the circular patch antenna in Figure 4.10 because the resonance curve in Figure 4.10 is the return loss of the circular patch in single

tissue layer of the skin phantom. In the skin layer the circular patch antenna is resonating at 915 MHz. The resonance curve is shifted slightly to a lower value in the muscle layer, but it has gone to a higher value when antenna was simulated in fat layer. It can be seen in Table 5.1 that the conductivity of skin, fat and muscle tissues at 915 MHz is 0.872, 0.051 and 0.948 S/m while the permittivity of skin, fat and muscle at 915 MHz is 41.33, 5.46 and 54.99. The conductivity of skin and muscle tissues has minor difference but the conductivity of the fat tissue is much lower than skin and muscle tissues at 915 MHz. Similarly, the permittivity of the skin and muscle tissues has not very large difference whereas the permittivity of fat tissue is very low as compared to skin and muscle tissues at 915 MHz. Because of the small difference in electrical properties of skin and muscle tissues at 915 MHz, the resonance curve is almost identical in skin and muscle tissues. The bandwidth of the antenna has minor change.

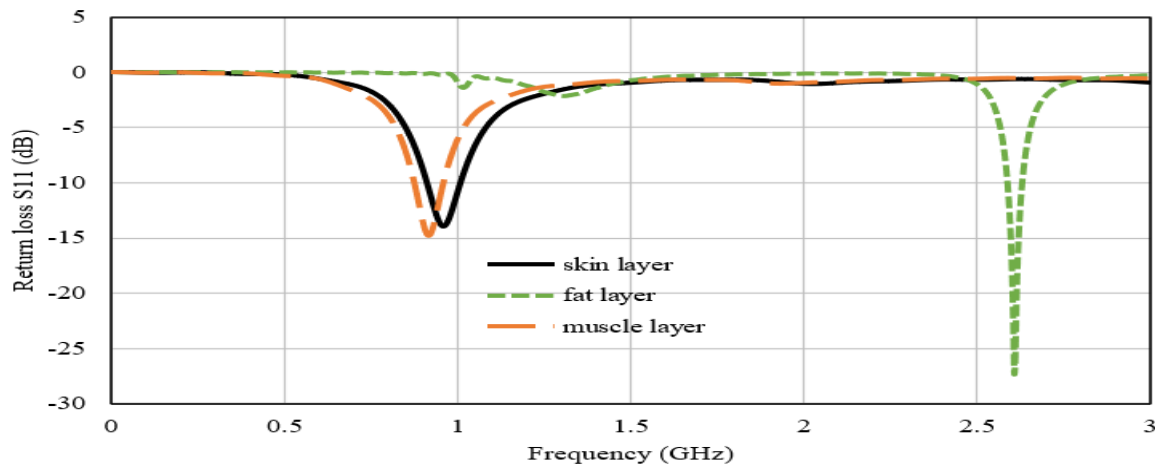


Figure 5.2- Circular patch antenna return loss in multilayer tissues (skin, fat and muscle)

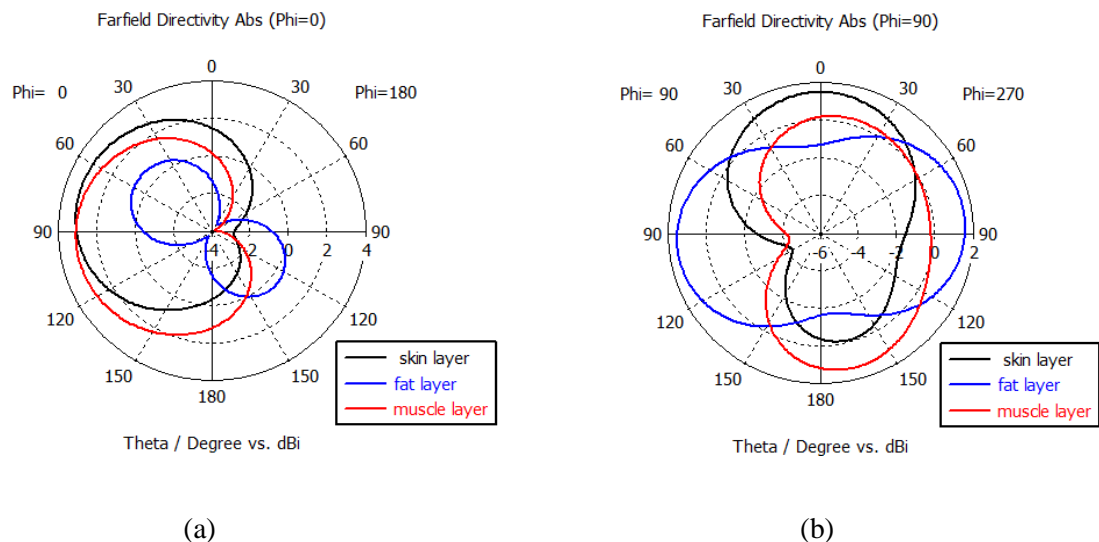


Figure 5.3- Polar plot of radiation pattern of the circular patch antenna in multilayer tissues (skin, fat and muscle) at 915 MHz (a) E-plane (b) H-plane

The E-plane and H-plane radiation pattern of the antenna at 915 MHz in skin, fat and muscle layer is shown in Figure 5.3. The circular patch antenna is designed to operate at 915 MHz for the implants inside the skin layer. The resonant frequency of the circular patch antenna has shifted to a higher value of around 2.6 GHz when simulated in fat layer. In Figure 5.3(a) the angle theta is constant and the value of angle phi is zero to show the E-plane radiation pattern whereas in Figure 5.3(b) the angle theta is constant and the value of angle phi is 90 to represent the H-plane radiation pattern. The directivity of the antenna is lowest in fat layer at 915 MHz as the antenna is not resonating at this frequency in fat layer. The directivity of antenna is approximately same at 915 MHz in skin and muscle layer. The peak realized gain of the antenna in skin layer is -28.7 dBi, -27.2 dBi in muscle layer and -47.8 dBi in fat layer at 915 MHz.

### 5.2.2 Performance analysis of rectangular patch antenna in multilayer tissues

Figure 5.4 shows the return loss plot of the rectangular patch antenna when it was simulated in skin, fat and muscle layer. The resonance curve for the fat layer in Figure 5.4 is identical to the resonance curve for the single tissue layer of the fat phantom in Figure 4.19 which shows that the antenna maintains its resonance for the fat layer in multilayer tissue phantom. The bandwidth of rectangular patch antenna is 880 MHz in skin layer, 260 MHz in fat layer and 720 MHz in muscle layer around 2.4 GHz.

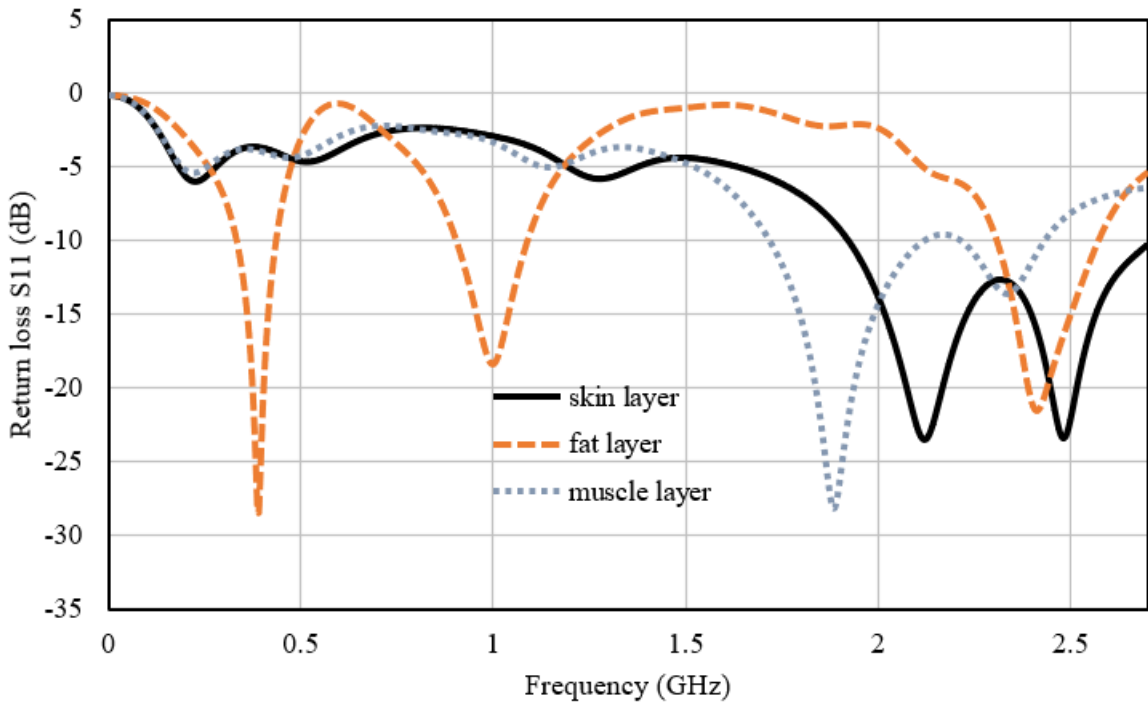


Figure 5.4- Return loss of the rectangular patch antenna in multilayer tissues (skin, fat and muscle)

The E-plane and H-plane radiation pattern of rectangular patch antenna in skin, fat and muscle layer at 2.4 GHz is given in Figure 5.5. The main lobe of radiation in E-plane in skin layer is 1.97 dBi, 2.48 dBi in muscle layer and 3.5 dBi in fat layer. The H-plane main lobe radiation magnitude is 2.35 dBi in skin layer, 3.53 dBi in fat layer and 2.19 dBi in muscle layer. The main lobe magnitude of radiation is higher in fat layer than both skin and muscle layer. The 3dB angular width of main lobe of radiation is approximately same for skin and fat layer in E-plane and H-plane but for the muscle layer the 3dB angular width of main lobe of radiation is wider than skin and fat layer in E-plane and H-plane. The directivity of the antenna at 2.4 GHz is highest in fat layer with a value of 3.62 dBi whereas the directivity in skin and muscle layer is 3.06 dBi and 3.29 dBi. Peak realized gain of the rectangular patch antenna at 2.4 GHz in skin layer is -30.8 dBi, -20.9 dBi in fat layer and -31.4 dBi in muscle layer.

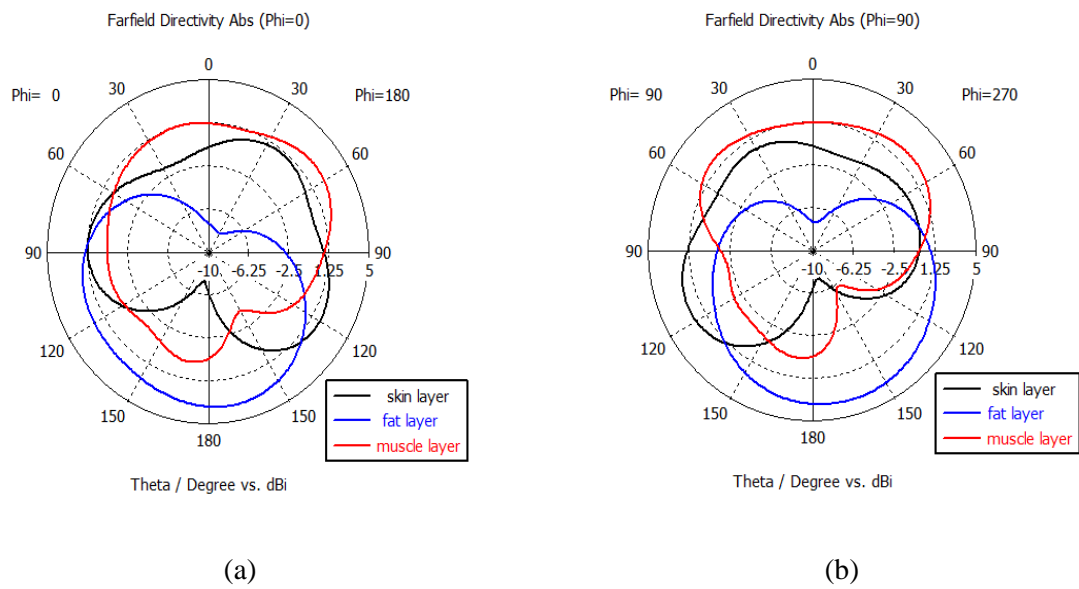


Figure 5.5- Polar plot of radiation pattern of the rectangular patch antenna in multilayer tissues (skin, fat and muscle) at 2.4 GHz (a) E-plane (b) H-plane

### 5.2.3 Performance analysis of compact size antenna in multilayer tissues

The return loss plot of the compact size antenna at 915 MHz in skin, fat and muscle layer is shown in Figure 5.6. It is evident from the return loss plot that this antenna is resonating at 915 MHz in skin, fat and muscle layer. It can be seen in Table 5.1 that there is a minor difference between the electrical properties of skin and muscle tissues at 915 MHz. So, the return loss plot curve inside skin and muscle layer is almost identical. The -10 dB bandwidth of the compact size antenna at 915 MHz in skin, fat and muscle layer is 18%, 2.18% and 17.48%. The bandwidth of implantable antennas become wider when implanted inside body tissues because of power absorption. The conductivity of skin and muscle layer at 915 MHz is greater than the conductivity of the fat layer at 915 MHz as given in Table 5.1. The bandwidth in fat layer is narrower because the fat layer absorbs less power due to its lower conductivity as compared to skin and muscle layer which absorb more power because of their higher conductivity and their bandwidth become wider.

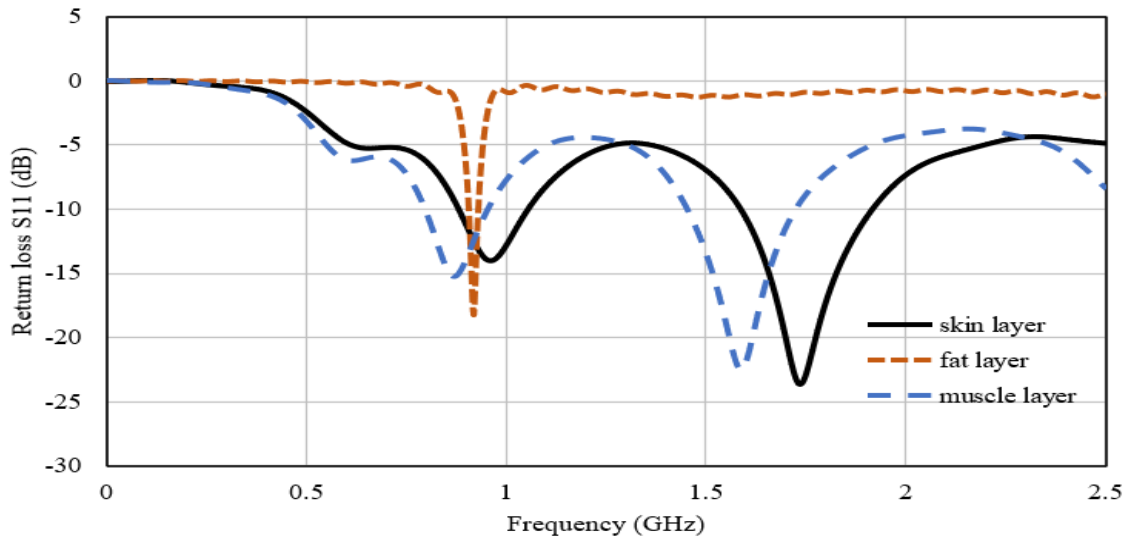


Figure 5.6- Return loss of compact size antenna at 915 MHz in multilayer tissues (skin, fat and muscle) The radiation pattern of the compact size antenna is shown in Figure 5.7. The skin layer and muscle layer radiation pattern are much similar to each other with minor variations. In E-plane the magnitude of main lobe of radiation for skin, fat and muscle layers at 915 MHz is 1.89 dBi, 1.92 dBi and 1.52 dBi. Whereas in H-plane the magnitude of main lobe of radiation for skin, fat and muscle layer is 1.99 dBi, 2.77 dBi and 2.07 dBi. The directivity of the antenna is lower in skin and muscle layer than in the fat layer. The directivity of the antenna in skin, fat and muscle layer at 915 MHz is 2 dBi, 2.79 dBi and 2.07 dBi. The peak realized gain of the antenna in skin layer is -34.7 dBi, -35.1 dBi in fat layer and -34.7 dBi in muscle layer.

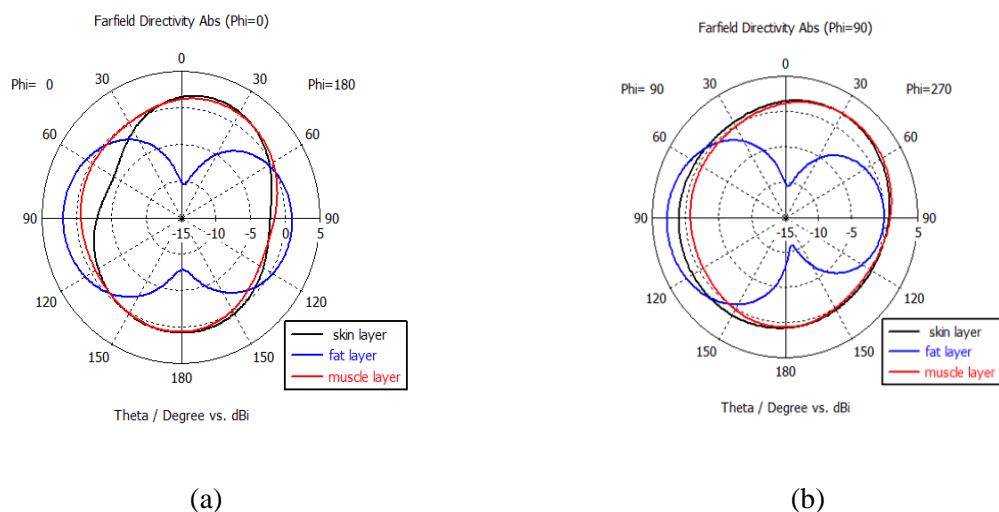


Figure 5.7- Polar plot of radiation pattern of compact size antenna in multilayer tissues (skin, fat and muscle) at 915 MHz (a) E-plane (b) H-plane

### **5.3 Performance Evaluation of Designed Antennas with Different Implant depths**

Implant depth of implantable antennas has major effect on antenna performance. The performance of the designed antennas is analysed at different implants depths inside the tissue layer for which they have been designed. The circular patch antenna and compact size antenna performance is analysed at different implant depths inside simplified skin layer phantom while the rectangular patch antenna performance is analysed inside simplified fat layer phantom. We have used single tissue layers of the simplified body model to evaluate the designed antenna performance for different implant depths inside a specific tissue layer.

#### *5.3.1 Performance evaluation of compact size antenna with different implant depths in skin layer phantom*

The compact size antenna was tested in simplified skin layer phantom with four implantation depths. The antenna was inserted 1mm, 3mm, 5mm and 15mm deep into the skin layer and the results were analysed. The return loss of the compact size antenna is shown in Figure 5.8. There is a minor difference between resonance curve for the different depths. The -10 dB bandwidth is also same. However, the implant depth effects the radiation efficiency. The radiation efficiency of the compact size antenna at 1mm and 3mm implant depth is -36.6 dB and -36.4 dB but at 5mm depth radiation efficiency has decreased to -37.5 dB. At 15mm implant depth the radiation efficiency has further decreased to -40.8 dB. The radiation efficiency has decreased at deeper implants because of more power absorption. The gain of the antenna also decreased with increased implant depth.

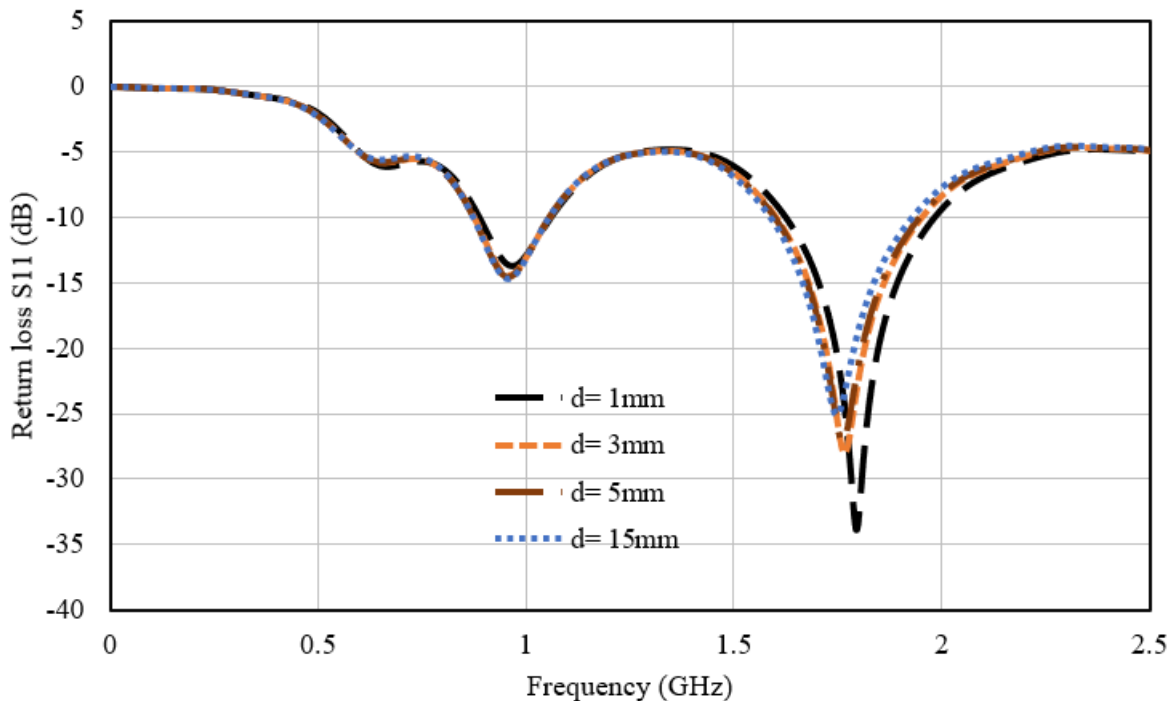


Figure 5.8- Return loss of compact size antenna in skin layer phantom with different implant depths

The depth of the implant also effects the radiation pattern of the antenna. The E-plane and H-plane radiation pattern of the compact size antenna is shown in Figure 5.9. The E-plane radiation pattern at 1mm, 3mm, 5mm depth is almost same in magnitude but at depth of 15 mm the magnitude of main lobe of radiation has increased by 0.016%.

The direction of main lobe of radiation is same at 1mm and 3mm implant depth and, 5mm and 15mm implant has same direction of radiation with a 14-degree shift in angle of 15 mm implant. In H-plane the magnitude of main lobe of radiation is less than 2 dBi for 1mm,3mm and 5mm while it is 2.26 dBi at 15mm implant depth. The direction of radiation is same for 3mm and 5mm implant. For 1mm and 15mm the direction of radiation is same with a shifted angle of 7 degrees.

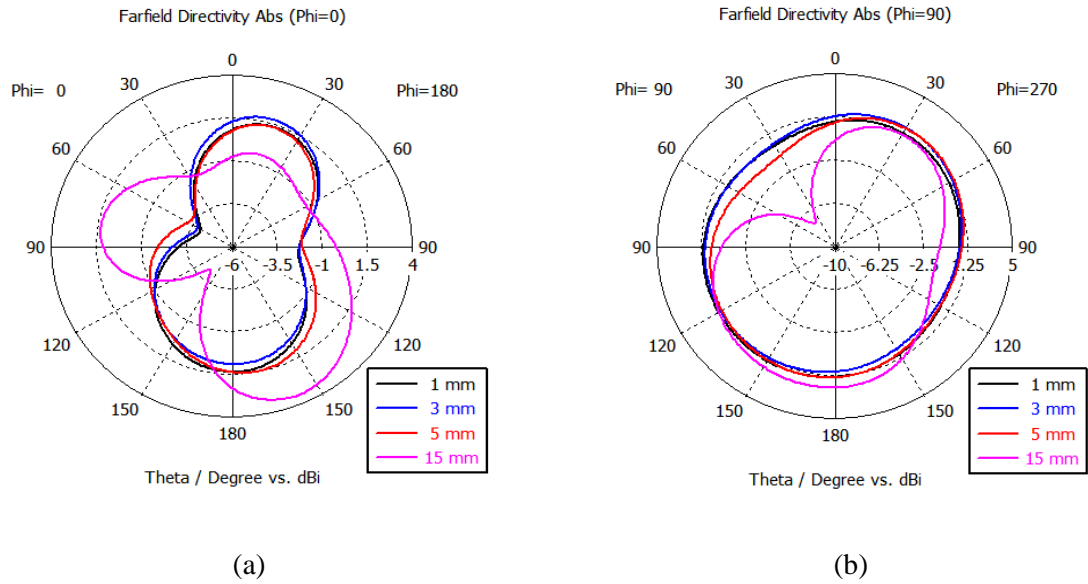


Figure 5.9- Polar plot of the radiation pattern of the compact size antenna with different implant depths in skin layer phantom at 915 MHz (a) E-plane (b) H-plane

### 5.3.2 Performance evaluation of circular patch antenna with different implant depths in skin layer phantom

Figure 5.10 shows the return loss of the circular patch antenna when it was simulated in 1mm, 3mm, 5mm and 15mm simplified skin layer phantom. The return loss and bandwidth of the antenna are slightly affected with various implant depths. The radiation efficiency of the antenna has little difference at 1mm, 3mm and 5mm depth while it has decreased by 0.01% at 15mm implant depth. The effect of the implant depth on the gain of the antenna is same as the effect on the efficiency.

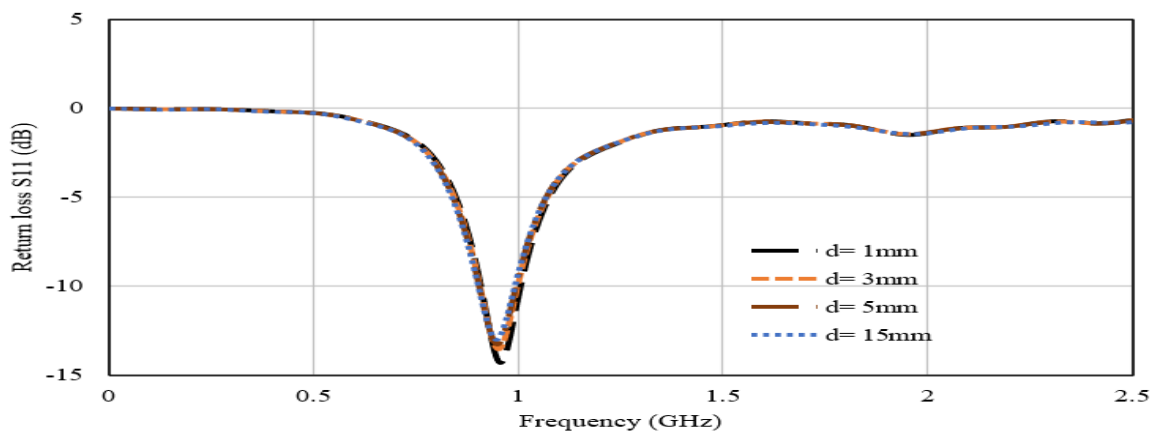


Figure 5.10- Return loss of circular patch antenna with different implant depths in skin layer

Polar plot of radiation pattern of the circular patch antenna with different implant depths in skin layer is shown in Figure 5.11. In E-plane the magnitude of main lobe of radiation has increased with increasing implant depth till 5mm while it has decreased at 15mm implant depth. The direction of radiation at all implant depths is same with a minor shift in angle of radiation. In H-plane the magnitude of main lobe of radiation has showed increase with increasing implant depth. The direction of radiation is at around 0-degree angle at 3mm and 5mm implant depth, at an angle of around 180 degrees for 1mm implant depth and its angle is around 90 degrees for 15mm implant depth. The implant depths in terms of wavelength are  $0.003 \lambda_0$ (1mm),  $0.009 \lambda_0$  (3mm),  $0.015 \lambda_0$ (5mm) and  $0.045 \lambda_0$  (15mm).  $\lambda_0$  is free space wavelength at 915 MHz and its value is 0.328m.

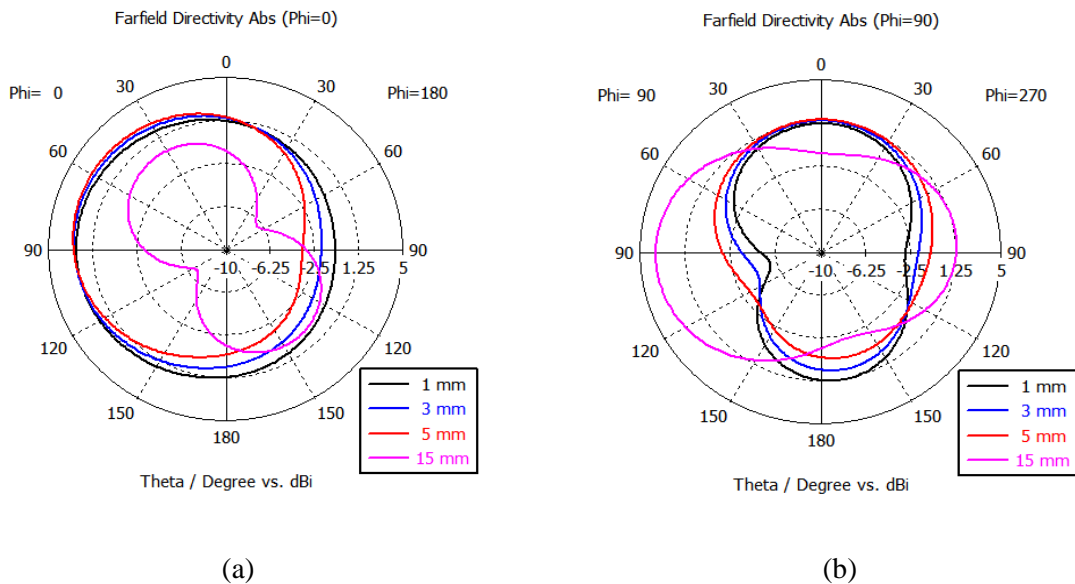


Figure 5.11- Polar plot of radiation pattern of the circular patch antenna with different implant depths in skin layer at 915 MHz (a) E-plane (b) H-plane

### 5.3.3 Performance evaluation of rectangular patch antenna in fat layer phantom with different implant depths

The rectangular patch antenna was simulated in 1mm, 3mm, 5mm and 15mm simplified fat layer phantom. The return loss of the rectangular patch antenna in Figure 5.12 shows that the implant depth has not affected the return loss or bandwidth of the antenna. The efficiency and gain of the antenna have increased with deeper implantation.

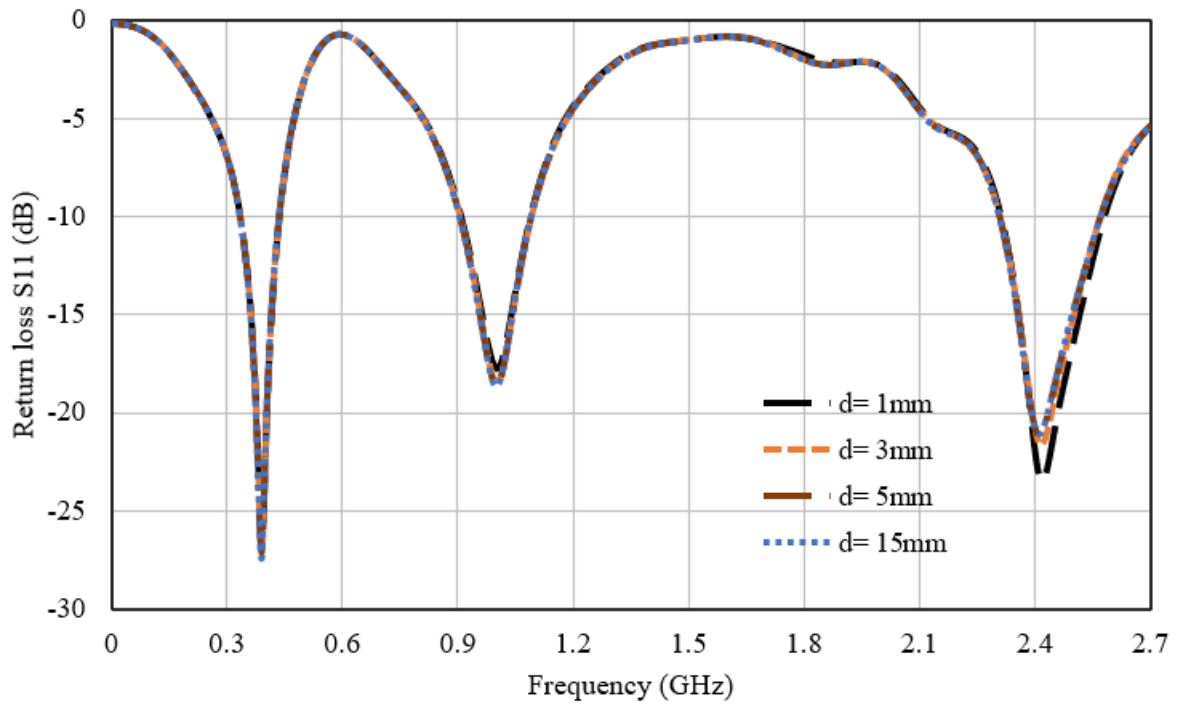


Figure 5.12- Return loss of the rectangular patch antenna with different implant depths in fat layer

Figure 5.13 shows the polar plot of radiation pattern of the rectangular patch antenna with different implant depths. The magnitude of main lobe of radiation in E-plane increases with increase in implant depth. The direction of radiation at 1mm, 3mm and 5mm is same with a slight shift in angle while at 15mm implant depth the direction angle is shifted with a difference of around 27 degrees. In H-plane the magnitude of main lobe of radiation has also increased with increasing implant depth. The direction of main lobe of radiation is 144 degrees at 1mm, 143 degrees at 3mm, 2 degrees at 5mm and 179 degrees at 15mm implant depth.

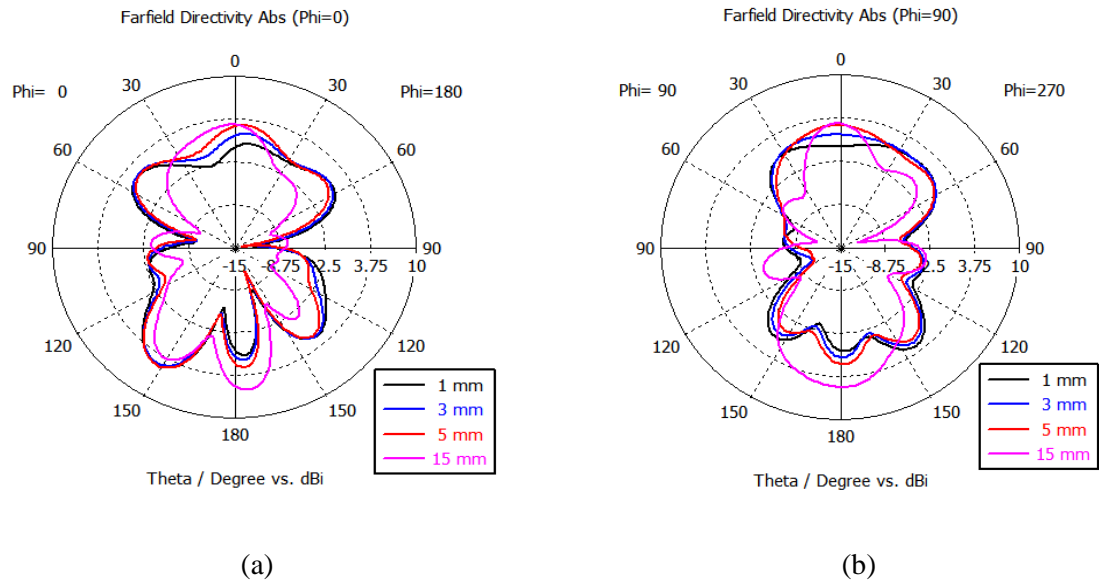


Figure 5.13- Radiation pattern of rectangular patch antenna at 2.4 GHz with varied implant depths (a)- E plane (b)- H plane

#### 5.4 Performance Evaluation of Compact Size Antenna in Different Size Phantoms

The size, shape and resolution of the body phantom also effect the antenna performance even if the depth of the implant is kept same. A circular and a rectangular phantom was used and the compact size antenna was placed 4mm deep inside the skin equivalent phantom as shown in Figure 5.14. The size of rectangular phantom is  $110 \times 70 \times 30 \text{ mm}^3$  and circular phantom is  $\pi \times 30^2 \times 49 \text{ mm}^3$ .

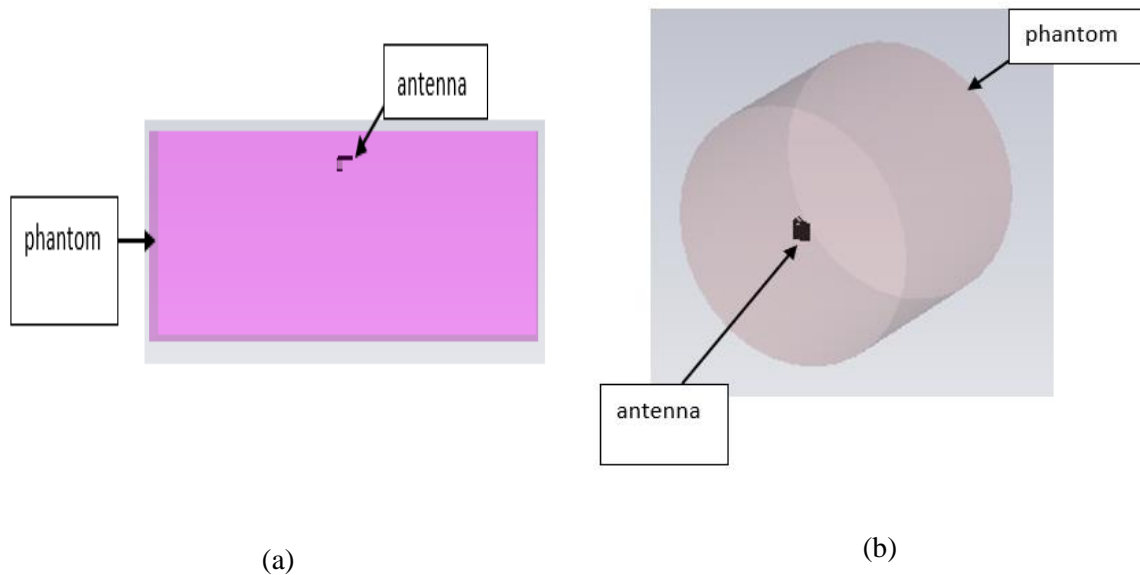


Figure 5.14- Antenna placement in circular and rectangular phantoms

The overall size of the phantoms is same but the shape and resolution is different. The simulation results shows that the return loss and bandwidth of the antenna are not affected by using different shape phantoms. The gain of the antenna is different for the same volume but different shape phantoms as shown in Figure 5.15. The efficiency of the antenna has also reduced in circular shape phantom. Because of the geometry of the circular phantom, the antenna orientation is changed inside circular phantom and more power is absorbed which decreases antenna efficiency. The shape of the phantom has also effected the radiation pattern of the antenna.

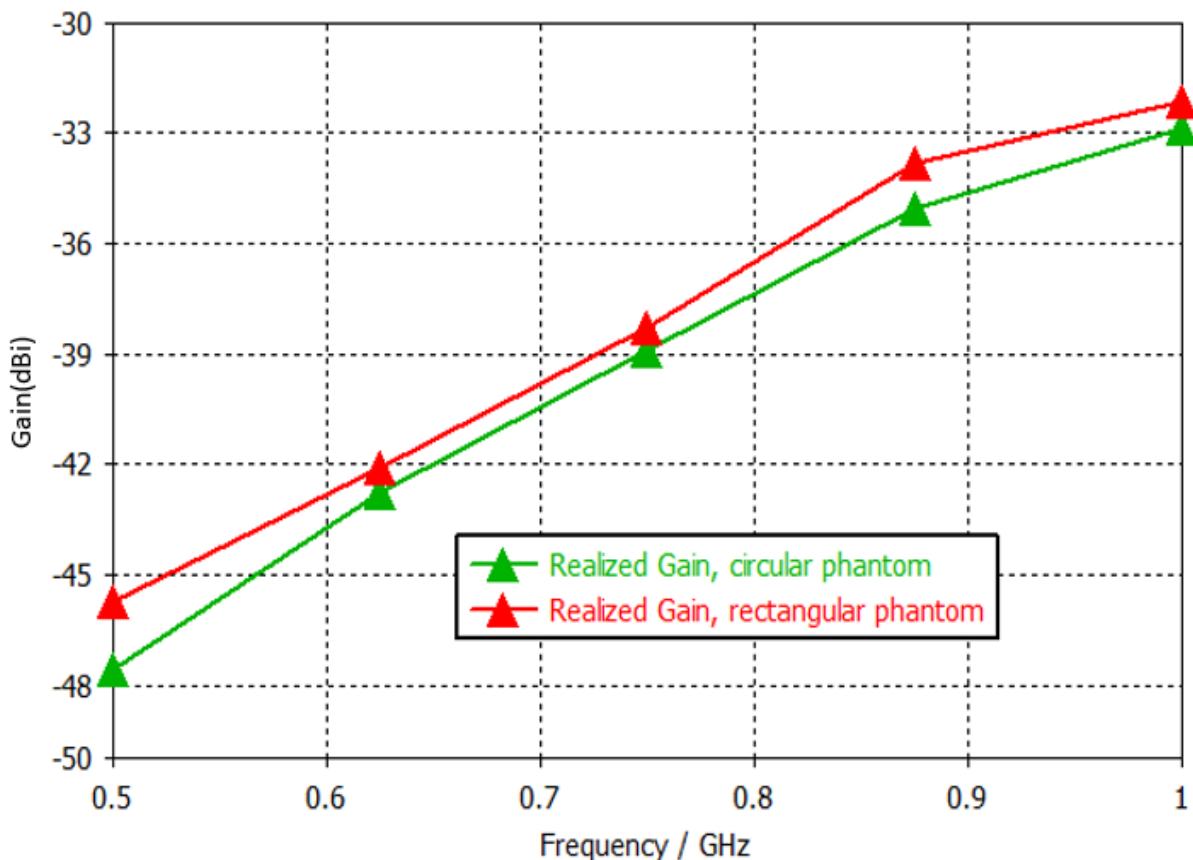


Figure 5.15- Gain of compact size antenna at 915 MHz in rectangular and circular shape phantoms

## 5.5 Effect of Insulation Layer on Rectangular Patch Antenna performance

The implantable antennas are encapsulated for biocompatibility purposes depending on the application. The insulation layer around the antenna can alter the resonance by effecting the antenna performance. We have used two different thicknesses of insulation layer (0.25mm and 0.5mm) to analyse the performance of rectangular patch antenna. Ceramic alumina is used as insulation layer material. There

is a negligible difference in gain and efficiency of the antenna when simulated with and without insulation layer. The resonance curve in Figure 5.16 shows that the antenna return loss has minor change at lower frequency but at 2.4 GHz the return loss has decreased and -10 dB bandwidth of the antenna at this frequency has increased. The conductivity of body tissues increases at higher frequencies. The insulation layer minimizes the power absorption in the body tissues. At lower frequencies, the power absorption in the body tissues is less and effect of insulation layer is minimum. Whereas at 2.4 GHz, the power absorption in body tissues was more which was reduced by insulation layer showing its increased effect on resonance curve as compared to lower frequencies.

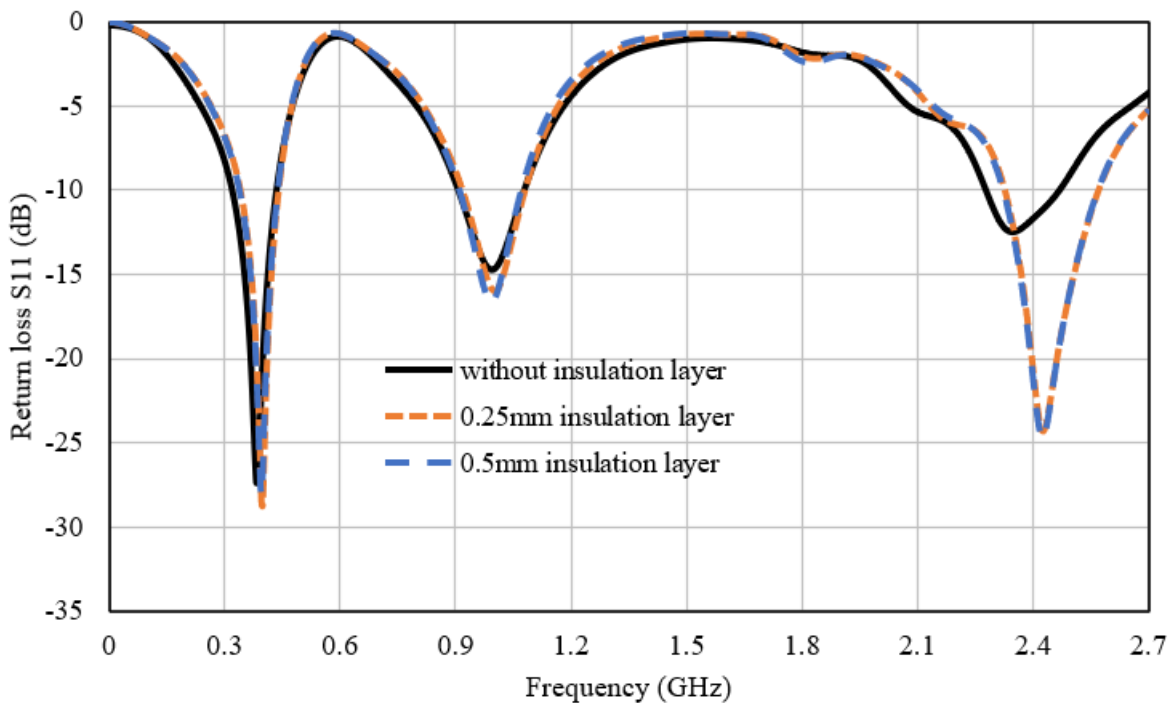


Figure 5.16- Return loss of rectangular patch antenna with insulation layer

## 5.6 Analysis of Circuit Components Effect on Designed Antennas Performance

The integration of antenna with sensor component can also pose a challenge. The antenna performance can be effected caused by the interference of other circuit components. For simulation we have assumed copper material to mimic battery and FR-4 for other components [5]. The block representation of the antenna with circuit components is shown in Figure 5.17. We have placed rectangular patch antenna

with circuit components inside the fat layer phantom. A skin layer phantom was used to simulate the circular patch and compact size antenna with circuit components. An implant depth of 5mm is used to simulate the antennas with circuit components.

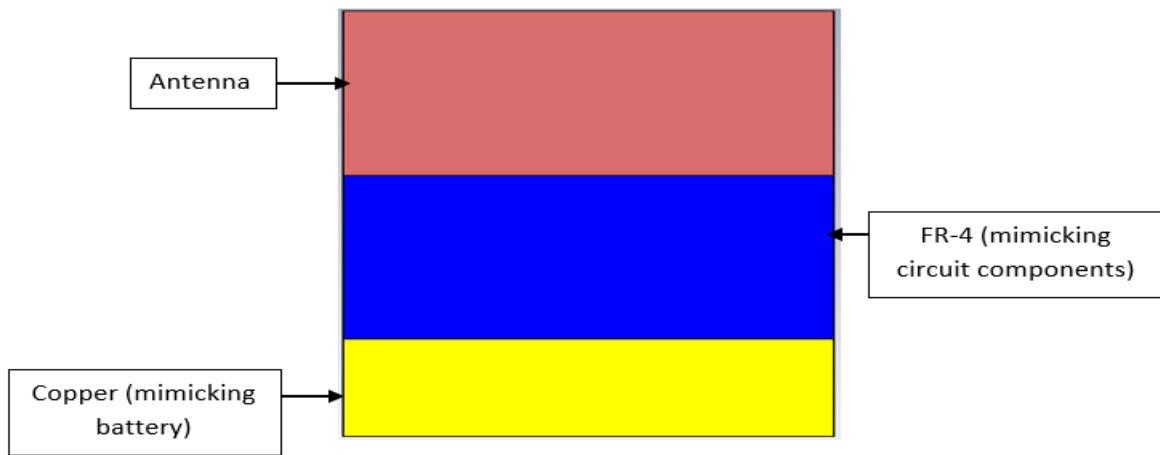


Figure 5.17- Block representation of antenna and circuit components

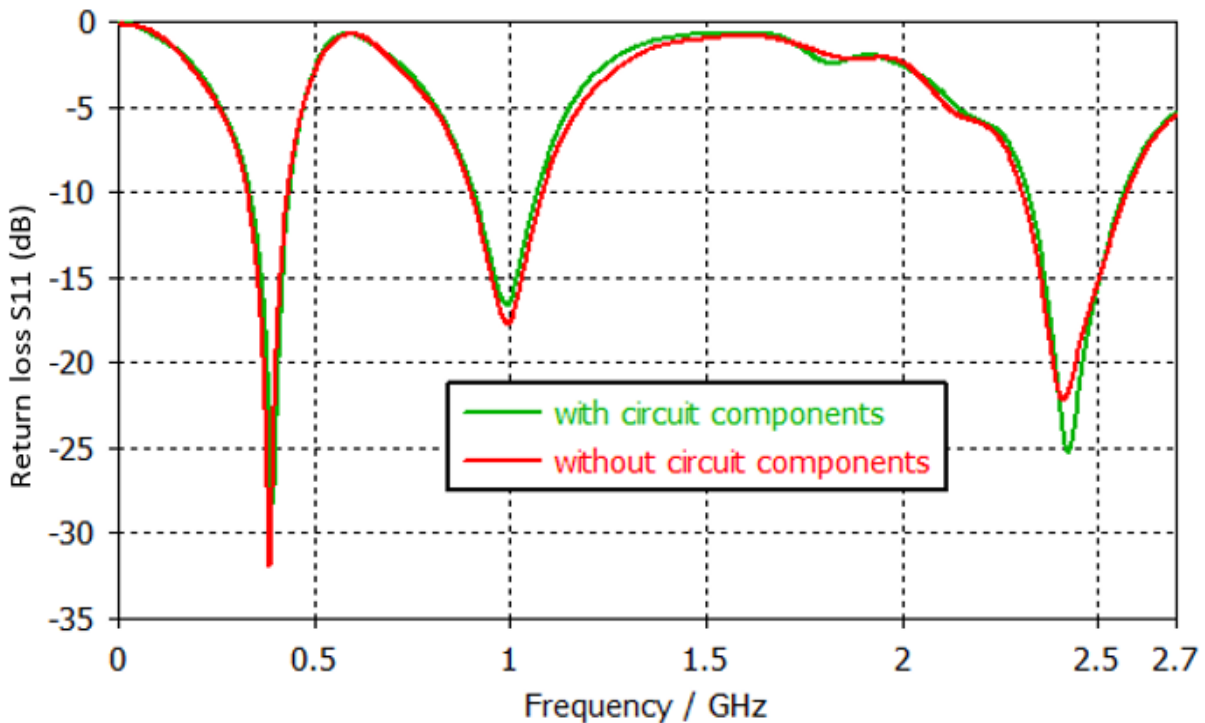


Figure 5.18- Return loss of rectangular patch antenna when simulated without and with circuit components

The return loss of the rectangular patch antenna, circular patch antenna and compact size antenna is shown in Figure 5.18, Figure 5.19 and Figure 5.20. The results analysis shows that there is a good

agreement between the simulation results of the antennas when they were simulated without and with circuit components.

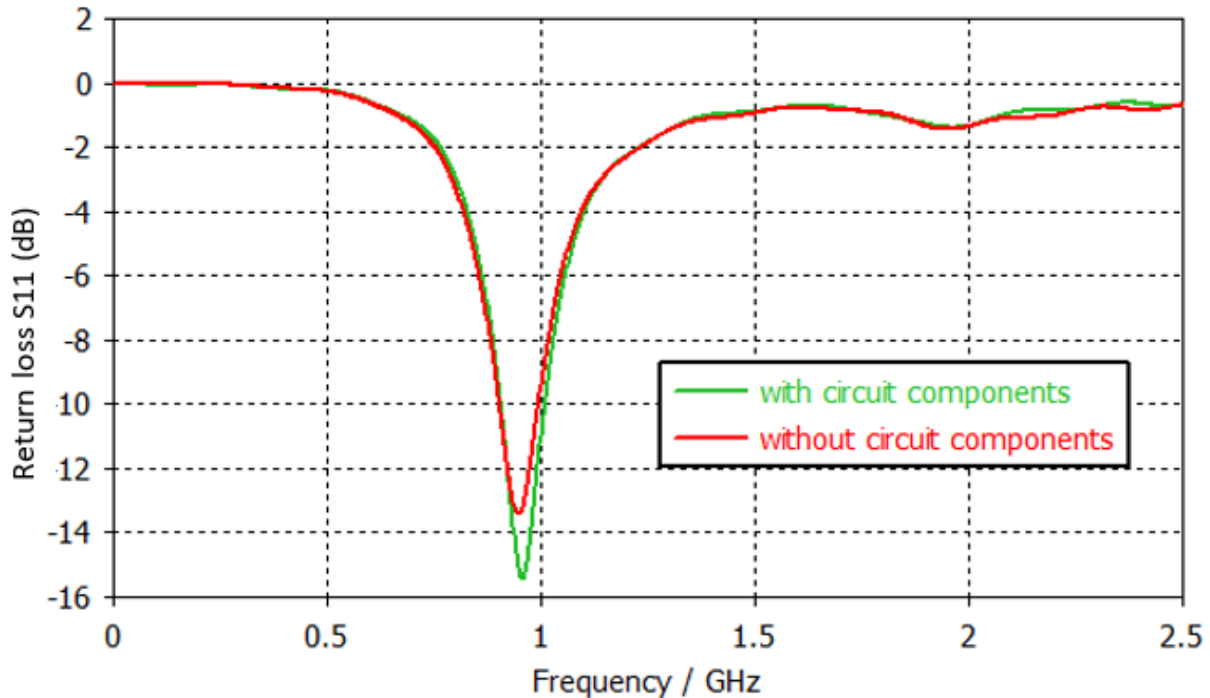


Figure 5.19- Return loss of the circular patch antenna without and with circuit components

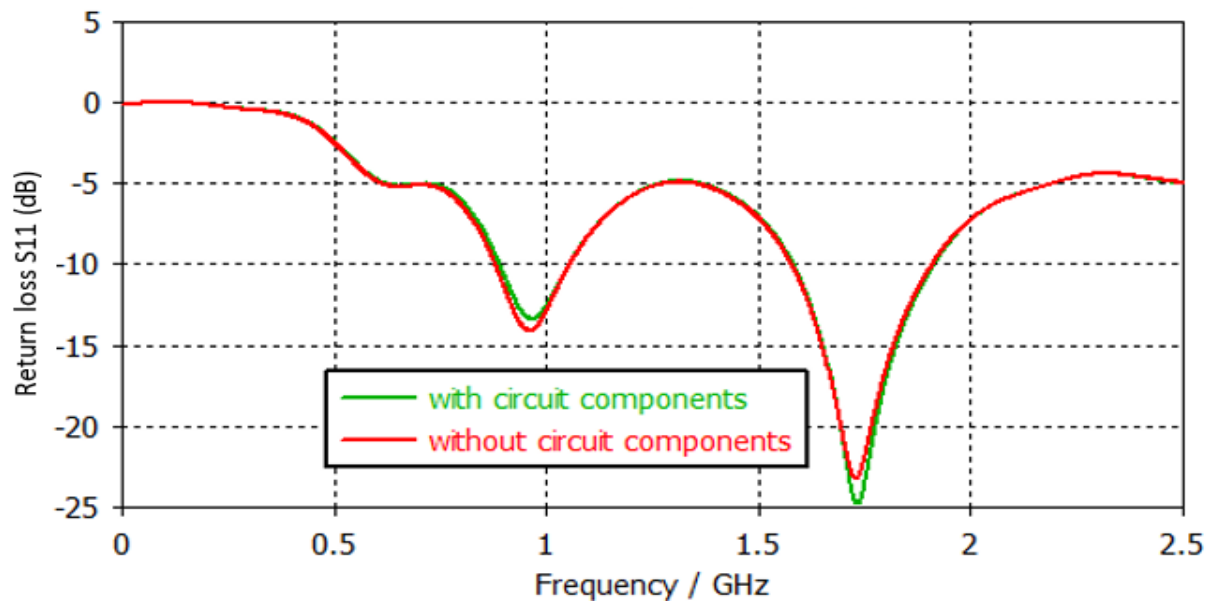


Figure 5.20- Return loss of the compact size antenna when simulated without and with circuit components

## 5.7 Designed Antennas Performance Evaluation in Anatomical Body Model

Though the antenna simulation results of the simplified body model are reliable, but the performance of the antenna need to be evaluated in the anatomical body model because the simulation results of the anatomical body model are closer to the real results. All of the designed antennas are simulated in human voxel model. The whole-body simulation takes a lot of time and memory. To reduce the simulation time only upper half of the body is used for simulation. The simulation time and memory used by the designed antennas when simulated in anatomical body model is given in Table 5.2. The block diagram of the implanted antenna inside the arm of voxel model is shown in Figure 5.21.

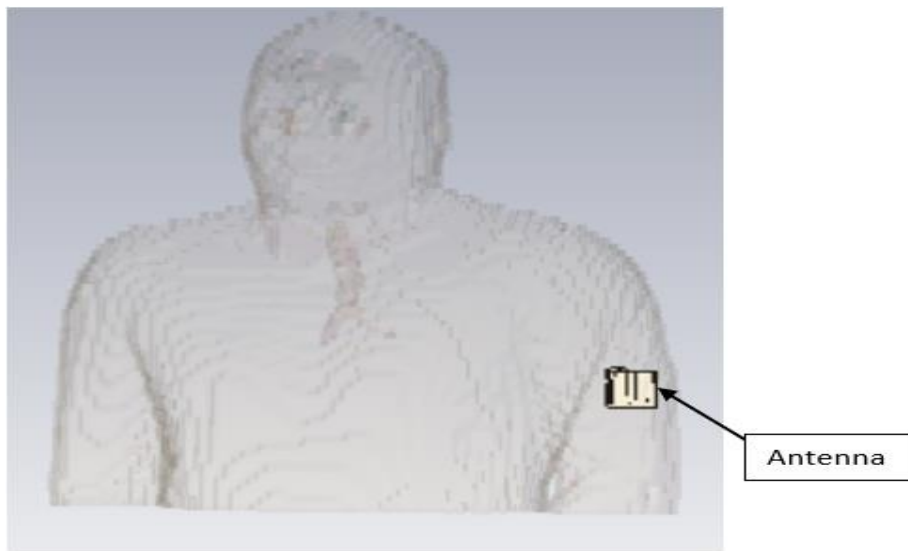


Figure 5.21- Block diagram of antenna inside anatomical body model

Table 5.2- Simulation time and memory used by designed antennas in anatomical body model

Antenna type	Simulation time (s)	Peak memory used (kB)	Number of mesh cells
Circular patch antenna	5231	710652	1568336
Rectangular patch antenna	7020	1076704	2055455
Compact size antenna	4709	858740	1580569

### 5.7.1 Performance evaluation of compact size antenna in anatomical body model

The compact size antenna was implanted inside the skin layer of the anatomical body model. The simulated return loss of the compact size antenna in anatomical body model and simplified skin layer phantom is given in Figure 5.22. The antenna resonates at 915 MHz with a slight shift in resonance curve as compared to simplified skin layer phantom. The -10 dB bandwidth of the antenna comes out as 154 MHz at resonant frequency in anatomical body model while in simplified skin layer phantom the bandwidth is 170 MHz. The radiation efficiency of the antenna has decreased to -43 dB in anatomical body model. The radiation efficiency of the antenna in simplified skin layer phantom is -36.5 dB.

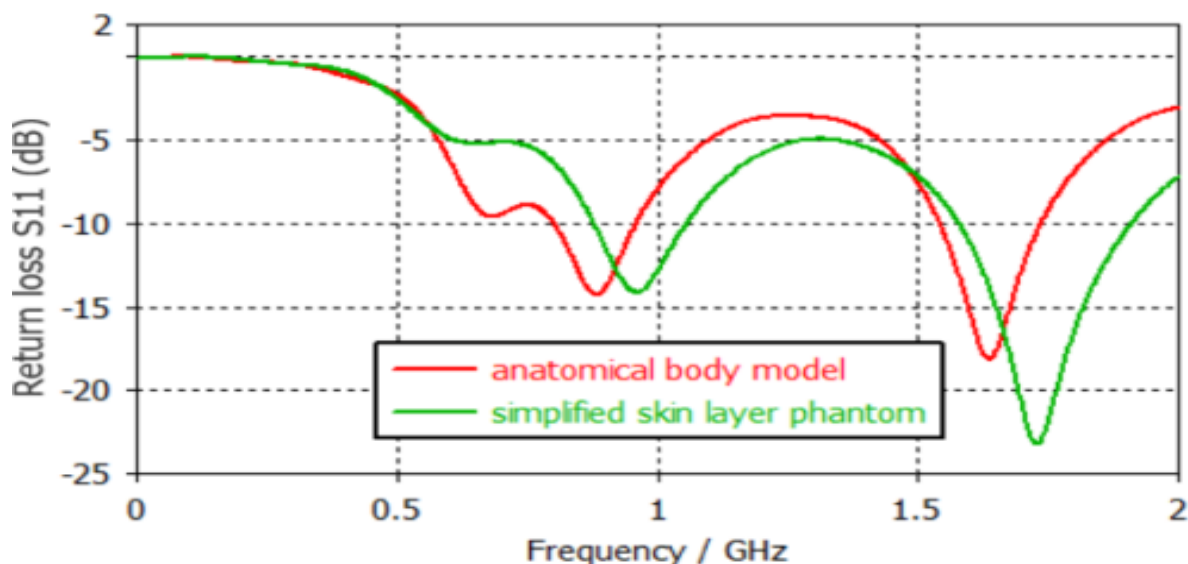


Figure 5.22- Return loss of compact size antenna in anatomical body model and simplified skin layer phantom

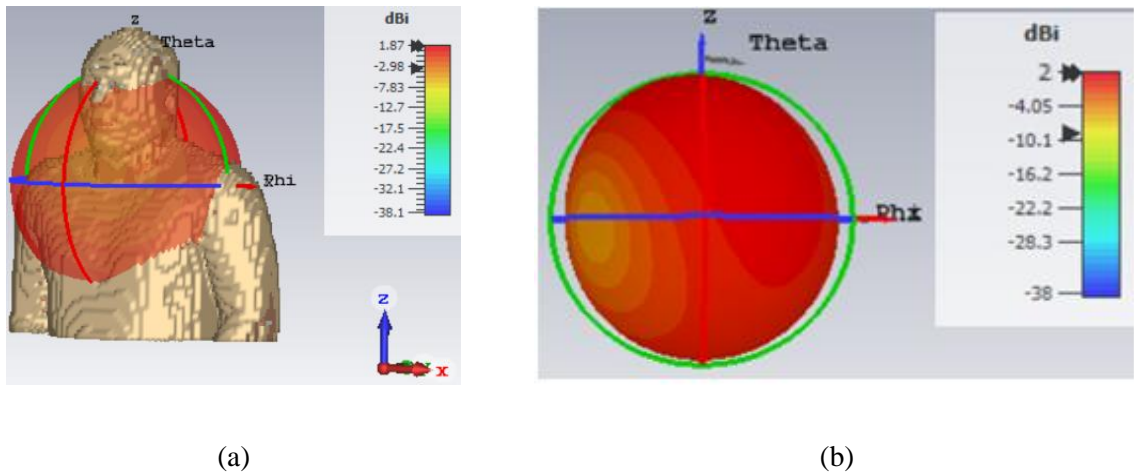


Figure 5.23- 3D Radiation pattern of the compact size antenna at 915 MHz (a) anatomical body model (b) simplified skin layer phantom

The 3D radiation pattern of the compact size antenna in anatomical body model and simplified skin layer phantom is shown in Figure 5.23. It can be seen in Figure 5.23 that the directivity of the compact size antenna inside anatomical body model has decreased. The realized gain of the compact size antenna in anatomical body model is -41 dBi while in simplified skin layer phantom, the gain is -34.7 dBi.

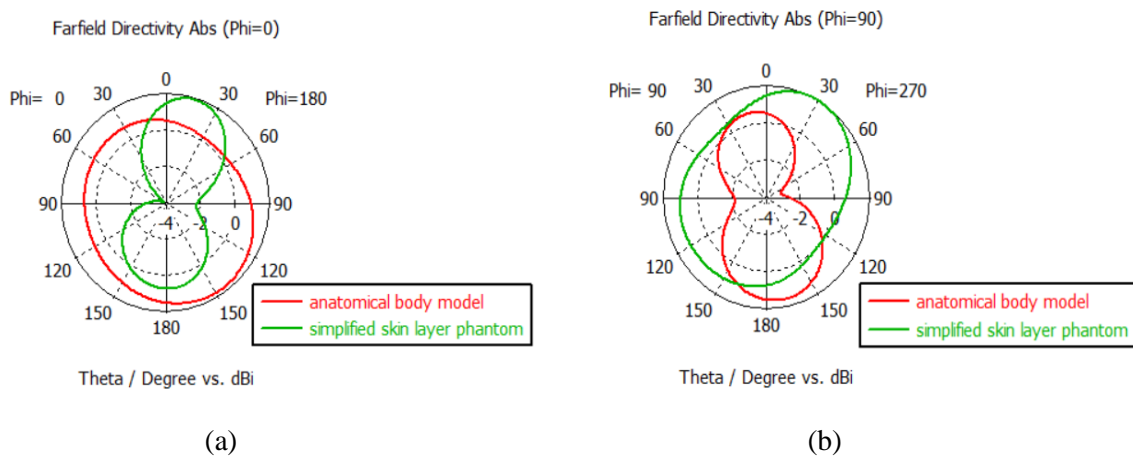


Figure 5.24- Polar plot of radiation pattern of the compact size antenna in anatomical body model and simplified skin layer phantom at 915 MHz (a) E-plane (b) H-plane

Figure 5.24 shows the E-plane and H-plane radiation pattern of the antenna at 915 MHz in anatomical body model and simplified skin layer phantom. The compact size antenna is designed for applications operating at 915 MHz, so the radiation pattern is presented at 915 MHz frequency only. It can be seen in Figure 5.24 that the radiation pattern of the compact size antenna for both E and H-planes has changed in anatomical body model as compared to simplified skin layer phantom. The direction of main lobe of radiation in E-plane has changed from 17 degrees in simplified skin layer phantom to 149 degrees in

anatomical body model. Similarly, the direction of main lobe of radiation in H-plane has changed from 30 degrees in simplified skin layer phantom to 171 degrees in anatomical body model. The difference of antenna performance in anatomical body model and simplified body model depends on many factors such as implant depth, implant position, size of the anatomical body model and simplified body model etc. Specific absorption rate of the compact size antenna in anatomical body model and simplified skin layer phantom is shown in Figure 5.25 and Figure 5.26. The SAR values of the antenna in anatomical body model are higher than in simplified skin layer phantom.

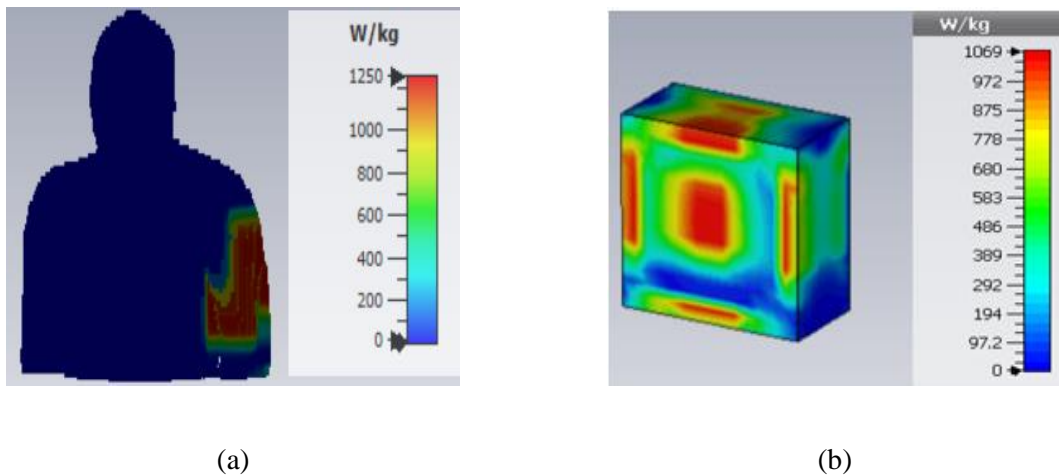


Figure 5.25- Compact size antenna 1g avg. SAR (a) anatomical body model (b) simplified skin layer phantom

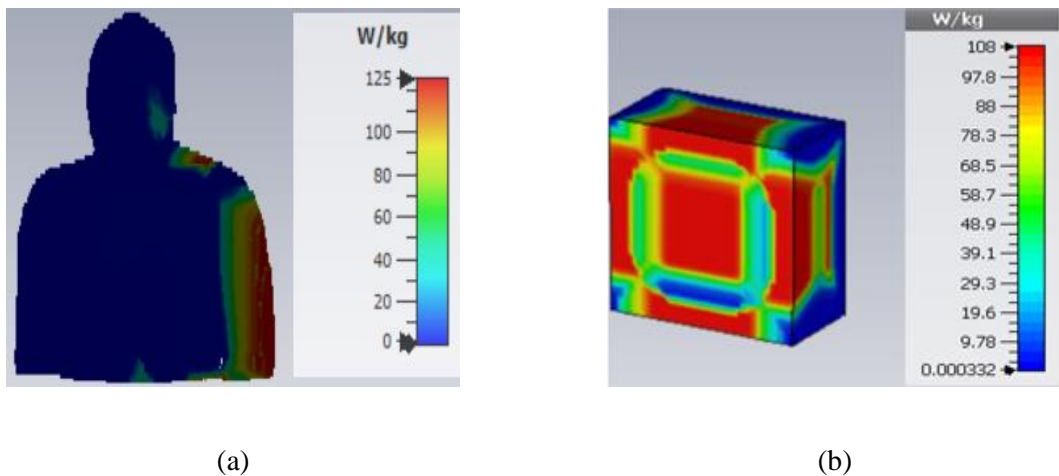


Figure 5.26- Compact size antenna 10g avg. SAR (a) anatomical body model (b) simplified skin layer phantom

### 5.7.2 Performance evaluation of rectangular patch antenna in anatomical body model

The rectangular patch antenna was simulated inside fat layer of anatomical body model. The return loss plot of the rectangular patch antenna when simulated in anatomical body model and simplified fat layer phantom is given in Figure 5.27. The rectangular patch antenna is resonating at 402 MHz, 915 MHz and 2.4 GHz in anatomical body model and fat layer phantom. The -10 dB bandwidth of the rectangular patch antenna in anatomical body model at resonant frequencies is 108 MHz, 206 MHz and 150 MHz while the bandwidth in simplified fat layer phantom is 108 MHz, 170 MHz and 250 MHz. The radiation efficiency of the rectangular patch antenna has decreased from -50 dB in simplified fat layer phantom to -53 dB in anatomical body model at 402 MHz. At 915 MHz the radiation efficiency of the rectangular patch antenna in simplified fat layer phantom is -42 dB while in anatomical body model the radiation efficiency is -44 dB. The radiation efficiency of the rectangular patch antenna at 2.4 GHz has increased from -32 dB in simplified fat layer phantom to -26 dB in anatomical body model.

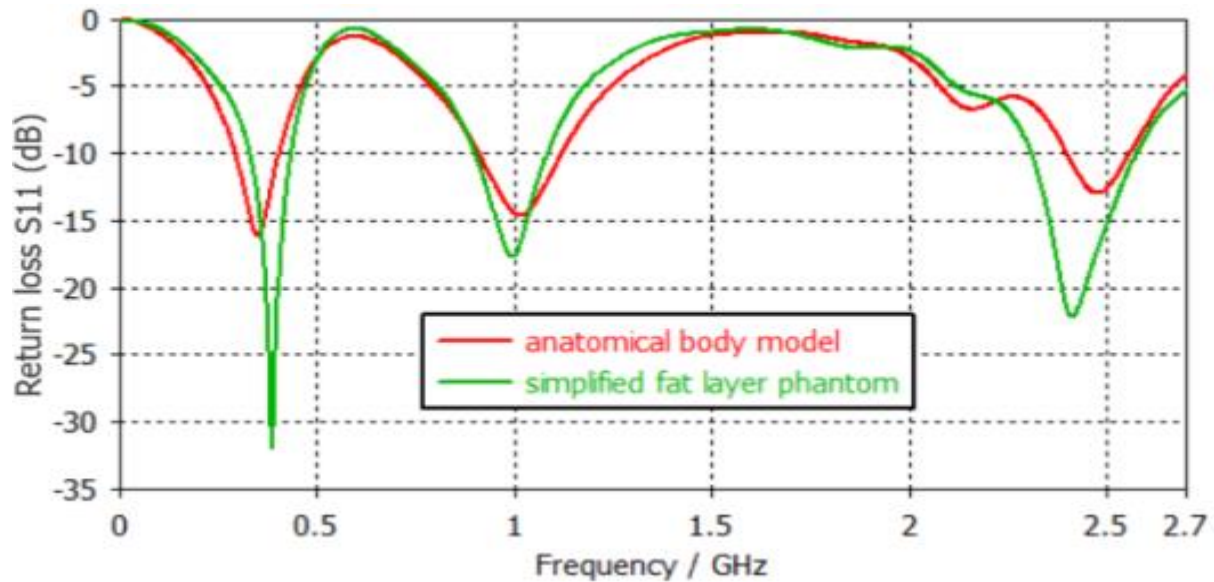


Figure 5.27- Return loss of the rectangular patch antenna in anatomical body model and simplified fat layer phantom

It can be seen in Figure 5.28 and Figure 5.29 that the directivity of the rectangular patch antenna when simulated in anatomical body model has increased at 402 MHz as compared to the directivity in simplified fat layer phantom at this frequency. At 915 MHz and 2.4 GHz the directivity of the rectangular patch antenna in anatomical body model has decreased as compared to the directivity in

simplified fat layer phantom at these frequencies. The realized gain of the rectangular patch antenna at 402 MHz, 915 MHz and 2.4 GHz in anatomical body model is -50.9 dBi, -42.2 dBi and -23.2 dBi whereas in simplified fat layer phantom the realized gain at these frequencies is -47.7 dBi, -37.2 dBi and -25.5 dBi.

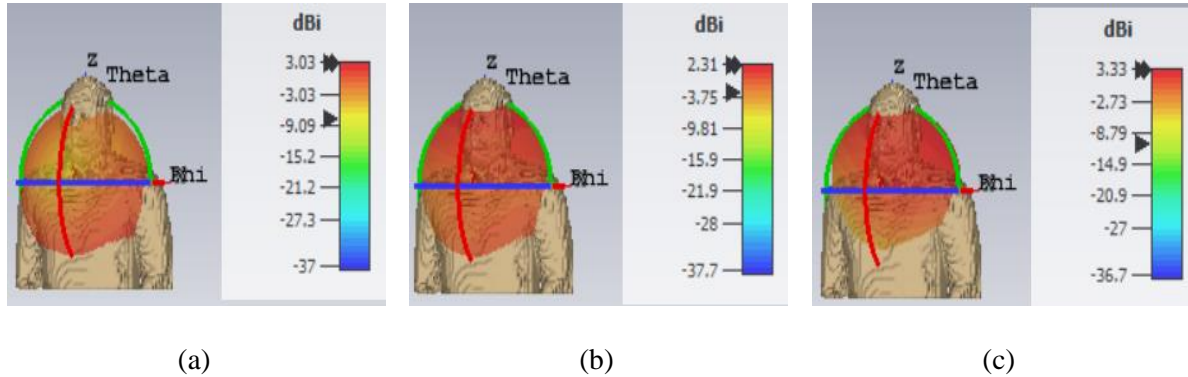


Figure 5.28- 3D radiation pattern of the rectangular patch antenna in anatomical body model (a) 402 MHz (b) 915 MHz (c) 2.4 GHz

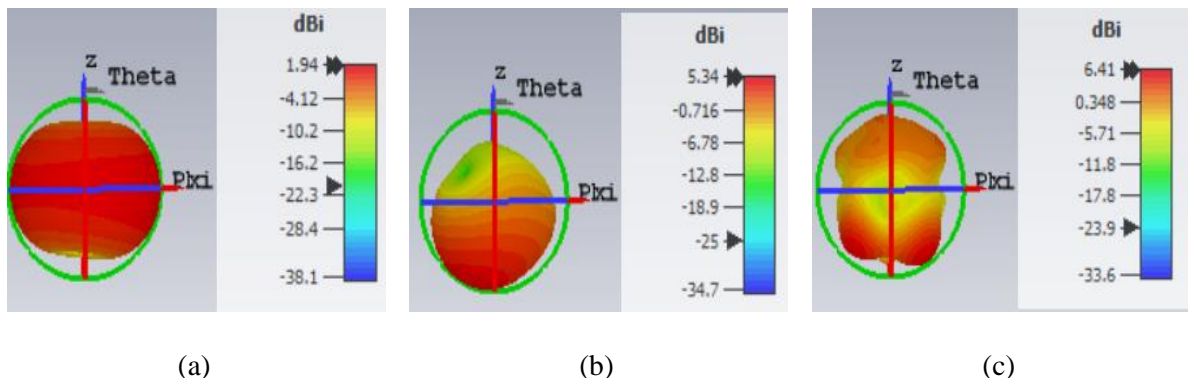


Figure 5.29- 3D radiation pattern of the rectangular patch antenna in simplified fat layer phantom (a) 402 MHz (b) 915 MHz (c) 2.4 GHz

Figure 5.30 and Figure 5.31 shows the polar plot of radiation pattern of the rectangular patch antenna in anatomical body model and simplified fat layer phantom. In E and H-plane the 3 dB angular width of main lobe of radiation for anatomical body model is greater than the 3 dB angular width of main lobe of radiation for simplified fat layer phantom at 402 MHz, 915 MHz and 2.4 GHz. The direction of main lobe of radiation in E and H-plane for anatomical body model at 402 MHz is 174 and 179 degrees while at this frequency the direction of main lobe of radiation in both E and H-plane is 95 degrees for simplified fat layer phantom. At 915 MHz the direction of main lobe of radiation in E and H-plane for anatomical body model is 0 and 1 degree whereas for simplified fat layer phantom the direction of main

lobe of radiation in E and H-plane at 915 MHz is 157 and 158 degrees. The direction of main lobe of radiation at 2.4 GHz in E and H-plane for anatomical body model is 41 and 4 degrees while at this frequency the direction of main lobe of radiation in E and H-plane for simplified fat layer phantom is 148 and 143 degrees. The radiation pattern of the rectangular patch antenna has changed in anatomical body model as compared to simplified fat layer phantom because of power absorption in other tissues of anatomical body model.

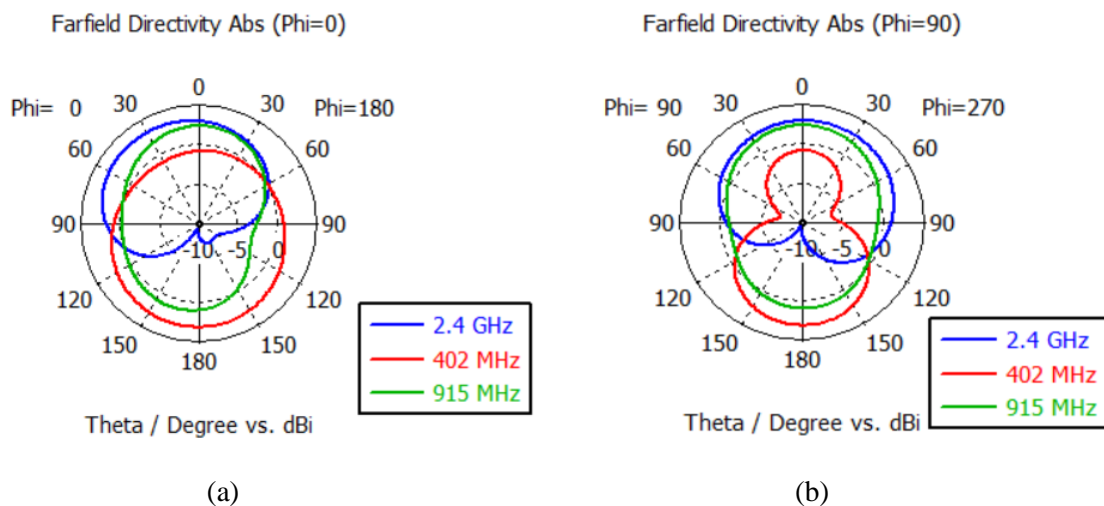


Figure 5.30- Polar plot of radiation pattern of rectangular patch antenna in anatomical body model (a) E-plane (b) H-plane

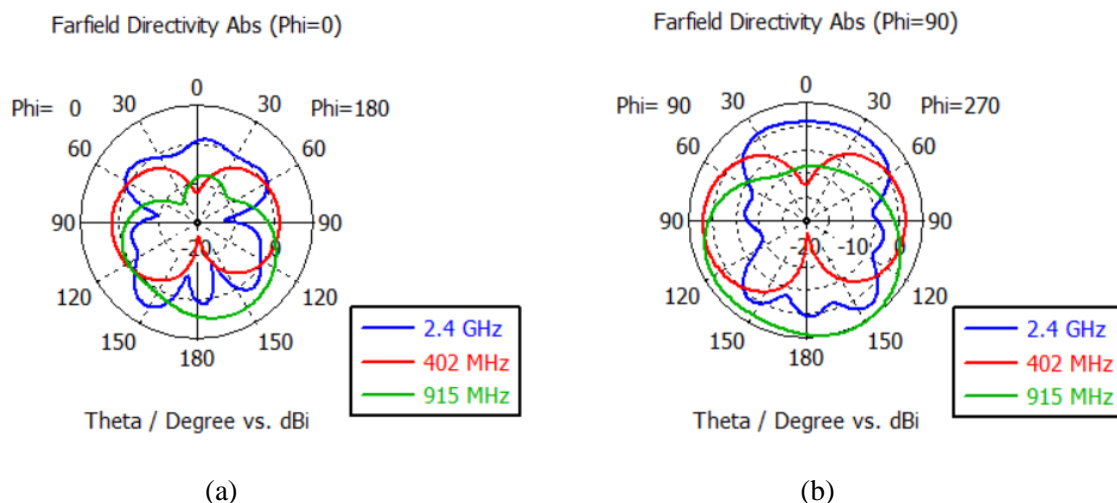
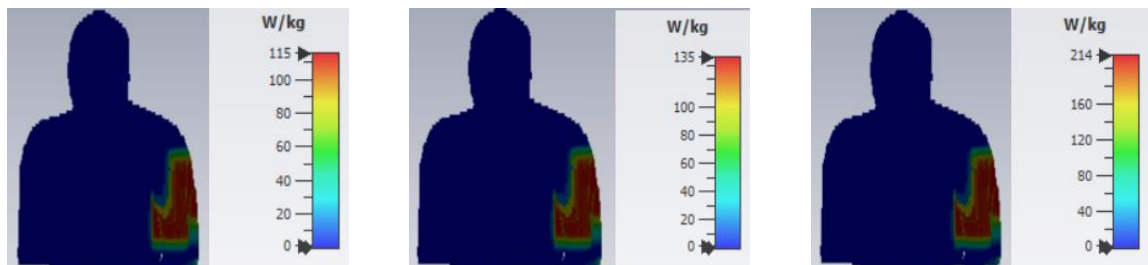


Figure 5.31- Polar plot of radiation pattern of rectangular patch antenna in simplified fat layer phantom (a) E-plane (b) H-plane

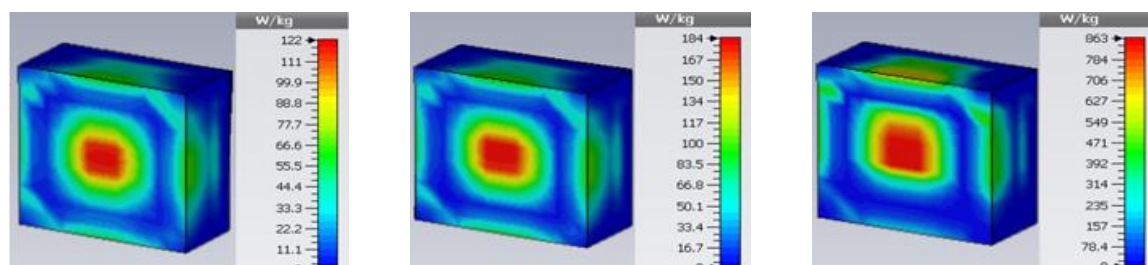


(a)

(b)

(c)

Figure 5.32 - 1g avg. SAR of the rectangular patch antenna in anatomical body model (a) 402 MHz  
(b) 915 MHz (c) 2.4 GHz

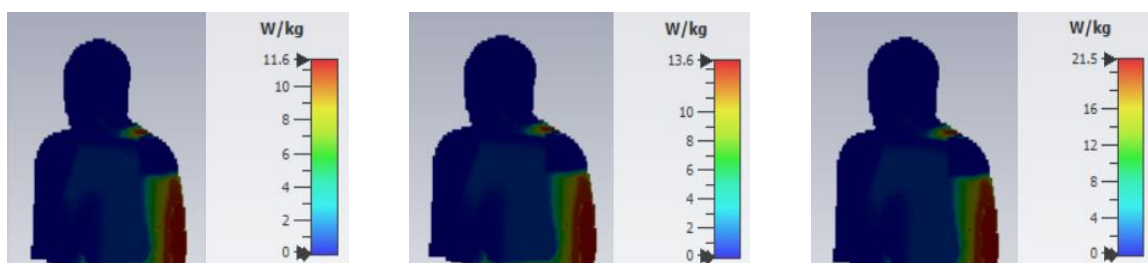


(a)

(b)

(c)

Figure 5.33- 1g avg. SAR of the rectangular patch antenna in simplified fat layer phantom (a) 402 MHz  
(b) 915 MHz (c) 2.4 GHz

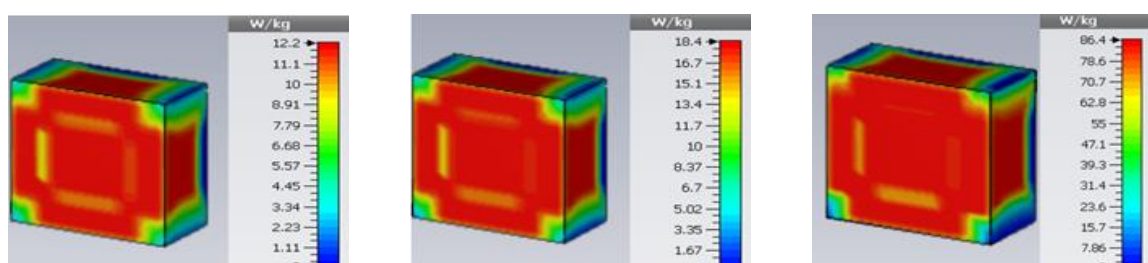


(a)

(b)

(c)

Figure 5.34- 10g avg. SAR of the rectangular patch antenna in anatomical body model (a) 402 MHz  
(b) 915 MHz (c) 2.4 GHz



(a)

(b)

(c)

Figure 5.35- 10g avg. SAR of the rectangular patch antenna in simplified fat layer phantom (a) 402 MHz  
(b) 915 MHz (c) 2.4 GHz

The 1g avg. SAR of the rectangular patch antenna in anatomical body model and simplified fat layer phantom is shown in Figure 5.32 and Figure 5.33 whereas the 10g avg. SAR of the rectangular patch antenna in anatomical body model and simplified fat layer phantom is shown in Figure 5.34 and Figure 5.35. The 1g and 10g avg. SAR of the rectangular patch antenna has reduced inside anatomical body model as compared to the SAR in simplified fat layer phantom. The SAR values are higher than the standard limits because the input power of the antenna was 0.5W. By applying the limited maximum allowed input power of the antenna, the SAR values can be reduced.

### *5.7.3 Performance evaluation of circular patch antenna in anatomical body model*

The circular patch antenna was implanted inside the skin layer of the anatomical body model. Figure 5.36 shows the resonance curve for the implantable circular patch antenna when simulated in anatomical body model and simplified skin layer phantom. The antenna resonates at 915 MHz with a bandwidth of around 90 MHz at centre frequency in anatomical body model and simplified skin layer phantom. The radiation efficiency of the circular patch antenna in simplified skin layer phantom is -31.6 dB while in anatomical body model the radiation efficiency of the circular patch antenna is -36 dB.

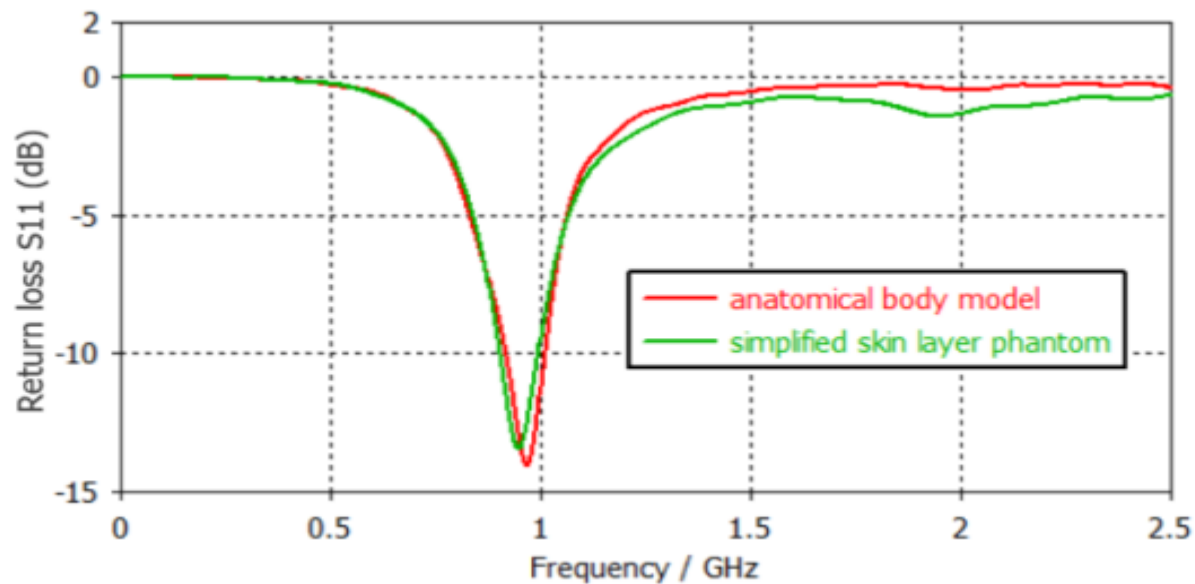


Figure 5.36- Return loss plot of the circular patch antenna in anatomical body model and simplified skin layer phantom

The 3D radiation pattern of the circular patch antenna in anatomical body model and simplified skin layer phantom is shown in Figure 5.37. The directivity of the circular patch antenna in Figure 5.37 is lower in anatomical body model than in simplified skin layer phantom. The realized gain of the circular patch antenna at 915 MHz is -34 dBi in anatomical body model whereas in simplified skin layer phantom the realized gain of the antenna is -28.8 dBi.

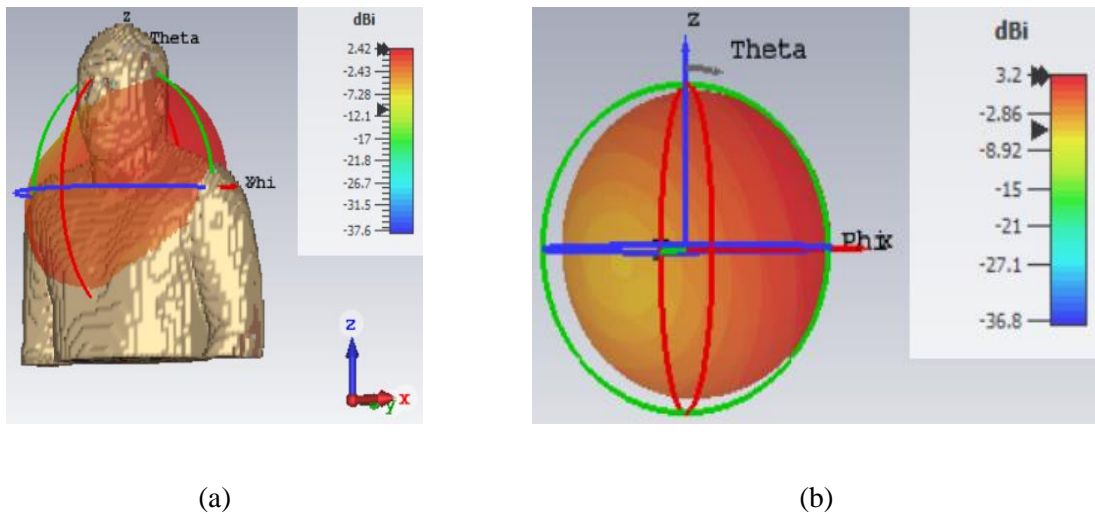


Figure 5.37- Circular patch antenna 3D radiation pattern (a) anatomical body model (b) simplified skin layer phantom

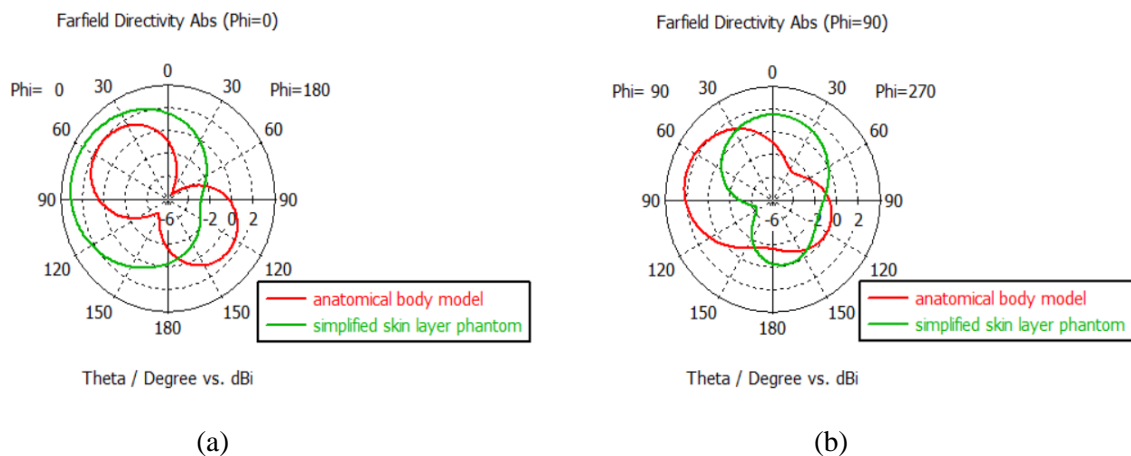


Figure 5.38- Polar plot of the radiation pattern of the circular patch antenna in anatomical body model and simplified skin layer phantom (a) E-plane (b) H-plane

The polar plot of the radiation pattern of the circular patch antenna in anatomical body model and simplified skin layer phantom is shown in Figure 5.38. The direction of main lobe of radiation in E-plane is 69 degrees in simplified skin layer phantom while in anatomical body model, the direction of

main lobe of radiation in E-plane is 52 degrees. In H-plane the direction of main lobe of radiation is 70 degrees in anatomical body model whereas the direction of main lobe of radiation in H-plane is 3 degrees in simplified skin layer phantom. The SAR values of circular patch antenna are lower in anatomical body model than in simplified body phantom as shown in Figure 5.39 and Figure 5.40. The SAR values in anatomical body model are higher than the standard limits and they can be reduced by limiting the antenna input power.

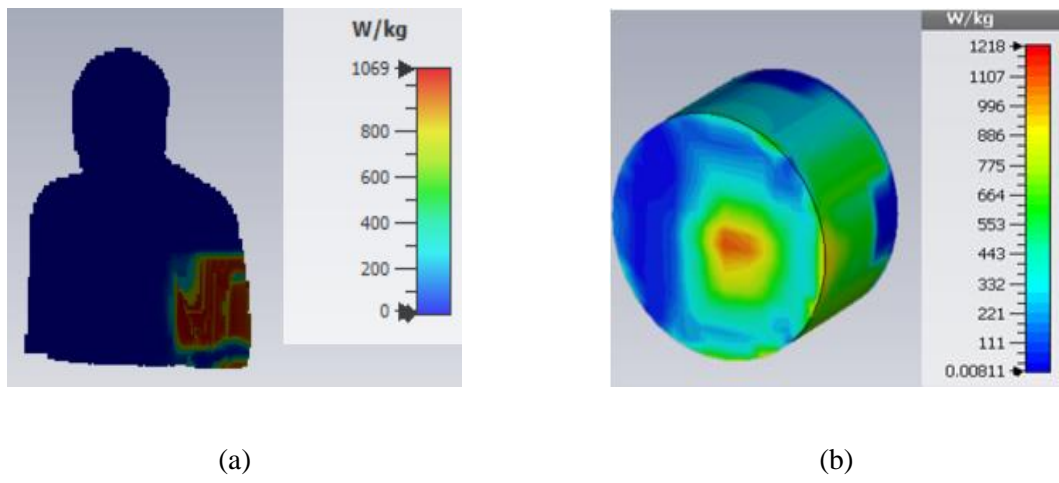


Figure 5.39- Circular patch antenna 1g avg. SAR (a) anatomical body model (b) simplified skin layer phantom

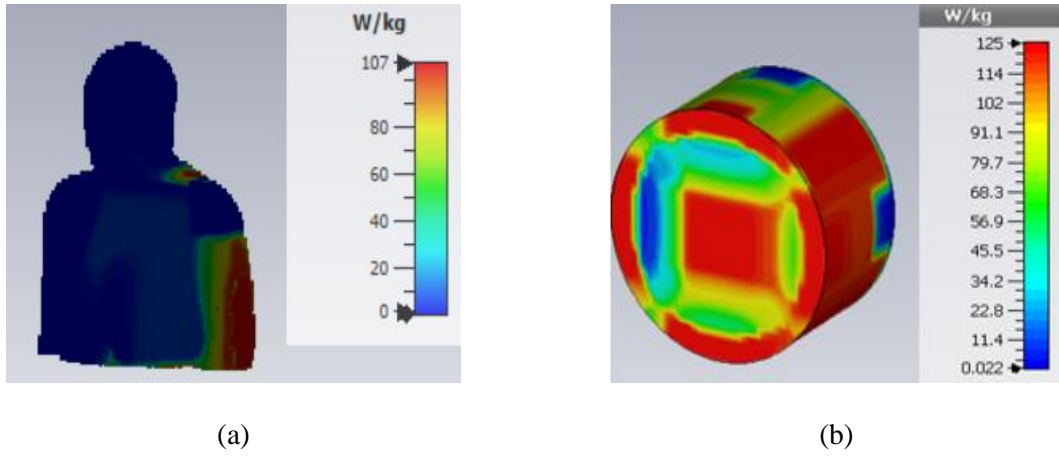


Figure 5.40- Circular patch antenna 10g avg. SAR (a) anatomical body model (b) simplified skin layer phantom

## **5.8 Designed Antennas SAR Calculation in Anatomical Body Model with Maximum Allowed Input Power**

In this section we have included the SAR results when maximum allowed input power was applied to the antenna to demonstrate that the antenna SAR can be reduced by lowering antenna input power. For easy comparison, in all other sections of the thesis we have included the results of antenna simulation with 0.5W input power which is set as default in CST Microwave Studio software because in literature other researchers have also used the software default input power.

The maximum allowed input power of the compact size antenna for anatomical body model is calculated from Figure 5.25(a) and Figure 5.26(a). For 1g avg. SAR the maximum allowed input power of the compact size antenna at 915 MHz is 1.28 mW and for 10g avg. SAR the maximum allowed input power of the compact size antenna at 915 MHz is 16 mW. The 1g avg. SAR of the compact size antenna in anatomical body when excited with maximum allowed input power at 915 MHz is 3.25 W/Kg whereas 10g avg. SAR is 0.04 W/Kg at this frequency as shown in Figure 5.41. The 1g avg. SAR is higher than the specified standard of 1.6 W/Kg because we have exited the antenna with maximum allowed input power. If the input power is decreased further, the SAR can also be decreased. For 10g avg. the SAR of the compact size antenna is within the specified standard of 2 W/Kg.

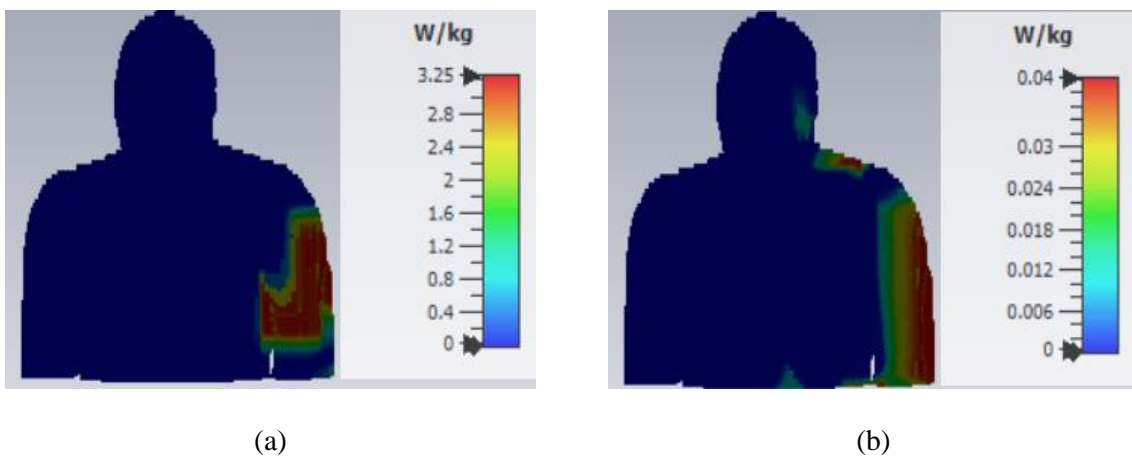


Figure 5.41- SAR of the compact size antenna in anatomical body model at 915 MHz when excited with maximum allowed input power (a) 1g (b) 10g

For the rectangular patch antenna the maximum allowed input power is calculated from Figure 5.32 and Figure 5.34. The maximum allowed input power of the rectangular patch antenna for 1g avg. SAR at

402 MHz, 915 MHz and 2.4 GHz is 14 mW, 12 mW and 7.4 mW whereas the maximum allowed input power for 10g avg. SAR at these frequencies is 172 mW, 147 mW and 193 mW. The 1g avg. SAR of the rectangular patch antenna in anatomical body model at resonant frequencies is 3.23 W/kg, 3.25 W/kg and 3.17 W/Kg whereas the 10g avg. SAR is 3.98 W/Kg, 3.99 W/Kg and 4 W/Kg as shown in Figure 5.42 and Figure 5.43. These SAR values are higher than the specified standards which can be reduced by further reducing antenna input power.

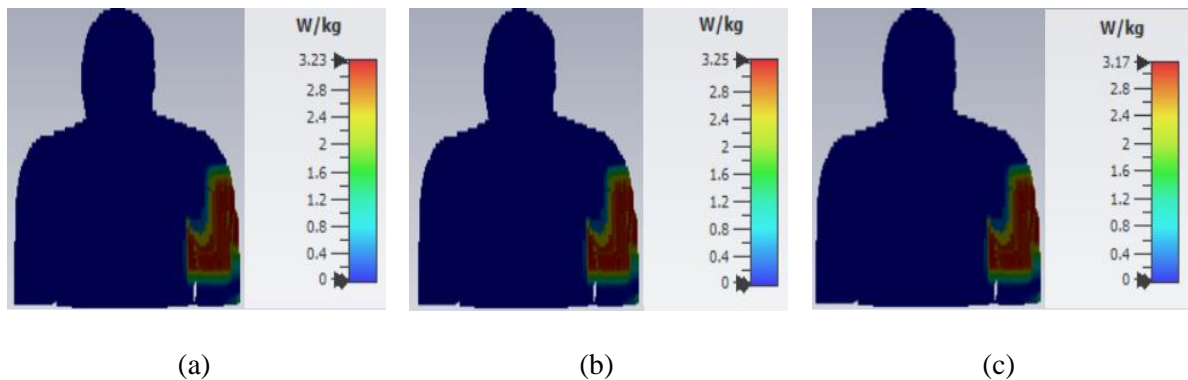


Figure 5.42- 1g avg. SAR of the rectangular patch antenna in anatomical body model when excited with maximum allowed input power (a) 402 MHz (b) 915 MHz (c) 2.4 GHz

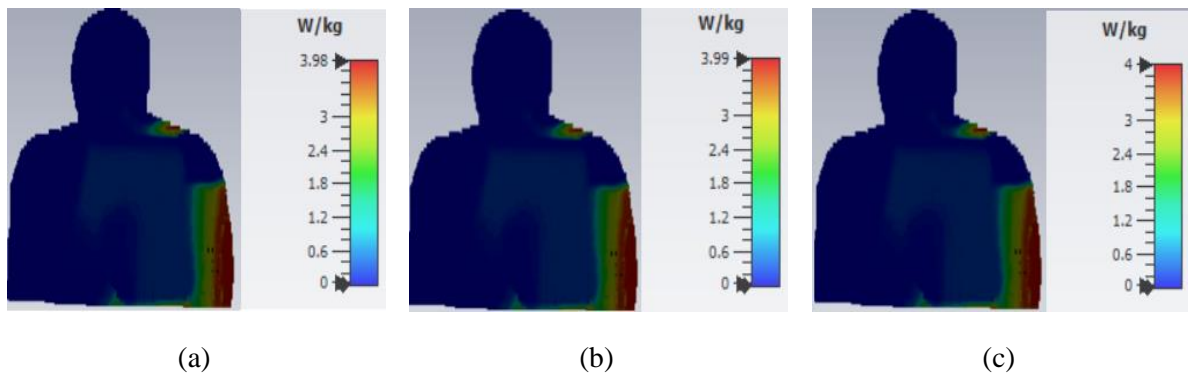


Figure 5.43- 10g avg. SAR of the rectangular patch antenna in anatomical body model when excited with maximum allowed input power (a) 402 MHz (b) 915 MHz (c) 2.4 GHz

The maximum allowed input power of the circular patch antenna for 1g avg. SAR calculated from Figure 5.39(a) is 1.5 mW at 915 MHz and for 10g avg. SAR the maximum allowed input power of the circular patch antenna calculated Figure 5.40(a) is 18.7 mW at 915 MHz. When the circular patch antenna is excited with maximum allowed input power, the 1g avg. SAR in anatomical body model is 3.21 W/Kg whereas 10g avg. SAR is 0.0401 W/Kg as shown in Figure 5.44. The 1g avg. SAR for this

antenna can be reduced further by reducing the antenna input power however the 10g avg. SAR is within specified standards.

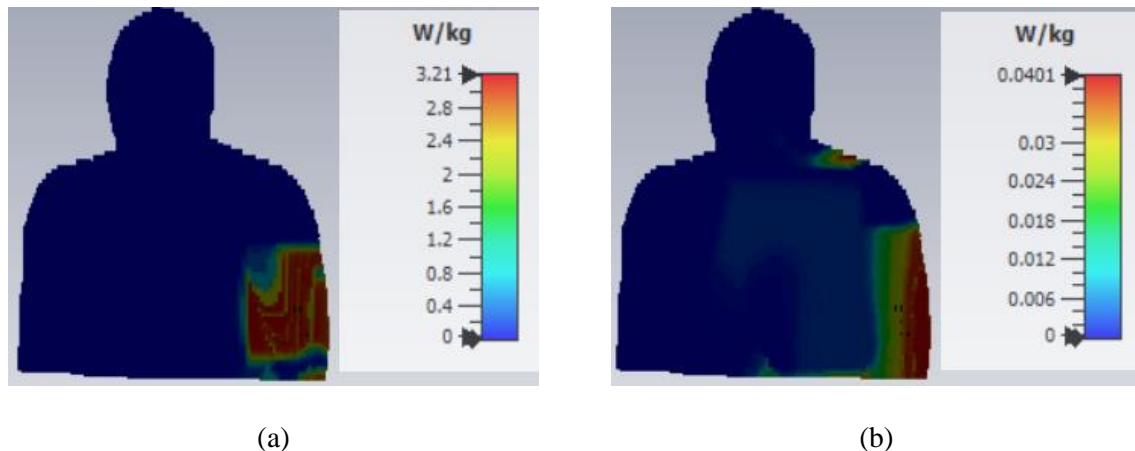


Figure 5.44- SAR of the circular patch antenna at 915 MHz in anatomical body model when excited with maximum allowed input power (a) 1g (b) 10 g

## 5.9 Chapter Summary

In this chapter a thorough study has been carried out on performance of designed antennas in multilayer tissues, different implant depths and different size phantoms. The antenna performance was also evaluated with different thicknesses of insulation layer. Mimicking circuit components were used to check the antenna integration with the sensor. The circular patch antenna was simulated in simplified skin, fat and muscle layer phantom. The simulation results show that the antenna resonates in skin and muscle layer at 915 MHz but the frequency was shifted to a higher value due to the difference between the conductivity of the fat tissue layer and other layers. The radiation pattern of the antenna was analysed for gain and radiation efficiency of the antenna. Simulation of rectangular patch antenna in skin, fat and muscle layer has shown that the antenna operates at three frequencies in fat layer while in skin and muscle layers it resonates only at 2.4 GHz. The antenna yields a wider bandwidth of 880 MHz and 720 MHz at this frequency in skin and muscle layer as compared to fat layer in which the bandwidth of antenna is 260 MHz. Multilayer simulation results of the compact size antenna shows that the antenna performs well in three layers, skin, fat and muscle by maintaining its operating frequency of 915 MHz ( $S_{11} \leq -10\text{dB}$ ). The antenna offers a wider bandwidth of 170 MHz with good performance characteristics. The designed antennas performance was evaluated at implant depths of 1mm, 3mm, 5mm and 15mm.

The return loss and bandwidth of all designed antennas has negligible difference. In case of circular patch antenna and compact size antenna the gain and efficiency has shown a decrease with increase in implant depth but these parameters have increased with deeper implantation for the rectangular patch antenna. As the size and shape of the simplified body phantoms effect the antenna performance, the compact size antenna performance was evaluated in skin equivalent phantoms of same volume and different shapes. The return loss and bandwidth of the antenna remained unaffected but the gain and efficiency were changed. The sensors and antennas are encapsulated with a biocompatible layer. The rectangular patch antenna was simulated with two thicknesses of alumina insulation layer in a simplified fat equivalent phantom. The frequency of the antenna has not been effected at lower bands but at 2.4 GHz the return loss was decreased and bandwidth became wider as compared to the resonance of the antenna without insulation layer. A copper material block was used to mimic the battery and a FR-4 material block was used to mimic the circuit components of the sensor. The antennas were placed on the top of the sensor to check their integration with the sensor. The antennas performed well with circuit components by showing a good match between the simulation results with and without circuit components. Designed antennas were simulated in anatomical body model to validate the free space simulation results.

# Chapter 6

## 6. Conclusion and Future Work

### 6.1 Conclusion

Implantable medical devices have gained a lot of attention in biotelemetry in recent years because of their advantages such as wireless capsule endoscopy, blood sugar level monitoring, blood glucose level monitoring, cardiac pacemakers, and many others. They are capable of monitoring the physiological data in real time. Design of such devices is a very challenging task as they consist of many small components. Among all these components the antenna is a major component because it works as a transmitting antenna or receiving antenna. In biotelemetry smaller size implantable sensors are preferable. The other components of the implantable sensors can be small and efficient at same time but it is very difficult to keep the antenna size small while maintaining its performance. So, design of an implantable antenna is a very challenging task. Three implantable antennas were designed to be used for implantable medical devices.

The design of a circular patch antenna was presented first. The antenna was simulated in multi-layer tissues and different implant depths. The antenna maintains its performance in skin and muscle phantom layer but the frequency was shifted towards higher bands in the fat phantom layer which can be optimized. A good performance was observed in all the antenna simulations. Specific absorption rate of the antenna was calculated for 1g avg. and 10g avg. SAR analysis shows that the antenna SAR values are within allowed limits. A rectangular patch antenna was designed for biotelemetry applications. The antenna has multiband operation. These frequency bands can be used for data transmission, wakeup signals and wireless power transfer applications. Both free space and implantable simulation results are analysed and showed a good match. The antenna performed well in multilayer tissues and at different implant depths. The gain and radiation efficiency of the antenna increased with increasing implant depths. SAR values for this antenna met the specified standards. The compact size antenna was designed

which is light weight and has very small overall volume. The antenna operates at the same frequency in multilayer tissues (skin, fat and muscle) which is the novelty of this antenna as it maintains its operating frequency despite of the different conducting properties of the body tissues and the fact that its size is very small. Small size antennas often give narrow bandwidth and higher frequencies of operation but this antenna has wider bandwidth of 170 MHz and lower ISM resonance frequency of 915 MHz. The antenna showed good performance even at deeper implantation inside the phantom tissue layers. The antenna has low SAR values which makes it the best match for implantable sensors. The comparative analysis of all the designed antennas has proved that the designed antennas have smaller size and improved performance as compared to previously designed antennas presented in open literature. The circular patch antenna comparison with other similar antennas in Table 4.2 showed that the circular patch has an overall size reduction of 15% with an overall performance improvement of 9%. A size reduction of around 29% is achieved in rectangular patch antenna design with an overall performance improvement of 15% as given in comparison Table 4.4. It can be seen in Table 4.7 that the compact size antenna has an overall performance improvement of 12% with the size reduction of around 47% as compared to the similar antennas presented in literature.

The designed antenna performance was analysed for different implantable scenarios. The compact size antenna was simulated in different shape phantoms with the same volume. The antenna return loss and bandwidth were not effected but the gain and radiation efficiency were changed. The rectangular patch antenna performance was analysed with different layers of insulation. Antenna performance has negligible difference at lower frequencies for different layers of thickness but at higher ISM band the bandwidth of the antenna was increased with a reduction in return loss. Mimicking circuit components were used to check the designed antennas integration with sensors. The simulation results showed that the antennas performed well with circuit components. The designed antennas also showed a good agreement between the simulation results of simplified body model and anatomical body model.

## **6.2 Future Work**

There are lot of issues faced during this research. The limited facilities prevented us from fabricating the prototype because of restrictions imposed as a result of COVID-19. The extension of this research work could be following.

### *6.2.1 Antenna Fabrication*

All of the designed antennas in the software can be fabricated and tested. Tissue simulating liquid or minced meat could be used for the fabricated antennas performance evaluation. Antennas can be subjected to different implantation depths and mounting scenarios to quantify their working mechanism and performance. Simulation results of free space and implantable conditions can be compared with the experimental results of the fabricated antennas for any optimization if needed. The antenna communication channel can be characterized and path losses could be calculated to ensure the reliable communication link.

### *6.2.2 Wireless power transfer*

Wireless power transfer is very interesting topic of the current age because of its applications in biotelemetry. The batteries used to power the implantable device can occupy a considerable space resulting in bigger size of the whole implant. The battery life also poses a challenge because the sensors are needed to be replaced quite often because of the battery lifetime. If the power is transferred wirelessly to the implantable device the aforementioned issue will be eliminated. The antennas with multiband operation can be used for such application. Lower band can be used for data transmission and higher band can be used for wireless power transfer.

### *6.2.3 Antenna design*

There is a new way of designing antennas with biodegradable materials. The materials degrade over time and surgery is not needed to remove them. There is a need for designing more such antennas. Metamaterials inspired implantable antennas also show good performance. Metamaterials should be used to improve the overall implant performance. The path losses between the implanted antennas and

the external devices are normally calculated but the path losses between the two implants should also be investigated for better communication link.

#### *6.2.4 Realization of the implantable device*

The designed implantable antennas are meant to be used with implantable sensors. The development of a complete sensor by integrating the designed antenna with it could be the future work. The device can be tested to transmit data from in-body to off-body (external receiver). This needs a lot of work because the sensors deal with two different fields of science, biological sciences and engineering. The whole implantable device can be used for wireless power transfer.

## References

- [1] K. S. Nikita, "Implantable Devices," in *Handbook of Biomedical Telemetry*, John Wiley & Sons, 2014, ch. 1, pp. 15-18, .
- [2] E. Topsakal, M. Ghovanloo and R. Bashirullah, "Guest Editorial: IEEE AWPL special cluster on wireless power and data telemetry for medical applications," *IEEE Antennas and Wireless Propagation Letters*, vol. 11, pp. 1638-1641, 2012.
- [3] J. Lin and Y. Wang, "An implantable microwave antenna for interstitial hyperthermia," *IEEE Proceedings*, vol. 75, (8), pp. 1132-1133, 1987.
- [4] S. M. Rao, A. Mhatre, D. Popa, J. Chiao, T. Ativanichayaphong, J. Sin and H. E. Stephanou, "MEMS based implantable drug delivery system," *Proceedings of VII International Conference on Micro Electro Mechanical Systems*, El Paso, TX, USA, Sep. 21-22, 2005, pp. 1-4.
- [5] R. Alrawashdeh, "Implantable Antennas for Biomedical Applications." PhD dissertation, University of Liverpool, UK, 2015.
- [6] Federal Communications Commission, "Medical implant communications service (MICS) federal register," *Rules Register*, vol. 64, (240), pp. 69926-69934, 1999.
- [7] IEEE Standard for Safety Levels with Respect to Human Exposure to Radio Frequency Electromagnetic Fields, 3 kHz to 300 GHz, IEEE Standard C95.1-1999, 1999.
- [8] L. J. Xu, Y. X. Guo and W. Wu, "Miniaturized Circularly Polarized Loop Antenna for Biomedical Applications," *IEEE Transactions on Antennas and Propagation*, vol. 63, (3), pp. 922-930, 2015.
- [9] S. Maity, K. R. Barman and S. Bhattacharjee, "Silicon-based technology: Circularly polarized microstrip patch antenna at ISM band with miniature structure using fractal geometry for biomedical application," *Microwave and Optical Technology Letters*, vol. 60, (1), pp. 93-101, 2018.
- [10] Y. Fu, J. Lei, X. Zou and J. Guo, "Flexible antenna design on PDMS substrate for implantable bioelectronics applications," *Electrophoresis*, vol. 40, (8), pp. 1186-1194, 2019.
- [11] S. A. Kumar and T. Shanmuganantham, "Coplanar waveguide-fed ISM band implantable crossed-type triangular slot antenna for biomedical applications," *International Journal of Microwave and Wireless Technologies*, vol. 6, (2), pp. 167-172, 2014.
- [12] Z. Bao, Y. Guo and R. Mittra, "An Ultrawideband Conformal Capsule Antenna With Stable Impedance Matching," *IEEE Transactions on Antennas and Propagation*, vol. 65, (10), pp. 5086-5094, 2017.
- [13] O. Knecht, Y. Jundt and J. W. Kolar, "Planar inverted-F antenna design for a fully implantable mechanical circulatory support system," *IEEE International Conference on Industrial Technology (ICIT)*, Toronto, Canada, 2017, pp. 1366-1371.
- [14] P. Leelatien, K. Ito, K. Saito, A. Alomainy, M. Sharma and Y. Hao, "Radio telemetry performance of liver implanted ultra wideband antenna," *11th European Conference on Antennas and Propagation (EUCAP)*, Paris, France, 2017, pp. 685-688.

- [15] S. Surapan, S. Kawdungta, H. C. Yang and Chih-Kuang Wu, "Design of dual band implantable antenna for biomedical applications," *13th International Conference on Electrical Engineering/Electronics, Computer, Telecommunications and Information Technology (ECTI-CON)*, Chiang Mai, Thailand, 2016, pp. 1-4.
- [16] S. Hashemi and J. Rashed-Mohassel, "Miniaturization of dual band implantable antennas," *Microwave and Optical Technology Letters*, vol. 59, (1), pp. 36-40, 2017.
- [17] D. Nikolayev, M. Zhadobov, P. Karban and R. Sauleau, "434 MHz ISM band antenna for in-body biotelemetry capsules," *11th European Conference on Antennas and Propagation (EUCAP)*, Paris, France, 2017, pp. 1035-1038.
- [18] N. A. Malik, T. Ajmal, P. Sant and M. Ur-Rehman, "A tri-band implantable antenna for biotelemetry applications," *IEEE International Conference on UK-China Emerging Technologies (UCET)*, Glasgow, UK, 2020, pp. 1-4.
- [19] N. A. Malik, T. Ajmal, P. Sant and M. Ur-Rehman, "A compact size implantable antenna for bio-medical applications," *International Conference on UK-China Emerging Technologies (UCET)*, Glasgow, UK, 2020, pp. 1-4.
- [20] N. A. Malik, P. Sant, T. Ajmal and M. Ur-Rehman, "Implantable antennas for bio-medical applications," *IEEE Journal of Electromagnetics, RF and Microwaves in Medicine and Biology*, vol. 5, (1), pp. 84-96, March 2021.
- [21] M. Zaeimbashi, H. Lin, C. Dong, X. Liang, M. Nasrollahpour, H. Chen, N. Sun, "NanoNeuroRFID: A wireless implantable device based on magnetoelectric antennas," *IEEE Journal of Electromagnetics, RF and Microwaves in Medicine and Biology*, vol. 3, (3), pp. 206-215, 2019.
- [22] Y. Peng, K. Saito and K. Ito, "Dual-band antenna design for wireless capsule endoscopic image transmission in the MHz band based on impulse radio technology," *IEEE Journal of Electromagnetics, RF and Microwaves in Medicine and Biology*, vol. 3, (3), pp. 158-164, 2019.
- [23] Y. Fan, J. Huang, T. Chang and X. Liu, "A miniaturized four-element MIMO antenna with EBG for implantable medical devices," *IEEE Journal of Electromagnetics, RF and Microwaves in Medicine and Biology*, vol. 2, (4), pp. 226-233, 2018.
- [24] O. Hammouda and A. Allam, "Utilizing implanted antennas to detect the presence of oral cancers," *Research Journal of Engineering Sciences*, vol. 2278, pp. 9472, 2014.
- [25] Z. Xiao, X. Tan, X. Chen, S. Chen, Z. Zhang, H. Zhang, J. Wang, "An implantable RFID sensor tag toward continuous glucose monitoring," *IEEE Journal of Biomedical and Health Informatics*, vol. 19, (3), pp. 910-919, 2015.
- [26] A. Chauhan, G. K. Chauhan and G. Kaur, "Implantable antennas in biomedical applications," *International Conference on Computational Intelligence and Communication Networks (CICN)*, Jabalpur, India, 2015, pp. 25-29.
- [27] Safety code, "Limits of human exposure to radiofrequency electromagnetic fields in the frequency range from 3 kHz to 300 GHz," *Environmental Health Directorate, Health Protection Branch, Health Canada, Canada*, 1999.

- [28] A. Kiourtzi, A. Kaltampani and K. S. Nikita, "A novel algorithm for implantable antenna design: Size and radiation performance considerations," *The 8th European Conference on Antennas and Propagation (EuCAP 2014)*, 2014, pp. 864-867.
- [29] A. Kiourtzi and K. S. Nikita, "A review of implantable patch antennas for biomedical telemetry: Challenges and solutions [wireless corner]," *IEEE Antennas and Propagation Magazine*, vol. 54, (3), pp. 210-228, 2012.
- [30] P. Soontornpipit, C. M. Furse and Y. C. Chung, "Miniaturized biocompatible microstrip antenna using genetic algorithm," *IEEE Transactions on Antennas and Propagation*, vol. 53, (6), pp. 1939-1945, 2005.
- [31] T. Chien, C. Cheng, H. Yang, J. Jiang and C. Luo, "Development of nonsuperstrate implantable low-profile CPW-fed ceramic antennas," *IEEE Antennas and Wireless Propagation Letters*, vol. 9, pp. 599-602, 2010.
- [32] J. Kim and Y. Rahmat-Samii, "Planar inverted-F antennas on implantable medical devices: Meandered type versus spiral type," *Microwave and Optical Technology Letters*, vol. 48, (3), pp. 567-572, 2006.
- [33] A. Kiourtzi, M. Christopoulou and K. S. Nikita, "Performance of a novel miniature antenna implanted in the human head for wireless biotelemetry," *IEEE International Symposium on Antennas and Propagation (APSURSI)*, Spokane, WA, USA, 2011, pp. 392-395.
- [34] L. Xu, Y. Guo and W. Wu, "Bandwidth enhancement of an implantable antenna," *IEEE Antennas and Wireless Propagation Letters*, vol. 14, pp. 1510-1513, 2015.
- [35] C. Liu, Y. Guo and S. Xiao, "Capacitively loaded circularly polarized implantable patch antenna for ISM band biomedical applications," *IEEE Transactions on Antennas and Propagation*, vol. 62, (5), pp. 2407-2417, 2014.
- [36] M. Ur-Rehman, N. A. Malik, X. Yang, Q. H. Abbasi, Z. Zhang and N. Zhao, "A low profile antenna for millimeter-wave body-centric applications," *IEEE Transactions on Antennas and Propagation*, vol. 65, (12), pp. 6329-6337, 2017.
- [37] T. Karacolak, A. Z. Hood and E. Topsakal, "Design of a dual-band implantable antenna and development of skin mimicking gels for continuous glucose monitoring," *IEEE Transactions on Microwave Theory and Techniques*, vol. 56, (4), pp. 1001-1008, 2008.
- [38] W. Xia, K. Saito, M. Takahashi and K. Ito, "Performances of an implanted cavity slot antenna embedded in the human arm," *IEEE Transactions on Antennas and Propagation*, vol. 57, (4), pp. 894-899, 2009.
- [39] L. Wakrim, S. Ibnyaich and M. M. Hassani, "The study of the ground plane effect on a Multiband PIFA Antenna by using Genetic Algorithm and Particle Swarm Optimization," *Journal of Microwaves, Optoelectronics and Electromagnetic Applications*, vol. 15, (4), pp. 293-308, 2016.
- [40] J. C. Lin, "Safety standards for human exposure to radio frequency radiation and their biological rationale," *IEEE Microwave Magazine*, vol. 4, (4), pp. 22-26, 2003.
- [41] Radiofrequency Electromagnetic Fields, "Evaluating compliance with FCC guidelines for human exposure to radiofrequency electromagnetic fields," *OET Bulletin*, vol. 65, (10), 1997.

- [42] Exposure to Electromagnetic Fields, "Guidelines for limiting human exposure to electromagnetic fields up to 300 GHz," *Rwanda Utilities Regulatory Agency*, 2009.
- [43] C. Liu, Y. Guo and S. Xiao, "A review of implantable antennas for wireless biomedical devices," *Forum for Electromagnetic Research Methods and Application Technologies (FERMAT)*, 2016, .
- [44] F. Merli, "Implantable Antennas for Biomedical Applications." PhD dissertation, EPFL University, Lausanne, Switzerland, 2011.
- [45] P. Soontornpipit, C. M. Furse and Y. C. Chung, "Design of implantable microstrip antenna for communication with medical implants," *IEEE Transactions on Microwave Theory and Techniques*, vol. 52, (8), pp. 1944-1951, 2004.
- [46] R. Warty, M. Tofighi, U. Kawoos and A. Rosen, "Characterization of implantable antennas for intracranial pressure monitoring: Reflection by and transmission through a scalp phantom," *IEEE Transactions on Microwave Theory and Techniques*, vol. 56, (10), pp. 2366-2376, 2008.
- [47] T. Karacolak, R. Cooper, J. Butler, S. Fisher and E. Topsakal, "In vivo verification of implantable antennas using rats as model animals," *IEEE Antennas and Wireless Propagation Letters*, vol. 9, pp. 334-337, 2010.
- [48] A. K. Skrivervik and F. Merli, "Design strategies for implantable antennas," *Loughborough Antennas and Propagation Conference (LAPC)*, Loughborough, UK, 2011, pp. 1-5.
- [49] J. Abadia, F. Merli, J. Zurcher, J. R. Mosig and A. K. Skrivervik, "3D-spiral small antenna design and realization for biomedical telemetry in the MICS band," *Radioengineering*, vol. 18, (4), pp. 359-367, 2009.
- [50] B. Mohamadzade, R. M. Hashmi, R. B. Simorangkir, R. Gharaei, S. Ur Rehman and Q. H. Abbasi, "Recent advances in fabrication methods for flexible antennas in wearable devices: State of the art," *Sensors*, vol. 19, (10), pp. 2312, 2019.
- [51] K. P. Esselle, "Antennas for Wireless Medical Devices," in *Antennas for Small Mobile Terminals*, Artech House, 2018, ch. 11, pp. 183-202, .
- [52] A. Nag, R. B. Simorangkir, E. Valentin, T. Björnin, L. Ukkonen, R. M. Hashmi and S. C. Mukhopadhyay, "A transparent strain sensor based on PDMS-embedded conductive fabric for wearable sensing applications," *IEEE Access*, vol. 6, pp. 71020-71027, 2018.
- [53] R. B. Simorangkir, Y. Yang, R. M. Hashmi, T. Björnin, K. P. Esselle and L. Ukkonen, "Polydimethylsiloxane-embedded conductive fabric: Characterization and application for realization of robust passive and active flexible wearable antennas," *IEEE Access*, vol. 6, pp. 48102-48112, 2018.
- [54] B. Mohamadzade, R. B. Simorangkir, R. M. Hashmi and A. Lalbakhsh, "Communication A Conformal Ultrawideband Antenna with Monopole-Like Radiation Patterns," *IEEE Transactions on Antennas and Propagation*, vol. 68, (8), pp. 6383-6388, Aug. 2020.
- [55] G. Wang, J. Fang and X. Dong, "Resolution of near-field microwave target detection and imaging by using flat LHM lens," *IEEE Transactions on Antennas and Propagation*, vol. 55, (12), pp. 3534-3541, 2007.
- [56] Y. Gong and G. Wang, "Superficial tumor hyperthermia with flat left-handed metamaterial lens," *Progress in Electromagnetics Research*, vol. 98, pp. 389-405, 2009.

- [57] S. Bhattacharjee, S. Maity, S. R. B. Chaudhuri and M. Mitra, "Metamaterial-inspired wideband biocompatible antenna for implantable applications," *IET Microwaves, Antennas & Propagation*, vol. 12, (11), pp. 1799-1805, 2018.
- [58] M. Zada, I. A. Shah and H. Yoo, "Metamaterial-loaded compact high-gain dual-band circularly polarized implantable antenna system for multiple biomedical applications," *IEEE Transactions on Antennas and Propagation*, vol. 68, (2), pp. 1140-1144, 2019.
- [59] O. M. Khan, R. M. Shubair, Q. U. Islam and I. Rashid, "Triband metamaterial embedded implantable antenna for biotelemetry applications," *IEEE International Symposium on Antennas and Propagation & USNC/URSI National Radio Science Meeting*, Boston, MA, USA, 2018, pp. 213-214.
- [60] C. J. Sánchez-Fernández, O. Quevedo-Teruel, J. Requena-Carrion, L. Inclan-Sánchez, E. Rajo-Iglesias and M. N. M. Kehn, "Dual-band implantable antenna based on short-circuited SRR," *Proceedings of the 4th European Conference on Antennas and Propagation (EuCAP)*, Barcelona, Spain, 2010, pp. 1-4.
- [61] K. Jaiswal, "Probe-Fed Wideband Implantable Microstrip Patch Antenna for Biomedical and Telemetry Applications," in *Soft Computing and Signal Processing*, Springer, 2019, pp. 635-642, .
- [62] S. A. A. Shah and H. Yoo, "Scalp-implantable antenna systems for intracranial pressure monitoring," *IEEE Transactions on Antennas and Propagation*, vol. 66, (4), pp. 2170-2173, 2018.
- [63] N. S. N. Samsuri, M. Rahim, F. Seman and M. Inam, "Compact Meander Line Telemetry Antenna for Implantable Pacemaker Applications," *Indonesian Journal of Electrical Engineering and Computer Science*, vol. 10, (3), pp. 883-889, 2018.
- [64] S. H. Zainud-Deen, H. A. E. Malhat and A. A. Balabel, "Octafilar Helical Antenna for Circular Polarization Wireless Capsule Endoscopy Applications," *Wireless Personal Communications*, vol. 108, (1), pp. 569-579, 2019.
- [65] X. Wang, J. Shi, L. Xu and J. Wang, "A wideband miniaturized implantable antenna for biomedical application at HBC band," *2018 Cross Strait Quad-Regional Radio Science and Wireless Technology Conference (CSQRWC)*, Xuzhou, China, 2018, pp. 1-3.
- [66] S. H. Lee, K. Chang, K. J. Kim and Y. J. Yoon, "A conical spiral antenna for wideband capsule endoscope system," *IEEE Antennas and Propagation Society International Symposium*, San Diego, CA, USA, 2008, pp. 1-4.
- [67] R. Li, Y. Guo and G. Du, "A conformal circularly polarized antenna for wireless capsule endoscope systems," *IEEE Transactions on Antennas and Propagation*, vol. 66, (4), pp. 2119-2124, 2018.
- [68] K. N. Ketavath, D. Gopi and S. S. Rani, "In-Vitro Test of Miniaturized CPW-Fed Implantable Conformal Patch Antenna at ISM Band for Biomedical Applications," *IEEE Access*, vol. 7, pp. 43547-43554, 2019.
- [69] K. Zhang, C. Liu, X. Liu, H. Cao, Y. Zhang, X. Yang and H. Guo, "A conformal differentially fed antenna for ingestible capsule system," *IEEE Transactions on Antennas and Propagation*, vol. 66, (4), pp. 1695-1703, 2018.
- [70] N. Mahalakshmi and A. Thenmozhi, "Design of hexagon shape bow-tie patch antenna for implantable bio-medical applications," *Alexandria Engineering Journal*, vol. 56, (2), pp. 235-239, 2017.

- [71] L. Xu, Y. Bo, W. Lu, L. Zhu and C. Guo, "Circularly Polarized Annular Ring Antenna With Wide Axial-Ratio Bandwidth for Biomedical Applications," *IEEE Access*, vol. 7, pp. 59999-60009, 2019.
- [72] I. A. Shah, M. Zada and H. Yoo, "Design and Analysis of a Compact-Sized Multiband Spiral-Shaped Implantable Antenna for Scalp Implantable and Leadless Pacemaker Systems," *IEEE Transactions on Antennas and Propagation*, vol. 67, (6), pp. 4230-4234, 2019.
- [73] G. Samanta and D. Mitra, "Dual-Band Circular Polarized Flexible Implantable Antenna Using Reactive Impedance Substrate," *IEEE Transactions on Antennas and Propagation*, vol. 67, (6), pp. 4218-4223, 2019.
- [74] S. Das and D. Mitra, "A compact wideband flexible implantable slot antenna design with enhanced gain," *IEEE Transactions on Antennas and Propagation*, vol. 66, (8), pp. 4309-4314, 2018.
- [75] K. Zhang, C. Liu, X. Liu, H. Guo and X. Yang, "Miniaturized circularly polarized implantable antenna for ISM-band biomedical devices," *International Journal of Antennas and Propagation*, vol. 2017, 2017.
- [76] R. Li, B. Li, G. Du, X. Sun and H. Sun, "A Compact Broadband Antenna with Dual-Resonance for Implantable Devices," *Micromachines*, vol. 10, (1), pp. 59, 2019.
- [77] L. Luo, B. Hu, J. Wu, T. Yan and L. Xu, "Compact dual-band antenna with slotted ground for implantable applications," *Microwave and Optical Technology Letters*, vol. 61, (5), pp. 1314-1319, 2019.
- [78] C. Liu, Y. Zhang and X. Liu, "Circularly polarized implantable antenna for 915 MHz ISM-band far-field wireless power transmission," *IEEE Antennas and Wireless Propagation Letters*, vol. 17, (3), pp. 373-376, 2018.
- [79] A. E. Mohamed, M. S. Sharawi and A. Muqaibel, "Implanted dual-band circular antenna for biomedical applications," *Microwave and Optical Technology Letters*, vol. 60, (5), pp. 1125-1132, 2018.
- [80] F. Faisal and H. Yoo, "A Miniaturized Novel-Shape Dual-Band Antenna for Implantable Applications," *IEEE Transactions on Antennas and Propagation*, vol. 67, (2), pp. 774-783, 2018.
- [81] H. Zhang, L. Li, C. Liu, Y. Guo and S. Wu, "Miniaturized implantable antenna integrated with split resonate rings for wireless power transfer and data telemetry," *Microwave Opt Technol Lett*, vol. 59, (3), pp. 710-714, 2017.
- [82] S. A. Kumar and T. Shanmuganantham, "Design of clover slot antenna for biomedical applications," *Alexandria Engineering Journal*, vol. 56, (3), pp. 313-317, 2017.
- [83] M. Fazeli, Y. Hong, W. Lee and J. Park, "Implantable ferrite antenna for biomedical applications," *Microwave and Optical Technology Letters*, vol. 58, (11), pp. 2745-2749, 2016.
- [84] H. Li, Y. Guo and S. Xiao, "Broadband circularly polarised implantable antenna for biomedical applications," *Electronics Letters*, vol. 52, (7), pp. 504-506, 2016.
- [85] S. A. Kumar, T. Shanmuganantham and G. Sasikala, "Design and development of implantable CPW fed monopole U slot antenna at 2.45 GHz ISM band for biomedical applications," *Microwave and Optical Technology Letters*, vol. 57, (7), pp. 1604-1608, 2015.

- [86] S. A. Kumar and T. Shanmuganantham, "Design and analysis of implantable CPW fed bowtie antenna for ISM band applications," *AEU-International Journal of Electronics and Communications*, vol. 68, (2), pp. 158-165, 2014.
- [87] S. A. Kumar and T. Shanmuganantham, "Implanted CPW Fed Monopole Antenna for Biomedical Applications," in *Advances in Computing and Information Technology*, Springer, 2013, pp. 97-105, .
- [88] X. Li, M. Jalilvand, W. You, W. Wiesbeck and T. Zwick, "An implantable stripline-fed slot antenna for biomedical applications," *IET International Radar Conference*, Xi'an, China, 14-16 April 2013, pp. 1-4.
- [89] Calculation of the dielectric properties of body tissues, "Institute for Applied Physics, Italian National Research Council", <http://niremf.ifac.cnr.it/tissprop/>.
- [90] P. Zakavi, N. C. Karmakar and I. Griggs, "Wireless orthopedic pin for bone healing and growth: Antenna development," *IEEE Transactions on Antennas and Propagation*, vol. 58, (12), pp. 4069-4074, 2010.
- [91] A. Kiourti and K. S. Nikita, "Miniature scalp-implantable antennas for telemetry in the MICS and ISM bands: design, safety considerations and link budget analysis," *IEEE Transactions on Antennas and Propagation*, vol. 60, (8), pp. 3568-3575, 2012.
- [92] A. Alomainy and Y. Hao, "Modeling and characterization of biotelemetric radio channel from ingested implants considering organ contents," *IEEE Transactions on Antennas and Propagation*, vol. 57, (4), pp. 999-1005, 2009.
- [93] Y. Huang and K. Boyle, *Antennas: From Theory to Practice*. John Wiley & Sons, 2008.
- [94] R. Moore, "Effects of a surrounding conducting medium on antenna analysis," *IEEE Transactions on Antennas and Propagation*, vol. 11, (3), pp. 216-225, 1963.
- [95] C. Tsao, "Radiation resistance of antennas in lossy media," *IEEE Transactions on Antennas and Propagation*, vol. 19, (3), pp. 443-444, 1971.
- [96] T. Wittig, "SAR Overview", <https://www.cst.com/Content/Events/UGM2007/05-Witting.pdf>.
- [97] H. Oraizi and B. Rezaei, "Improvement of antenna radiation efficiency by the suppression of surface waves," *Journal of Electromagnetic Analysis and Applications*, vol. 3, (03), pp. 79, 2011.
- [98] D. Nikolayev, M. Zhadobov, P. Karban and R. Sauleau, "Increasing the radiation efficiency and matching stability of in-body capsule antennas," *10th European Conference on Antennas and Propagation (EuCAP)*, Davos, Switzerland, 2016, pp. 1-5.
- [99] H. Li, Y. Guo, C. Liu, S. Xiao and L. Li, "A miniature-implantable antenna for medradio-band biomedical telemetry," *IEEE Antennas and Wireless Propagation Letters*, vol. 14, pp. 1176-1179, 2015.
- [100] S. M. Islam, K. P. Esselle, D. Bull and P. M. Pilowsky, "Bandwidth enhancement of an implantable RFID tag antenna at 900 MHz ISM band for RF telemetry," *International Symposium on Communications and Information Technologies (ISCIT)*, Gold Coast, QLD, Australia, 2012, pp. 741-745.

- [101] C. Huang, C. Tsai and C. Yang, "Compact broadband implantable monopole antenna with gain enhancement," *IEEE Antennas and Propagation Society International Symposium (APSURSI)*, Memphis, TN, USA, 2014, pp. 1590-1591.
- [102] C. Schmidt, F. Casado, A. Arriola, I. Ortego, P. D. Bradley and D. Valderas, "Broadband UHF implanted 3-D conformal antenna design and characterization for in-off body wireless links," *IEEE Transactions on Antennas and Propagation*, vol. 62, (3), pp. 1433-1444, 2014.
- [103] M. Mark, T. Björninen, Y. D. Chen, S. Venkatraman, L. Ukkonen, L. Sydänheimo, J. M. Carmena and J. M. Rabaey, "Wireless channel characterization for mm-size neural implants," *Annual International Conference of the IEEE Engineering in Medicine and Biology*, Buenos Aires, Argentina, 2010, pp. 1565-1568.
- [104] F. Huang, C. Lee, C. Chang, L. Chen, T. Yo and C. Luo, "Rectenna application of miniaturized implantable antenna design for triple-band biotelemetry communication," *IEEE Transactions on Antennas and Propagation*, vol. 59, (7), pp. 2646-2653, 2011.
- [105] Z. Chen, H. Sun and W. Geyi, "Maximum Wireless Power Transfer to the Implantable Device in the Radiative Near Field," *IEEE Antennas and Wireless Propagation Letters*, vol. 16, pp. 1780-1783, 2017.
- [106] R. Das, Y. Cho and H. Yoo, "High efficiency unidirectional wireless power transfer by a triple band deep-tissue implantable antenna," *IEEE MTT-S International Microwave Symposium (IMS)*, San Francisco, CA, USA, 2016, pp. 1-4.
- [107] A. Alomainy and Y. Hao, "Modeling and characterization of biotelemetric radio channel from ingested implants considering organ contents," *IEEE Transactions on Antennas and Propagation*, vol. 57, (4), pp. 999-1005, 2009.
- [108] M. R. Basar, Malek, Mohd Fareq Bin Abd, K. M. Juni, M. I. M. Saleh, M. S. Idris, L. Mohamed, N. Saudin, "The use of a human body model to determine the variation of path losses in the human body channel in wireless capsule endoscopy," *Progress in Electromagnetics Research*, vol. 133, pp. 495-513, 2013.
- [109] S. Park, W. Kim, J. Lee, Y. Chung and C. Cheon, "A new receiver antenna with buffer layer for wireless capsule endoscopy in human body," *IEEE Antennas and Propagation Society International Symposium*, San Diego, CA, USA, 2008, pp. 1-4.
- [110] A. C. Gordillo and I. Balasingham, "On directive antennas application to implant-on-body UWB communications," *The 19th Annual Wireless and Optical Communications Conference (WOCC 2010)*, Shanghai, China, 2010, pp. 1-5.
- [111] Y. Yang, G. Fang, E. Dutkiewicz and D. Shen, "Statistical characterization of the 400 mhz in-body propagation channel in in-door environments," *International Symposium on Communications and Information Technologies (ISCIT)*, Gold Coast, QLD, Australia, 2012, pp. 48-53.
- [112] T. H. Hubing, "Survey of numerical electromagnetic modeling techniques," *Department of Electrical Engineering, University of Missouri-Rolla, USA*, 1991.
- [113] C. A. Balanis, *Antenna Theory: Analysis and Design*. 4th ed. John wiley & sons, 2015.
- [114] P. Shubtidze, R. Jobava, R. Beria, I. Shamatava, R. Zaridze and D. Karkashadze, "Application of FDTD to dispersive media," *DIPED-99. Direct and Inverse Problems of Electromagnetic and*

*Acoustic Wave Theory. Proceedings of 4th International Seminar/Workshop (IEEE Cat. no. 99TH8402), Lviv, Ukraine, 1999, pp. 112-116.*

[115] K. Yee, "Numerical solution of initial boundary value problems involving Maxwell's equations in isotropic media," *IEEE Transactions on Antennas and Propagation*, vol. 14, (3), pp. 302-307, 1966.

[116] T. Weiland, "A discretization model for the solution of Maxwell's equations for six-component fields," *Archiv Elektronik Und Uebertragungstechnik*, vol. 31, pp. 116-120, 1977.

[117] V. Grout, M. O. Akinsolu, B. Liu, P. I. Lazaridis, K. K. Mistry and Z. D. Zaharis, "Software Solutions for Antenna Design Exploration: A Comparison of Packages, Tools, Techniques, and Algorithms for Various Design Challenges," *IEEE Antennas and Propagation Magazine*, vol. 61, pp. 48-59, June 2019.

[118] Antenna Design, "*RFID Antenna Design using Zeland Tools*", <https://www.rfglobalnet.com/doc/rfid-antenna-design-using-zeland-tools-0001>.

[119] Zeland Inc., "*IE3D User Manual*", 2019, <http://www.zeland.com>.

[120] Ansys HFSS, "*3D High Frequency Simulation Software*", <https://www.ansys.com/en-gb/products/electronics/ansys-hfss>.

[121] Altair Engineering Inc., "*Altair Feko*", <https://www.altair.com/feko/>.

[122] CST Studio Suite 3D EM simulation and analysis software, "*CST Microwave Studio User Manual*", 2019, <https://www.3ds.com/products-services/simulia/products/cst-studio-suite/>.

[123] The MathWorks Inc., "*Antenna Toolbox*", <https://uk.mathworks.com/products/antenna.html>.

[124] CADES Research Centre, "*Antenna Design Explorer, ADE 1.0*", <http://cadescenter.com/antenna-design/explorer/>.

[125] Electromagnetic Analysis, "*Full Wave Solutions to Maxwell's Equations*", <https://www.microwavejournal.com/articles/29299-electromagnetic-analysis>.

[126] Alexej Grudiev, "*Simulation Packages and Review of Codes*", [https://indico.cern.ch/event/164082/contributions/246170/attachments/195880/274792/Simulation\\_packages\\_and\\_Review\\_of\\_Codes\\_AG.pdf](https://indico.cern.ch/event/164082/contributions/246170/attachments/195880/274792/Simulation_packages_and_Review_of_Codes_AG.pdf).

[127] M. Mokhtar, K. Kamardin, Y. Yamada, R. H. M. Baharin, N. H. Abd Rahman, N. Zainudin, T. A. Latef and M. N. M. Yasin, "Implantable patch antenna for body communication," *2nd International Conference on Telematics and Future Generation Networks (TAFGEN)*, Kuching, Malaysia, 2018, pp. 77-80.

[128] S. D. Hossain, K. A. Sobahan and M. Al-Amin, "A circular microstrip patch antenna to operate in dual band for wireless communications," *Journal of Physics: Conference Series*, vol. 1718, (1), pp. 012014, 2021.

[129] Y. Zhang, C. Liu, X. Liu, K. Zhang and X. Yang, "A wideband circularly polarized implantable antenna for 915 MHz ISM-band biotelemetry devices," *IEEE Antennas and Wireless Propagation Letters*, vol. 17, (8), pp. 1473-1477, 2018.

- [130] Y. Liu, Y. Chen, H. Lin and F. H. Juwono, "A Novel Differentially Fed Compact Dual-Band Implantable Antenna for Biotelemetry Applications," *IEEE Antennas and Wireless Propagation Letters*, vol. 15, pp. 1791-1794, 2016.
- [131] H. Werfelli, K. Tayari, M. Chaoui, M. Lahiani and H. Ghariani, "Design of rectangular microstrip patch antenna," *2nd International Conference on Advanced Technologies for Signal and Image Processing (ATSIP)*, Monastir, Tunisia, 2016, pp. 798-803.
- [132] M. Q. Qi, H. Xu, H. F. Ma, M. P. Jin, W. Wang and T. J. Cui, "A wideband waveguide antenna with nearly equal E-and H-plane radiation patterns," *Hindawi*, vol. 2013, 2013.
- [133] N. Nkordeh, F. Idachaba and O. Oni, "Microstrip patch antenna: Comparing performance of a rectangular and a circular patch at LTE bluetooth and GSM frequencies," *Proceedings of the World Congress on Engineering WCE*, London, UK, July 1 - 3, 2015, pp. 1-6.
- [134] IEEE Standard Definitions of Terms for Antennas, "*IEEE Std 145-1993*", pp.1-32, 18 July 1993.

## Appendix A

### Human Body Tissues Properties at Different Frequencies

#### At 450 MHz

Tissue	Num	Eps	Mue	Kappa [s/m]	Rho [kg/m^3]	K [W/mK]	HeatCap [kJ/K/kg]	BloodFlow [W/K/m^3]	MetabolicRate [W/m^3]
Marrow	1	5.643264	1.0	0.030226	1030	0.624	2.7	32000	5700
FatTissue	2	5.560525	1.0	0.041934	1100	0.201	2.5	1700	300
Bones	3	13.038851	1.0	0.095831	1850	0.410	1.3	3400	610
WhiteSubstance	4	41.484737	1.0	0.459431	1030	0.502	3.6	17280	7100
GraySubstance	5	56.550674	1.0	0.758460	1030	0.502	3.7	40000	7100
Skin	6	45.753101	1.0	0.708836	1100	0.293	3.5	9100	1620
Eye	7	57.244282	1.0	1.018697	1010	0.624	4.178	10300	14250
SkeletonMuscle	8	58.482101	1.0	0.851437	1040	0.460	3.6	2700	480
Blood	9	63.675682	1.0	1.366503	1000	0.505	3.9	0	0
NeuronalFabric	11	54.736618	1.0	1.056018	1030	0.624	3.5	40000	7100
Lens	12	47.872349	1.0	0.679023	1050	0.624	3.0	0	0
NervusOpticus	13	34.081126	1.0	0.459844	1030	0.624	3.5	40000	7100
Cartilages	14	44.995184	1.0	0.603635	1030	0.624	3.5	9000	1600
MucousMembrane	15	49.196331	1.0	0.686908	1100	0.624	3.3	9000	1600
Air	16	1.000000	1.0	0.000000	1.3	0.025	1.005	0	0
Lung	17	23.479828	1.0	0.382735	1020	0.624	3.6	9500	1700
Intestine	18	61.746040	1.0	0.880119	1020	0.624	3.7	53000	9500
Kidney	19	65.002380	1.0	1.127501	1020	0.499	3.9	270000	48000
Liver	20	50.435566	1.0	0.674515	1020	0.469	3.6	68000	12000
Glands	22	61.229324	1.0	0.890586	1020	0.624	3.6	360000	64000
Spleen	23	62.096809	1.0	1.052154	1020	0.543	3.7	82000	15000
Stomach	24	67.058762	1.0	1.018782	1020	0.624	3.6	29000	5200
Pancreas	25	67.058762	1.0	1.018782	1020	0.624	3.5	41000	7300
Bladder	26	19.580004	1.0	0.331574	1010	0.624	3.3	9000	1600
GallBladder	27	60.742165	1.0	1.148203	1020	0.624	3.9	0	0
IntestineContents	28	64.091296	1.0	1.930395	1020	0.624	4.2	0	0
VentriclesRight	30	64.970528	1.0	0.992743	1000	0.493	4.2	0	0
VentriclesLeft	31	64.970528	1.0	0.992743	1000	0.493	4.2	0	0
ForecourtRight	32	64.970528	1.0	0.992743	1000	0.493	3.7	54000	9600
ForecourtLeft	33	64.970528	1.0	0.992743	1000	0.493	3.7	54000	9600
BloodV	43	63.675682	1.0	1.366503	1000	0.493	3.9	0	0
BloodA	44	63.675682	1.0	1.366503	1000	0.493	3.9	0	0

## At 900 MHz

Tissue	Num	Eps	Mue	Kappa [s/m]	Rho [kg/m^3]	K [W/mK]	HeatCap [kJ/K/kg]	BloodFlow [W/K/m^3]	MetabolicRate [W/m^3]
Marrow	1	5.504309	1.0	0.040201	1030	0.624	2.7	32000	5700
FatTissue	2	5.461937	1.0	0.051039	1100	0.201	2.5	1700	300
Bones	3	12.453704	1.0	0.143304	1850	0.410	1.3	3400	610
WhiteSubstance	4	38.086288	1.0	0.590815	1030	0.502	3.6	17280	7100
GraySubstance	5	52.724701	1.0	0.942193	1030	0.502	3.7	40000	7100
Skin	6	41.405334	1.0	0.866780	1100	0.293	3.5	9100	1620
Eye	7	55.270130	1.0	1.166726	1010	0.624	4.178	10300	14250
SkeletonMuscle	8	56.879063	1.0	0.995364	1040	0.460	3.6	2700	480
Blood	9	61.360718	1.0	1.538069	1000	0.505	3.9	0	0
NeuronalFabric	11	49.443092	1.0	1.262649	1030	0.624	3.5	40000	7100
Lens	12	46.572613	1.0	0.793379	1050	0.624	3.0	0	0
NervusOpticus	13	32.530067	1.0	0.573612	1030	0.624	3.5	40000	7100
Cartilages	14	42.653103	1.0	0.782333	1030	0.624	3.5	9000	1600
MucousMembrane	15	46.080399	1.0	0.844670	1100	0.624	3.3	9000	1600
Air	16	1.000000	1.0	0	1.3	0.025	1.005	0	0
Lung	17	21.999969	1.0	0.456663	1020	0.624	3.6	9500	1700
Intestine	18	57.939129	1.0	1.079813	1020	0.624	3.7	53000	9500
Kidney	19	58.675552	1.0	1.392205	1020	0.499	3.9	270000	48000
Liver	20	46.833118	1.0	0.854965	1020	0.469	3.6	68000	12000
Glands	22	59.683323	1.0	1.038448	1020	0.624	3.6	360000	64000
Spleen	23	57.178375	1.0	1.272679	1020	0.543	3.7	82000	15000
Stomach	24	65.061401	1.0	1.186670	1020	0.624	3.6	29000	5200
Pancreas	25	65.061401	1.0	1.186670	1020	0.624	3.5	41000	7300
Bladder	26	18.936157	1.0	0.383049	1010	0.624	3.3	9000	1600
GallBladder	27	59.141594	1.0	1.256896	1020	0.624	3.9	0	0
IntestineContents	28	59.487000	1.0	2.164847	1020	0.624	4.2	0	0
VentriclesRight	30	59.892677	1.0	1.229882	1000	0.493	4.2	0	0
VentriclesLeft	31	59.892677	1.0	1.229882	1000	0.493	4.2	0	0
ForecourtRight	32	59.892677	1.0	1.229882	1000	0.493	3.7	54000	9600
ForecourtLeft	33	59.892677	1.0	1.229882	1000	0.493	3.7	54000	9600
BloodV	43	61.360718	1.0	1.538069	1000	0.493	3.9	0	0
BloodA	44	61.360718	1.0	1.538069	1000	0.493	3.9	0	0

## At 1800 MHz

Tissue	Num	Eps	Mue	Kappa [s/m]	Rho [kg/m^3]	K [W/mK]	HeatCap [kJ/K/kg]	BloodFlow [W/K/m^3]	MetabolicRate [W/m^3]
Marrow	1	5.371605	1.0	0.068468	1030	0.624	2.7	32000	5700
FatTissue	2	5.349368	1.0	0.078385	1100	0.201	2.5	1700	300
Bones	3	11.780735	1.0	0.275193	1850	0.410	1.3	3400	610
WhiteSubstance	4	37.010921	1.0	0.914969	1030	0.502	3.6	17280	7100
GraySubstance	5	50.078876	1.0	1.391190	1030	0.502	3.7	40000	7100
Skin	6	38.871057	1.0	1.184768	1100	0.293	3.5	9100	1620
Eye	7	53.567787	1.0	1.601727	1010	0.624	4.178	10300	14250
SkeletonMuscle	8	55.335312	1.0	1.437796	1040	0.460	3.6	2700	480
Blood	9	59.372261	1.0	2.043690	1000	0.505	3.9	0	0
NeuronalFabric	11	46.113232	1.0	1.708732	1030	0.624	3.5	40000	7100
Lens	12	45.352734	1.0	1.147332	1050	0.624	3.0	0	0
NervusOpticus	13	30.866894	1.0	0.842816	1030	0.624	3.5	40000	7100
Cartilages	14	40.215481	1.0	1.286782	1030	0.624	3.5	9000	1600
MucousMembrane	15	43.850479	1.0	1.232065	1100	0.624	3.3	9000	1600
Air	16	1.000000	1.0	0.000000	1.3	0.025	1.005	0	0
Lung	17	20.945705	1.0	0.637096	1020	0.624	3.6	9500	1700
Intestine	18	55.147705	1.0	1.576100	1020	0.624	3.7	53000	9500
Kidney	19	54.426064	1.0	1.949712	1020	0.499	3.9	270000	48000
Liver	20	44.210804	1.0	1.289116	1020	0.469	3.6	68000	12000
Glands	22	58.142151	1.0	1.500078	1020	0.624	3.6	360000	64000
Spleen	23	53.847534	1.0	1.779962	1020	0.543	3.7	82000	15000
Stomach	24	63.226818	1.0	1.697995	1020	0.624	3.6	29000	5200
Pancreas	25	63.226818	1.0	1.697995	1020	0.624	3.5	41000	7300
Bladder	26	18.341116	1.0	0.535134	1010	0.624	3.3	9000	1600
GallBladder	27	58.213646	1.0	1.642106	1020	0.624	3.9	0	0
IntestineContents	28	55.902672	1.0	2.695574	1020	0.624	4.2	0	0
VentriclesRight	30	56.322693	1.0	1.771246	1000	0.493	4.2	0	0
VentriclesLeft	31	56.322693	1.0	1.771246	1000	0.493	4.2	0	0
ForecourtRight	32	56.322693	1.0	1.771246	1000	0.493	3.7	54000	9600
ForecourtLeft	33	56.322693	1.0	1.771246	1000	0.493	3.7	54000	9600
BloodV	43	59.372261	1.0	2.043690	1000	0.493	3.9	0	0
BloodA	44	59.372261	1.0	2.043690	1000	0.493	3.9	0	0

## At 2450 MHz

Tissue	Num	Eps	Mue	Kappa [s/m]	Rho [kg/m^3]	K [W/mK]	HeatCap [kJ/K/kg]	BloodFlow [W/K/m^3]	MetabolicRate [W/m^3]
Marrow	1	5.296872	1.0	0.095031	1030	0.624	2.7	32000	5700
FatTissue	2	5.280096	1.0	0.104517	1100	0.201	2.5	1700	300
Bones	3	11.381223	1.0	0.394277	1850	0.410	1.3	3400	610
WhiteSubstance	4	36.166599	1.0	1.215008	1030	0.502	3.6	17200	7100
GraySubstance	5	48.911255	1.0	1.807664	1030	0.502	3.7	40000	7100
Skin	6	38.006660	1.0	1.464073	1100	0.293	3.5	9100	1620
Eye	7	52.627628	1.0	2.033048	1010	0.624	4.178	10300	14250
SkeletonMuscle	8	54.417614	1.0	1.882011	1040	0.460	3.6	2700	480
Blood	9	58.263756	1.0	2.544997	1000	0.505	3.9	0	0
NeuronalFabric	11	44.803696	1.0	2.101270	1030	0.624	3.5	40000	7100
Lens	12	44.625317	1.0	1.504036	1050	0.624	3.0	0	0
NervusOpticus	13	30.145145	1.0	1.088474	1030	0.624	3.5	40000	7100
Cartilages	14	38.771160	1.0	1.755682	1030	0.624	3.5	9000	1600
MucousMembrane	15	42.852562	1.0	1.591928	1100	0.624	3.3	9000	1600
Air	16	1.000000	1.0	0.000000	1.3	0.025	1.005	0	0
Lung	17	20.476801	1.0	0.804128	1020	0.624	3.6	9500	1700
Intestine	18	53.878193	1.0	2.038204	1020	0.624	3.7	53000	9500
Kidney	19	52.742668	1.0	2.429709	1020	0.499	3.9	270000	48000
Liver	20	43.034443	1.0	1.686411	1020	0.469	3.6	68000	12000
Glands	22	57.200367	1.0	1.967798	1020	0.624	3.6	360000	64000
Spleen	23	52.449310	1.0	2.238070	1020	0.543	3.7	82000	15000
Stomach	24	62.158325	1.0	2.210518	1020	0.624	3.6	29000	5200
Pancreas	25	62.158325	1.0	2.210518	1020	0.624	3.5	41000	7300
Bladder	26	18.000759	1.0	0.685294	1010	0.624	3.3	9000	1600
GallBladder	27	57.633728	1.0	2.059032	1020	0.624	3.9	0	0
IntestineContents	28	54.424351	1.0	3.172779	1020	0.624	4.2	0	0
VentriclesRight	30	54.814018	1.0	2.256186	1000	0.493	4.2	0	0
VentriclesLeft	31	54.814018	1.0	2.256186	1000	0.493	4.2	0	0
ForecourtRight	32	54.814018	1.0	2.256186	1000	0.493	3.7	54000	9600
ForecourtLeft	33	54.814018	1.0	2.256186	1000	0.493	3.7	54000	9600
BloodV	43	58.263756	1.0	2.544997	1000	0.493	3.9	0	0
BloodA	44	58.263756	1.0	2.544997	1000	0.493	3.9	0	0

## **Appendix B**

### **Ethics Form**

#### **UNIVERSITY OF BEDFORDSHIRE**

##### **Research Ethics Scrutiny (Postgraduate Research Students)**

**When completing this form please ensure that you read and comply with the following:**

Researchers must demonstrate clear understanding of an engagement with the following:

1. *Integrity* - The research has been carried out in a rigorous and professional manner and due credit has been attributed to all parties involved.
2. *Plagiarism* - Proper acknowledgement has been given to the authorship of data and ideas.
3. *Conflicts of Interest* - All financial and professional conflicts of interest have been properly identified and declared.
4. *Data Handling* - The research draws upon effective record keeping, proper storage of date in line with confidentiality, statute and University policy.
5. *Ethical Procedures* - Proper consideration has been given to all ethical issues and appropriate approval sought and received from all relevant stakeholders. In addition the research should conform to professional codes of conduct where appropriate.
6. *Supervision* - Effective management and supervision of staff and student for whom the researcher(s) is/are responsible
7. *Health and Safety*- Proper training on health and safety issues has been received and completed by all involved parties. Health and safety issues have been identified and appropriate assessment and action have been undertaken.

The **Research Institutes** are responsible for ensuring that all researchers abide by the above. It is anticipated that ethical approval will be granted by each Research Institute. Each Research Institute will give guidance and approval on ethical procedures and ensure they conform to the requirements of relevant professional bodies. As such Research Institutes are required to provide the University Research Ethics Committee with details of their procedures for ensuring adherence to relevant ethical requirements. This applies to any research whether it be, or not, likely to raise ethical issues. Research proposals involving vulnerable groups; sensitive topics; groups requiring gatekeeper permission; deception or without full informed consent; use of personal/confidential information; subjects in stress, anxiety, humiliation or intrusive interventions must be referred to the University Research Ethics Committee.

Research projects involving participants in the NHS will be submitted through the NHS National Research Ethics Service (NRES). The University Research Ethics Committee will normally accept the judgement of NRES (it will never approve a proposal that has been rejected by NRES), however NRES approval will need to be verified before research can commence and the nature of the research will need to be verified.

Where work is conducted in collaboration with other institutions ethical approval by the University and the collaborating partner(s) will be required.

The **University Research Ethics Committee** is a sub-committee of the Academic Board and is chaired by a member of the Vice Chancellor's Executive Group, appointed by the Vice-Chancellor and includes members external to the University

**Research Misconduct:** Allegations of Research Misconduct against staff or postgraduate (non-taught) research students should be made to the Director of Research Development.

## **UNIVERSITY OF BEDFORDSHIRE**

### **Research Ethics Scrutiny (Annex to RS1 form)**

#### **SECTION A To be completed by the candidate**

Registration No: 1331792

Candidate: Nabeel Ahmed Malik

Degree of: PhD

Research Institute: SSWT (IRAC)

Research Topic: Design of Implantable Antennas for Bio-medical applications

External Funding:

The candidate is required to summarise in the box below the ethical issues involved in the research proposal and how they will be addressed. In any proposal involving human participants the following should be provided:

- clear explanation of how informed consent will be obtained,
- how will confidentiality and anonymity be observed,
- how will the nature of the research, its purpose and the means of dissemination of the outcomes be communicated to participants,
- how personal data will be stored and secured
- if participants are being placed under any form of stress (physical or mental) identify what steps are being taken to minimise risk

If protocols are being used that have already received University Research Ethics Committee (UREC) ethical approval then please specify. Roles of any collaborating institutions should be clearly identified. Reference should be made to the appropriate professional body code of practice.

The research work involves design of implantable antennas for biomedical applications. The software simulations would be confirmed through experimental measurements. The measurements would not require any human subjects for the implant. Instead, I will make use of well-established techniques of liquid gel phantoms/sheep meat (a portion as large as 3cm\*3cm and not more than 300g in weight) obtained from food stores. Therefore, there is no risk to personal health and personal data and no informed consent is required for this work.

Answer the following question by deleting as appropriate:

1. Does the study involve vulnerable participants or those unable to give informed consent (e.g. children, people with learning disabilities, your own students)?

Yes  No

If YES: Have/will Researchers be DBS checked?

Yes  No

2. Will the study require permission of a gatekeeper for access to participants (e.g. schools, self-help groups, residential homes)?

Yes  No

3. Will it be necessary for participants to be involved without consent (e.g. covert observation in non-public places)?

Yes  No

4. Will the study involve sensitive topics (e.g. sexual activity, substance abuse)?

Yes  No

5. Will blood or tissue samples be taken from participants?

Yes  No

6. Will the research involve intrusive interventions (e.g. drugs, hypnosis, physical exercise)?

Yes  No

7. Will financial or other inducements be offered to participants (except reasonable expenses)?

Yes  No

8. Will the research investigate any aspect of illegal activity?

Yes  No

9. Will participants be stressed beyond what is normal for them?

Yes  No

10. Will the study involve participants from the NHS (e.g. patients) or participants who fall under the requirements of the Mental Capacity Act 2005?

Yes\*  No

If you have answered yes to any of the above questions or if you consider that there are other significant ethical issues then details should be included in your summary above. If you have answered yes to Question 1 then a clear justification for the importance of the research must be provided.

\*Please note if the answer to Question 10 is yes then the proposal should be submitted through **NHS research ethics approval procedures** to the appropriate **NRES**. The UREC should be informed of the outcome.

Checklist of documents which should be included:

Project proposal (with details of methodology) & source of funding	<input checked="" type="checkbox"/>
Documentation seeking informed consent (if appropriate)	
Information sheet for participants (if appropriate)	
Questionnaire (if appropriate)	

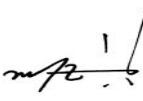
(Tick as appropriate)

**Applicant declaration**

I understand that I cannot collect any data until the application referred to in this form has been approved by all relevant parties. I agree to carry out the research in the manner specified and comply with the statement of ethical requirements on page 1 of this form. If I make any changes to the approved method I will seek further ethical approval for any changes.

Signature of Applicant: 

Date: 26/11/2017

Signature of Director of Studies: 

Date: 27/11/2017

*This form together with a copy of the research proposal should be submitted to the Research Institute Director for consideration by the Research Institute Ethics Committee/Panel*

**Note you cannot commence collection of research data until this form has been approved**

**SECTION B To be completed by the Research Institute Ethics Committee:**

Comments:

**There is no serious ethical issue involved but the disposal organs can be potentially a problem. Can you please clarify how this will be done?**

Approved

Signature Chair of Research Institute Ethics Committee:



Date: 7/2/18

*This form should then be filed on the student's record*

If in the judgement of the committee there are significant ethical issues for which there is not agreed practice then further ethical consideration is required before approval can be given and the proposal with the committees comments should be forwarded to the secretary of the UREC for consideration.

**There are significant ethical issues which require further guidance**

Signature Chair of Research Institute Ethics Committee:

Date:

*This form together with the recommendation and a copy of the research proposal should then be submitted to the University Research Ethics Committee*